THE MICROWAVE AND INFRA-RED SPECTRA OF SOME UNSTABLE GASEOUS MOLECULES

By

HELEN MARGARET JEMSON

B.Sc. (Hons.), The University of Otago, 1981

A THESIS SUBMITTED IN PARTIAL FULFILLMENT OF

THE REQUIREMENTS FOR THE DEGREE OF

DOCTOR OF PHILOSOPHY

in

THE FACULTY OF GRADUATE STUDIES

(Department of Chemistry)

We accept this thesis as conforming

to the required standard

THE UNIVERSITY OF BRITISH COLUMBIA

December 1986

In presenting this thesis in partial fulfilment of the requirements for an advanced degree at the University of British Columbia, I agree that the Library shall make it freely available for reference and study. I further agree that permission for extensive copying of this thesis for scholarly purposes may be granted by the head of my department or by his or her representatives. It is understood that copying or publication of this thesis for financial gain shall not be allowed without my written permission.

Department of CHEMISTRY

The University of British Columbia
1956 Main Mall
Vancouver, Canada
V6T 1Y3

Date 15 DEC 1986

ABSTRACT

The microwave spectra of three unstable molecules, bromine isocyanate (BrNCO), iodine isocyanate (INCO), and bromine thiocyanate (BrSCN), have been observed and analyzed in the frequency range 16-54 GHz. The infra-red spectrum of aminodifluoroborane (BF_2NH_2) has been investigated in the region 3700-400 cm^{-1}, and one band, the 2_0^1 vibrational band has been recorded at a resolution of 0.004 cm^{-1}, and the rotational structure analyzed.

BrNCO: BrNCO was generated from the flow reaction of Br_2 with silver cyanate. The spectra of two isotopic species were observed: ^{79}BrNCO and ^{81}BrNCO. They contain strong a-type transitions as well as some weaker b-type transitions which could not initially be assigned. In addition, the transitions show both Br and N quadrupole hyperfine structure. A novel method has been developed which uses perturbations in the Br structure to evaluate all the rotational constants, as well as the Br quadrupole tensor, entirely from a-type R branch transitions using a global least-squares fitting programme. This has allowed some b-type transitions to be assigned. The molecule has been shown to be planar and a partial r_0 structure was determined. The principal values of the Br quadrupole tensor have been evaluated and have provided some information about the type of bonding involved in the Br-N bond.

INCO: INCO was observed in the flow reaction of I_2 with silver cyanate. Many strong a-type transitions were observed as well as some very weak b-type transitions. These transitions showed I and N quadrupole hyperfine structure; many perturbations in the I structure were observed. The method developed in the analysis of the spectrum of BrNCO using such perturbations to obtain otherwise unobtainable rotational constants was extended to include centrifugal distortion constants. The planarity of INCO has been confirmed and a partial r_0 structure was determined. The principal values of the I quadrupole tensor have been evaluated and have provided some information about the type of bonding involved in the I-N bond.

BrSCN: BrSCN was generated in the flow reaction of Br_2 with silver thiocyanate. The spectra contained both a- and b-type transitions, all of which showed Br quadrupole hyperfine structure. The rotational constants and all five quartic centrifugal distortion constants were obtained for two isotopic species: ^{79}BrSCN and ^{81}BrSCN. The rotational constants confirm the thiocyanate configuration, and a partial r_0 structure has been obtained. Also, the principal values of the Br quadrupole tensor were evaluated which show that the Br-S bond is essentially covalent, with small amounts of π and ionic character.

BF_2NH_2: BF_2NH_2 was generated by heating solid BF_3NH_3. The wavenumbers of 7 of the vibrational fundamentals have been

obtained, and from the analysis of the 2_0^1 band, an accurate set of rotational and quartic centrifugal distortion constants of the ground vibrational state have been obtained and the rotational and quartic centrifugal distortion constants of the 2^1 level have been evaluated. Also a Coriolis type perturbation was observed, probably due to the combination level $\nu_7 + \nu_{11}$, which has provided an estimate of the wavenumber of the ν_{11} fundamental which has not yet been observed.

TABLE OF CONTENTS

Chapter		Page
I.	Introduction	1
	Bibliography	8
II.	Theory	
	2.1 Introduction	10
	2.2 The Rigid Rotor	11
	2.3 Rigid Rotor Selection Rules	15
	2.4 Centrifugal Distortion	17
	2.5 Structural Data	21
	2.6 Nuclear Spin Statistics	25
	2.7 Nuclear Quadrupole Coupling	26
	2.8 Stark Effect	32
	2.9 The Harmonic Oscillator	37
	2.10 Vibration Selection Rules	39
	2.11 Coriolis Perturbations	41
	Bibliography	46
III.	Experimental Methods	
	3.1 The Microwave Spectrometer	48
	3.2 The FT-IR Interferometric Spectrometer	52
	Bibliography	59
IV.	The Microwave Spectrum of Bromine Isocyanate, BrNCO	
	4.1 Introduction	60
	4.2 Experimental Methods	60
	4.3 Initial Assignments	61
	4.4 Determination of A	65
	4.5 Analysis of a-type Transitions	68
	4.6 b-type Transitions	69
	4.7 The Structure of BrNCO	101
	4.8 Br and ^{14}N Quadrupole Coupling	105
	4.9 Discussion	111
	Bibliography	113
V.	The Microwave Spectrum of Iodine Isocyanate, INCO	
	5.1 Introduction	115
	5.2 Experimental Methods	116
	5.3 Analysis of a-type Transitions	117
	5.4 Analysis of b-type Transitions	121
	5.5 Structure of INCO	145
	5.6 ^{127}I and ^{14}N Quadrupole Coupling	148
	5.7 Discussion	150
	Bibliography	155

Table of Contents (Continued)

Chapter		Page
VI.	The Microwave Spectrum of Bromine Thiocyanate, BrSCN	
6.1	Introduction	155
6.2	Experimental Methods	156
6.3	Analysis of the Microwave Spectrum	158
6.4	The Structure of BrSCN	182
6.5	Bromine Quadrupole Coupling	185
6.6	Discussion	189
	Bibliography	191
VII.	The Infra-Red Spectrum of Aminodifluoroborane, BF_2NH_2	
7.1	Introduction	193
7.2	Experimental Methods	194
7.3	Analysis of the Infra-red Spectrum	196
7.4	Analysis of the Rotational Structure of the 2^1 Band	199
7.5	Discussion	224
	Bibliography	226

LIST OF TABLES

Table		Page
4.1	Spectroscopic constants of BrNCO from a-type transitions.	70
4.2	Correlation coefficients of the spectroscopic constants of BrNCO derived from a-type transitions only.	71
4.3	Spectroscopic constants of ^{79}BrNCO.	78
4.4	Spectroscopic constants of ^{81}BrNCO.	79
4.5	Measured rotational transitions (in MHz) of ^{79}BrNCO.	80
4.6	Measured rotational transitions (in MHz) of ^{81}BrNCO.	86
4.7	Observed hyperfine transition frequencies in (MHz) of $^{79}Br^{14}NCO$ b-type transitions.	92
4.8	Observed hyperfine transition frequencies in (MHz) of $^{81}Br^{14}NCO$ b-type transitions.	97
4.9	Bromine quadrupole coupling constants in principal inertial axes.	101
4.10	^{14}N quadrupole coupling constants in principal inertial axes.	102
4.11	Structural parameters of bromine isocyanate.	103
4.12	Comparison of structural parameters of BrNCO with values in other molecules.	104
4.13	Principal values of the bromine quadrupole coupling tensor.	107
4.14	Comparison of experimentally determined ^{14}N quadrupole coupling constants with values calculated using theoretical calculations.	111
5.1	Spectroscopic constants of ^{127}INCO from a-type transitions only.	123
5.2	Correlation coefficients of the spectroscopic constants of ^{127}INCO calculated from a-type transitions.	125
5.3	Spectroscopic Constants of ^{127}INCO.	128

List of Tables (Continued)

Table		Page
5.4	Correlation coefficients of the spectroscopic constants of ^{127}INCO.	129
5.5	Measured rotational transitions (in MHz) of INCO.	131
5.6	Observed hyperfine transition frequencies (in MHz) of $^{127}I^{14}$NCO b-type Q branch transitions.	139
5.7	Quadrupole coupling constants of ^{14}N in principal inertial axes.	145
5.8	Structural parameters of INCO.	146
5.9	Comparison of structural parameters of INCO with other molecules.	147
5.10	Quadrupole coupling constants of ^{127}I in principal inertial axes.	148
5.11	Quadrupole coupling constants of ^{127}I in principal quadrupole axes.	148
5.12	Comparison of ^{14}N quadrupole coupling constants obtained experimentally with theoretically calculated values.	150
5.13	Ionic bond character of the halogen isocyanates.	153
6.1	The rotational constants of bromine thiocyanate and bromine isothiocyanate calculated from model structures.	159
6.2	Spectroscopic constants of bromine thiocyanate.	164
6.3	Closest near degeneracies having the correct symmetry to cause perturbations in hyperfine structure in the spectrum of bromine thiocyanate.	166
6.4	Measured rotational transitions (in MHz) of ^{79}BrSCN.	167
6.5	Measured rotational transitions (in MHz) of ^{81}BrSCN.	175
6.6	Comparison of the measured rotational constants of bromine thiocyanate with those calculated from model structures.	183

List of Tables (Continued)

Table		Page
6.7	Structural parameters of bromine thiocyanate.	183
6.8	Comparison of structural parameters of BrSCN with structures of other molecules.	184
6.9	Quadrupole coupling constants of bromine thiocyanate in the principal inertial axes system.	186
6.10	Principal values of the bromine quadrupole coupling tensor of bromine thiocyanate.	186
7.1	Vibrational frequencies of BF_2NH_2 (in cm^{-1}).	200
7.2	Vibrational Frequencies of BF_2NH_2 (in cm^{-1}).	201
7.3	Rotational constants of the 2^1 level of $^{11}BF_2NH_2$.	206
7.4	Rotational constants of the 2^1 level of $^{11}BF_2NH_2$.	207
7.5	Observed infrared transitions of $^{11}BF_2NH_2$.	209

LIST OF FIGURES

Figure		Page
3.1	Block diagram showing basic design of microwave spectrometer.	49
3.2	Schematic design of interferometer.	54
4.1	Broadband scan of the microwave spectrum of BrNCO in the frequency range 32.7-38.6 GHz.	63
4.2	$J = 6 \leftarrow 5$ a-type R branch of BrNCO in the frequency range 24.8 - 26.2 GHz.	64
4.3	Rotational energy levels of ^{81}BrNCO.	73
4.4	The energy levels of the $11_{0,11} - 10_{0,10}$ transitions of ^{81}BrNCO.	72
4.5	Hyperfine splitting patterns of some $K_a = 0$ transitions of ^{81}BrNCO.	74
4.6	The $17_{1,16} - 17_{0,17}$ transitions of ^{79}BrNCO showing both ^{79}Br and ^{14}N nuclear quadrupole effects.	76
4.7	The atoms of BrNCO in its principal inertial axis system according to structure II (Table 4.11).	104
5.1	Broadband scan of the $J = 9 \leftarrow 8$ a-type R branch of INCO in the frequency range 29.68 - 30.71 GHz.	118
5.2	The $12_{0,12} - 11_{0,11}$ transitions of INCO.	120
5.3	The rotational energy levels of INCO showing several important near-degeneracies.	122
5.4	The energy levels of $17_{2,15}$ and $19_{1,19}$ of INCO.	127
5.5	The relative positions of the atoms of INCO in its principal inertial axis system (from structure II in Table 5.8).	147
6.1	Preparation of BrSCN.	157
6.2	The transition $13_{2,11} - 13_{1,12}$ for ^{79}BrSCN and ^{81}BrSCN.	162

List of Figures (Continued)

Figure		Page
6.3	Broadband scan of the spectrum of BrSCN from 31.57 - 31.87 GHz.	163
6.4	The positions of the atoms of BrSCN relative to its principal inertial axis system.	185
7.1	The configuration of the atoms of BF_2NH_2.	197
7.2	Low-resolution transmittance spectrum of gaseous BF_2NH_2 in the region 750-3700 cm^{-1}.	198
7.3	Medium resolution transmittance spectrum of the ν_2 fundamental of gaseous BF_2NH_2.	202
7.4	High resolution absorbance spectrum of a portion of the ^PP branch side of the 2_0^1 band of gaseous BF_2NH_2.	204
7.5	High resolution absorbance spectrum of a portion of the ^PP branch side of the 2_0^1 band of BF_2NH_2 indicating a small Coriolis perturbation.	208
7.6	Relative positions of the K stacks of the 2^1 and perturbing level for a particular value of J.	223

ACKNOWLEDGEMENT

I would like to thank my supervisor Dr. M.C.L. Gerry for his guidance, encouragement and approachability throughout my time at U.B.C.

I would also like to thank Dr. W. Lewis-Bevan and Dr. N.P.C. Westwood for their many helpful discussions.

Finally, I would like to thank my husband James for his support and encouragement.

CHAPTER I: INTRODUCTION

Every molecule possesses a unique set of energy levels. These energy levels, associated with the motions of the nuclei and electrons in the molecule, depend on such factors as atomic masses, interatomic distances, the electron distribution and interparticle forces. Molecular spectroscopic studies examine the absorption or emission of electromagnetic radiation arising from transitions between these energy levels. The frequency of the radiation depends on the type of transition.

Pure rotational transitions, between levels in the same electronic and vibrational state, usually occur in the microwave region which extends from approximately 1 GHz to 1000 GHz, while infra-red radiation is usually used to determine the frequency of transitions between vibrational states.

The rapid technological advances associated with the development of radar during World War II provided the instrumentation for spectroscopically analyzing molecules in the microwave region of the electromagnetic spectrum. Since then, the available frequency range has expanded and the sensitivity and resolution have improved considerably. Instead of doing laborious calculations using explicit energy formulas, or using perturbation theory to account for centrifugal distortion, quadrupole coupling or other effects, computers have allowed increasingly complex formulations to be used to analyze microwave spectra in order to find exact solutions for the

energies associated with rotational motion. From the analysis of microwave spectra we can obtain, in addition to the rotational constants of molecules, quadrupole coupling constants, dipole moments, structural information and force field determinations (1). The spectroscopic constants of the ground vibrational state of a molecule obtained from microwave spectra can be useful when assigning rotational structure in vibrational transitions.

Not only have a large number of gaseous stable molecules been investigated using microwave spectroscopy, but also the spectra of many unstable gases have been analyzed, and more recently, gaseous free radicals and molecular ions have been studied spectroscopically.

The applications of techniques using microwave radiation are numerous. For example, microwave - microwave double resonance, involving a simultaneous irradiation with two frequencies, is useful in assigning transitions in complex spectra, and is also useful in studying molecular collision processes (2). One extremely interesting use of microwave spectroscopy is the observation of spectral lines of a variety of molecular free radicals, ions and stable molecules in interstellar space (3).

Infra-red spectroscopy has long been used as a tool for investigating the physical and chemical properties of molecules in the gaseous, liquid and solid phases. The infra-red region extends from approximately 2-50 μm. Transitions of gaseous

molecules in this region involve simultaneous changes in rotational and vibrational quantum numbers, and analyses of these transitions provide spectroscopic constants for both the ground and excited vibrational levels, while the frequencies of the fundamental vibrations can be used in force-field calculations.

Dispersive techniques, involving the use of a monochromator, have been superseded for many applications by the technique of Fourier-Transform Infra-Red Spectroscopy (4). Such applications include the measurement of extremely high-resolution spectra, the measurement of weak bands and the study of short-lived species.

This thesis reports the spectroscopic studies of some unstable gaseous molecules: bromine isocyanate, iodine isocyanate, bromine thiocyanate and difluoroaminoborane. This follows a general theme that has been followed within this research group in recent years where several unstable molecules have been studied using both microwave and infra-red spectroscopy. Each of the four molecules investigated is sufficiently unstable that it was generated and studied in a flow system.

The microwave spectra of the first three molecules, BrNCO, INCO and BrSCN were analyzed in order to determine their rotational constants, centrifugal distortion constants and quadrupole coupling constants of the quadrupolar nuclei in the molecules, and to determine some structural information.

These molecules all belong to a class of molecules known as the pseudohalides, which have similar chemical properties to the halides. Other examples of pseudohalides are the azides, cyanides and cyanamides. The structures of many pseudohalide molecules have been studied in the gas phase using both electron diffraction and microwave spectroscopy (5-19). Many interesting features have been found.

Molecules containing the NCO group are either cyanates or isocyanates depending on whether the rest of the molecule is linked via the oxygen or nitrogen atom respectively. The structures of all the cyanate molecules which have been studied so far in the gas phase, have been shown, with one exception, to be linked via the nitrogen atom, and are therefore isocyanates (XNCO) (6-11). Only F_5SeOCN has been demonstrated to have a cyanate structure (12). The X-N-C angle in the isocyanates is found to vary widely, depending on the substituent X; for example it is effectively 180° in the ground state of SiH_3NCO (6), ≃124° in HNCO (7) and ≃118° for ClNCO (8,9).

Until the structure of ClNCO was determined, the -NCO chain was assumed to be linear in all isocyanate molecules; however in ClNCO it was found that it is in fact non-linear, with the O atom bent away from the N-C bond axis by ≃9° in a trans configuration to Cl (8,10). The O atom has since also been shown to lie slightly off the N-C axis in HNCO as well as in other isocyanate molecules (7,11).

These structural variations are not unique. The isocyanate

molecules are isoelectronic with the azide molecules (XN_3) (13,14). The azides exhibit rather similar structural trends, although the X-N-N angles are somewhat smaller than the corresponding X-N-C angles of the isocyanates (e.g. in ClN_3 it is ≈109° (13)). There is also a slight tilt of the N-N-N group with <(N-N-N)=171.9° in ClN_3, almost identical with the NCO angle in ClNCO.

The thiocyanates are also a rather interesting group of molecules. They contain the -SCN group, which is ambidentate, meaning that it can bond at either the N atom or the S atom to form both isothiocyanates (XNCS) and thiocyanates (XSCN). There seems to be no prior indication as to whether a molecule has the isothiocyanate or thiocyanate configuration, and in fact, the methyl derivative has been found to exist in both forms: CH_3SCN and CH_3NCS (15). The isothiocyanates, for example SiH_3NCS (16) and the parent acid HNCS (17), show the same trends in the variation of the X-N-C angle as do the isocyanates, although on average the X-N-C angle is ≈7° wider. On the other hand, the thiocyanates, for example NCSCN (18) and ClSCN (19) do not show such trends and the X-S-C angle is ≈99° in all cases.

Of the halogen pseudohalides, the microwave spectra and therefore the gas phase structures of the chlorine derivatives have been analyzed, eg. ClNCO (8,9), ClSCN (19), and ClN_3 (13). However few of the bromine and iodine containing pseudohalides have been examined spectroscopically. This may be partly due to the difficulty in analyzing the quadrupole hyperfine structure

in the microwave spectra of such molecules. Bromine and iodine have large quadrupole moments, and in many cases, this causes the hyperfine structure not to follow a simple first order pattern. This makes the spectra of molecules containing these atoms difficult to analyze.

The microwave spectra of BrNCO, INCO and BrSCN have not been investigated prior to the studies reported here. In fact, little is known about these molecules in the gaseous phase. All three molecules were expected to show non first-order quadrupole hyperfine splitting due to the halogen nuclei. However a computer programme had been written, which uses the exact quadrupole Hamiltonian, to simultaneously evaluate the rotational, centrifugal distortion and quadrupole coupling constants of a molecule (20). This was expected to aid considerably in the analysis of the spectra of these molecules.

The infra-red spectrum of BF_2NH_2 was examined in the region 3700-400 cm^{-1} using Fourier Transform infra-red spectroscopy. BF_2NH_2 belongs to the extensive group of inorganic molecules containing a boron-nitrogen bond. The properties of these molecules are of interest because they are isoelectronic with hydrocarbons containing a C-C linkage such as alkenes, alkynes and benzenes. For example, borazine, $N_3B_3H_6$, which has a ring structure, is isoelectronic with benzene, and in fact it has been called the 'inorganic benzene' (21,22).

The amineboranes, e.g. $R_3N:BR'_3$, are co-ordination compounds of an amine with a borane and are the B-N analogues of the

alkanes. They are, however, much less stable than their aliphatic counterparts because of the nature of the very polar donor - acceptor bonding, and they decompose easily to more stable compounds, which include aminoboranes.

The aminoboranes, e.g. $R_2N\text{-}BR'_2$, are isoelectronic with the alkenes. While structurally they are found to be planar, with C_{2v} symmetry like their organic analogues, the double bond character of the B-N bond is considerably less than in the C=C bond in ethylene, reflecting the different nature of the bonding (23-25). The π bonding in the aminoboranes arises from the transfer of lone pair of electrons from the nitrogen atom to the empty p orbital on the boron. Consequently these molecules are considerably less stable than the hydrocarbons and have a tendency to polymerize (26).

The parent compound, aminoborane, BH_2NH_2, has been characterized in the gas phase by microwave spectroscopy (23), and more recently an extensive infra-red study, which is still in progress, has been reported (27). It was therefore decided to investigate the infra-red spectrum of BF_2NH_2 to determine the wavenumbers of the fundamental vibrations. A high resolution study of the ν_2 fundamental was also carried out.

Bibliography

1. W. Gordy, R.L. Cook, "Microwave Molecular Spectra," 3rd ed. in "Techniques of Chemistry" (A. Weissberger, Ed.), Vol. 18, Wiley, New York, 1984.

2. J.G. Baker, "Microwave-Microwave Double Resonance," pp. 65-122, in "Modern Aspects of Microwave Spectroscopy, "(G.W. Chantry, Ed.), Academic, London, 1979.

3. G. Winnewisser, E. Churchwell, C.M. Walmsley, "Astrophysics of Interstellar Molecules", pp. 313-503, in "Modern Aspects of Microwave Spectroscopy", (G.W. Chantry, Ed.), Academic, London, 1979.

4. P.R. Griffiths, "Chemical Infrared Fourier Transform Spectroscopy", Wiley, New York, 1975.

5. C. Glidewell, Inorg. Chem. Acta, 11, 257-282, (1974).

6. J.A. Duckett, A.G. Robiette, M.C.L. Gerry, J. Mol. Spectrosc. 90, 374-393, (1981).

7. K. Yamada, J. Mol. Spectrosc., 79, 323-344, (1980).

8. W.H. Hocking, M.C.L. Gerry, J. Mol. Spectrosc. 42, 547-566, (1972).

9. W.H. Hocking, M.L. Williams, M.C.L. Gerry, J. Mol. Spectrosc. 58, 250-260, (1975).

10. H. Oberhammer, Z. Naturforsch, a26, 280-286, (1971).

11. H. Oberhammer, K. Seppelt, R. Mews, J. Mol. Struct. 101, 325-331, (1983).

12. K. Seppelt, H. Oberhammer, Inorg. Chem. 24, 1227-1229, (1985).

13. R.L. Cook, M.C.L. Gerry, J. Chem. Phys. 53, 2525-2528, (1970).

14. M. Winnewisser, R.L. Cook, J. Chem. Phys. 41, 999-1004, (1964).

15. R.G. Lett, W.H. Flygare, J. Chem. Phys. 47, 4730-4750, (1967).

16. D.R. Jenkins, R. Kewley, T.M. Sugden, Trans. Faraday Soc. 58, 1284-1290, (1962).

17. K. Yamada, M. Winnewisser, G. Winnewisser, L.B. Szalanski, M.C.L. Gerry, J. Mol. Spectrosc. 79, 295-313, (1980).

18. L. Pierce, R. Nelson, C.H. Thomas, J. Chem. Phys. 43, 3423-3431, (1967).

19. R.J. Richards, R.W. Davis, M.C.L. Gerry, J. Chem. Soc. Chem. Comm., 915-916, (1980).

20. M.C.L. Gerry, W. Lewis - Bevan, N.P.C. Westwood, J. Chem. Phys. 79, 4655-4663, (1983).

21. N. Niedenzu, J.W. Dawson, "Boron-Nitrogen Compounds", Academic Press, New York, 1965.

22. E.L. Muetterties, "The Chemistry of Boron and its Compounds", Wiley, New York, 1967.

23. M. Sugie, H. Takeo, C. Matsumura, Chem. Phys. Lett., 64, 573-575, (1974).

24. F.J. Lovas, D.R. Johnson, J. Chem. Phys. 59, 2347-2353 (1973).

25. F.B. Clippard, L.S. Bartell, Inorg. Chem., 9, 2439-2442, (1970).

26. S.Y. Pusatcioglu, H.A. McGee, A.L. Fricke, J. C. Hassler, J. Appl. Sci. 21, 1561-1567, (1977).

27. M.C.L. Gerry, W. Lewis-Bevan, A.J. Merer, N.P.C. Westwood, J. Mol. Spectrosc., 110, 153-163, (1985).

CHAPTER II: THEORY

2.1 Introduction

Mathematical models describing the motion of the electrons and nuclei in a molecule are used for the analysis of molecular spectra. This enables us to find solutions for the energy levels associated with these motions. The assignment of the quantum numbers involved in the transitions between levels, and the derived energy expressions for these levels, allow various parameters to be obtained which can be interpreted in terms of molecular properties.

Assumptions are often made to simplify the mathematics. In interpreting vibrational and rotational spectra in particular, the energies associated with the vibrational and rotational motions are usually much different in magnitude and can be treated independently. This allows them to be calculated separately.

The two basic models adopted for vibration and rotation are the harmonic oscillator and rigid rotor respectively. These models, however, do not exactly reproduce the rotational and vibrational energies, and corrections must be made to allow for other factors such as anharmonicity in the case of vibrational energies, and for non-rigidity of bonds when calculating rotational energies. Sometimes even the assumption that the vibrational and rotational energies can be calculated independently breaks down. In addition, transitions may have

observable splittings due to factors such as nuclear quadrupole moments, or external magnetic or electric fields. These factors all require corrections to the Hamiltonian.

Once the correct model is chosen, a least-squares fitting procedure is used to fit the observed frequencies, giving parameters such as vibrational frequencies, moments of inertia and quadrupole coupling constants. These spectroscopic constants can then in turn be used to calculate molecular properties such as structures, bonding characteristics such as estimates of ionic or double bond character, and dipole moments.

2.2 The Rigid Rotor

The coarse features of the rotational spectrum of a molecule can be accounted for reasonably well by the rigid rotor model. The Hamiltonian for this model, referred to the principal axes of inertia of the molecule, is given by:

$$H_r = B_x J_x^2 + B_y J_y^2 + B_z J_z^2 \qquad (2.1)$$

where J_x, J_y and J_z are the components of the rotational angular momentum about each of the principal axes of inertia. B_x, B_y and B_z are the rotational constants of the molecule which are related to the principal moments of inertia by:

$$B_\alpha = \frac{h}{8\pi^2 I_\alpha} \qquad \alpha = x, y, z \qquad (2.2)$$

The non-zero matrix elements of this Hamiltonian (in

frequency units) are:

$$\langle J,K,M|H_r|J,K,M\rangle = \tfrac{1}{2}(B_x+B_y)J(J+1) + [B_z - \tfrac{1}{2}(B_x+B_y)]K^2 \quad (2.3)$$

$$\langle J,K\pm2,M|H_r|J,K,M\rangle = \tfrac{1}{4}(B_x-B_y)\{[J(J+1)-K(K\pm1)] \times [J(J+1)-(K\pm1)(K\pm2)]\}^{1/2} \quad (2.4)$$

By convention, J_z is chosen as the component of the angular momentum for which there exist simultaneous eigenstates with J^2. J is the rotational quantum number representing the total rotational angular momentum of the molecule, K is the quantum number representing the component of J along the principal z-axis with values J, (J-1),....(-J+1), -J, and the quantum number M gives the component of the total angular momentum along the space-fixed Z axis.

The principal axes of a molecule are usually labelled a, b, and c with $I_a \leq I_b \leq I_c$. The a, b and c axes can be identified with the x, y and z axis according to various representations. The three right-handed representations are (8):

I^r $\quad x \rightarrow b \; ; \; y \rightarrow c \; ; \; z \rightarrow a$

II^r $\quad x \rightarrow c \; ; \; y \rightarrow a \; ; \; z \rightarrow b$

III^r $\quad x \rightarrow a \; ; \; y \rightarrow b \; ; \; z \rightarrow c$ (2.5)

The I^r representation is the one most commonly used.

For some special types of molecules, the Hamiltonian has diagonal matrix elements only, and simple expressions for the

rigid rotor energy can be derived:

(a) Spherical Top: $I_a = I_b = I_c$

$$E_r = hBJ(J+1) \qquad (2.6)$$

(b) Linear Molecules: $I_b = I_c$; $I_a = 0$

$$E_r = hBJ(J+1) \qquad (2.7)$$

(c) Symmetric Top: (i) prolate rotors: $I_b = I_c > I_a$

$$E_r = h[BJ(J+1)+(A-B)K^2] \qquad (2.8)$$

(ii) oblate rotors: $I_a = I_b < I_c$

$$E_r = h[BJ(J+1)+(C-B)K^2] \qquad (2.9)$$

Most molecules, however, fall into the class of asymmetric rotors with $I_a < I_b < I_c$. For these molecules, the off-diagonal matrix elements of the Hamiltonian are non-zero. There are no explicit expressions for the rotational energies, except at low J, and the resulting spectra can be quite complex.

The complete Hamiltonian must be diagonalised in order to determine the exact energy. This procedure can be considerably simplified by first using the Wang transformation (9) to introduce a new set of basis functions:

$$|J,0^+\rangle = |J,0\rangle$$

$$|J,K^+\rangle = \tfrac{1}{\sqrt{2}}\,[|J,K\rangle + |J,-K\rangle] \qquad (K>0)$$

$$|J,K^-\rangle = \tfrac{1}{\sqrt{2}}\,[|J,K\rangle - |J,-K\rangle] \qquad (K>0) \qquad (2.10)$$

Because there are no K+1 terms to connect odd and even K matrix elements, and following the Wang transformation there are no elements connecting $|J,K^+\rangle$ and $|J,K^-\rangle$ terms, the matrix can be converted to four smaller submatrixes designated E^+, E^-, O^+ and O^-. These smaller submatrices are then diagonalised to find the energies.

While the matrices are diagonal in J, they are non-diagonal in K. K is no longer a 'good' quantum number. The notation that is most commonly used to describe the energy levels of an asymmetric rotor is J_{K_a,K_c} (8), where K_a represents the K quantum number in the prolate symmetric top limit and K_c is the K quantum number in the oblate symmetric top limit.

Various parameters can be used as measures of how close a molecule is to being a symmetric top. One convenient parameter is Ray's asymmetry parameter κ (10):

$$\kappa = \frac{2B-A-C}{A-C} \qquad (2.11)$$

The limiting values of κ are -1 and +1 corresponding to prolate and oblate symmetric tops respectively. Another such parameter is Wang's asymmetry parameter b_p (9) , where:

$$b_p = \frac{C-B}{2A-B-C} \qquad \text{with } -1 \leq b_p \leq 0 \qquad (2.12)$$

$b_p = 0$ in the prolate limit and $b_p = -1$ in the oblate limit. Expressions for the energy levels of an asymmetric top have been derived in terms of the asymmetry parameters e.g.:

$$E_r = h\{\tfrac{1}{2}(B+C)J(J+1) - [A-\tfrac{1}{2}(B+C)]W(b_p)\} \qquad (2.13)$$

$W(b_p)$ is called the reduced energy. It is usually obtained by diagonalising the Hamiltonian. For a near symmetric top it can be expressed approximately as a power series in b_p:

$$W(b_p) = K^2 + C_1 b_p + C_2 b_p{}^2 + \ldots\ldots \qquad (2.14)$$

2.3 Rigid Rotor Selection Rules

Rotational transitions are induced by the interaction of the electric field component of electromagnetic radiation with the permanent electric dipole moment of a molecule. Because the microwaves are plane polarised, with the electric field E(t) along the space fixed Z axis, perpendicular to their direction of propagation, the radiation interacts with the component of the molecular dipole moment along this direction:

$$H(t) = -\mu . E(t) = -\mu_Z E_Z(t) \qquad (2.15)$$

For a transition to be allowed, the matrix element $\langle J',K',M' | \mu_Z | J,K,M \rangle$ must be non-zero. μ_Z is related to the molecule-fixed axes by direction cosines (ϕ_{Zg}):

$$\mu_Z = \sum_g \mu_g \phi_{Zg} \qquad g=a,b,c \qquad (2.16)$$

In a symmetric top, where the dipole moment lies along the

direction of the symmetry axis, the following selection rules can be derived:

$$K>0;\ \Delta J = 0, \pm 1\ ;\ \Delta K=0\ ;\ \Delta M=0$$
$$K=0;\ \Delta J = \pm 1\ ;\ \Delta K=0\ ;\ \Delta M=0 \qquad (2.17)$$

Asymmetric rotor selection rules are more complex. The dipole moment is not necessarily aligned along any of the principal axes of inertia, and therefore there is a possibility of a-, b- and c-type transitions, depending on whether the component of the dipole moment along each of these axes is non-zero. The expression:

$$\langle J', \tau' | \phi_{Zg} | J, \tau \rangle \qquad \text{where} \qquad \tau = K_a - K_c \qquad (2.18)$$

must transform according to the totally symmetric representation A in the D_2 point group which is the symmetry group of the asymmetric rotor eigenfunctions. The eigenfunctions are classified according to one of the symmetry species A, B_a, B_b, B_c of this group.

The selection rules are: $\Delta J = 0, \pm 1\ ;\ \Delta M=0$

	$K_a' K_c' \leftrightarrow K_a K_c$
a-type $\mu_a \neq 0$	ee ↔ eo
	oe ↔ oo
b-type $\mu_b \neq 0$	ee ↔ oo
	eo ↔ oe

c-type $\mu_c \neq 0$	ee ↔ oe	
	oo ↔ eo	(2.19)

e and o refer to the even or odd nature of K_a and K_c.

2.4 Centrifugal Distortion

While rigid rotor theory provides a reasonable approximation of observed rotational spectra, many discrepancies are observed between measured and calculated frequencies, particularly for lighter molecules, and at high values of J and K. Real molecules are not rigid. Flexible bonds and angles result in centrifugal distortions in molecules as they rotate. Corrections to the rigid-rotor Hamiltonian, which involve higher order angular momentum terms, must be made (11).

$$H_d = \frac{1}{4} \sum_{\alpha\beta\gamma\delta} \tau_{\alpha\beta\gamma\delta} J_\alpha J_\beta J_\gamma J_\delta \qquad \alpha,\beta,\gamma,\delta, = x,y,z \tag{2.20}$$

The parameters $\tau_{\alpha\beta\gamma\delta}$ can be directly interpreted in terms of the inverse harmonic force constants:

$$\tau_{\alpha\beta\gamma\delta} = \frac{1}{2I_{\alpha\alpha}I_{\beta\beta}I_{\gamma\gamma}I_{\delta\delta}} \sum_{i=1}^{3N-6} \sum_{j=1}^{3N-6} \frac{\partial I_{\alpha\beta}}{\partial R_i} \frac{\partial I_{\gamma\delta}}{\partial R_j} (f^{-1})_{ij} \tag{2.21}$$

R_i and R_j belong to the set of 3N-6 internal displacement coordinates while $(f^{-1})_{ij}$ is an element of the inverse force constant matrix where a force constant is defined in the harmonic potential energy by:

$$V = \frac{1}{2} \sum_{i,j} f_{ij} R_i R_j \qquad (2.22)$$

Symmetry restrictions and commutation relations reduce the number of possible τ's to 21. Many of these are equivalent, which leave only 6 τ's: τ'_{aaaa}, τ'_{bbbb}, τ'_{cccc}, τ'_{aabb}, τ'_{bbcc} and τ'_{aacc} (12).

$$H'_d = \frac{1}{4} \sum_{\alpha\beta} \tau'_{\alpha\alpha\beta\beta} J_\alpha^2 J_\beta^2 \qquad (2.23)$$

However these 6 τ's cannot all be determined simultaneously from experimental data (13,14). Watson (15,16) has solved this indeterminacy problem starting from the standard form of the rotational Hamiltonian as a power series in the components of angular momentum:

$$H_{rot} = \sum_{pqr} h_{pqr} (J_x^p J_y^q J_z^r + J_x^r J_y^q J_z^p) \qquad (2.24)$$

In practice this power series converges rapidly. Because of various physical properties and symmetry considerations of the Hamiltonian, only a certain number of terms of each degree are possible. Once again, for an asymmetric rotor, this means there will be 6 centrifugal distortion constants of 4th degree. The indeterminacy is removed by further reducing the number of parameters by a unitary transformation of the Hamiltonian. This is analogous to the rigid rotor problem where a rotation of the axes diagonalizes the inertia tensor.

The number of quartic centrifugal distortion constants is

thus reduced to five and a small vibrational correction is introduced into the rotational constants.

There is no unique reduction. However, there are two that are commonly used. Including the sextic distortion constants (terms in the angular momentum to the sixth degree) these are (17):

(i) Asymmetric top (A) reduction

The A reduction is the most commonly used reduction. The matrix elements of the Hamiltonian are all of the form $\Delta K = 0$, $\Delta K = \pm 2$, thus preserving the same structure of the submatrices as for a rigid asymmetric top. In frequency units:

$$\begin{aligned}\langle J,K|H_A|J,K\rangle = {} & \tfrac{1}{2}(B+C)J(J+1) + [A - \tfrac{1}{2}(B+C)]K^2 \\ & - \Delta_J J^2(J+1)^2 - \Delta_{JK} J(J+1)K^2 - \Delta_K K^4 \\ & + \Phi_J J^3(J+1)^3 + \Phi_{JK} J^2(J+1)^2K^2 + \Phi_{KJ} J(J+1)K^4 \\ & + \Phi_K K^6 \end{aligned} \qquad (2.25)$$

$$\begin{aligned}\langle J,K\pm2|H_A|J,K\rangle = {} & \{\tfrac{1}{4}(B-C) - \delta_J J(J+1) - \tfrac{1}{2}\delta_K[(K\pm2)^2+K^2] \\ & + \phi_J J^2(J+1)^2 + \tfrac{1}{2}\phi_{JK} J(J+1)[(K\pm2)^2+K^2] \\ & + \tfrac{1}{2}\phi_K[(K\pm2)^4+K^4]\}\{[J(J+1)-K(K\pm1)] \\ & \times [J(J+1)-(K\pm1)(K\pm2)]\}^{1/2} \end{aligned} \qquad (2.26)$$

The disadvantage of this reduction is that the constant δ_K becomes indeterminate for an accidental near-symmetric top. In this case the S-reduction is used.

(ii) Symmetric top (S) reduction

In the symmetric top reduction there is no J_z - dependence in the off-diagonal matrix elements. The result is that the matrix elements are of the form $\Delta K=0, \pm2, \pm4, \pm6$. In frequency units:

$$\begin{aligned}\langle J,K|H_S|J,K\rangle = {} & \tfrac{1}{2}(B+C)J(J+1) + [A-\tfrac{1}{2}(B+C)]K^2 \\ & -D_J J^2(J+1)^2 - D_{JK}J(J+1)K^2 - D_K K^4 \\ & -H_J J^3(J+1)^3 + H_{JK}J^2(J+1)^2K^2 \\ & +H_{KJ}J(J+1)K^4 + H_K K^6 \end{aligned} \tag{2.27}$$

$$\begin{aligned}\langle J,K\pm2|H_S|J,K\rangle = {} & \{\tfrac{1}{4}(B-C) + d_1 J(J+1) + h_1 J^2(J+1)^2\} \\ & \times\{[J(J+1)-K(K\pm1)][J(J+1)-(K\pm1)(K\pm2)]\}^{1/2}\end{aligned} \tag{2.28}$$

$$\begin{aligned}\langle J,K\pm4|H_S|J,K\rangle = {} & \{d_2 + h_2 J(J+1)\}\{[J(J+1)-K(K\pm1)] \\ & \times[J(J+1)-(K\pm1)(K\pm2)][J(J+1)-(K\pm2)(K\pm3)] \\ & \times[J(J+1)-(K\pm3)(K\pm4)]\}^{1/2}\end{aligned} \tag{2.29}$$

$$\begin{aligned}\langle J,K\pm6|H_S|J,K\rangle = {} & h_3\{[J(J+1)-K(K\pm1)[J(J+1)-(K\pm1)(K\pm2)] \\ & \times[J(J+1)-(K\pm2)(K\pm3)][J(J+1)-(K\pm3)(K\pm4)] \\ & \times[J(J+1)-(K\pm4)(K\pm5)][J(J+1)-(K\pm5)(K\pm6)]^{1/2}\end{aligned} \tag{2.30}$$

The disadvantage of this reduction is that the diagonalization procedure takes longer because of the greater number of off-diagonal matrix elements. In all the spectroscopic studies reported in this thesis, Watson's A-

reduction in the I^r representation is used.

In many earlier papers the effects of distortion are often reported in terms of the τ's. However the quartic distortion constants from Watson's A-reduction are simply related to the τ's. In the I^r representation (16,18):

$$\Delta_J = -\tfrac{1}{8}\{\tau'_{bbbb} + \tau'_{cccc}\}$$

$$\Delta_{JK} = \tfrac{3}{8}\{\tau'_{bbbb} + \tau'_{cccc}\} - \tfrac{1}{4}\{\tau'_{ccaa} + \tau'_{bbaa} + \tau'_{bbcc}\}$$

$$\Delta_K = -\tfrac{1}{4}\{\tau'_{bbbb} + \tau'_{cccc} + \tau'_{aaaa}\} + \tfrac{1}{4}\{\tau'_{ccaa} + \tau'_{bbcc} + \tau'_{aabb}\}$$

$$\delta_J = -\tfrac{1}{16}\{\tau'_{bbbb} - \tau'_{cccc}\}$$

$$\delta_K = \tfrac{1}{8}\tau'_{bbbb}\,(B-A)/(B-C) + \tfrac{1}{8}\tau'_{cccc}\,(C-A)/(B-C) + \tfrac{1}{8}\{\tau'_{ccaa} - \tau'_{bbaa} + \tau'_{bbcc}\,(2A-B-C)/(B-C)\}$$

$$\tau'_1 = \tau'_{aabb} + \tau'_{bbcc} + \tau'_{ccaa}$$

$$\tau'_2 = (A/S)\tau'_{bbcc} + (B/S)\tau'_{aacc} + (C/S)\tau'_{aabb} \qquad (S = A+B+C) \qquad (2.31)$$

2.5 Structural Data

In the gas phase, structures of molecules can be calculated using both electron diffraction and microwave spectroscopy. The structural parameters extracted from such studies are of particular importance, as they can be considered free of intermolecular forces. Trends in bond lengths and angles over a series of similar molecules give insights into the nature of the chemical bonds involved in connecting the atoms of a molecule. Information may be derived such as ionic character and double bond character.

Structural information is contained in the moments of inertia calculated from the spectroscopic rotational constants A, B and C (see equation 2.2). The moments of inertia are simply related to the masses of the atoms in a molecule and their co-ordinates in the principal inertial axes:

$$I_{xx} = \sum_i m_i \ (y_i^2 + z_i^2)$$

$$I_{yy} = \sum_i m_i \ (z_i^2 + x_i^2)$$

$$I_{zz} = \sum_i m_i \ (x_i^2 + y_i^2) \qquad (2.32)$$

However, the accuracy of the bond lengths and angles obtained from the moments of inertia is not as precise as the uncertainties in the rotational constants would suggest. This is because the dimensions of a molecule are affected by its zero point motion. Therefore the moments of inertia in the ground state, obtained by rotational spectroscopy, are only directly relevant to the ground vibrational state structural parameters.

Several different types of structure can be calculated from the available data.

The structure that would be the most ideal to determine is the equilibrium or r_e structure, which is the configuration of the molecule at the minimum of the vibrational potential surface; however its calculation requires a knowledge of the rotational constants for enough isotopes in all the excited vibrational states, which are not known for many molecules.

The effective structure, r_o, is obtained directly from the ground state spectroscopic moments of inertia via the moment of inertia and first moment equations. For a planar asymmetric rotor these are:

$$I_{aa} = \sum_i m_i b_i^2 \quad I_{bb} = \sum_i m_i a_i^2 \quad I_{ab} = I_{ba} = \sum_i m_i a_i b_i = 0$$

$$\sum_i m_i a_i = 0 \qquad \sum_i m_i b_i = 0 \qquad (2.33)$$

Obviously more information than the moments of inertia of a single isotopic species would be required to completely determine the structure of a molecule. To be able to solve the above equations for all structural parameters, isotopic substitution must be used. These structural parameters must be assumed to remain constant with isotopic substitution which is not always a good assumption, especially for lighter atoms.

A common representation of the structure of a molecule is the substitution structure, r_s, which is calculated using equations developed by Kraitchman (19). These equations calculate the coordinates of each atom in a molecule using the changes in the moments of inertia upon the isotopic substitution of the atom. Costain (20) has shown that the r_s structure is closer to the r_e structure than the r_o one is, because some of the ground-state vibrational effects have been averaged out.

The disadvantage of the r_s structure is that is lacks a well-defined physical meaning. One structure, however, that can be readily compared to electron diffraction data is the ground-

state average or r_z structure, which represents the average configuration of the atoms. A knowledge of the harmonic force constants is required to calculate r_z and these are not always available because their calculation requires vibrational frequencies, and other data such as distortion constants and inertial defects for more than one isotopic species. If an r_z structure is obtained then it may in turn be used to obtain an approximation for the equilibrum structure (21,22).

An important parameter used for testing the planarity of a molecule is the inertial defect.

$$\Delta = I_c^\circ - I_a^\circ - I_b^\circ \qquad (2.34)$$

For a planar molecule in its equilibrium configuration, Δ would be zero. However, Δ is usually a small positive number, largely because of in-plane vibrational effects, but it also contains some contribution from out-of plane vibrational effects and electronic and centrifugal effects (23). Inertial defects can also be useful in obtaining an estimate of a rotational constant in cases when only two of them can be determined: eg. only B and C are ordinarily determinable if a molecule exhibits a strong a-type R branch spectrum only. A knowledge of Δ from similar molecules could be used to estimate a value of A.

Herschbach and Laurie (24) have developed a simple approximation for the relationship between the inertial defect

and the frequency of the lowest in-plane bending vibration:

$$\Delta \approx \frac{4K}{\omega} \qquad (2.35)$$

with ω in cm^{-1} and $K = h/8\pi^2$. This vibrational frequency could also be estimated from the intensities of vibrational satellites if the excited vibrational states are sufficiently populated at the temperature of the experiment.

2.6 Nuclear Spin Statistics

A number of molecules contain two or more identical nuclei, i.e. nuclei that can be exchanged by a rotation of the molecule by less than 2π degrees about a symmetry axis, so that the configuration is indistinguishable from the original. For such an exchange of nuclei the overall wave-function must either remain unchanged (symmetric) or else change sign only (antisymmetric). For Bose particles (integral or zero spin) the overall wave functions are symmetric, while for Fermi particles (half-integral spin) the overall wave-functions are antisymmetric with respect to an operation which exchanges identical particles (25).

Asymmetric rotors often contain one or more pairs of identical nuclei. For molecules with one pair of such nuclei the relative weight of the symmetric to antisymmetric spin functions is $(I+1)(2I+1):I(2I+1)$. For a molecule in its ground electronic and vibrational state (symmetric), the parity of the

rotational wave function with respect to the symmetry axis is important e.g. if the symmetry axis is the b-axis the rotational wave functions with $K_a K_c$ = ee or oo are symmetric with respect to the b-axis, while the functions with $K_a K_c$ = eo or oe are antisymmetric. Therefore the relative intensities of b-type transitions of a molecule obeying Bose statistics is ee↔oo: eo ↔oe = (2I+1)(I+1):I(2I+1)

If a molecule has more than one pair of identical nuclei the resultant statistics and relative intensities of the transitions are derived by considering the simultaneous exchange of each pair. For example, for the simultaneous exchange of two pairs of equivalent fermions, the total wavefunction is symmetric.

2.7 Nuclear Quadrupole Coupling

An important hyperfine interaction in rotational spectroscopy is the interaction between the quadrupole moment of a nucleus and the electric field gradient at the nucleus due to the electron charge distribution.

All atoms with a nuclear spin greater than 1/2 have a quadrupole moment. Because the electric field gradient, and therefore the magnitude of the interaction, depends upon the rotational state of the molecule, the interaction effectively couples the rotational angular momentum and the nuclear spin. The resultant new total angular momentum is designated F.

$$\mathbf{J} + \mathbf{I} = \mathbf{F} \tag{2.36}$$

The rotational energy levels are split into components which have different values of F where F = J+I, J+I-1,....|J-I|. The spectroscopic consequence of this coupling is the hyperfine splitting of all rotational transitions according to the additional selection rules $\Delta F = 0, \pm 1$. The most intense hyperfine components are those with $\Delta F = \Delta J$.

The quadrupole interaction arises from the second non-vanishing term in the multipole expansion of the electrostatic interaction between a nucleus and the various electrons surrounding it. The quadrupole Hamiltonian is

$$H_Q = \tfrac{1}{6}\, \mathbf{Q} : \nabla\mathbf{E} \tag{2.37}$$

Q and ∇E are second-rank tensors where Q is the electric quadrupole moment operator (dependent on the nuclear co-ordinates) and ∇E refers to the gradient of the electric field.

The matrix elements of this Hamiltonian are diagonal in F but off-diagonal in J and K. Exact quadrupole energies must therefore be calculated by diagonalizing matrices with dimensions (2F+1)(2I+1) × (2F+1)(2I+1) which can rapidly become large at high values of J.

However, quadrupole energies are in general small compared to the overall rotational energy and a first-order approximation, diagonal in J, accurately predicts most hyperfine

structure. In this case the generalized expression for the field gradient operator is:

$$\nabla(E_{ij}) = \frac{q_J}{J(2J-1)} [\tfrac{3}{2}(J_i J_j + J_j J_i) - \delta_{ij} J^2] \qquad i,j = X,Y,Z \qquad (2.38)$$

where $q_J = \langle J, M_J = J | \nabla E_{zz} | J, M_J = J \rangle$ (2.39)

q_J is the field gradient coupling constant. Similarly:

$$Q_{ij} = \frac{eQ}{I(2I-1)} [\tfrac{3}{2}(I_i I_j + I_j I_i) - \delta_{ij} I^2] \qquad i,j = X,Y,Z \qquad (2.40)$$

where $eQ = \langle I, M_I = I | Q_{zz} | I, M_I = I \rangle$ (2.41)

Q is defined as the quadrupole moment of the nucleus. A simplification of terms yields the more compact form of the quadrupole energy:

$$E_Q = \frac{eQq_J}{2J(2J-1)I(2I-1)} [\tfrac{3}{4} C(C+1) - J(J+1)I(I+1)] \qquad (2.42)$$

where $C = F(F+1) - J(J+1) - I(I+1)$ (2.43)

Because the quantity q_J is defined in the space-fixed reference system, it must be transformed into a molecule-fixed axis system using the direction cosines. The principal inertial axes are chosen even though in general they are not the principal quadrupolar axes. In terms of direction cosines:

$$\nabla E_{zz} = q_{aa}\phi_{Za}^2+q_{bb}\phi_{Zb}^2+q_{cc}\phi_{Zc}^2+2q_{ab}\phi_{Za}\phi_{Zb}+2q_{bc}\phi_{Zb}\phi_{Zc}+2q_{ac}\phi_{Za}\phi_{Zc} \tag{2.44}$$

The last 3 terms make no contribution to the first-order quadrupole energy. Using Laplace's relationship:

$$\chi_{aa} + \chi_{bb} + \chi_{cc} = 0 \qquad (\chi_{gg} = eQq_{gg}) \tag{2.45}$$

which indicates that only two quadrupole coupling constants (χ_{gg}) can be independently determined, together with the expression:

$$\langle J,\tau,M_J=J|\phi_{Zg}^2|J,\tau,M_J=J\rangle = \frac{2}{(J+1)(2J+3)}\langle J,\tau|J_g^2|J,\tau\rangle + \frac{1}{(2J+3)} \tag{2.46}$$

the first order quadrupole energy may conveniently be expressed in terms of the reduced energy and χ_{aa} and $\chi_{bb}-\chi_{cc}$:

$$E_Q = \frac{3C(C+1) - 4I(I+1)J(J+1)}{8I(2I-1)J(2J-1)(J+1)(2J+3)}\{[3\langle J_a^2\rangle - J(J+1)]\chi_{aa} + (1/b_p)[\langle J_a^2\rangle - W(b_p)](\chi_{bb} - \chi_{cc})\} \tag{2.47}$$

Once values for χ_{aa}, χ_{bb} and χ_{cc} have been obtained, they can be transformed into the principal quadrupole axes system to find χ_{zz}, χ_{yy} and χ_{xx}. These quantities can give valuable information about the nature of the chemical bonding in a

molecule e.g. covalent or ionic character, or π bonding character.

The assumption that only the first-order quadrupole energy is significant breaks down for molecules that have relatively large quadrupole energies, in particular, bromine and iodine containing molecules. In this case, second-order perturbation theory must also be considered. The resulting correction terms are usually very small but they may become appreciable, particularly if near - degeneracies of the correct symmetry occur (see Chapter IV).

When a molecule has more than one quadrupole coupling nucleus, the relative magnitudes of the coupling due to each nucleus determines the coupling scheme (27).

For example, if there are two nuclei with similar coupling; the coupling scheme is:

$$\begin{aligned} \mathbf{I}_1 + \mathbf{I}_2 &= \mathbf{I} \\ \mathbf{J} + \mathbf{I} &= \mathbf{F} \end{aligned} \qquad (2.48)$$

A total nuclear spin I is formed by the coupling of I_1 and I_2. I then couples to the rotational angular momentum J to give a total angular momentum F.

A much simpler two nuclei case is where one nucleus couples much more strongly than the other. The coupling scheme is:

$$J + I_1 = F_1$$
$$F_1 + I_2 = F \qquad (2.49)$$

The strongly coupling nucleus I_1 couples with the rotational angular momentum J to form a resultant F_1 to which the spin of the second nucleus I_2 couples. The total resultant is **F**. The associated quantum numbers are:

$$F_1 = (J + I_1), (J + I_1 - 1), \ldots\ldots\ldots\ldots\ldots |J - I_1|$$

and

$$F = (F_1 + I_2), (F_1 + I_2 - 1), \ldots\ldots\ldots\ldots |F_1 - I_2| \qquad (2.50)$$

If H_{Q1} represents the interaction of I_1 and J, and H_{Q2} represents the Hamiltonian for the interaction of I_2 and J, with the sum of these Hamiltonians representing the overall interaction, then in the first order approximation, H_{Q1} has the same eigenvalues as the Hamiltonian for a single coupling nucleus (equation 2.46), while H_{Q2} is treated as a perturbation on H_{Q1}. The overall quadrupole energy is the sum of the energies resulting from each Hamiltonian:

$$E_Q = \langle F, F_1 \mid H_{Q1}(I_1, J) + H_{Q2}(I_2, J) \mid F, F_1 \rangle$$

$$= \frac{3\,A_0\,(A_0+1) - 4I_1(I_1+1)J(J+1)}{8I_1(2I_1-1)J(2J-1)(J+1)(2J+3)} \{[3\langle J_a^2\rangle - J(J+1)]\chi_{aa}(1) +$$

$$(1/b_p)\,[\langle J_a^2\rangle - W(b_p)](\chi_{bb}(1) - \chi_{cc}(1)) +$$

$$\frac{[3A_1(A_1+1)-4I_2(I_2+1)F_1(F_1+1)][3A_2(A_2+1)-4J(J+1)F_1(F_1+1)]}{16I_2(2I_2-1)J(J+1)(2J-1)(2J+3)F_1(2F_1-1)(F_1+1)(2F_1+3)} \times$$

$$\{[3\langle J_a^2\rangle - J(J+1)]\chi_{aa}(2)+(1/b_p)[\langle J_a^2\rangle - W(b_p)](\chi_{bb}(2)-\chi_{cc}(2))\} \quad (2.51)$$

$$A_0 = F_1(F_1+1)-I_1(I_1+1)-J(J+1)$$
$$A_1 = F(F+1)-I_2(I_2+1)-F_1(F_1+1)$$
$$A_2 = I_1(I_1+1)-J(J+1)-F_1(F_1+1) \quad (2.52)$$

The resulting rotational spectrum can become extremely complicated even in this simplest case.

2.8 Stark Effect

The Stark effect is induced when an external electric field interacts with the dipole moment of a molecule. The interaction lifts or partially lifts the degeneracy in M - the quantum number representing the component of the total angular momentum along the space-fixed Z axis.

The Stark Hamiltonian is given by:

$$H_S = -\mu.E \quad (2.53)$$

μ is the permanent dipole moment of a molecule, defined in terms of the molecule-fixed axes, and E is an external electric field which is kept constant in magnitude, and by convention lies along the direction of the space-fixed Z axis. In terms of

direction cosines:

$$H_S = -E \sum_g \mu_g \phi_{Zg} \qquad g = x,y,z \qquad (2.54)$$

Although exact Stark energies can be calculated, they are relatively small, and perturbation theory is generally used to calculate both the first and second order Stark energies with sufficient accuracy to describe the interaction.

In the case of a symmetric top molecule the first order Stark energy is

$$\begin{aligned} E_S^{(1)} &= \langle J,K,M_J | H_S | J,K,M_J \rangle \\ &= \frac{-\mu E K M_J}{J(J+1)} \end{aligned} \qquad (2.55)$$

The M degeneracy is completely lifted and the energy is linear in the electric field strength.

When K = 0 for a symmetric top, the first order Stark effect becomes zero and these lines exhibit a second order Stark effect only, as do the transitions of linear molecules in $^1\Sigma$ states. The second order Stark energy is given by:

$$\begin{aligned} E_S^{(2)} = \frac{\mu^2 E^2}{2hB} \{ & [(J^2-K^2)(J^2-M^2)/[J^3(2J+1)(2J-1)] \\ & - [(J+1)^2-K^2][(J+1)^2-M^2]/[(J+1)^3(2J+1)(2J+3)] \} \end{aligned} \qquad (2.56)$$

The M-degeneracy is only partially lifted and the energy is quadratic in μE.

When the electric field is parallel to the direction of the electric vector of the microwaves, the selection rule is $\Delta M_J=0$.

The expression for the Stark energy of an asymmetric rotor is much more complicated because of the possibility of components of the dipole moment along each of the principal axes. Golden and Wilson (28) have developed the theory for the Stark energy of an asymmetric rotor.

Except for the special case of a near-degeneracy, symmetry restrictions preclude the possibility of a first order Stark effect for asymmetric rotors; the Stark energy is second order.

The energy shift for each component of the dipole is

$$(E_g^{(2)})_{J\tau M} = \mu_g^2 E^2 \left[\frac{(J^2-M^2)}{4J^2(4J^2-1)} \sum_{\tau'} \frac{|\langle J,\tau|\phi_{Zg}|JH,\tau'\rangle|^2}{E^\circ_{J,\tau} - E^\circ_{J-1,\tau'}} + \frac{M^2}{4J^2(J+1)^2} \sum_{\tau'} \frac{|\langle J,\tau|\phi_{Zg}|J,\tau'\rangle|^2}{E^\circ_{J,\tau'} - E^\circ_{J,\tau'}} + \frac{(J+1)^2 - M^2}{4(J+1)^2(2J+1)(2J+3)} \sum_{\tau'} \frac{|\langle J,\tau|\phi_{Zg}|J+1,\tau'\rangle|^2}{E^\circ_{J,\tau} - E^\circ_{J+1,\tau'}} \right] \tag{2.57}$$

When the M dependent and independent terms are factored out a general expression is:

$$(E_g^{(2)})_{J\tau M} = \frac{2\mu_g^2 E^2}{A+C} [A_{J,\tau} + M^2 B_{J,\tau}] \tag{2.58}$$

This is a second order Stark effect.

In asymmetric rotors, near-degeneracies are quite common; both near-symmetric rotor degeneracies and accidental near-degeneracies of various types can occur. Consequently, using the Van Vleck transformation (29), a 2 x 2 submatrix involving matrix elements due only to the two interacting levels needs to be diagonalized to find the Stark energy:

$$\begin{vmatrix} H_{11}-W & H_{12} \\ H_{12} & H_{22}-W \end{vmatrix} = 0 \qquad (2.59)$$

H_{11} and H_{22} refer to the two energies of the degenerate or near-degenerate levels:

$$H_{ii} = E_{ii}^{(0)} + E_{ii}^{(2)} \qquad (2.60)$$

where $E_{ii}^{(2)}$ is the second-order contribution of the remaining non-degenerate levels.

The off-diagonal term differs for various kinds of near-degeneracy. Golden and Wilson (28) have given expressions for the various cases. If it is a near-degeneracy between the members of an asymmetry doublet, then the expression for H_{12} is:

$$\begin{aligned} |H_{12}|^2 &= |\langle J,\tau,M|H_S|J,\tau',M\rangle|^2 \\ &= \mu_g^2 E^2 \frac{M^2}{4J^2(J+1)^2} |\langle J,\tau|\phi_{Zg}|J,\tau'\rangle|^2 \end{aligned} \qquad (2.61)$$

where g = a or c depending on the symmetry of the two levels.

The dependence of the energy on the electric field strength depends on the relative size of the difference in energy between the two interacting levels compared to the magnitude of the off-diagonal elements.

When the levels are very close together with $|H_{12}| >> |(H_{11} - H_{22})|$, a first order Stark dependence is introduced:

$$W = \tfrac{1}{2} (E^{\circ}_{J,\tau} + E^{\circ}_{J,\tau'}) \pm \mu_g E \frac{|M|}{2J(J+1)} \langle J,\tau|\phi_{Zg}|J,\tau'\rangle \qquad (2.62)$$

This is a linear function of the electric field.

When the two levels are reasonably far apart with $|(H_{11} - H_{22}) >> H_{12}|$, the energy expression reduces to the second-order expression.

The Stark effect can be extremely useful in aiding the assignment of rotational transitions. For example, the number of resolved Stark lobes (for low J lines) gives the value of the smaller of the two J values involved in the transition. Also, the intensity pattern of the Stark lobes differs for Q and R branches, where the Stark lobe intensity increases with M for Q-branch lines and decreases for R branch lines.

In addition, the dependence on the field strength for any given transition can provide clues as to the assignment of this transition. For example, for a prolate rotor, the Stark effect may be used to distinguish transitions within an a-type R branch group of lines having the same value of J. The $K_a = 0$

transition will have a typical second-order effect, while any degenerate or near-degenerate asymmetry pair will exhibit a first order Stark effect and the Stark lobes will move away from the unsplit transition frequency very rapidly with an increase in field strength. Asymmetry pairs at low K_a, which have relatively large asymmetry splittings also show a second-order effect, although in general they are modulated more quickly than the $K_a = 0$ transition.

The most important chemical application of the Stark effect is the measurement of dipole moments from the displacements of the Stark components as a function of the field strength.

The Stark effect is also important when measuring rotational spectra. Zero-based square-wave Stark modulation is one of the most commonly used modulation techniques to improve sensitivity (see Section 3.1).

2.9 The Harmonic Oscillator

The vibrational Hamiltonian in terms of the normal co-ordinates is:

$$H_V = \tfrac{1}{2} \sum_{i=1}^{3N-6} P_i^2 + \tfrac{1}{2} \sum_{i=1}^{3N-6} \lambda_i Q_i^2 \qquad (2.63)$$

where Q_i is the normal co-ordinate, P_i is the momentum conjugate to Q_i ($P_i = -i\hbar(\partial/\partial Q_i)$), and λ_i is a constant related to the frequency ν_i ($\lambda_i = 4\pi^2\nu_i^2$).

Substituting this into the quantum mechanical Schroedinger equation gives:

$$\frac{-h^2}{8\pi^2} \sum_{i=1}^{3N-6} [(\partial^2 \psi_v / \partial Q_i^2) + \tfrac{1}{2} \lambda_i^2 \, Q_i^2 \, \psi_v - E_v \, \psi_v] = 0 \qquad (2.64)$$

Assuming that the molecule is a harmonic oscillator, the vibrations (normal co-ordinates) are independent, so that ψ_v is just the product of the individual $\psi(Q_i)$ for the normal modes.

$$\psi_v = \prod_{i}^{3N-6} \psi_i(Q_i) \qquad (2.65)$$

and the overall energy is the sum of the energies of each of the normal modes.

$$E_v = \sum_{i=1}^{3N-6} E_v(Q_i) \qquad (2.66)$$

where $E_v(Q_i) = (v_i + \frac{1}{2})h\omega_i \qquad v_i = 0, 1, 2 \ldots .$ (2.67)

v_i is the vibrational quantum number for the ith normal mode and ω_i is the fundamental frequency of the ith normal mode.

The normal modes are numbered according to their symmetry properties. Each of the 3N-6 normal modes has the same symmetry properties as one of the irreducible representations of the point group to which the molecule belongs. The lowest numbers

are given to the normal modes which have the highest symmetry, and for normal modes having the same symmetry properties, the lowest number goes to the vibration with the highest frequency.

2.10 Vibration Selection Rules

If a vibrational transition is to occur, a change in the dipole moment in some direction is required.

The dipole moment can be written in terms of its 3 space-fixed components:

$$\mu = \mu_x + \mu_y + \mu_z \qquad (2.68)$$

Considering one of these components only (μ_F: F = X, Y, Z), its Taylor expression in terms of the normal co-ordinates is:

$$\mu_F = \mu_F^{\circ} + \sum_{i=1}^{3N-6} (\partial \mu_F / \partial Q_i)_o \, Q_i + \ldots\ldots\ldots \qquad (2.69)$$

The transition moment matrix element for this component of the dipole moment is:

$$(\mu_F)_{mn} = \langle m | \mu_F^{\circ} | n \rangle + \sum_{i=1}^{3N-6} \langle m | (\partial \mu_F / \partial Q_i)_o Q_i | n \rangle + \ldots. \qquad (2.70)$$

The wave functions can be separated into their vibrational and rotational parts and μ_F can be written in terms of its

components along the molecule-fixed axes.

$$(\mu_F)_{mn} = \sum_{g=x,y,z} \{\langle v_m|\mu_g^\circ|v_n\rangle\langle r_m|\phi_{Fg}|r_n\rangle + \sum_i (\partial\mu_g/\partial Q_i)_o \langle v_m|Q_i|v_n\rangle\langle r_m|\phi_{Fg}|r_n\rangle\} \quad (2.71)$$

The first part of this expression is strictly a pure rotational term because $\langle v_m|\mu_g^\circ|v_n\rangle = 0$ unless m = n (i.e. no change in vibrational state).

For the second term to be non-zero, $(\partial\mu_g/\partial Q_i)_o$ must be non-zero; there must be a change in at least one component of the dipole moment with vibration.

The expression $\langle v_m|Q_i|v_n\rangle$ leads to the selection rules for a harmonic oscillator:

$$\langle v_m|Q_i|v_n\rangle = \langle\psi_1^m|\psi_1^n\rangle\langle\psi_2^m|\psi_2^n\rangle\ldots\langle\psi_i^m|Q_i|\psi_i^n\rangle\ldots \ldots\langle\psi_{3N-6}^m|\psi_{3N-6}^n\rangle$$

$$\langle\psi_i^m|Q_i|\psi_i^n\rangle = 0 \text{ unless } \Delta v_i = \pm 1$$

$$\langle\psi_j^m|\psi_j^n\rangle = \delta_{mn} \quad \therefore \quad \Delta v_j (i\neq j) = 0 \quad (2.72)$$

Each normal coordinate therefore absorbs radiation independently.

The rotational part of the expression gives the same selection rules as for a pure rotational problem, except that it is the direction of $(\partial\mu_g/\partial Q_i)_o$ that determines the a-, b- or c-type selection rules.

Real molecules are anharmonic oscillators so that the strict selection rules of a harmonic oscillator break down.

Overtones are allowed with $\Delta v_i = \pm 1, \pm 2, \pm 3, \ldots$, each with diminishing intensity. Overtones are not exact multiples of the fundamental frequency because of the anharmonicity. Combination bands are also allowed. These involve the simultaneous changes in the vibrational quantum numbers of more than one normal mode.

2.11 Coriolis Perturbations

While in most cases the rotation and vibration terms in the overall rotation-vibration Hamiltonian can be considered separately, the situation can arise when a vibration-rotation interaction term becomes significant. This is the case when there are degenerate modes of vibration, or when two vibrational levels having the appropriate symmetry are near-degenerate. Perturbations in the rotational structure are observed.

The overall rotation-vibration Hamiltonian can be written:

$$H = \sum_k \tfrac{1}{2}(P_k^2 + \lambda_k Q_k^2) + \frac{(J_x - p_x)^2}{2I_x} + \frac{(J_y - p_y)^2}{2I_y} + \frac{(J_z - p_z)^2}{2I_z} \qquad (2.73)$$

This is just the sum of a pure vibrational term and a rotational term. p_α is the component of vibrational angular momentum about the α axis, and in terms of the normal coordinates is defined by:

$$p_\alpha = \sum_r \sum_{s>r} \zeta^\alpha_{r,s} [Q_r P_s - Q_s P_r] \qquad (2.74)$$

The zeta constants ($\zeta^{\alpha}_{r,s}$) relate a pair of normal coordinates through rotation about one of the axes α, e.g.:

$$\zeta^{\alpha}_{r,s} = \sum_{j=1}^{N} (\partial q_{xj}/\partial Q_r)(\partial q_{yj}/\partial Q_s) - (\partial q_{xj}/\partial Q_s)(\partial q_{yj}/\partial Q_r) \quad (2.75)$$

The $q_{\alpha j}$ are the mass weighted Cartesian displacement coordinates of atom j. The overall Hamiltonian can be separated into a rigid rotor Hamiltonian, a harmonic oscillator Hamiltonian and a perturbation term.

$$H = H_r + H_v + H' \quad (2.76)$$

$$H' = \frac{-p_x J_x}{I_x} - \frac{p_y J_y}{I_y} - \frac{p_z J_z}{I_z} + \frac{p_x^2}{2I_x} + \frac{p_y^2}{2I_y} + \frac{p_z^2}{2I_z} \quad (2.77)$$

The p_α^2 terms have no rotational dependence and generally make a very small contribution; therefore it is the $p_\alpha J_\alpha$ terms that are responsible for the Coriolis perturbation.

J_α and p_α commute; J_α operates only on the rotational wave functions and p_α operates only on the vibrational wave functions. Therefore the matrix elements for the first three terms of the perturbation Hamiltonian can be factorized:

$$\langle v',r'|-(p_\alpha J_\alpha)/I_\alpha|v,r\rangle = -(1/I_\alpha)\langle v'|p_\alpha|v\rangle\langle r'|J_\alpha|r\rangle \quad (2.78)$$

$|v\rangle$ and $|r\rangle$ are the vibrational and rotational wave functions

respectively.

(i) Vibrational part $\langle v' | p_\alpha | v \rangle$

The vibrational wave functions are assumed to be simple products of the harmonic oscillator functions in the normal coordinates. v and v' must differ only in two of their vibrational quantum numbers (v_r and v_s). In addition these two quantum numbers must vary only by one unit between the two states. This gives matrix elements of two types:

$$\text{(a) } \langle v_r+1, v_s | p_\alpha | v_r, v_s+1 \rangle \quad \text{(b) } \langle v_r+1, v_s+1 | p_\alpha | v_r, v_s \rangle \tag{2.79}$$

Only terms of type (a) are important since they connect levels which may have similar energy, while terms of type (b) are only likely to connect levels which have different energies.

Evaluation of term (a) gives:

$$\langle v_r+1, v_s | p_\alpha | v_r, v_s+1 \rangle = ih\, \zeta^\alpha_{r,s}\, \Omega_{r,s} [(v_r+1)(v_s+1)]^{1/2}$$

$$\Omega_{r,s} = [(\omega_r/\omega_s)^{1/2} + (\omega_s/\omega_r)^{1/2}] \tag{2.80}$$

An important special case relates the first excited states of 2 different normal modes:

$$\langle 1,0 | p_\alpha | 0,1 \rangle = -ih\zeta^\alpha_{r,s}\, \Omega_{r,s} \quad (v_r = v_s = 0) \tag{2.81}$$

For matrix elements of p_α to be non-zero they must be totally symmetric. Therefore $\langle v_r', v_s' | v_r, v_s \rangle$ must have the same symmetry as p_α which has the symmetry properties of a rotation about the α axis (R_α). When this condition is met for two vibrational levels, and the energy levels are close in energy, then angular momentum is induced about the α-axis.

(ii) Rotational part $\langle r' | J_\alpha | r \rangle$

The non-zero matrix elements for the components of the total angular momentum are given by the standard formulae, assuming that the molecule is a symmetric top:

$$\langle J,K | J_z | J,K \rangle = K\hbar$$

$$\langle J,K | J_x \pm iJ_y | J,K\pm1 \rangle = \hbar[J(J+1)-K(K\pm1)]^{1/2} \qquad (2.82)$$

These equations are a good enough approximation when determining the symmetry of a Coriolis perturbation in a near-symmetric rotor.

The perturbation has the symmetry of a rotation about one of the axes (R_x, R_y or R_z). The symmetry species of each of these is determined by the point group to which the molecule belongs. The symmetry species of the perturbing mode is easily determined from the relationship:

$$\Gamma(v) \times \Gamma(v') = \Gamma(R_\alpha) \qquad (2.83)$$

For a Coriolis interaction inducing angular momentum about the z-axis, the selection rule is $\Delta K = 0$, while $\Delta K = \pm 1$ for angular momentum induced about the x or y axis. $\Delta J = 0$ for all three cases.

Bibliography

1. W. Gordy, R.L. Cook, "Microwave Molecular Spectra, "3rd. ed., in "Techniques of Chemistry" (A. Weissberger, Ed.), Vol. 18, Wiley, New York, 1984.

2. H.W. Kroto, "Molecular Rotation Spectra," Wiley, London, 1975.

3. J.E. Wollrab, "Rotational Spectra and Molecular Structure," Academic Press, New York, 1967.

4. C.H. Townes, A.L. Schawlow, "Microwave Spectroscopy," McGraw-Hill, New York, 1955.

5. T.M. Sugden, C.N. Kenny, "Microwave Spectroscopy of Gases," Van Nostrand, London, 1965.

6. G. Herzberg, "Infrared and Raman Spectra of Polyatomic Molecules.", Van Nostrand, New York, 1945.

7. H.C. Allen, P.C. Cross, "Molecular Vib-Rotors," Wiley, New York, 1963.

8. G.W. King, R.M. Hainer, P.C. Cross, J. Chem. Phys., 11, 27-42, (1943).

9. S.C. Wang, Phys. Rev., 34, 243-252, (1929)

10. B.S. Ray, Z. Physik, 78, 74-91, (1983).

11. E.B. Wilson, J.B. Howard. J. Chem. Phys., 4, 260-268, (1936).

12. D. Kivelson, E.B. Wilson, J. Chem. Phys., 20, 1575-1579, (1952).

13. H. Dreizler, G.Z. Dendl, Z. Naturforsh, 20a, 30-37, (1965).

14. H. Dreizler, H.D. Rudolph, Z. Naturforsh, 20a, 749-751, (1965).

15. J.K.G. Watson, J. Chem. Phys. 46, 1935-1949, (1967).

16. J.K.G. Watson, J. Chem Phys. 48, 4517-4524, (1968).

17. J.K.G. Watson, "Aspects of Quartic and Sextic Centrifugal Effects on Rotational Energy Levels", In Vibrational Spectra and Structure, J.R. Durig, Ed., Vol. 6, Marcel Dekker, New York, (1977).

18. W. Kirchhoff, J. Mol. Spectrosc., 41, 333-380, (1972).

19. J. Kraitchman, Am. J. Phys.. 21, 17-24, (1953).

20. C. Costain, J. Chem Phys., 29, 864-874, (1958).

21. K. Kuchitsu, J. Chem. Phys., 49, 4456-4462, (1968).

22. K. Kuchitsu, T. Fukuyama, Y. Morino, J. Mol. Struct., 1, 463-479, (1968); J Mol. Struct., 4, 41-50, (1969).

23. T. Oka, Y. Morino, J. Mol. Spectrosc., 6, 472-482, (1961).

24. D.R. Herschbach, V.W. Laurie, J. Chem. Phys. 40, 3142-3153, (1964).

25. E. Bright Wilson, Jr., J. Chem. Phys., 3, 276-285, (1935).

26. J.K. Bragg, Phys. Rev., 75, 735-738, (1949).

27. J. Bardeen, C.H. Townes, Phys. Rev. 73, 97-105, (1948).

28. S. Golden, E.B. Wilson, J. Chem. Phys., 16, 669-685, (1948).

29. J.H. Van Vleck, Phys. Rev. 33, 467-506, (1929).

30. I.M. Mills., Pure and Appl. Chem., 2, 325-344, (1965).

CHAPTER III: EXPERIMENTAL METHODS

3.1 The Microwave Spectrometer

Microwave spectrometers have three basic components. These are a source of microwave radiation, an absorption cell which contains the gas being studied and allows the microwaves to pass through it, and a means to detect and display the absorption signal.

The basic design of the microwave spectrometer used to study the rotational spectra of BrNCO, INCO and BrSCN is shown in Figure 3.1.

In the microwave region, sources of radiation are electronically generated and are tunable and essentially monochromatic. In the early days of microwave technology reflex-klystrons were used as sources. Other tube-type sources followed, such as backward-wave oscillators, which allowed for a wider electronic tuning range. Nowadays, solid state devices, microwave frequency synthesizers, may be used. For all three molecules studied in the microwave region, the fundamental source used was a Watkins Johnson 1291A Microwave Synthesizer which operates between 8-18 GHz and allows step sizes as small as 10 Hz. Measurements were referenced to a crystal in the synthesiser of accuracy 1 in 10^{10}. Higher frequencies were obtained by multiplying the output of the synthesizer with a Honeywell-Space Kom 14-27 doubler and a T-K_a1 tripler to give a total frequency range of 8-54 GHz.

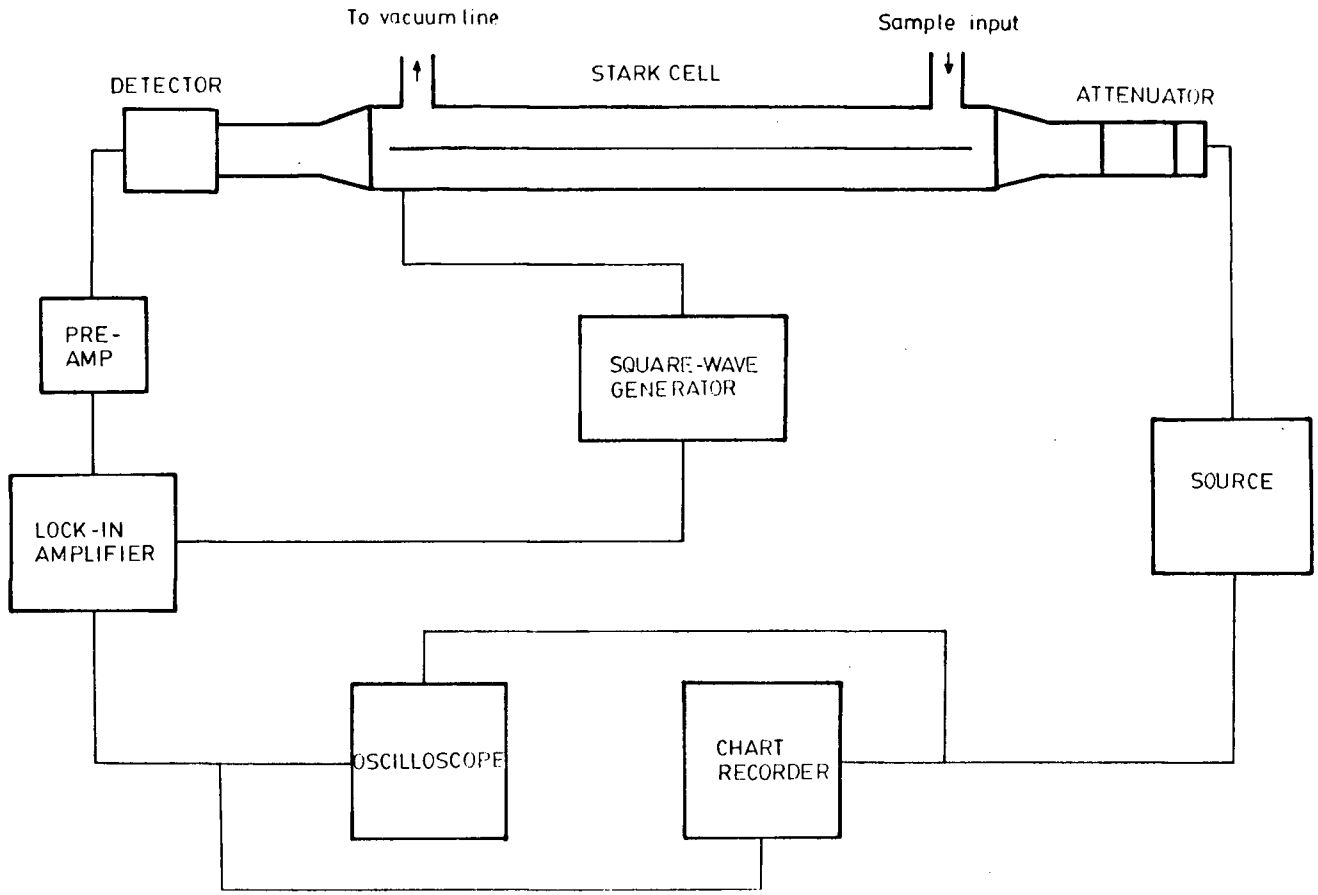

Figure 3.1 Block diagram showing basic design of microwave spectrometer.

The absorption cell used was a 6-ft. Hewlett-Packard X-band Stark cell which was attached to a vacuum line and sealed at either end with mica windows which are transparent to microwave radiation. Between the microwave source and the cell there was an attenuator to prevent power saturation. For frequency ranges other than X-band, the ends of the cell were tapered at either end to the correct waveguide dimensions for the frequency. The detectors used were diode crystal rectifiers.

In the microwave region, absorption coefficients are very small, with less than ≈0.1% of the incident power being absorbed. Any absorption signals would therefore be swamped without some form of modulation, by such factors as variations in the power output of the source with frequency, variations in transmission due to reflections in the wave guide and thermal noise in the detector. Although several methods of modulation may be used, Stark modulation is the most common one, and was used in all the work described in this thesis. It makes use of the shift in the absorption frequency upon application of an external electric field.

A flat metal strip or septum is placed halfway between and parallel to the broad faces of the cell. It is held in place by strips of teflon which insulate the septum from the rest of the cell. A 0-2000 volt zero-based square-wave voltage is applied between the septum and wave guide, and because the applied electric field is parallel to the electric vector of the electromagnetic radiation, only transitions with $\Delta M = 0$ occur

when the field is on. This electric field is turned on and off at a frequency of 30 - 100 kHz above which modulation broadening can become a problem. For the spectrometer used in this study a 100 kHz square-wave generator was used.

The signal passes through a pre-amplifier to the lock-in amplifier. A reference signal from the square-wave generator also goes to the lock-in amplifier, so that only those signals which are oscillating at this reference frequency at the correct phase are selected. Background characteristics are ignored; the radiation is modulated only when a molecular resonance occurs. The resulting signal discriminates between a field-free transition and its Stark components which arise when the electric field is on. The unsplit transition and its Stark components are displayed 180° out of phase with each other.

The signal was displayed on an oscilloscope or, for a more permanent record, it was recorded on chart paper using an X-Y chart recorder; the X component of the trace comes from a voltage ramp out of the Watkins-Johnson synthesizer and the Y component comes from the lock-in amplifier.

Frequencies were swept using the microprocessor in the Watkins-Johnson Synthesizer. For the work on BrNCO and INCO the sweeps were controlled using the front panel controls of the synthesizer, and all the transition frequencies were measured by tracing each individual line onto paper and interpolating the frequency of the centre of the peak from frequency markers placed on either side of the peak.

In the work on the microwave spectrum of BrSCN, the Watkins Johnson Frequency Synthesizer was interfaced to a Micro PDP 11/23+ microcomputer via a General Purpose Interface Bus (GPIB IEEE-488 1975 standard) which controls the functions of the Synthesizer. The computer is interrupt driven so that data acquisition and the stepping of the frequency can take place in real time.

The signal from the output of the lock-in amplifier is shared with the oscilloscope, chart recorder, and the computer through an A/D converter which is connected to a buffer amplifier.

The operating system of the microcomputer was RSX-11M and software programmes have been written in Fortran-77 and Macro-11 which signal average, oversample, store and display the signal, and aid the measurement of the transition frequencies. Each measured line was recorded using sweeps both up and down in frequency, and the average of the two were taken to remove the effects of different time constants in the system.

The measurement accuracy for all the measured transitions was ±0.03 MHz.

3.2 The FT-IR Interferometric Spectrometer

Although the Michelson interferometer was designed by Michelson in the late nineteenth century, it has taken the technological advances of more recent times, particularly in computer technology, for Fourier transform infra-red

spectroscopy to reach its potential as a high-resolution spectroscopic technique.

The basic interferometer design is shown in Figure 3.2. It consists of an infra-red source directed at a beamsplitter which is designed to transmit 50% of the incoming radiation and reflect the rest. The beamsplitter is commonly made from a film of germanium supported on a single crystal such as KCl or CsI. At lower wavenumbers, unsupported Mylar of different thicknesses can be used. One of the beams is reflected back to the beamsplitter from a stationary mirror, while the second beam is reflected back from a moving mirror. The two beams recombine constructively or destructively at the beam splitter, depending on the difference in distance each beam has travelled to and from the moving and static mirrors. If the incoming radiation is monochromatic, then a sinusoidal plot of intensity versus the optical retardation (twice the displacement of the moving mirror) will result. When a broad band radiation source is used, the interference pattern seen at the detector is much more complex, being the sum of the interference patterns due to all wavelengths. This is called an interferogram.

The intensity of the detector signal is given by:

$$I(\delta) = \int_{o}^{\infty} 0.50\ I(\nu)(1 + \cos 2\pi\nu\delta)\,d\nu \qquad (3.1)$$

where $I(\nu)$ is the intensity of the source as a function of

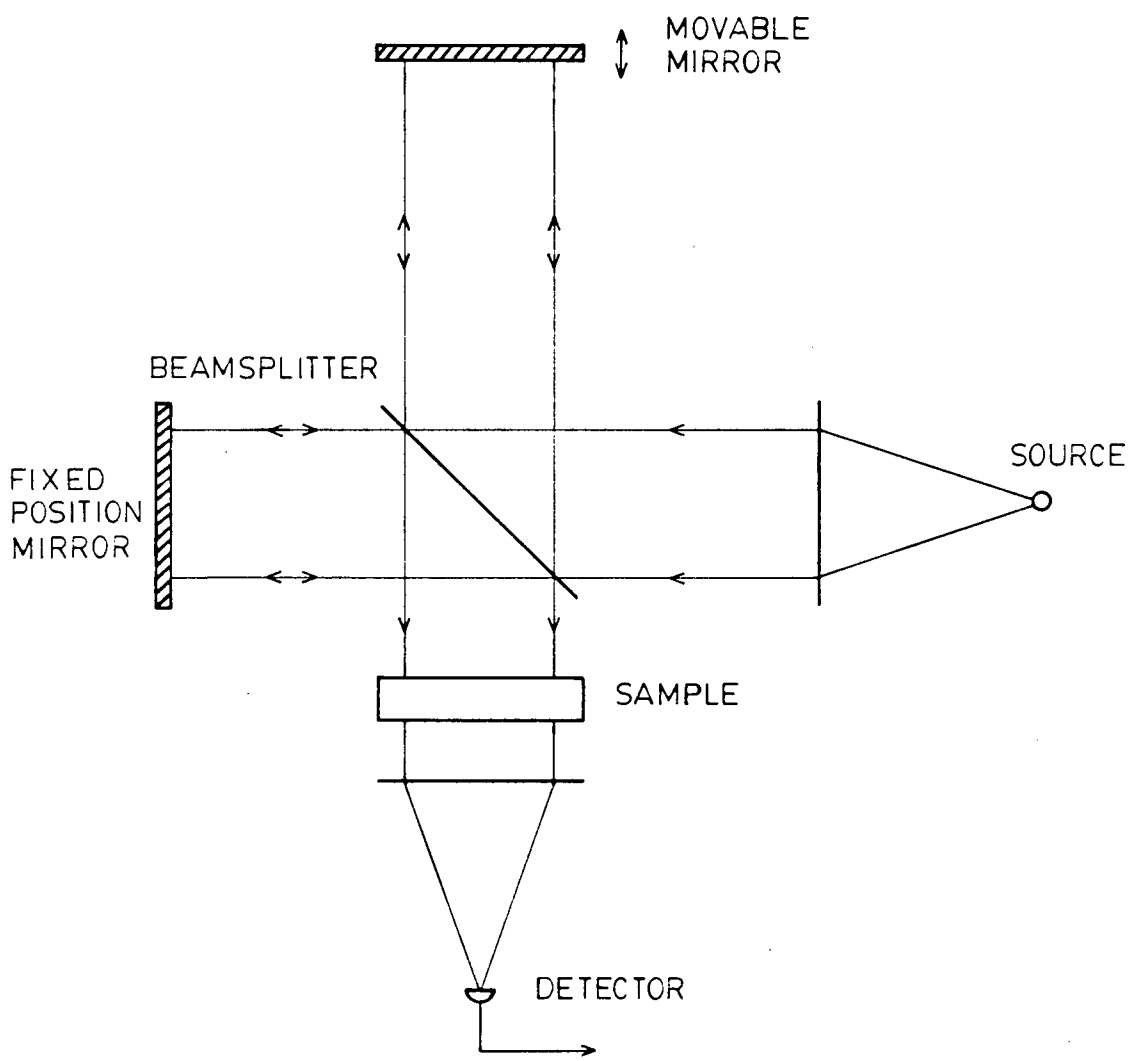

Figure 3.2 Schematic design of interferometer.

frequency ν, and δ is the path difference.

One part of this equation is a constant; the other is a modulated component which is important spectroscopically. Thus the equation for the interferogram is given by:

$$I(\delta) = \int_{0}^{\infty} B(\nu)\cos(2\pi\nu\delta)\,d\nu \qquad (3.2)$$

$B(\nu)$ takes into account such factors as beamsplitter efficiency, detector response and amplifier characteristics.

Equation (3.2) can be transformed mathematically to the more conventional form of the spectrum by a Fourier transformation:

$$B(\nu) = \int_{-\infty}^{+\infty} I(\delta)\cos(2\pi\nu\delta)\,d\delta \qquad (3.3)$$

This expression implies that the mirror must be moved an infinite distance to obtain the complete spectrum, and the Fourier transform involves a continuous integration over the interferogram function. Instead, the spectrum is approximated by a summation of a finite set of discrete points multiplied by the calculated cosine values performed using a high speed computer. Also, because the mirror only moves a finite distance, the interferogram is effectively truncated (known as boxcar truncation). The net result is the broadening of all the spectral features which are accompanied by side lobes, which

oscillate with diminishing frequencies away from the central frequency. This effect is called ringing. Such baseline irregularities can be reduced by using an apodization function which scales the ends of the interferogram so that it goes smoothly to zero. A number of different apodization functions can be used. However, while reducing the ringing effects, they will also serve to reduce the resolution.

While the coarse spectral features come from parts of the interferogram close to the centre burst (at zero path difference), the higher resolution information comes from the wings of the interferogram so that the further the moving mirror travels, the higher the attainable resolution. Theoretically, the limit of resolution for a spectrometer is:

$$\Delta(\nu) = 1/2x \text{ cm}^{-1} \qquad (3.4)$$

where x is the maximum displacement of the mirror.

In measuring a high resolution spectrum, it is extremely important that the exact position of the moving mirror is monitored. This is achieved by passing a stabilized He-Ne laser beam through the centre of the IR beam. Being a monochromatic source, the resulting sinusoidal interferogram allows a precise measurement of the mirror position.

Typically a background spectrum is taken as well as the sample spectrum, so that the two can be ratioed to give the familiar transmittance spectrum.

The advantages of FTIR over the conventional dispersive technique are well-known. The best-known is Fellget's advantage, or the multiplex advantage, and arises because the interferometer detects and measures all wavelengths simultaneously rather than successively as for dispersive spectroscopy. It results in much faster data acquisition in FTIR, or a better signal to noise ratio for the same source and detector operating for the same measurement time.

The Jacquinot or throughput advantage refers to the amount of energy reaching the detector. In a dispersive spectrometer, the entrance and exit slits of the monochromator, which must be very narrow for high resolution spectra, restrict the amount of light reaching the detector. In an interferometric system, the amount of light reaching the detector is limited solely by the efficiency of the beam splitter and the size of the source aperture, resulting in a much greater efficiency in utilization of the light source.

A third and very important advantage is Connes advantage which arises from the use of the He-Ne laser to reference the position of the moving mirror. The accuracy of the frequency is far superior to that of the dispersive instrument.

To measure the infra-red spectrum of BF_2NH_2, a Bomem DA3.002 interferometric spectrophotometer was used. Spectra were recorded between 400 and 3700 cm^{-1} at varying resolutions. The radiation source was a Globar which is a black-body continuum source. A KCl beamsplitter was used down to 550 cm^{-1}

below which a Mylar beamsplitter was used. The cell was a multiple reflection cell which was set to give a path length of 8.25 m. Above 1900 cm^{-1} a liquid nitrogen-cooled InSb detector was used, from 700-1800 cm^{-1} a liquid nitrogen-cooled HgCdTe detector was used, while below 700 cm^{-1}, the detector used was a liquid helium cooled Ge:Cu detector. Digital and optical filters were used to restrict the amplifier band width so that only the range of interest was collected. Both background and sample spectra were recorded, both of which were transformed and then ratioed to give a transmittance spectrum which in turn could be converted to absorbance.

Bibliography

1. H.W. Kroto, "Molecular Rotation Spectra," pp. 250-256, Wiley, London, 1975.

2. T.M. Sugden, C.N. Kenny, "Microwave Spectroscopy of Gases," pp. 191-242, Van Nostrad, 1965.

3. W.D. Perkins, J. Chem. Ed., 63, A5-10, (1986).

4. G. Horlick, Appl. Spectroscopy, 22, 617-626, (1968).

5. P.R. Griffiths, "Chemical Infrared Fourier Transform Spectroscopy", Wiley, New York, 1975.

CHAPTER IV: THE MICROWAVE SPECTRUM OF BROMINE ISOCYANATE, BrNCO

4.1 Introduction

Bromine isocyanate, BrNCO, was first prepared in the gas phase by Gottardi, in the reaction of Br_2 vapour with solid AgNCO at 150°C (1), and also by the vacuum thermolysis of tribromoisocyanuric acid (2). The infra-red spectra of BrNCO in both the solid and gas phase have been reported (2), as has the He(I) photoelectron spectrum of gaseous BrNCO (3).

No structural data are available for BrNCO; however the similarity of the photoelectron spectra of ClNCO and BrNCO (3) makes it likely that their structures will be similar.

Of the halogen isocyanates, only ClNCO has previously been studied using microwave spectroscopy (4,5). The aim of this study was therefore to analyse the microwave spectrum of BrNCO in order to derive its rotational and other spectroscopic constants, to deduce some structural information from these constants.

4.2 Experimental Methods

BrNCO was prepared in a flow system by passing Br_2 vapour over heated silver cyanate at ≃150°C at a pressure of ≃30 mTorr.

$$AgNCO_{(s)} + Br_{2(g)} \rightarrow BrNCO_{(g)} + AgBr_{(s)} \qquad (4.1)$$

The AgNCO was previously prepared by mixing $AgNO_3$ and KNCO.

The resulting precipitate was washed and then dried thoroughly under vacuum at 150°C for several hours before use. This step is extremely important because BrNCO tends to hydrolyse easily (2). Indeed, lines due to both NH_3 and HNCO, which are products of the hydrolysis of BrNCO, were usually observed before the spectrum of BrNCO started to appear.

For observations of the a-type transitions, the cell was kept at room temperature. However, to help resolve the nitrogen hyperfine splitting in the b-type lines, the cell was cooled slightly using dry ice under the cell, although care had to be taken not to cool the cell completely down to dry ice temperature because the BrNCO gas condenses.

4.3 Initial Assignments

There are two isotopic species of bromine in natural abundance: ^{79}Br and ^{81}Br. They are in approximately equal abundance; the spectra of $^{79}BrNCO$ and $^{81}BrNCO$ therefore have approximately equal intensities.

Initial calculations for the rotational constants of both isotopes were made using structural parameters transferred from ClNCO (4,5) and a shortened Br-N bond length from BrNO (6). Bromine quadrupole coupling constants were estimated using 4p-orbital populations from a CNDO calculation in the equations of Townes and Dailey (7) (see section 4.8), and by assuming that the Br-N bond is a principal axis of the Br quadrupole tensor.

BrNCO was predicted to be a planar near-symmetric prolate

rotor having both a- and b-type transitions. A preliminary inspection of the spectrum showed only a series of equally spaced groups of lines (Figure 4.1). These are the a-type R branch transitions which are spaced by ≃(B+C). No b-type lines were evident in these early observations.

While the spectra of the two isotopes are overlapped, (B+C) for each isotope are sufficiently different that the clusters of lines for each could be easily distinguished, with those of ^{81}BrNCO to lower frequency. The spectrum was additionally complicated by the presence of lines corresponding to transitions within excited vibrational states of the molecule. Each transition was also split into a quartet structure because of the quadrupole coupling of the bromine nucleus (I = 3/2 for both isotopes). No ^{14}N (I=1) hyperfine splitting was observed for any of the a-type transitions.

The first transitions to be assigned were from the J = 6 ← 5 a-type R branch, which is shown in Figure 4.2. The asymmetry split K_a = 1 transitions were easily distinguished to the high and low frequency sides of the main cluster of lines for both the ground state, and for at least two excited vibrational states. The K_a = 0 transition was identified by its distinctive Stark effect (see section 2.8).

K_a = 1 and K_a = 0 transitions for other values of J were similarly assigned. The asymmetry splitting is dependent on (B-C); therefore preliminary values of B and C could be calculated. For most transitions, the bromine hyperfine

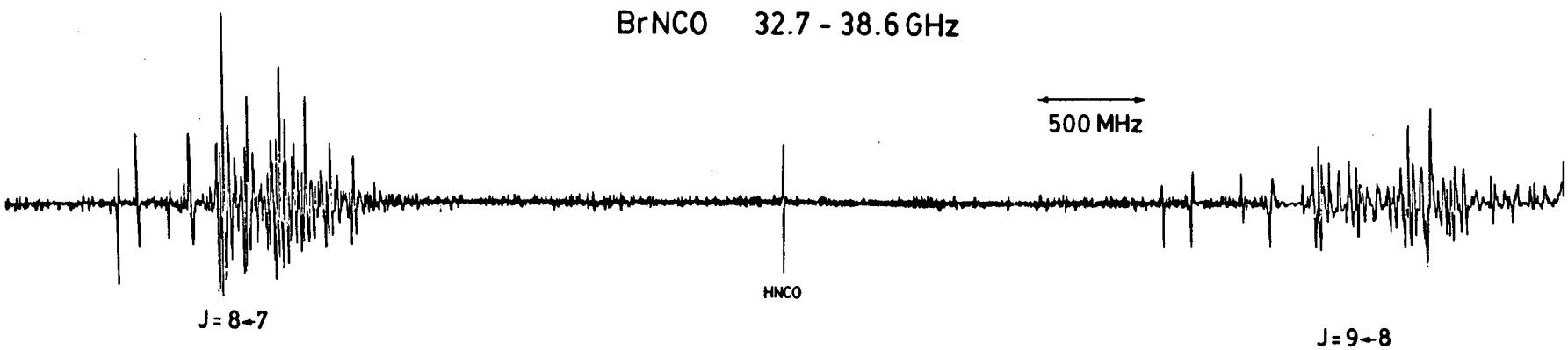

Figure 4.1 Broadband scan of the microwave spectrum of BrNCO in the frequency range 32.7-38.6 GHz.

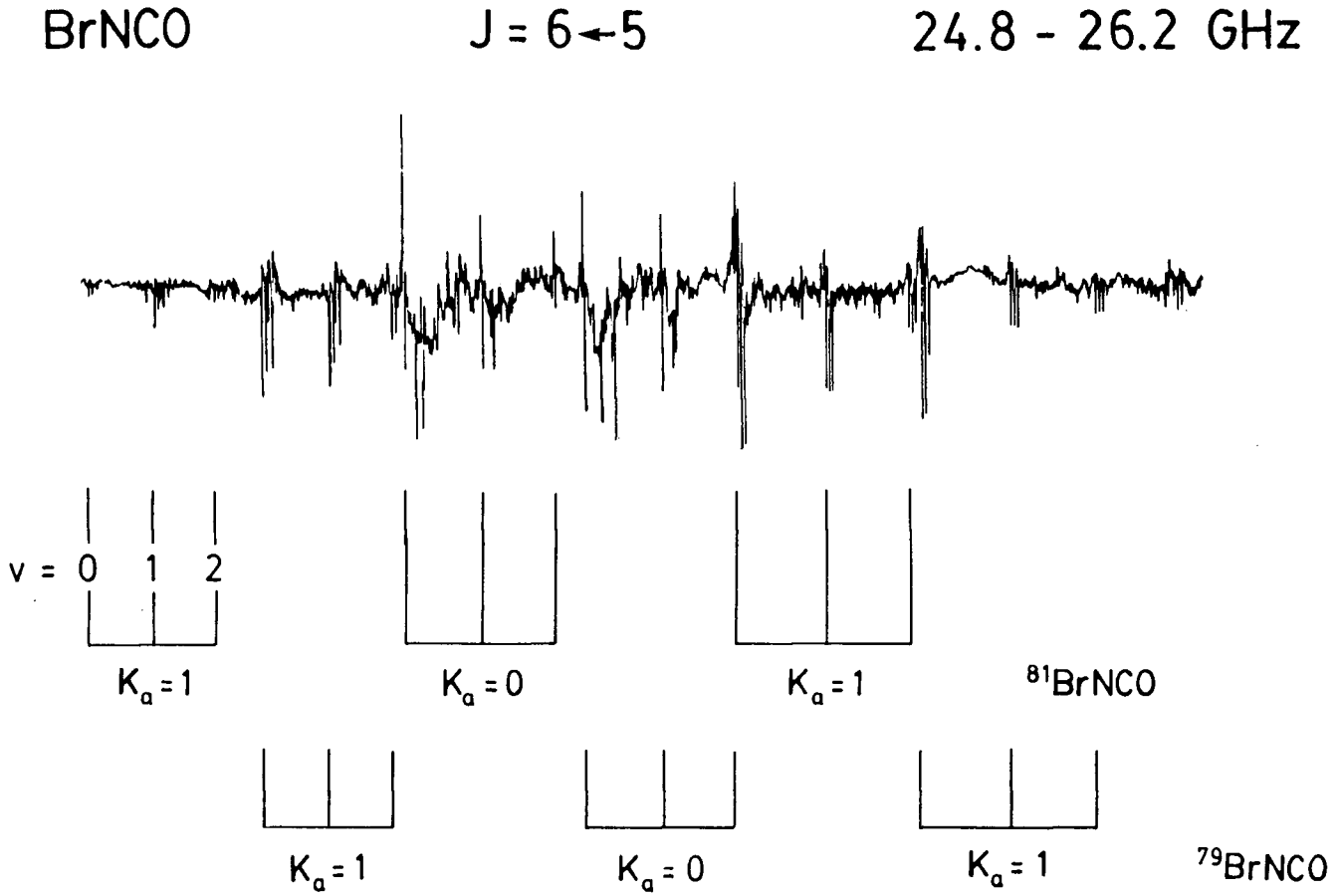

Figure 4.2 J = 6 ← 5 a-type R branch of BrNCO in the frequency range 24.8 - 26.2 GHz. $K_a = 0$ and $K_a = 1$ transitions for both isotopes in the ground and two excited vibrational states are indicated.

splitting patterns were symmetric quartets as predicted from first-order theory. However, some transitions had anomalous splitting patterns which could not initially be explained.

The determination of an accurate value of A was a problem. An approximate value of A can sometimes be obtained from a-type R branches alone, from the $K_a = 2$ asymmetry splittings. However, these splittings were very small for BrNCO (≈20 MHz for $J = 8 \leftarrow 7$ for ^{81}BrNCO). They were also difficult to assign unambiguously because of their large predicted quadrupole splittings, and they were difficult to measure because of lineshape distortion by the Stark components. A could not be obtained via this route.

A can usually be determined by assigning b-type transitions. However, they were impossible to assign at this stage of the study because they were very weak compared to the a-type transitions. In addition, they had large predicted Br quadrupole splitting, the spectra of the two isotopes were of equal intensity, and transitions within excited vibrational states were present.

It was the anomalies of the hyperfine structure of the a-type transitions that provided the route to an accurate determination of A.

4.4 Determination of A

For molecules containing nuclei that produce relatively large quadrupole splittings, such as iodine or bromine

containing molecules, the first order analysis of the quadrupole coupling due to a single nucleus given in section 2.7 is usually inadequate to describe the observed hyperfine splitting patterns (8). Sometimes, even molecules containing a nucleus with much smaller quadrupole coupling constants, such as chlorine, have a small number of transitions which do not fit the predicted pattern (9,10). In this case, second-order perturbation theory could be used to get a closer approximation of the actual quadrupole energies. Better still, the complete quadrupole Hamiltonian could be diagonalized to determine the exact energies.

I have developed a procedure which uses non first-order quadrupole hyperfine structure to calculate an accurate value of the rotational constant A solely from a-type R branch spectra.

For planar molecules containing a single quadrupole nucleus, the field gradient tensor can be written:

$$\nabla E_{ZZ} = q_{aa}\phi_{Za}^2 + q_{bb}\phi_{Zb}^2 + q_{cc}\phi_{Zc}^2 + 2q_{ab}\phi_{Za}\phi_{Zb} \qquad (4.2)$$

The first 3 terms contribute to first order and usually account for most of the hyperfine structure. However the fourth term, which contributes to higher order, may have a significant effect. This occurs when χ_{ab}, the off diagonal term in the quadrupole tensor, is large. For χ_{ab} to be large, two conditions must be met. The first is that the quadrupole moment of the quadrupolar nucleus should be large, which is true for

bromine. The second condition is that the principal quadrupole axes should be at a large angle to the principal inertial axes. In BrNCO the angle between the z-axis of the quadrupole tensor and the a-inertial axis is calculated to be ≈28° (see section 4.7). The effect of a large χ_{ab} is particularly significant, and can produce relatively large perturbations in the hyperfine structure, when near-degeneracies of the correct type occur. The selection rules for these near-degeneracies for a planar molecule like BrNCO are $\Delta F=0$; $\Delta J=0, \pm1, \pm2$ and $K_a K_c$ = ee ↮ oe or eo ↮ oo. Since these near-degeneracies depend on all three rotational constants, and to a lesser extent on the centrifugal distortion constants, deviations from first-order hyperfine structure can provide extra information on these constants, as well as on χ_{ab}. Therefore in principle, it should be possible to use these perturbations to determine constants that would not otherwise be determinable from the observed transitions. For example, it should be possible to evaluate A from a-type R branches alone for molecules where there are several near-degeneracies of the correct symmetry and a quadrupolar nucleus with a large χ_{ab}. BrNCO would seem to be an ideal candidate. This method has previously been proposed for trans-1-bromopropene (10); and in propadienone, an anomalous Stark effect, caused by near-degeneracies, gave A by an analogous method (12). However, an exact treatment had not been carried out before.

A computer programme has been written which does a

simultaneous least-squares fit to the rotational, centrifugal distortion and quadrupole coupling constants of a molecule containing a single quadrupolar nucleus (9). The matrix elements for the quadrupole Hamiltonian are those of Benz et al (13). The matrix elements involving the off-diagonal term χ_{ab} are of the form $\langle J',K\pm1|H_Q|J,K\rangle$; therefore, after the Wang transformation, the matrix can no longer be broken down into 4 smaller submatrices for a given value of F. The complete matrix has to be diagonalized to find the energies, with each matrix being diagonal in F and of the order of (2F+1)(2I+1). These matrices rapidly become large, and the fitting procedure requires a great deal of computing time. Consequently, these global least-squares fits were done using the CRAY-1 Vector Computer of the Atmospheric Environment Service of Environment Canada.

4.5 Analysis of a-type Transitions

Values for A_o and χ_{ab} were estimated as described earlier. They were then used to predict the hyperfine splitting patterns of some perturbed transitions. Assignments of transitions were made on a trial and error basis; and by an iterative procedure, values of the constants from one fit were used to predict the frequencies of more transitions, which were then measured and included in the next least squares fit to further refine the constants. $K_a = 0$ and $K_a = 1$ lines were measured for J = 3 to 13. Values obtained for A_o and χ_{ab} were well-determined for

both isotopes, and they are essentially not correlated with each other or with any other constant (see Table 4.2). The accuracy of A_o within one standard deviation is less than 0.4 MHz. This is several orders of magnitude better than is normally obtained for molecules having spectra with a-type R branches only (14). B, C, Δ_J, Δ_{JK}, δ_J, as well as χ_{aa} and $\chi_{bb}-\chi_{cc}$ for bromine were also well determined (see Table 4.1).

An energy level diagram for ^{81}BrNCO is shown in Figure 4.3. It shows two of the closest near-degeneracies which cause perturbations in the hyperfine structure. These are between $10_{0,10}$ and $9_{1,8}$ which are 426.34 MHz apart and the $5_{0,5}$ and $3_{1,3}$ levels which are 844.13 MHz apart. Another significant near-degeneracy is between the $14_{1,13}$ and $12_{2,11}$ levels which are 2159.37 MHz apart. These cause the largest shifts in frequency from a first order calculation; however, much smaller shifts can be detected for transitions involving the $8_{0,8}$ and $7_{1,6}$ levels, even though they are 6983 MHz apart. In fact, not one of the measured $K_a = 0$ transitions, which are predicted to appear as a doublet of barely resolvable doublets, was unperturbed. The shifts in frequency range from 0.5 MHz for $8_{0,8}-7_{0,7}$ to 33 MHz for one of the hyperfine components of the $10_{0,10}-9_{0,9}$ transition (see Figures 4.4 & 4.5).

4.6 b-type Transitions

The constants derived from the a-type lines were used to predict the positions of some $K_a = 1 \leftarrow 0$ b-type transitions.

Table 4.1

Spectroscopic constants of BrNCO from a-type transitions

Parameter	^{79}BrNCO	^{81}BrNCO
Rotational Constants (MHz)		
A_o	41188.71(23)[1]	41142.57(39)
B_o	2175.6311(13)	2159.5035(13)
C_o	2063.1025(11)	2048.4716(10)
Centrifugal Distortion Constants (kHz)		
Δ_J	1.1366(22)	1.1258(23)
Δ_{JK}	-172.72(16)	-171.00(12)
δ_J	0.1692(29)	0.1690(26)
Bromine Nuclear Quadrupole Coupling Constants (MHz)		
χ_{aa}	608.16(48)	508.40(47)
$\chi_{bb}-\chi_{cc}$	279.4(11)	230.8(11)
χ_{ab}	549.85(11)	458.30(22)
Number of Rotational Transitions		
	26	29
Standard Deviation of fit (MHz)		
	0.028	0.029

[1] Numbers in parentheses are one standard deviation in units of the last significant figures.

Table 4.2

Correlation coefficients of the spectroscopic constants of BrNCO derived from a-type transitions only

^{79}BrNCO

A_o	1.00							
B_o	0.10	1.00						
C_o	-0.13	-0.73	1.00					
Δ_J	-0.03	0.48	0.15	1.00				
Δ_{JK}	0.06	0.00	0.05	-0.27	1.00			
δ_J	0.11	0.88	-0.84	0.27	-0.06	1.00		
χ_{aa}	-0.05	-0.10	-0.04	-0.14	0.03	0.02	1.00	
$\chi_{bb}-\chi_{cc}$	0.26	0.25	-0.29	0.01	0.01	0.23	-0.19	1.00
χ_{ab}	0.30	0.09	0.16	0.05	-0.03	-0.11	-0.28	-0.16

^{81}BrNCO

A_o	1.00							
B_o	0.11	1.00						
C_o	-0.05	-0.70	1.00					
Δ_J	0.07	0.57	0.08	1.00				
Δ_{JK}	0.09	0.10	0.10	-0.10	1.00			
δ_J	0.09	0.88	-0.79	0.44	-0.05	1.00		
χ_{aa}	-0.13	-0.13	-0.01	-0.14	-0.03	-0.05	1.00	
$\chi_{bb}-\chi_{cc}$	0.26	0.26	-0.30	0.02	0.02	-0.23	-0.14	1.00
χ_{ab}	-0.88	-0.11	0.10	-0.05	-0.06	-0.11	-0.12	-0.16

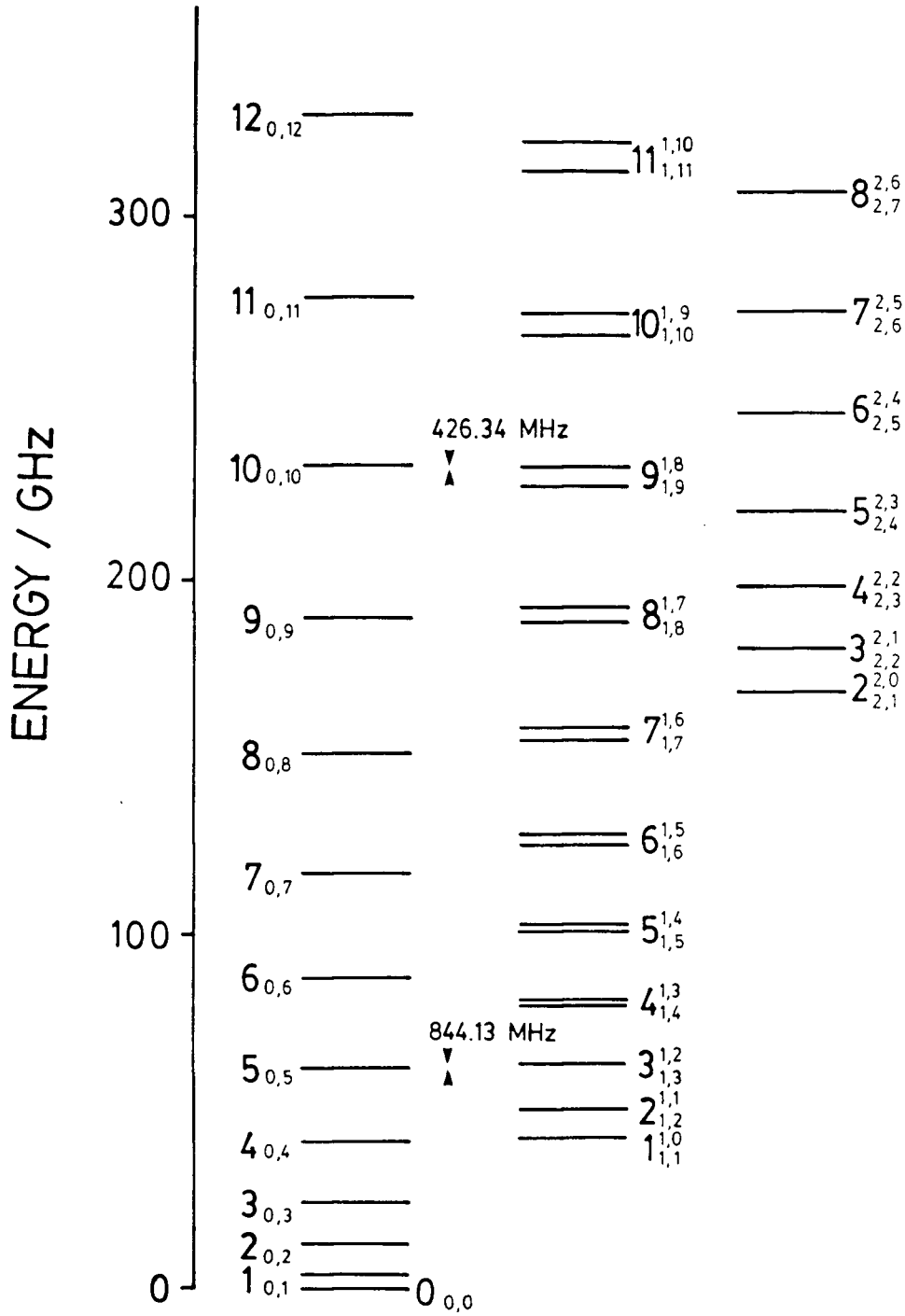

Figure 4.3 Rotational energy levels of ^{81}BrNCO. Two important near-degeneracies are indicated.

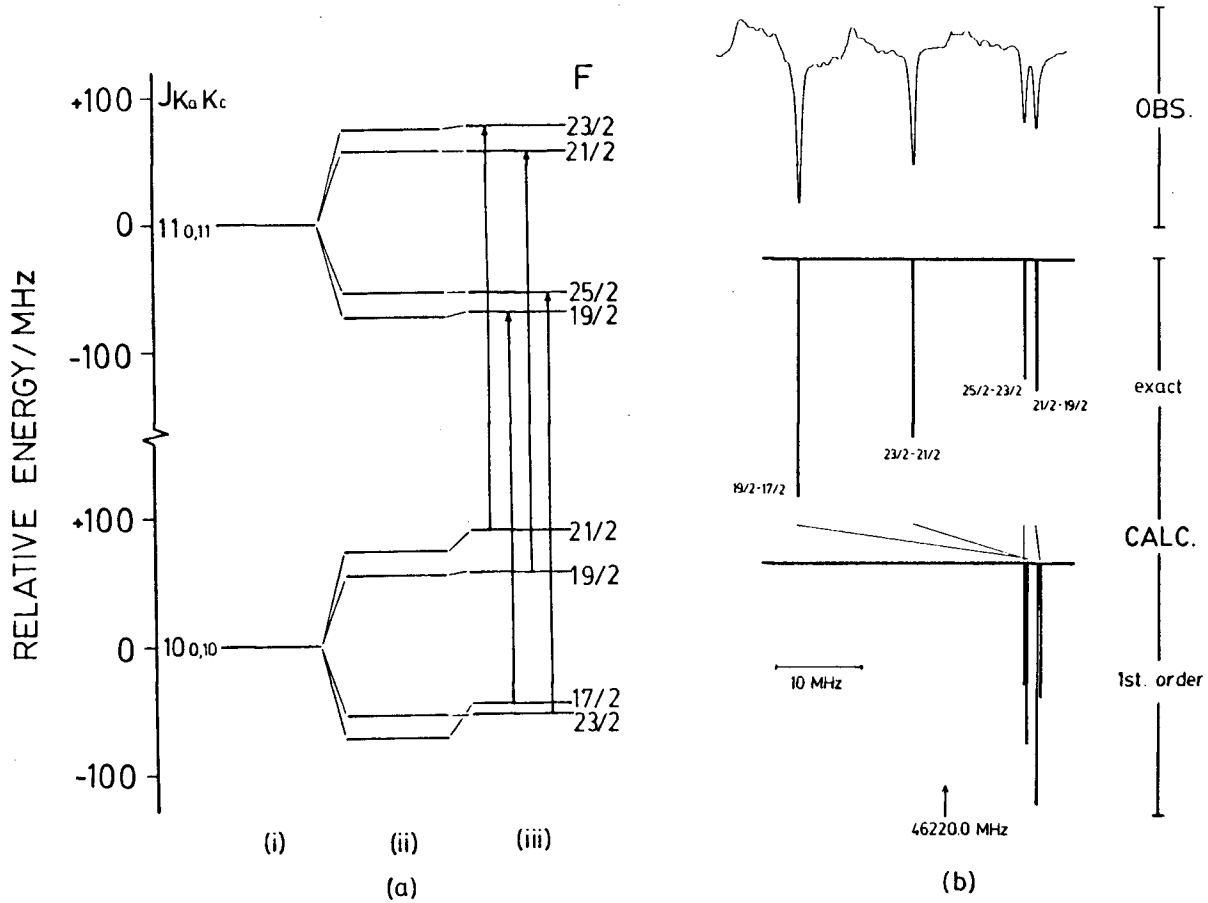

Figure 4.4 The energy levels of the $11_{0,11}$ - $10_{0,10}$ transitions of ^{81}BrNCO. (a) The energy levels: (i) the hypothetical unsplit rotational energies; (ii) predicted first-order bromine quadrupole energy levels; (iii) bromine quadrupole energy levels derived from the exact Hamiltonian. (b) The observed transitions compared with the calculated first-order and exact patterns.

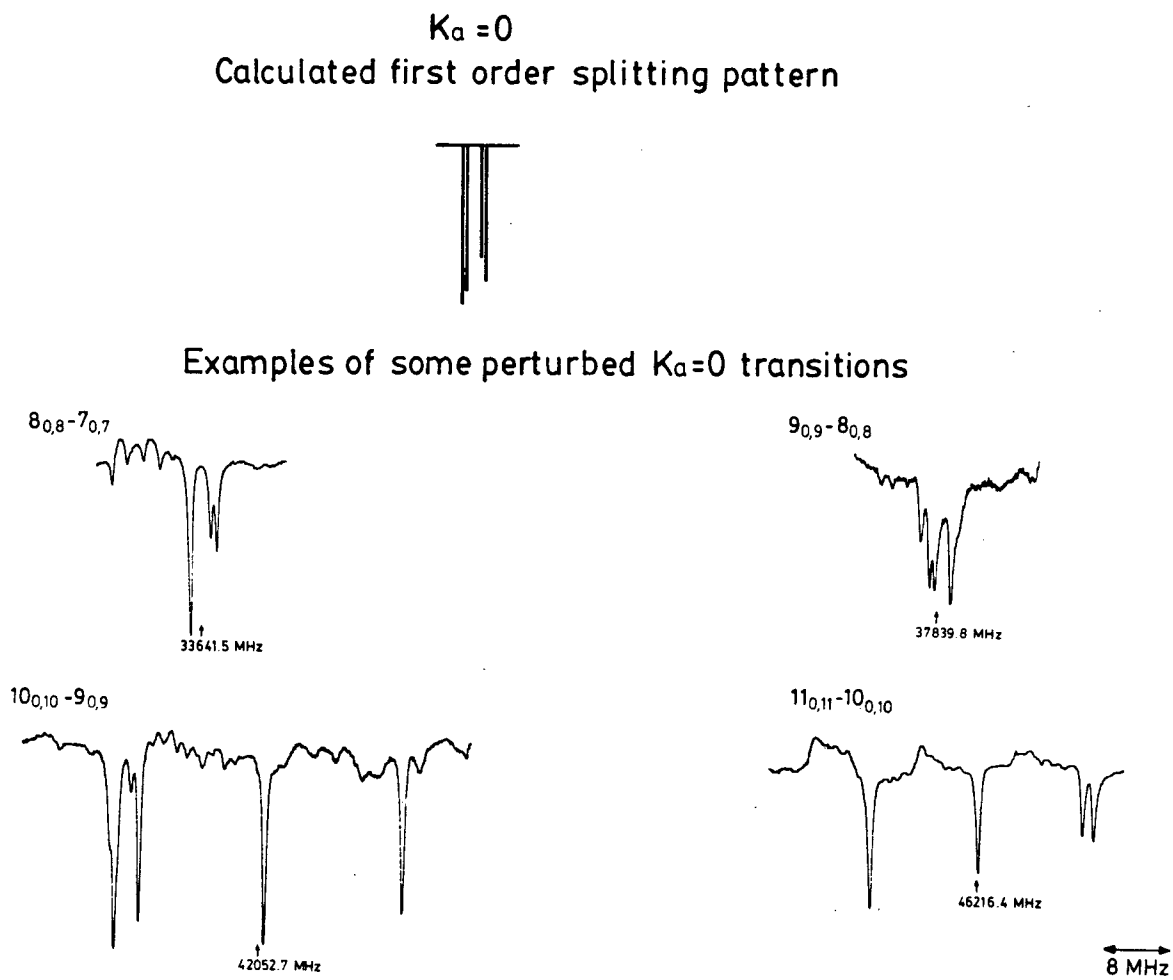

Figure 4.5 Hyperfine splitting patterns of some $K_a = 0$ transitions of ^{81}BrNCO.

These lines were much weaker than the a-type lines and could not initially be assigned. All the transitions were found within 1 MHz of their predicted frequencies. Thus, the value of A_0 was confirmed. Both R and Q branch lines were measured for J up to 20.

All the b-type lines showed ^{14}N quadrupole splitting. An example is given in Figure 4.6. The effect of the nitrogen quadrupole splitting had to be subtracted from these transitions before the bromine quadrupole coupling constants and the other spectroscopic constants could be further refined. This was done using a programme which fits the coupling constants of two quadrupolar nuclei. The coupling scheme used was ($J + I_{Br} = F_1$; $F_1 + I_N = F$). This is a good approximation for BrNCO, because the nitrogen quadrupole coupling constants are much smaller than those for bromine. The programme fits to the differences between frequencies of the hyperfine components of the same transition. χ_{aa} and $\chi_{bb}-\chi_{cc}$ for the nitrogen nucleus were determined by including in the fit only the splittings of lines having the same value of F_1 but different values of F. These splittings are independent of the bromine quadrupole coupling constants, which were held constant in the fit. The ^{14}N quadrupole coupling constants for both isotopes are included in Tables 4.3 and 4.4.

The effect of the nitrogen quadrupole coupling was subtracted from the b-type transitions. All the transitions, both a and b-type, were then included in a global least-squares fit to

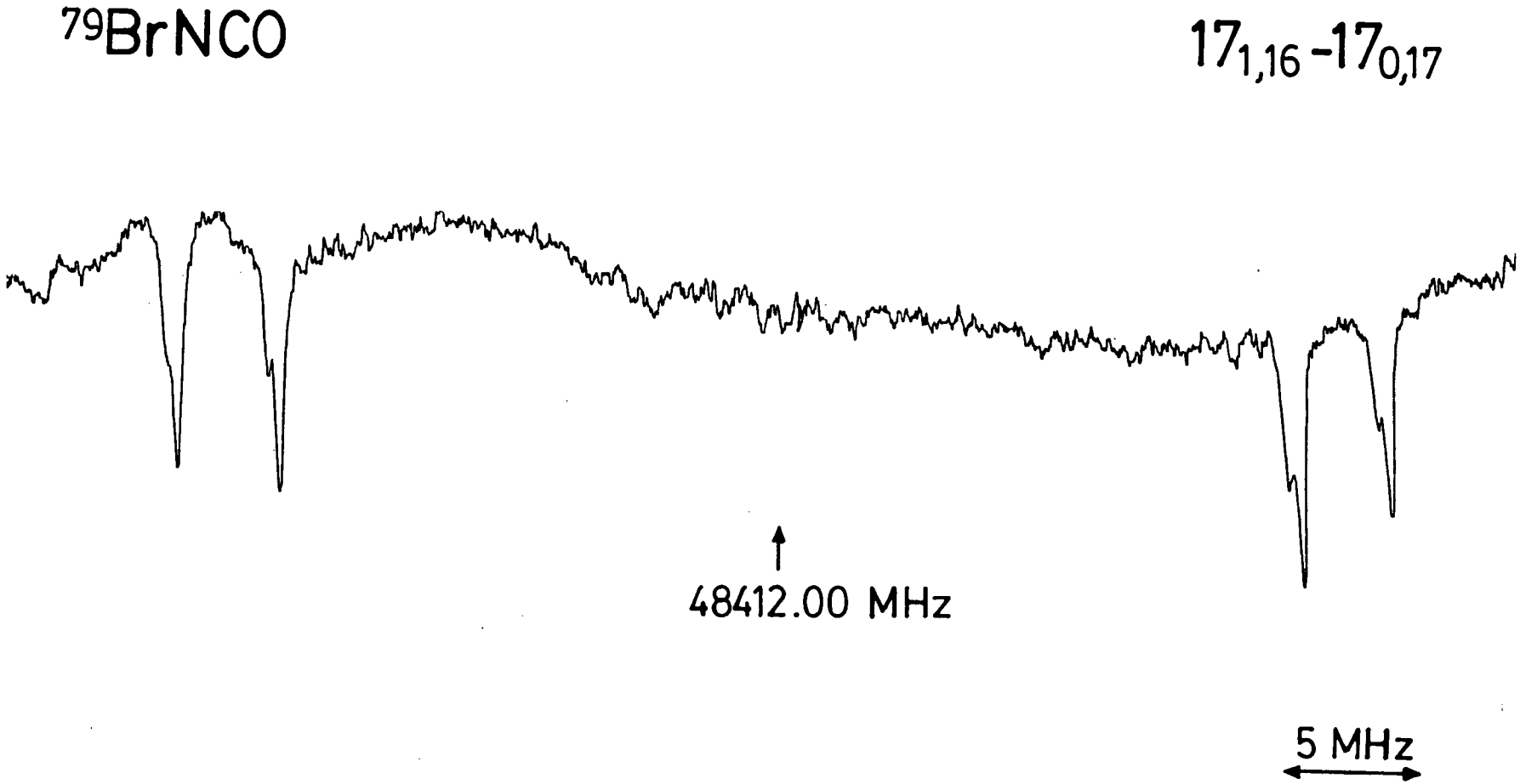

Figure 4.6 The $17_{1,16} - 17_{0,17}$ transitions of ^{79}BrNCO showing both ^{79}Br and ^{14}N nuclear quadrupole effects.

determine the final rotational, centrifugal distortion and bromine quadrupole coupling constants. These are shown in Table 4.3 for ^{79}BrNCO and Table 4.4 for ^{81}BrNCO, along with a comparison with the constants derived from the a-type transitions only. Watson's A-reduction in the I^r representation is used throughout. Unfortunately only Δ_J, Δ_{JK} and δ_J and Φ_{KJ} could be determined because of the limited number of branches available. The measured frequencies, along with the residuals which are calculated with χ_{ab} included and omitted, are shown in Tables 4.5 and 4.6. The effect of χ_{ab} is clear.

Table 4.3

Spectroscopic Constants of ^{79}BrNCO

Parameter	a-type Transitions	All Transitions
Rotational Constants (MHz)		
A_o	41188.71(23)[1]	41189.506(25)
B_o	2175.6311(13)	2175.63391(52)
C_o	2063.1025(11)	2063.09857(53)
Centrifugal Distortion Constants (kHz)		
Δ_J	1.1366(22)	1.1370(19)
Δ_{JK}	-172.72(16)	-173.97(14)
δ_J	0.1692(29)	0.17367(26)
Φ_{KJ}	–	-0.248(19)
Bromine Nuclear Quadrupole Coupling Constants (MHz)		
χ_{aa}	608.16(48)	608.41(52)
$\chi_{bb}-\chi_{cc}$	279.4(11)	280.086(64)
χ_{ab}	549.85(11)	549.67(12)
Nitrogen Nuclear Quadrupole Coupling Constants (MHz)		
χ_{aa}	–	5.09(78)
$\chi_{bb}-\chi_{cc}$	–	1.811(19)
Inertial defect (a.m.u. Å^2)		
	–	0.400
Number of Rotational Transitions		
	26	43
Standard Deviation of Distortion Fit (MHz)		
	0.028	0.032

[1] Numbers in parentheses are one standard deviation in units of the last significant figures.

Table 4.4

Spectroscopic Constants of ^{81}BrNCO

Parameter	a-type Transitions	All Transitions
Rotational Constants (MHz)		
A_o	41142.57(39)[1]	41141.914(29)
B_o	2159.5035(13)	2159.50429(53)
C_o	2048.4716(10)	2048.47014(55)
Centrifugal Distortion Constants (kHz)		
Δ_J	1.1258(23)	1.1281(18)
Δ_{JK}	-171.00(12)	-172.23(14)
δ_J	0.1690(26)	0.17004(31)
Φ_{KJ}	–	-0.214(19)
Bromine Nuclear Quadrupole Coupling Constants (MHz)		
χ_{aa}	508.40(47)	508.49(52)
$\chi_{bb}-\chi_{cc}$	230.8(11)	233.311(70)
χ_{ab}	458.30(22)	458.60(12)
Nitrogen Nuclear Quadrupole Coupling Constants (MHz)		
χ_{aa}	–	4.75(51)
$\chi_{bb}-\chi_{cc}$	–	1.912(12)
Inertial defect (a.m.u. Å^2)		
	–	0.401
Number of Rotational Transitions		
	29	46
Standard Deviation of Distortion Fit (MHz)		
	0.029	0.034

[1] Numbers in parentheses are one standard deviation in units of the last significant figures.

Table 4.5 Measured rotational transitions (in MHz) of ^{79}BrNCO

Transition F' - F"	Normalised[1] Weight	Observed[2] Frequency	Residuals[3] Without χ_{ab}	Residuals[3] With χ_{ab}
$4_{1,4}$ - $3_{1,3}$				
11/2 - 9/2	1.000	16697.064	-23.577	-0.082
9/2 - 7/2	1.000	16725.798	-9.839	0.001
5/2 - 3/2	1.000	16732.136	-0.012	-0.006
7/2 - 5/2	1.000	16747.530	-0.162	-0.065
$5_{1,5}$ - $4_{1,4}$				
13/2 - 11/2	1.000	20907.007	0.769	0.039
11/2 - 9/2	1.000	20914.295	0.519	0.028
7/2 - 5/2	1.000	20915.140	0.011	0.029
9/2 - 7/2	1.000	20922.857	-0.036	0.028
$5_{0,5}$ - $4_{0,4}$				
9/2 - 7/2	1.000	21174.479	-20.928	-0.058
11/2 - 9/2	1.000	21185.088	-0.136	-0.028
13/2 - 11/2	1.000	21185.088	0.077	0.052
7/2 - 5/2	1.000	21187.013	-8.273	0.041
$5_{1,4}$ - $4_{1,3}$				
13/2 - 11/2	1.000	21470.377	0.197	0.004
7/2 - 5/2	1.000	21474.140	-0.019	-0.005
11/2 - 9/2	1.000	21477.657	-0.015	-0.010
9/2 - 7/2	1.000	21482.051	0.128	-0.037
$6_{1,6}$ - $5_{1,5}$				
15/2 - 13/2	1.000	25090.043	0.275	0.036
13/2 - 11/2	1.000	25094.279	0.162	0.002
9/2 - 7/2	1.000	25096.468	0.020	0.040
11/2 - 9/2	1.000	25100.904	-0.003	0.044
$6_{0,6}$ - $5_{0,5}$				
13/2 - 11/2	0.100	25420.588	-0.183	-0.010
15/2 - 13/2	0.100	25420.588	0.094	0.073
9/2 - 7/2	1.000	25436.877	9.568	-0.068
11/2 - 9/2	1.000	25451.129	23.585	0.062

[1] Measurements were weighted according to $1/\sigma^2$, where σ is the uncertainty in the measurements. Unit weight corresponded to an uncertainty of 0.03 MHz.

[2] Nitrogen hyperfine splitting has been subtracted from the b-type transitions.

[3] Observed frequency minus the frequency calculated using the constants in Table 4.3

Table 4.5 (Continued)

Transition F' - F"	Normalised Weight	Observed Frequency	Residuals Without χ_{ab}	Residuals With χ_{ab}
$6_{1,5}$ - $5_{1,4}$				
15/2 - 13/2	1.000	25766.036	0.310	-0.009
9/2 - 7/2	1.000	25769.092	-0.051	-0.031
13/2 - 11/2	1.000	25770.035	-0.016	-0.016
11/2 - 9/2	1.000	25773.916	0.312	-0.016
$7_{1,7}$ - $6_{1,6}$				
17/2 - 15/2	1.000	29272.172	0.151	0.030
15/2 - 13/2	1.000	29274.880	0.099	0.018
11/2 - 9/2	1.000	29277.094	-0.042	-0.021
13/2 - 11/2	1.000	29279.874	-0.082	-0.045
$7_{0,7}$ - $6_{0,6}$				
17/2 - 15/2	1.000	29654.116	0.048	0.030
15/2 - 13/2	1.000	29654.116	-0.286	0.018
11/2 - 9/2	0.100	29658.081	-0.854	-0.010
13/2 - 11/2	0.100	29658.504	-0.744	-0.030
$7_{1,6}$ - $6_{1,5}$				
17/2 - 15/2	1.000	30060.726	0.660	-0.007
11/2 - 9/2	1.000	30062.800	-0.048	-0.023
15/2 - 13/2	1.000	30062.800	-0.013	-0.024
13/2 - 11/2	1.000	30066.356	0.686	-0.041
$8_{1,8}$ - $7_{1,7}$				
19/2 - 17/2	1.000	33453.349	0.067	-0.007
17/2 - 15/2	1.000	33455.203	0.039	-0.010
13/2 - 11/2	1.000	33457.276	-0.020	0.002
15/2 - 13/2	1.000	33459.210	-0.004	0.029
$8_{0,8}$ - $7_{0,7}$				
17/2 - 15/2	0.100	33885.400	-0.578	0.076
19/2 - 17/2	0.100	33885.612	0.023	0.006
13/2 - 11/2	1.000	33888.327	-0.918	-0.011
15/2 - 13/2	1.000	33889.384	-0.238	0.002
$8_{1,7}$ - $7_{1,6}$				
17/2 - 15/2	0.100	34355.372	0.081	0.018
13/2 - 11/2	0.100	34355.688	0.014	0.043
19/2 - 17/2	0.100	34355.688	2.272	-0.080
15/2 - 13/2	1.000	34360.044	2.450	-0.044
$9_{1,9}$ - $8_{1,8}$				
21/2 - 19/2	1.000	37633.739	0.091	0.041
19/2 - 17/2	1.000	37635.076	0.069	0.035
15/2 - 13/2	1.000	37636.850	-0.021	0.003
17/2 - 15/2	1.000	37638.241	-0.012	0.020

Table 4.5 (Continued)

Transition F' - F"	Normalised Weight	Observed Frequency	Residuals Without χ_{ab}	Residuals With χ_{ab}
$9_{0\,9}$ - $8_{0\,8}$				
19/2 - 17/2	1.000	38112.998	-2.304	0.038
21/2 - 19/2	0.100	38114.961	0.101	0.086
15/2 - 13/2	0.100	38114.961	-2.746	-0.150
17/2 - 15/2	1.000	38117.988	-0.153	0.023
$9_{1\,8}$ - $8_{1\,7}$				
17/2 - 15/2	1.000	38617.849	-31.213	0.0
21/2 - 19/2	1.000	38626.908	-18.916	0.007
19/2 - 17/2	1.000	38646.382	-0.800	-0.054
15/2 - 13/2	1.000	38647.578	-0.097	-0.063
$10_{1\,10}$ - $9_{1\,9}$				
23/2 - 21/2	1.000	41813.185	0.051	0.015
21/2 - 19/2	1.000	41814.197	0.032	0.009
17/2 - 15/2	1.000	41815.738	-0.035	-0.006
19/2 - 17/2	1.000	41816.788	-0.031	0.003
$10_{0\,10}$ - $9_{0\,9}$				
23/2 - 21/2	1.000	42341.688	0.033	0.019
19/2 - 17/2	1.000	42345.109	0.686	0.009
21/2 - 19/2	1.000	42361.038	18.890	-0.042
17/2 - 15/2	1.000	42375.034	31.099	-0.037
$10_{1\,9}$ - $9_{1\,8}$				
17/2 - 15/2	1.000	42938.775	-0.031	0.014
21/2 - 19/2	1.000	42938.775	0.473	-0.023
23/2 - 21/2	1.000	42949.302	12.032	-0.026
19/2 - 17/2	1.000	42962.772	22.914	-0.030
$11_{1\,11}$ - $10_{1\,10}$				
25/2 - 23/2	1.000	45991.765	0.049	0.021
23/2 - 21/2	1.000	45992.565	0.034	0.016
19/2 - 17/2	1.000	45993.878	-0.035	0.0
21/2 - 19/2	1.000	45994.713	-0.026	0.014
$11_{0\,11}$ - $10_{0\,10}$				
19/2 - 17/2	1.000	46544.577	-23.029	-0.014
23/2 - 21/2	1.000	46554.253	-12.030	0.021
25/2 - 23/2	1.000	46565.779	0.039	0.027
21/2 - 19/2	1.000	46567.612	-0.534	0.010
$11_{1\,10}$ - $10_{1\,9}$				
23/2 - 21/2	0.100	47228.576	0.060	0.030
19/2 - 17/2	0.100	47228.888	-0.100	-0.032
25/2 - 23/2	0.100	47228.888	1.192	-0.023
21/2 - 19/2	1.000	47231.377	1.555	-0.012

Table 4.5 (Continued)

Transition F' - F"	Normalised Weight	Observed Frequency	Residuals Without χ_{ab}	Residuals With χ_{ab}
$12_{1\,12}$ - $11_{1\,11}$				
27/2 - 25/2	1.000	50169.384	0.031	0.009
25/2 - 23/2	1.000	50170.039	0.017	0.005
21/2 - 19/2	1.000	50171.143	-0.066	-0.015
23/2 - 21/2	1.000	50171.830	-0.056	0.002
$12_{0\,12}$ - $11_{0\,11}$				
25/2 - 23/2	0.100	50786.288	-1.180	0.028
21/2 - 19/2	0.100	50786.863	-1.567	0.087
27/2 - 25/2	0.100	50786.863	-0.012	-0.023
23/2 - 21/2	1.000	50788.988	-0.033	0.033
$12_{2\,11}$ - $11_{2\,10}$				
27/2 - 25/2	1.000	50858.400	-2.650	0.001
25/2 - 23/2	1.000	50860.909	-2.348	0.038
21/2 - 19/2	1.000	50862.154	-0.063	-0.056
23/2 - 21/2	1.000	50864.420	-0.040	-0.035
$12_{3\,10}$ - $11_{3\,9}$				
27/2 - 25/2	1.000	50900.357	0.058	0.049
21/2 - 19/2	0.100	50900.950	-0.006	-0.003
25/2 - 23/2	1.000	50905.033	0.055	0.048
23/2 - 21/2	0.100	50905.691	-0.020	-0.016
$12_{3\,9}$ - $11_{3\,8}$				
27/2 - 25/2	0.100	50900.950	-0.007	-0.016
21/2 - 19/2	1.000	50901.565	-0.051	-0.048
25/2 - 23/2	0.100	50905.691	0.066	0.059
23/2 - 21/2	1.000	50906.313	-0.047	-0.043
$12_{1\,11}$ - $11_{1\,10}$				
27/2 - 25/2	0.100	51517.502	0.474	0.012
25/2 - 23/2	0.100	51517.724	0.018	0.017
21/2 - 19/2	0.100	51518.023	-0.104	0.025
23/2 - 21/2	1.000	51519.258	0.443	-0.014
$13_{1\,12}$ - $13_{0\,13}$				
27/2 - 27/2	1.000	44441.733	-0.997	0.019
25/2 - 25/2	1.000	44445.392	-1.927	0.001
29/2 - 29/2	1.000	44482.980	-0.613	0.044
23/2 - 23/2	1.000	44486.143	-2.094	0.042
$14_{1\,13}$ - $14_{0\,14}$				
29/2 - 29/2	1.000	45314.448	-0.808	-0.019
27/2 - 27/2	1.000	45320.417	0.871	-0.062
31/2 - 31/2	1.000	45355.799	-0.496	0.019
25/2 - 25/2	1.000	45361.203	0.569	0.020

Table 4.5 (Continued)

Transition F' - F"	Normalised Weight	Observed Frequency	Residuals Without χ_{ab}	Residuals With χ_{ab}
$15_{1\ 14}$ - $15_{0\ 15}$				
31/2 - 31/2	1.000	46261.617	-0.690	-0.030
29/2 - 29/2	1.000	46266.069	-0.277	-0.020
33/2 - 33/2	1.000	46303.187	-0.428	-0.007
27/2 - 27/2	1.000	46307.165	-0.533	0.012
$16_{1\ 15}$ - $16_{0\ 16}$				
33/2 - 33/2	1.000	47285.651	-0.631	-0.049
31/2 - 31/2	1.000	47289.727	-0.382	-0.033
35/2 - 35/2	1.000	47327.565	-0.372	-0.018
29/2 - 29/2	1.000	47331.196	-0.607	-0.001
$17_{1\ 16}$ - $17_{0\ 17}$				
35/2 - 35/2	1.000	48389.145	-0.530	0.009
33/2 - 33/2	1.000	48392.993	-0.327	0.024
37/2 - 37/2	1.000	48431.442	-0.299	0.005
31/2 - 31/2	1.000	48434.850	-0.572	0.036
$18_{1\ 17}$ - $18_{0\ 18}$				
35/2 - 35/2	1.000	49578.252	-0.292	0.042
39/2 - 39/2	1.000	49617.344	-0.243	0.023
33/2 - 33/2	1.000	49620.528	-0.582	0.029
$19_{1\ 18}$ - $19_{0\ 19}$				
37/2 - 37/2	1.000	50848.120	-0.327	-0.011
41/2 - 41/2	1.000	50887.846	-0.245	-0.010
35/2 - 35/2	1.000	50890.884	-0.627	0.002
$20_{1\ 19}$ - $20_{0\ 20}$				
41/2 - 41/2	1.000	52201.741	-0.566	0.001
39/2 - 39/2	1.000	52205.209	-0.298	-0.002
43/2 - 43/2	1.000	52245.672	-0.237	-0.026
37/2 - 37/2	1.000	52248.464	-0.677	-0.002
$21_{1\ 20}$ - $21_{0\ 21}$				
41/2 - 41/2	0.010	53652.430	-0.186	0.093
$14_{0\ 14}$ - $13_{1\ 13}$				
29/2 - 27/2	1.000	24966.261	0.964	0.002
27/2 - 25/2	1.000	24970.004	0.270	-0.017
31/2 - 29/2	1.000	24993.737	0.032	0.011
25/2 - 23/2	1.000	24999.436	1.343	0.009
$15_{0\ 15}$ - $14_{1\ 14}$				
31/2 - 29/2	1.000	29875.048	0.837	0.030
29/2 - 27/2	1.000	29878.788	0.545	0.018
33/2 - 31/2	1.000	29902.383	0.004	-0.011
27/2 - 25/2	1.000	29907.698	1.330	-0.020

Table 4.5 (Continued)

Transition F' - F"	Normalised Weight	Observed Frequency	Residuals Without χ_{ab}	Residuals With χ_{ab}
$16_{0\ 16}$ - $15_{1\ 15}$				
33/2 - 31/2	1.000	34816.506	0.721	0.018
31/2 - 29/2	0.0	34823.144	3.680	0.305
35/2 - 33/2	1.000	34843.644	0.025	0.016
29/2 - 27/2	0.0	34850.568	3.310	0.134
$17_{0\ 17}$ - $16_{1\ 16}$				
35/2 - 33/2	1.000	39787.743	0.624	-0.004
33/2 - 31/2	1.000	39789.729	-0.756	0.057
37/2 - 35/2	1.000	39814.522	-0.014	-0.020
31/2 - 29/2	1.000	39817.797	-0.070	-0.017
$18_{0\ 18}$ - $17_{1\ 17}$				
37/2 - 35/2	1.000	44785.796	0.611	0.038
35/2 - 33/2	1.000	44787.977	-0.294	0.082
39/2 - 37/2	1.000	44812.050	-0.067	-0.071
33/2 - 31/2	1.000	44815.420	0.249	-0.047
$19_{0\ 19}$ - $18_{1\ 18}$				
39/2 - 37/2	1.000	49807.390	0.544	0.013
37/2 - 35/2	1.000	49809.383	-0.253	-0.003
41/2 - 39/2	1.000	49833.206	-0.028	-0.029
35/2 - 33/2	1.000	49836.343	0.337	-0.025

Table 4.6 Measured rotational transitions (in MHz) of ^{81}BrNCO

Transition F' - F"	Normalised[1] Weight	Observed[2] Frequency	Residuals[3] Without χ_{ab}	Residuals[3] With χ_{ab}
$4_{1,4} - 3_{1,3}$				
11/2 - 9/2	1.000	16590.877	-11.334	-0.006
9/2 - 7/2	0.100	16609.323	-5.455	0.147
5/2 - 3/2	1.000	16611.856	-0.020	-0.016
7/2 - 5/2	1.000	16624.686	-0.142	-0.074
$5_{1,5} - 4_{1,4}$				
13/2 - 11/2	1.000	20757.792	0.560	0.022
11/2 - 9/2	1.000	20763.937	0.389	0.028
7/2 - 5/2	1.000	20764.629	-0.057	-0.045
9/2 - 7/2	1.000	20771.106	-0.055	-0.010
$5_{0,5} - 4_{0,4}$				
9/2 - 7/2	0.100	21031.080	-9.510	-0.034
11/2 - 9/2	0.100	21031.924	-0.127	-0.053
13/2 - 11/2	0.100	21031.924	0.053	0.035
7/2 - 5/2	0.100	21035.953	-4.522	-0.003
$5_{1,4} - 4_{1,3}$				
13/2 - 11/2	1.000	21313.553	0.119	-0.012
7/2 - 5/2	1.000	21316.760	-0.050	-0.041
11/2 - 9/2	1.000	21319.707	-0.011	-0.007
9/2 - 7/2	1.000	21323.394	0.109	-0.004
$6_{1,6} - 5_{1,5}$				
15/2 - 13/2	1.000	24910.652	0.191	0.018
13/2 - 11/2	1.000	24914.219	0.114	-0.001
9/2 - 7/2	1.000	24916.049	-0.009	0.005
11/2 - 9/2	1.000	24919.733	-0.046	-0.013
$6_{0,6} - 5_{0,5}$				
13/2 - 11/2	0.100	25236.625	-0.169	-0.052
15/2 - 13/2	0.100	25236.625	0.061	0.046
9/2 - 7/2	1.000	25247.673	5.400	-0.064
11/2 - 9/2	1.000	25253.866	11.392	0.044

[1] Measurements were weighted according to $1/\sigma^2$, where σ is the uncertainty in the measurements. Unit weight corresponded to an uncertainty of 0.03 MHz.

[2] Nitrogen hyperfine splitting has been subtracted from the b-type transitions.

[3] Observed frequency minus the frequency calculated using the constants in Table 4.4

Table 4.6 (Continued)

Transition F' - F"	Normalised Weight	Observed Frequency	Residuals Without χ_{ab}	Residuals With χ_{ab}
6_{15} - 5_{14}				
15/2 - 13/2	1.000	25577.458	0.215	0.0
9/2 - 7/2	1.000	25580.091	-0.039	-0.025
13/2 - 11/2	1.000	25580.857	-0.012	-0.012
11/2 - 9/2	1.000	25584.055	0.203	-0.018
7_{17} - 6_{16}				
17/2 - 15/2	1.000	29062.671	0.122	0.035
15/2 - 13/2	1.000	29064.944	0.084	0.026
11/2 - 9/2	1.000	29066.810	-0.024	-0.009
13/2 - 11/2	1.000	29069.148	-0.039	-0.013
7_{07} - 6_{06}				
17/2 - 15/2	0.100	29439.508	0.075	0.062
15/2 - 13/2	0.100	29439.508	-0.202	0.003
11/2 - 9/2	1.000	29442.917	-0.594	0.004
13/2 - 11/2	1.000	29443.243	-0.530	-0.003
7_{16} - 6_{15}				
17/2 - 15/2	1.000	29840.398	0.436	-0.004
11/2 - 9/2	1.000	29842.269	-0.039	-0.023
15/2 - 13/2	1.000	29842.269	0.004	-0.003
13/2 - 11/2	1.000	29845.134	0.471	-0.012
8_{18} - 7_{17}				
19/2 - 17/2	1.000	33213.759	0.035	-0.018
17/2 - 15/2	1.000	33215.310	0.011	-0.025
13/2 - 11/2	1.000	33217.031	-0.055	-0.040
15/2 - 13/2	1.000	33218.628	-0.058	-0.036
8_{08} - 7_{07}				
17/2 - 15/2	0.100	33640.279	-0.364	0.067
19/2 - 17/2	0.100	33640.279	-0.043	-0.054
13/2 - 11/2	1.000	33642.755	-0.630	-0.018
15/2 - 13/2	1.000	33643.526	-0.172	0.0
8_{27} - 7_{26}				
19/2 - 17/2	1.000	33666.139	0.041	0.013
13/2 - 11/2	1.000	33667.381	0.0	0.004
17/2 - 15/2	1.000	33672.197	0.049	0.028
15/2 - 13/2	1.000	33673.552	0.003	0.010
8_{26} - 7_{25}				
19/2 - 17/2	1.000	33686.085	-0.017	-0.038
13/2 - 11/2	1.000	33687.347	-0.069	-0.066
17/2 - 15/2	1.000	33691.803	-0.019	-0.034
15/2 - 13/2	1.000	33693.217	-0.038	-0.033

Table 4.6 (Continued)

Transition F' - F"	Normalised Weight	Observed Frequency	Residuals Without χ_{ab}	Residuals With χ_{ab}
$8_{3\,6}$ - $7_{3\,5}$				
13/2 - 11/2	0.010	33681.647	0.062	0.065
19/2 - 17/2	0.010	33682.607	0.078	0.073
15/2 - 13/2	0.010	33695.368	0.074	0.079
17/2 - 15/2	0.010	33696.133	0.128	0.125
$8_{3\,5}$ - $7_{3\,4}$				
13/2 - 11/2	0.010	33681.647	-0.019	-0.016
19/2 - 17/2	0.010	33682.607	-0.002	-0.008
15/2 - 13/2	0.010	33695.368	-0.004	0.0
17/2 - 15/2	0.010	33696.133	0.050	0.048
$8_{1\,7}$ - $7_{1\,6}$				
17/2 - 15/2	0.100	34103.358	0.028	-0.011
19/2 - 17/2	0.100	34103.358	1.599	0.141
13/2 - 11/2	0.100	34103.581	-0.081	-0.061
15/2 - 13/2	1.000	34106.842	1.578	-0.007
$9_{1\,9}$ - $8_{1\,8}$				
21/2 - 19/2	1.000	37364.100	0.044	0.009
19/2 - 17/2	1.000	37365.212	0.019	-0.005
15/2 - 13/2	1.000	37366.723	-0.031	-0.015
17/2 - 15/2	1.000	37367.891	-0.017	0.005
$9_{0\,9}$ - $8_{0\,8}$				
19/2 - 17/2	1.000	37838.013	-1.379	0.072
21/2 - 19/2	1.000	37839.125	0.098	0.087
15/2 - 13/2	1.000	37839.817	-1.597	0.061
17/2 - 15/2	1.000	37841.727	-0.046	0.074
$9_{1\,8}$ - $8_{1\,7}$				
17/2 - 15/2	1.000	38332.348	-33.029	-0.037
21/2 - 19/2	1.000	38344.933	-17.728	0.059
19/2 - 17/2	1.000	38363.036	-0.762	-0.019
15/2 - 13/2	1.000	38364.182	-0.038	-0.014
$10_{1\,10}$ - $9_{1\,9}$				
23/2 - 21/2	1.000	41513.589	0.043	0.018
21/2 - 19/2	1.000	41514.434	0.027	0.010
17/2 - 15/2	1.000	41515.728	-0.027	-0.008
19/2 - 17/2	1.000	41516.617	-0.010	0.013
$10_{0\,10}$ - $9_{0\,9}$				
23/2 - 21/2	1.000	42035.331	0.005	-0.004
19/2 - 17/2	1.000	42038.338	0.698	0.005
21/2 - 19/2	1.000	42053.495	17.763	-0.030
17/2 - 15/2	1.000	42070.174	32.937	-0.001

Table 4.6 (Continued)

Transition F' - F"	Normalised Weight	Observed Frequency	Residuals Without χ_{ab}	Residuals With χ_{ab}
$10_{1\,9}$ - $9_{1\,8}$				
17/2 - 15/2	0.100	42623.983	0.053	0.084
21/2 - 19/2	0.100	42623.983	0.483	-0.089
23/2 - 21/2	1.000	42635.697	13.060	-0.036
19/2 - 17/2	1.000	42652.089	27.282	0.004
$11_{1\,11}$ - $10_{1\,10}$				
25/2 - 23/2	1.000	45662.225	0.062	0.042
23/2 - 21/2	1.000	45662.886	0.042	0.030
19/2 - 17/2	1.000	45664.006	0.003	0.028
21/2 - 19/2	1.000	45664.697	0.006	0.034
$11_{0\,11}$ - $10_{0\,10}$				
19/2 - 17/2	1.000	46203.181	-27.368	-0.041
23/2 - 21/2	1.000	46216.341	-13.090	0.001
25/2 - 23/2	1.000	46229.030	0.046	0.038
21/2 - 19/2	1.000	46230.414	-0.580	0.026
$11_{1\,10}$ - $10_{1\,9}$				
23/2 - 21/2	0.100	46882.334	0.024	0.001
25/2 - 23/2	0.100	46882.589	0.965	0.031
19/2 - 17/2	0.100	46882.589	-0.122	-0.077
21/2 - 19/2	1.000	46884.557	1.151	-0.045
$12_{1\,12}$ - $11_{1\,11}$				
27/2 - 25/2	1.000	49809.879	0.017	0.001
25/2 - 23/2	1.000	49810.417	-0.003	-0.013
21/2 - 19/2	1.000	49811.346	-0.070	-0.036
23/2 - 21/2	1.000	49811.887	-0.093	-0.055
$12_{0\,12}$ - $11_{0\,11}$				
25/2 - 23/2	0.100	50419.356	-0.899	0.030
27/2 - 25/2	0.100	50419.787	0.020	0.012
21/2 - 19/2	0.100	50419.787	-1.284	-0.029
23/2 - 21/2	1.000	50421.510	-0.047	0.002
$12_{2\,11}$ - $11_{2\,10}$				
27/2 - 25/2	1.000	50490.169	-2.229	0.004
25/2 - 23/2	1.000	50492.221	-2.023	0.035
21/2 - 19/2	1.000	50493.316	-0.064	-0.059
23/2 - 21/2	1.000	50495.218	-0.033	-0.029
$12_{3\,10}$ - $11_{3\,9}$				
27/2 - 25/2	1.000	50531.253	0.100	0.094
21/2 - 19/2	0.100	50531.756	0.046	0.048
25/2 - 23/2	1.000	50535.147	0.078	0.073
23/2 - 21/2	0.100	50535.675	-0.005	-0.002

Table 4.6 (Continued)

Transition F' - F"	Normalised Weight	Observed Frequency	Residuals Without χ_{ab}	Residuals With χ_{ab}
$12_{3\,9}$ - $11_{3\,8}$				
27/2 - 25/2	0.100	50531.756	-0.030	-0.036
21/2 - 19/2	1.000	50532.268	-0.076	-0.074
25/2 - 23/2	0.100	50535.675	-0.018	-0.023
23/2 - 21/2	1.000	50536.229	-0.075	-0.073
$12_{1\,11}$ - $11_{1\,10}$				
27/2 - 25/2	0.100	51139.918	0.371	0.029
25/2 - 23/2	0.100	51140.147	0.034	0.032
21/2 - 19/2	0.100	51140.415	-0.057	0.027
23/2 - 21/2	1.000	51141.417	0.372	0.025
$13_{1\,13}$ - $12_{1\,12}$				
29/2 - 27/2	1.000	53956.629	0.040	0.027
27/2 - 25/2	1.000	53957.085	0.023	0.016
23/2 - 21/2	0.100	53957.794	-0.124	-0.067
25/2 - 23/2	1.000	53958.365	-0.031	0.035
$13_{1\,12}$ - $13_{0\,13}$				
27/2 - 27/2	1.000	44338.710	-0.730	-0.003
25/2 - 25/2	1.000	44341.957	-1.300	-0.009
29/2 - 29/2	1.000	44373.009	-0.447	0.024
23/2 - 23/2	1.000	44375.878	-1.433	0.026
$14_{1\,13}$ - $14_{0\,14}$				
29/2 - 29/2	1.000	45198.833	-0.535	0.027
27/2 - 27/2	1.000	45203.962	1.027	-0.067
31/2 - 31/2	1.000	45233.165	-0.359	0.009
25/2 - 25/2	1.000	45237.912	0.787	-0.030
$15_{1\,14}$ - $15_{0\,15}$				
31/2 - 31/2	1.000	46132.138	-0.488	-0.021
29/2 - 29/2	1.000	46135.813	-0.171	-0.008
33/2 - 33/2	1.000	46166.698	-0.301	-0.002
27/2 - 27/2	1.000	46170.031	-0.356	0.011
$16_{1\,15}$ - $16_{0\,16}$				
33/2 - 33/2	1.000	47141.155	-0.399	0.011
31/2 - 31/2	1.000	47144.494	-0.240	0.0
35/2 - 35/2	1.000	47175.957	-0.253	-0.002
29/2 - 29/2	1.000	47179.023	-0.395	0.026
$17_{1\,16}$ - $17_{0\,17}$				
35/2 - 35/2	1.000	48228.193	-0.394	-0.015
33/2 - 33/2	1.000	48231.347	-0.268	-0.023
37/2 - 37/2	1.000	48263.357	-0.222	-0.007
31/2 - 31/2	1.000	48266.234	-0.398	0.025

Table 4.6 (Continued)

Transition F' - F"	Normalised Weight	Observed Frequency	Residuals Without χ_{ab}	Residuals With χ_{ab}
$18_{1\,17}$ - $18_{0\,18}$				
37/2 - 37/2	1.000	49395.853	-0.380	-0.015
35/2 - 35/2	1.000	49398.883	-0.248	-0.013
39/2 - 39/2	1.000	49431.438	-0.170	0.018
33/2 - 33/2	1.000	49434.146	-0.383	0.041
$20_{1\,19}$ - $20_{0\,20}$				
41/2 - 41/2	1.000	51983.271	-0.401	-0.011
43/2 - 43/2	1.000	52019.775	-0.151	-0.002
37/2 - 37/2	1.000	52022.159	-0.447	0.018
$14_{0\,14}$ - $13_{1\,13}$				
27/2 - 25/2	0.100	24515.044	0.276	0.083
31/2 - 29/2	0.100	24534.742	-0.024	-0.039
25/2 - 23/2	0.100	24539.294	0.864	-0.074
$15_{0\,15}$ - $14_{1\,14}$				
31/2 - 29/2	0.100	29382.081	0.538	-0.033
29/2 - 27/2	0.100	29385.286	0.383	0.041
33/2 - 31/2	1.000	29405.051	0.004	-0.006
27/2 - 25/2	1.000	29409.292	0.915	-0.015
$16_{0\,16}$ - $15_{1\,15}$				
33/2 - 31/2	1.000	34285.015	0.511	0.014
31/2 - 29/2	1.000	34289.226	1.655	0.096
35/2 - 33/2	1.000	34307.728	-0.008	-0.015
29/2 - 27/2	1.000	34312.549	1.774	0.015
$17_{0\,17}$ - $16_{1\,16}$				
35/2 - 33/2	1.000	39217.570	0.447	0.003
33/2 - 31/2	1.000	39219.283	-0.648	-0.001
37/2 - 35/2	1.000	39240.010	-0.006	-0.010
31/2 - 29/2	1.000	39242.688	-0.111	-0.006
$18_{0\,18}$ - $17_{1\,17}$				
37/2 - 35/2	1.000	44176.871	0.425	0.021
35/2 - 33/2	1.000	44178.762	-0.260	0.018
39/2 - 37/2	1.000	44198.933	-0.009	-0.011
33/2 - 31/2	1.000	44201.684	0.189	-0.007
$19_{0\,19}$ - $18_{1\,18}$				
37/2 - 35/2	1.000	49161.623	-0.136	0.045
41/2 - 39/2	1.000	49181.401	-0.056	-0.057
35/2 - 33/2	1.000	49183.967	0.177	-0.073

Table 4.7
Observed hyperfine transition frequencies in (MHz) of $^{79}Br^{14}NCO$
b-type transitions

Transition F_1'	F'	-	F_1''	F''	Observed Frequency
$13_{1\,12}$		-	$13_{0\,13}$		
27/2	27/2	-	27/2	27/2	44441.472
27/2	25/2	-	27/2	25/2	44441.863
27/2	29/2	-	27/2	29/2	44441.863
25/2	25/2	-	25/2	25/2	44445.128
25/2	23/2	-	25/2	23/2	44445.524
25/2	27/2	-	25/2	27/2	44445.524
29/2	29/2	-	29/2	29/2	44482.699
29/2	27/2	-	29/2	27/2	44483.120
29/2	31/2	-	29/2	31/2	44483.120
23/2	23/2	-	23/2	23/2	44485.883
23/2	21/2	-	23/2	21/2	44486.273
23/2	25/2	-	23/2	25/2	44486.273
$14_{1\,13}$		-	$14_{0\,14}$		
29/2	29/2	-	29/2	29/2	45314.176
29/2	27/2	-	29/2	27/2	45314.584
29/2	31/2	-	29/2	31/2	45314.584
27/2	27/2	-	27/2	27/2	45320.156
27/2	25/2	-	27/2	25/2	45320.548
27/2	29/2	-	27/2	29/2	45320.548
31/2	31/2	-	31/2	31/2	45355.548
31/2	29/2	-	31/2	29/2	45355.924
31/2	33/2	-	31/2	33/2	45355.924
25/2	25/2	-	25/2	25/2	45360.959
25/2	23/2	-	25/2	23/2	45361.325
25/2	27/2	-	25/2	27/2	45361.325
$15_{1\,14}$		-	$15_{0\,15}$		
31/2	31/2	-	31/2	31/2	46261.353
31/2	29/2	-	31/2	29/2	46261.749
31/2	33/2	-	31/2	33/2	46261.749
29/2	29/2	-	29/2	29/2	46265.801
29/2	27/2	-	29/2	27/2	46266.203
29/2	31/2	-	29/2	31/2	46266.203
33/2	33/2	-	33/2	33/2	46302.902
33/2	31/2	-	33/2	31/2	46303.329
33/2	35/2	-	33/2	35/2	46303.329
27/2	27/2	-	27/2	27/2	46306.888
27/2	25/2	-	27/2	25/2	46307.303
27/2	29/2	-	27/2	29/2	46307.303

Table 4.7 (Continued)

Transition F_1'	F'	-	F_1''	F''	Observed Frequency
$16_{1\ 15}$		-	$16_{0\ 16}$		
33/2	33/2	-	33/2	33/2	47285.376
33/2	31/2	-	33/2	31/2	47285.789
33/2	35/2	-	33/2	35/2	47285.789
31/2	31/2	-	31/2	31/2	47289.460
31/2	29/2	-	31/2	29/2	47289.860
31/2	33/2	-	31/2	33/2	47289.860
35/2	35/2	-	35/2	35/2	47327.280
35/2	33/2	-	35/2	33/2	47327.708
35/2	37/2	-	35/2	37/2	47327.708
29/2	29/2	-	29/2	29/2	47330.917
29/2	27/2	-	29/2	27/2	47331.335
29/2	31/2	-	29/2	31/2	47331.335
$17_{1\ 16}$		-	$17_{0\ 17}$		
35/2	35/2	-	35/2	35/2	48388.886
35/2	33/2	-	35/2	33/2	48389.274
35/2	37/2	-	35/2	37/2	48389.274
33/2	33/2	-	33/2	33/2	48392.722
33/2	31/2	-	33/2	31/2	48393.128
33/2	35/2	-	33/2	35/2	48393.128
37/2	37/2	-	37/2	37/2	48431.154
37/2	35/2	-	37/2	35/2	48431.557
37/2	39/2	-	37/2	39/2	48431.557
31/2	31/2	-	31/2	31/2	48434.573
31/2	29/2	-	31/2	29/2	48434.988
31/2	33/2	-	31/2	33/2	48434.988
$18_{1\ 17}$		-	$18_{0\ 18}$		
35/2	35/2	-	35/2	35/2	49577.931
35/2	33/2	-	35/2	33/2	49578.402
35/2	37/2	-	35/2	37/2	49578.402
39/2	39/2	-	39/2	39/2	49617.061
39/2	37/2	-	39/2	37/2	49617.485
39/2	41/2	-	39/2	41/2	49617.485
33/2	33/2	-	33/2	33/2	49620.243
33/2	31/2	-	33/2	31/2	49620.671
33/2	35/2	-	33/2	35/2	49620.671
$19_{1\ 18}$		-	$19_{0\ 19}$		
37/2	37/2	-	37/2	37/2	50847.848
37/2	35/2	-	37/2	35/2	50848.256
37/2	39/2	-	37/2	39/2	50848.256
41/2	41/2	-	41/2	41/2	50887.560
41/2	39/2	-	41/2	39/2	50887.989
41/2	43/2	-	41/2	43/2	50887.989

Table 4.7 (Continued)

Transition F_1'	F'	-	F_1''	F''	Observed Frequency
$19_{1\ 18}$		-	$19_{0\ 19}$		
35/2	35/2	-	35/2	35/2	50890.575
35/2	33/2	-	35/2	33/2	50891.039
35/2	37/2	-	35/2	37/2	50891.039
$20_{1\ 19}$		-	$20_{0\ 20}$		
41/2	41/2	-	41/2	41/2	52201.473
41/2	39/2	-	41/2	39/2	52201.875
41/2	43/2	-	41/2	43/2	52201.875
39/2	39/2	-	39/2	39/2	52204.966
39/2	37/2	-	39/2	37/2	52205.331
39/2	41/2	-	39/2	41/2	52205.331
43/2	43/2	-	43/2	43/2	52245.425
43/2	41/2	-	43/2	41/2	52245.795
43/2	45/2	-	43/2	45/2	52245.795
37/2	37/2	-	37/2	37/2	52248.189
37/2	35/2	-	37/2	35/2	52248.602
37/2	39/2	-	37/2	39/2	52248.602
$21_{1\ 20}$		-	$21_{0\ 21}$		
43/2	43/2	-	43/2	43/2	53652.121
43/2	41/2	-	43/2	41/2	53652.585
43/2	45/2	-	43/2	45/2	53652.585
$14_{0\ 14}$		-	$13_{1\ 13}$		
29/2	29/2	-	27/2	27/2	24966.079
29/2	27/2	-	27/2	25/2	24966.343
29/2	31/2	-	27/2	29/2	24966.343
27/2	27/2	-	25/2	25/2	24969.841
27/2	25/2	-	25/2	23/2	24970.086
27/2	29/2	-	25/2	27/2	24970.086
31/2	31/2	-	29/2	29/2	24993.569
31/2	29/2	-	29/2	27/2	24993.821
31/2	33/2	-	29/2	31/2	24993.821
25/2	25/2	-	23/2	23/2	24999.297
25/2	23/2	-	23/2	21/2	24999.506
25/2	27/2	-	23/2	25/2	24999.506
$15_{0\ 15}$		-	$14_{1\ 14}$		
31/2	31/2	-	29/2	29/2	29874.876
31/2	29/2	-	29/2	27/2	29875.134
31/2	33/2	-	29/2	31/2	29875.134
29/2	29/2	-	27/2	27/2	29878.588
29/2	27/2	-	27/2	25/2	29878.888
29/2	31/2	-	27/2	29/2	29878.888
33/2	33/2	-	31/2	31/2	29902.211
33/2	31/2	-	31/2	29/2	29902.469
33/2	35/2	-	31/2	33/2	29902.469

Table 4.7 (Continued)

Transition F_1' F'	-	F_1'' F"	Observed Frequency
$15_{0\ 15}$	-	$14_{1\ 14}$	
27/2 27/2	-	25/2 25/2	29907.525
27/2 25/2	-	25/2 23/2	29907.784
27/2 29/2	-	25/2 27/2	29907.784
$16_{0\ 16}$	-	$15_{1\ 15}$	
33/2 33/2	-	31/2 31/2	34816.338
33/2 31/2	-	31/2 29/2	34816.590
33/2 35/2	-	31/2 33/2	34816.590
31/2 31/2	-	29/2 29/2	34822.967
31/2 29/2	-	29/2 27/2	34823.232
31/2 33/2	-	29/2 31/2	34823.232
35/2 35/2	-	33/2 33/2	34843.459
35/2 33/2	-	33/2 31/2	34843.736
35/2 37/2	-	33/2 35/2	34843.736
29/2 29/2	-	27/2 27/2	34850.383
29/2 27/2	-	27/2 25/2	34850.660
29/2 31/2	-	27/2 29/2	34850.660
$17_{0\ 17}$	-	$16_{1\ 16}$	
35/2 35/2	-	33/2 33/2	39787.581
35/2 33/2	-	33/2 31/2	39787.824
35/2 37/2	-	33/2 35/2	39787.824
33/2 33/2	-	31/2 31/2	39789.581
33/2 31/2	-	31/2 29/2	39789.803
33/2 35/2	-	31/2 33/2	39789.803
37/2 37/2	-	35/2 35/2	39814.361
37/2 35/2	-	35/2 33/2	39814.602
37/2 39/2	-	35/2 37/2	39814.602
31/2 31/2	-	29/2 29/2	39817.639
31/2 29/2	-	29/2 27/2	39817.876
31/2 33/2	-	29/2 31/2	39817.876
$18_{0\ 18}$	-	$17_{1\ 17}$	
37/2 37/2	-	35/2 35/2	44785.638
37/2 35/2	-	35/2 33/2	44785.875
37/2 39/2	-	35/2 37/2	44785.875
35/2 35/2	-	33/2 33/2	44787.756
35/2 33/2	-	33/2 31/2	44788.008
35/2 37/2	-	33/2 35/2	44788.008
39/2 39/2	-	37/2 37/2	44811.872
39/2 37/2	-	37/2 35/2	44812.139
39/2 41/2	-	37/2 39/2	44812.139
33/2 33/2	-	31/2 31/2	44815.259
33/2 31/2	-	31/2 29/2	44815.500
33/2 35/2	-	31/2 33/2	44815.500

Table 4.7 (Continued)

Transition				Observed
F_1'	F'	- F_1''	F"	Frequency
$19_{0\ 19}$		- $18_{1\ 18}$		
39/2	39/2	- 37/2	37/2	49807.225
39/2	37/2	- 37/2	35/2	49807.472
39/2	41/2	- 37/2	39/2	49807.472
37/2	37/2	- 35/2	35/2	49809.219
37/2	35/2	- 35/2	33/2	49809.465
37/2	39/2	- 35/2	37/2	49809.465
41/2	41/2	- 39/2	39/2	49833.029
41/2	39/2	- 39/2	37/2	49833.294
41/2	43/2	- 39/2	41/2	49833.294
35/2	35/2	- 33/2	33/2	49836.161
35/2	33/2	- 33/2	31/2	49836.434
35/2	37/2	- 33/2	35/2	49836.434

Table 4.8

Observed hyperfine transition frequencies in (MHz) of $^{81}Br^{14}NCO$ b-type transitions

Transition F_1' F' - F_1'' F''	Observed Frequency
$13_{1\ 12}$ - $13_{0\ 13}$	
27/2 27/2 - 27/2 27/2	44338.456
27/2 25/2 - 27/2 25/2	44338.837
27/2 29/2 - 27/2 29/2	44338.837
25/2 25/2 - 25/2 25/2	44341.686
25/2 23/2 - 25/2 23/2	44342.092
25/2 27/2 - 25/2 27/2	44342.092
29/2 29/2 - 29/2 29/2	44372.756
29/2 27/2 - 29/2 27/2	44373.136
29/2 31/2 - 29/2 31/2	44373.136
23/2 23/2 - 23/2 23/2	44375.607
23/2 21/2 - 23/2 21/2	44376.013
23/2 25/2 - 23/2 25/2	44376.013
$14_{1\ 13}$ - $14_{0\ 14}$	
29/2 29/2 - 29/2 29/2	45198.579
29/2 27/2 - 29/2 27/2	45198.960
29/2 31/2 - 29/2 31/2	45198.960
27/2 27/2 - 27/2 27/2	45203.706
27/2 25/2 - 27/2 25/2	45204.090
27/2 29/2 - 27/2 29/2	45204.090
31/2 31/2 - 31/2 31/2	45232.888
31/2 29/2 - 31/2 29/2	45233.303
31/2 33/2 - 31/2 33/2	45233.303
25/2 25/2 - 25/2 25/2	45237.646
25/2 23/2 - 25/2 23/2	45238.045
25/2 27/2 - 25/2 27/2	45238.045
$15_{1\ 14}$ - $15_{0\ 15}$	
31/2 31/2 - 31/2 31/2	46131.887
31/2 29/2 - 31/2 29/2	46132.265
31/2 33/2 - 31/2 33/2	46132.265
29/2 29/2 - 29/2 29/2	46135.540
29/2 27/2 - 29/2 27/2	46135.950
29/2 31/2 - 29/2 31/2	46135.950
33/2 33/2 - 33/2 33/2	46166.433
33/2 31/2 - 33/2 31/2	46166.830
33/2 35/2 - 33/2 35/2	46166.830
27/2 27/2 - 27/2 27/2	46169.751
27/2 25/2 - 27/2 25/2	46170.171
27/2 29/2 - 27/2 29/2	46170.171

Table 4.8 (Continued)

Transition				Observed
F_1'	F'	- F_1''	F"	Frequency
$16_{1\ 15}$		- $16_{0\ 16}$		
33/2	33/2	- 33/2	33/2	47140.884
33/2	31/2	- 33/2	31/2	47141.290
33/2	35/2	- 33/2	35/2	47141.290
31/2	31/2	- 31/2	31/2	47144.231
31/2	29/2	- 31/2	29/2	47144.625
31/2	33/2	- 31/2	33/2	47144.625
35/2	35/2	- 35/2	35/2	47175.688
35/2	33/2	- 35/2	33/2	47176.091
35/2	37/2	- 35/2	37/2	47176.091
29/2	29/2	- 29/2	29/2	47178.762
29/2	27/2	- 29/2	27/2	47179.153
29/2	31/2	- 29/2	31/2	47179.153
$17_{1\ 16}$		- $17_{0\ 17}$		
35/2	35/2	- 35/2	35/2	48227.944
35/2	33/2	- 35/2	33/2	48228.317
35/2	37/2	- 35/2	37/2	48228.317
33/2	33/2	- 33/2	33/2	48231.028
33/2	31/2	- 33/2	31/2	48231.480
33/2	35/2	- 33/2	35/2	48231.480
37/2	37/2	- 37/2	37/2	48263.076
37/2	35/2	- 37/2	35/2	48263.497
37/2	39/2	- 37/2	39/2	48263.497
31/2	31/2	- 31/2	31/2	48265.959
31/2	29/2	- 31/2	29/2	48266.369
31/2	33/2	- 31/2	33/2	48266.369
$18_{1\ 17}$		- $18_{0\ 18}$		
37/2	37/2	- 37/2	37/2	49395.589
37/2	35/2	- 37/2	35/2	49395.985
37/2	39/2	- 37/2	39/2	49395.985
35/2	35/2	- 35/2	35/2	49398.620
35/2	33/2	- 35/2	33/2	49399.015
35/2	37/2	- 35/2	37/2	49399.015
39/2	39/2	- 39/2	39/2	49431.171
39/2	37/2	- 39/2	37/2	49431.572
39/2	41/2	- 39/2	41/2	49431.572
33/2	33/2	- 33/2	33/2	49433.866
33/2	31/2	- 33/2	31/2	49434.286
33/2	35/2	- 33/2	35/2	49434.286

Table 4.8 (Continued)

Transition F_1'	F'	-	F_1''	F''	Observed Frequency
$20_{1\ 19}$		-	$20_{0\ 20}$		
41/2	41/2	-	41/2	41/2	51982.974
41/2	39/2	-	41/2	39/2	51983.420
41/2	43/2	-	41/2	43/2	51983.420
43/2	43/2	-	43/2	43/2	52019.489
43/2	41/2	-	43/2	41/2	52019.918
43/2	45/2	-	43/2	45/2	52019.918
37/2	37/2	-	37/2	37/2	52021.875
37/2	35/2	-	37/2	35/2	52022.301
37/2	39/2	-	37/2	39/2	52022.301
$14_{0\ 14}$		-	$13_{1\ 13}$		
27/2	25/2	-	25/2	23/2	24515.015
27/2	29/2	-	25/2	27/2	24515.015
31/2	29/2	-	29/2	27/2	24534.838
31/2	33/2	-	29/2	31/2	24534.838
25/2	23/2	-	23/2	21/2	24539.391
25/2	27/2	-	23/2	25/2	24539.391
$15_{0\ 15}$		-	$14_{1\ 14}$		
31/2	29/2	-	29/2	27/2	29382.176
31/2	33/2	-	29/2	31/2	29382.176
29/2	27/2	-	27/2	25/2	29385.379
29/2	31/2	-	27/2	29/2	29385.379
33/2	33/2	-	31/2	31/2	29404.897
33/2	31/2	-	31/2	29/2	29405.129
33/2	35/2	-	31/2	33/2	29405.129
27/2	27/2	-	25/2	25/2	29409.124
27/2	25/2	-	25/2	23/2	29409.377
27/2	29/2	-	25/2	27/2	29409.377
$16_{0\ 16}$		-	$15_{1\ 15}$		
33/2	33/2	-	31/2	31/2	34284.843
33/2	31/2	-	31/2	29/2	34285.101
33/2	35/2	-	31/2	33/2	34285.101
31/2	31/2	-	29/2	29/2	34289.066
31/2	29/2	-	29/2	27/2	34289.307
31/2	33/2	-	29/2	31/2	34289.307
35/2	35/2	-	33/2	33/2	34307.549
35/2	33/2	-	33/2	31/2	34307.818
35/2	37/2	-	33/2	35/2	34307.818
29/2	29/2	-	27/2	27/2	34312.372
29/2	27/2	-	27/2	25/2	34312.628
29/2	31/2	-	27/2	29/2	34312.628

Table 4.8 (Continued)

Transition F_1'	F'	-	F_1''	F''	Observed Frequency
$17_{0\ 17}$		-	$16_{1\ 16}$		
35/2	35/2	-	33/2	33/2	39217.392
35/2	33/2	-	33/2	31/2	39217.659
35/2	37/2	-	33/2	35/2	39217.659
33/2	33/2	-	31/2	31/2	39219.118
33/2	31/2	-	31/2	29/2	39219.365
33/2	35/2	-	31/2	33/2	39219.365
37/2	37/2	-	35/2	35/2	39239.819
37/2	35/2	-	35/2	33/2	39240.106
37/2	39/2	-	35/2	37/2	39240.106
31/2	31/2	-	29/2	29/2	39242.507
31/2	29/2	-	29/2	27/2	39242.779
31/2	33/2	-	29/2	31/2	39242.779
$18_{0\ 18}$		-	$17_{1\ 17}$		
37/2	37/2	-	35/2	35/2	44176.713
37/2	35/2	-	35/2	33/2	44176.950
37/2	39/2	-	35/2	37/2	44176.950
35/2	35/2	-	33/2	33/2	44178.596
35/2	33/2	-	33/2	31/2	44178.845
35/2	37/2	-	33/2	35/2	44178.845
39/2	39/2	-	37/2	37/2	44198.763
39/2	37/2	-	37/2	35/2	44199.018
39/2	41/2	-	37/2	39/2	44199.018
33/2	33/2	-	31/2	31/2	44201.493
33/2	31/2	-	31/2	29/2	44201.780
33/2	35/2	-	31/2	33/2	44201.780
$19_{0\ 19}$		-	$18_{1\ 18}$		
37/2	37/2	-	35/2	35/2	49161.454
37/2	35/2	-	35/2	33/2	49161.708
37/2	39/2	-	35/2	37/2	49161.708
41/2	41/2	-	39/2	39/2	49181.244
41/2	39/2	-	39/2	37/2	49181.480
41/2	43/2	-	39/2	41/2	49181.480
35/2	35/2	-	33/2	33/2	49183.806
35/2	33/2	-	33/2	31/2	49184.084
35/2	37/2	-	33/2	35/2	49184.048

4.7 The Structure of BrNCO

The structural information that can be derived from BrNCO is somewhat limited because rotational constants were measured for only two isotopic species: ^{79}BrNCO and ^{81}BrNCO. However some reasonable deductions can be made.

The inertial defect, which is the same for both isotopes, is a small, positive number (see Tables 4.3 and 4.4). This implies that BrNCO is planar (see section 2.5). Furthermore, the ratios of the out of plane quadrupole coupling constants χ_{cc} (^{81}BrNCO) / χ_{cc}(^{79}BrNCO) = 0.835. This is close to the ratio of the quadrupole moments of the bromine atoms (0.8354) which supports the conclusion that BrNCO is planar.

Table 4.9

Bromine Quadrupole Coupling Constants in Principal Inertial Axes

	^{79}BrNCO	^{81}BrNCO
χ_{aa} (MHz)	608.41(52)	508.49(52)
χ_{bb} (MHz)	-164.16(26)	-137.59(26)
χ_{cc} (MHz)	-444.25(26)	-370.90(26)

The ^{14}N quadrupole coupling constants are consistent with the configuration BrNCO rather than BrOCN. If the structure were BrOCN, the C-N bond would probably be a principal axis in the

nitrogen quadrupole tensor. In this case χ_{zz} would be ≃ -4 MHz (15). Assuming cylindrical symmetry χ_{cc} would therefore be ≃ 2 MHz. Even with a large asymmetry about the C-N bond, χ_{cc} would still be expected to be positive. Table 4.10 shows that χ_{cc} for both isotopes is in fact negative, hence the configuration is probably BrNCO.

Table 4.10

^{14}N Quadrupole Coupling Constants in Principal Inertial Axes

	^{79}BrNCO	^{81}BrNCO
χ_{aa} (MHz)	5.09(78)	4.75(51)
χ_{bb} (MHz)	-1.64(39)	-1.41(26)
χ_{cc} (MHz)	-3.45(39)	-3.33(26)

A least squares fit was used to fit the rotational constants to the structural parameters. Because of the limited number of constants available, some of the structural parameters had to be held fixed. The N-C and C-O bond lengths were held fixed at their values in ClNCO(4). This is a reasonable assumption because these parameters do not change very much within the group of isocyanate molecules whose structures have been determined (16,17). The N-C-O angle was held fixed at values varying between 9.13° as in ClNCO, and 0° which corresponds to a linear NCO group. Three fits were done to determine values for the Br-N bond length and the Br-N-C angle. The resulting

Table 4.11

Structural parameters of bromine isocyanate

	I	II	III
r(Br-N)/Å	1.836	1.847	1.863
r(N-C)[1]/Å	1.225	1.225	1.225
r(C-O)[1]/Å	1.162	1.162	1.162
<(BrNC)	121.59°	119.44°	116.74°
<(NCO)[2]	0°	4°	9.13°
<(Br-N-a)[3]	28.5°	28.65°	28.8°

[1] Value fixed at that of ClNCO (5).

[2] Value fixed for each structural determination.

[3] Angle between Br-N bond and a-inertial axis.

parameters are shown in Table 4.11.

Table 4.12 shows some comparisons with other molecules. The BrNC angle is reasonable when compared with the ClNC angle in ClNCO. Also, the Br-N bond length agrees well with the Br-N bond lengths in other molecules.

For a more definitive structural derivation, moments of inertia of other isotopic species of BrNCO will have to be determined. The configuration of BrNCO relative to its principal inertial axes is shown in Figure 4.7.

Table 4.12

Comparison of Structural Parameters of BrNCO With Values in Other Molecules

	r(Br-N)(Å)	
	BrNCO[1]	1.85
	$CH_3C(O)NHBr$ (18)	1.82
	$C_6H_5C(O)NHBr$ (19)	1.82
	$BrN(COCH_2)_2$ (19)	1.84
	BrNO (11)	2.14
	Sum of single bond radii (20)	1.84
	<(XNC)	
	BrNCO[1]	119°
	ClNCO(4,5)	118°

[1]Values taken from Structure II

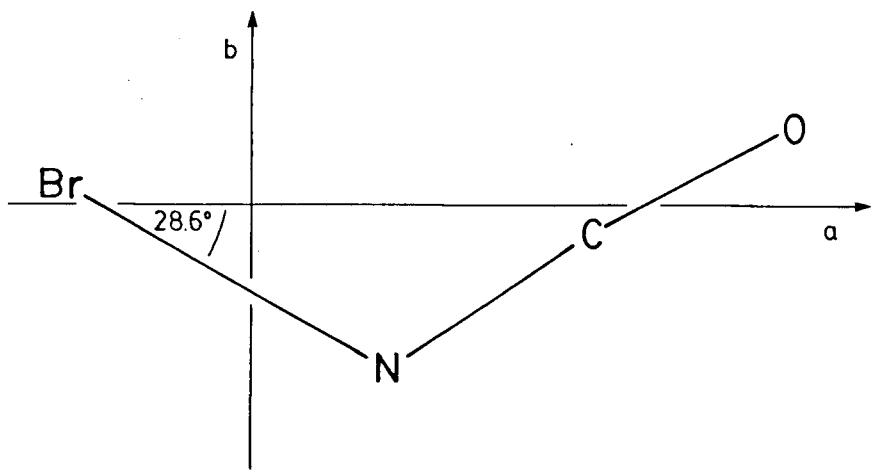

Figure 4.7 The atoms of BrNCO in its principal inertial axis system according to structure II (Table 4.11).

4.8 Br and ^{14}N Quadrupole Coupling

The quadrupole coupling constants of a nucleus in a molecule contain information about the distribution of charges in the molecule; therefore something can be learned about the nature of the chemical bonding involved.

First, however, the quadrupole coupling constants in the inertial axis system need to be transformed into the principal quadrupole axes system. The measurement of χ_{ab} has enabled us to do this. For a planar molecule this unitary transformation is:

$$\chi' = U \chi U^{-1}$$

$$\chi^1 = \begin{bmatrix} \chi_{zz} & 0 & 0 \\ 0 & \chi_{xx} & 0 \\ 0 & 0 & \chi_{yy} \end{bmatrix}$$

$$\chi = \begin{bmatrix} \chi_{aa} & \chi_{ab} & 0 \\ \chi_{ab} & \chi_{bb} & 0 \\ 0 & 0 & \chi_{cc} \end{bmatrix}$$

$$U = \begin{bmatrix} \cos\theta_{za} & \sin\theta_{za} & 0 \\ -\sin\theta_{za} & \cos\theta_{za} & 0 \\ 0 & 0 & 1 \end{bmatrix} \qquad (4.3)$$

where θ_{za} is the angle between the a-inertial axis and the z-principal quadrupole axis, and χ_{zz}, χ_{xx} and χ_{yy} are the principal values of the bromine quadrupole coupling tensor. The y-axis is defined to be perpendicular to the plane of the

molecule.

The resulting equations are:

$$\chi_{zz} = \chi_{aa}\cos^2\theta_{za} + 2\chi_{ab}\cos\theta_{za}\sin\theta_{za} + \chi_{bb}\sin^2\theta_{za}$$
$$\chi_{xx} = \chi_{aa}\sin^2\theta_{za} - 2\chi_{ab}\cos\theta_{za}\sin\theta_{za} + \chi_{bb}\cos^2\theta_{za}$$
$$\chi_{yy} = \chi_{cc} \qquad (4.4)$$

For many molecules χ_{ab} is not determined. However, χ_{zz} and χ_{xx} can still be calculated using the quadrupole coupling constants of isotopically substituted molecules, or by assuming that the principal quadrupole axis lies along the bond containing the quadrupole nucleus giving a value for θ_{za}. However, in BrNCO, χ_{ab} is well-determined and θ_{za} can be calculated from the relationship:

$$\tan 2\theta_{za} = \frac{2\chi_{ab}}{\chi_{aa} - \chi_{bb}} \qquad (4.5)$$

Comparison of θ_{za} with the angle between the bromine-nitrogen bond axis and the a-axis shows that the z-axis does indeed lie along the bond axis (see Table 4.11). The $\simeq 1°$ difference is probably not significant but further refinement of the structural parameters is required to confirm this.

The principal values of the bromine quadrupole coupling tensor are given in Table 4.13.

The interpretation of these quadrupole coupling constants in terms of the type of chemical bonding between the bromine and

Table 4.13

Principal Values of the Bromine Quadrupole Coupling Tensor

	^{79}BrSCN	^{81}BrSCN
χ_{zz} (MHz)	893.95(46)[1]	746.41(46)
χ_{xx} (MHz)	-449.70(36)	-375.51(31)
χ_{yy} (MHz)	-444.25(26)	-370.90(26)
θ_{za} (deg)[2]	27.45(1)	27.42(1)

[1] Uncertainties are one standard deviation in units of the last significant figures.

[2] θ_{za} is the angle between the z-principal quadrupole axis in the a-inertial axis.

nitrogen nuclei requires that several assumptions are made, such as neglect of orbital overlap, and s and p orbital hybridization. Derived quantities such as ionic bond character should not be taken to be exact, but rather as indications of the relative contributions of each possible resonance form.

One of the main assumptions is that the partially filled p orbitals are primarily responsible for the electric field gradients around a quadrupolar nucleus (7). These field gradients can therefore be related to the number or fractional number of electrons in the valence p orbitals. The equations of Townes and Dailey (7) are:

$$\chi_{gg} = eQq_g = -(U_p)_g \, eQq_{n\,l\,m} \qquad g = x, y, z \qquad (4.6)$$

$$(U_p)_x = \tfrac{1}{2}(n_y+n_z) - n_x$$

$$(U_p)_y = \tfrac{1}{2}(n_z+n_x) - n_y$$

$$(U_p)_z = \tfrac{1}{2}(n_x+n_y) - n_z \qquad (4.7)$$

n_x, n_y and n_z represent the number of electrons in the p_x, p_y and p_z orbitals.

For a single bromine atom $q_{n\,l\,m} = q_{4\,1\,0} = -q_z$ and $q_x = q_y = -1/2q_z$.

When the bromine atom is bound to another atom, the electric field gradients about the nucleus are modified, so that comparisons of experimental quadrupole coupling constants with those of a free bromine atom will give some measure of the type of bond involved, e.g. the degree of π bonding or the ionic or covalent character.

The three most likely resonance forms contributing to the overall structure of BrNCO are:

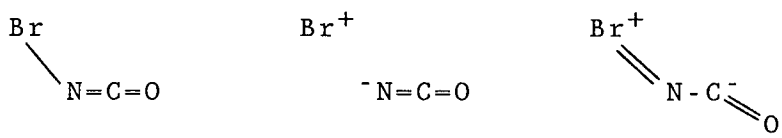

I II III

Form III shows a resonance form of BrNCO with an out-of-plane π bond between the Br and N nuclei. The difference in χ_{xx} and χ_{yy} is directly related to the number or fractional number of electrons lost from Br as a result of π bonding. The double bond character is denoted π and is given by (20):

$$\pi = \frac{2(\chi_{xx} - \chi_{yy})}{3\ eQq_{Br}} \qquad (4.8)$$

π also represents the fractional contribution of form III to the

overall structure of BrNCO. χ_{xx} and χ_{yy} are very close; $\pi \simeq 0.5\%$ implying that the Br-N bond is essentially cylindrically symmetric.

In ClNCO the amount of π character was calculated to be $\simeq 4\%$ from the chlorine quadrupole coupling constants (4). The resonance form for π bonding in ClNCO is

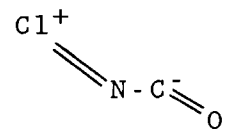

This is consistent with the 9.13° bend in the NCO group in ClNCO with the O atom trans to the Cl atom. The NCO group may be closer to being linear in BrNCO but no conclusions can be drawn before a further structural investigation is carried out.

A measure of the ionic character of the Br-N bond can be calculated using the Valence Bond theory proposed by Townes and Dailey. The weighted contributions of all possible resonance structures are considered. Here only forms I and II need to be considered; the contribution of form III may be neglected. Form II representing a totally ionic BrNCO is shown with the positive pole on the bromine atom since $|\chi_{zz}| > |\chi_{Br}|$. The contribution of this resonance structure is i and that of form I is (1-i). The p orbital populations of each of these structures are:

$$\begin{aligned} &\text{I} \quad n_x = n_y = 2 \; ; \; n_z = 1 \qquad (U_p)_z = 1 \\ &\text{II} \quad n_x = n_y = 2 \; ; \; n_z = 0 \qquad (U_p)_z = 2 \end{aligned} \tag{4.9}$$

The ionic character is obtained from:

$$\chi_{zz} = eQq_{Br} [(1-i) + 2i(1+\epsilon)] \qquad (4.10)$$

The contribution of form II must be multiplied by a factor $(1+\epsilon)$ to account for the decreased screening effect at the Br nucleus by the electrons. $\epsilon = 0.15$ for the halogens (22).

In BrNCO i $\simeq$ 12% and the single bond character $\simeq$87%. The ionic character of BrNCO is larger than in ClNCO which agrees with the lower electronegativity of Br compared to Cl.

It must be emphasized that the calculated contribution of each of the resonance structures is only very rough in view of the approximations made.

An attempt was made to reproduce the experimentally evaluated ^{14}N quadrupole coupling constants using a theoretical calculation. A modified CNDO calculation (CNDO/BW) was used to estimate the populations of the 2p orbitals of nitrogen along the direction of each of the inertial axes. These populations were then used in equations 4.6 and 4.7 to calculate the nitrogen quadrupole coupling constants. $eQq_{210}(^{14}N)$ = -10MHz (23). The theoretical p-orbital populations are: $n_a = 0.8770$; $n_b = 1.3553$; $n_c = 1.6776$. A comparison of the experimental and theoretical nitrogen quadrupole coupling constants are given in Table 4.14.

The theoretical calculations reproduce the experimentally determined values only moderately well. This may be because Br

Table 4.14

Comparison of experimentally determined ^{14}N quadrupole coupling constants with values calculated using theoretical calculations

	Experimental		Theoretical
	^{79}BrNCO	^{81}BrNCO	
χ_{aa} (MHz)	5.09(78)	4.75(51)	6.39
χ_{bb} (MHz)	-1.64(39)	-1.42(26)	-0.78
χ_{cc} (MHz)	-3.45(39)	-3.33(26)	-5.61

and N have similar electronegativities, demonstrating the need for improved theoretical calculations, particularly when dealing with molecules containing heavy atoms such as bromine.

4.9 Discussion

This is the first detailed analysis of a spectrum of bromine isocyanate in the gas phase, aside from the photoelectron study (3). Unfortunately only three of the five quartic centrifugal distortion constants and one sextic centrifugal distortion constant could be measured, partly because the b-type transitions were very weak which prevented any branches other than the $K_a = 1 \leftarrow 0$ R and Q branches to be measured.

This analysis, however, has amply demonstrated the worth of our global least-squares fitting procedure. For the first time an accurate value of A_o has been evaluated solely from the

analysis of a-type R branch transitions. This method has the potential to be applied to a large number of other molecules, although its application is restricted to molecules containing nuclei with large quadrupole moments (eg Br and I), with the additional limitation that θ_{za} lies between ≃20° and 70°. The precision of the constants derived using this method will be dependent on the number of near-degeneracies of the correct symmetry.

Several vibrational satellites were observed in the spectrum of BrNCO. Relative intensity measurements provide an estimate of the lowest vibrational frequency of BrNCO at ≃ 116 ± 40 cm^{-1}. This is probably the Br-N-C in plane bending vibration. The inertial defect (see Section 2.5) was also used to calculate this frequency at ≃ 168cm^{-1} which is slightly higher than the intensity measurements.

A partial r_o structure has also been determined for BrNCO. More isotopic data will be required to obtain a full substitution structure. Also, because the infra-red data (2) are incomplete, and only three out of five quartic centrifugal distortion constants have been determined in this study for each isotope, there are insufficient data to make a force-field determination for this molecule, which would enable an r_z structure to be calculated.

Finally, an analysis of the quadrupole coupling constants of BrNCO has shown the Br-N bond to be covalent, with a small amount of ionic character.

Bibliography

1. W. Gottardi, Angew Chem. Intl. Ed. 10, 416, (1971).

2. W. Gottardi, Monatsh. 103, 1150-1157, (1973).

3. D.C. Frost, C.B. MacDonald, C.A. McDowell, N.P.C. Westwood, Chem. Phys. 47, 111-124 (1980).

4. W.H. Hocking, M.C.L. Gerry, J. Mol. Spectrosc. 42, 547-566 (1972).

5. W.H. Hocking, M.L. Williams, M.C.L. Gerry, J. Mol. Spectrosc. 58, 250-260 (1975).

6. D.J. Millen, D. Mitra, Trans Faraday Soc., 66, 2414-2419 (1970).

7. W. Gordy, R.L. Cook, "Microwave Molecular Spectra," 3rd. ed., in "Techniques of Chemistry" (A Weissberger, Ed.), Vol. 18, pp. 725-802, Wiley, New York, 1984.

8. See for example C. Flanagan, L. Pierce, J. Chem. Phys. 38, 2963-2969, (1963); W. Gordy, J.W. Simmons, A.G. Smith, Phys. Rev. 74, 243-249, (1948).

9. M.C.L. Gerry, W. Lewis - Bevan, N.P.C. Westwood, J. Chem. Phys. 79, 4655-4663, (1983).

10. J.A. Howe, J. Chem. Phys. 34, 1247-1249, (1961).

11. R.A. Beaudet, J. Chem. Phys. 50, 2002-2011 (1969).

12. R.D. Brown, P.D. Godfrey, R. Champion, D. McNaughton, J. Am. Chem. Soc. 103, 5715-5719, (1981).

13. H.P. Benz, A. Bauder, Hs. H. Gunthard, J. Mol. Spectrosc. 21, 156-164 (1966).

14. R. Kewley, K.V.L.N. Sastry, M. Winnewisser, J. Mol. Spectrosc. 10, 418-441, (1963).

15. W.B. Moniz, H.S. Gutowsky, J. Chem. Phys. 38, 1155-1162, (1963).

16. K. Yamada, J. Mol. Spectrosc. 79, 323-344 (1980).

17. H. Oberhammer, K. Seppett, R. Mews, J. Mol. Struct. 101, 325-331, (1983).

18. R.J. Dubey, Acta Cryst, B. 27, 23-25 (1971).

19. O. Jabey, H. Pritzow, J. Jander, Z. Naturforsch. 32b, 1416-1420, (1977).

20. L. Pauling. "The Chemical Bond." Cornell University Press, Ithaca, New York, 1960.

21. J.H. Goldstein, J. Chem Phys. 24, 106-109 (1956).

22. C.H. Townes, A.L. Schawlow, "Microwave Spectroscopy", pp. 225-247, McGraw Hill Inc., New York, (1955).

23. E.A.C. Lucken, Trans. Faraday Soc., 57, 729-734, (1961).

CHAPTER V: THE MICROWAVE SPECTRUM OF IODINE ISOCYANATE, INCO

5.1 Introduction

Iodine isocyanate is the next in the series of halogen isocyanates. After the success in using the least-squares fitting procedure to determine simultaneously the rotational, centrifugal distortion and quadrupole coupling constants of BrNCO, it was decided to apply the same method to INCO. INCO is expected to have a similar structure to BrNCO and ClNCO, and therefore should also be a near-symmetric prolate rotor. Also, because iodine is a relatively heavy atom it should have a predominately strong a-type R branch spectrum and this, coupled with the fact that the iodine nucleus has a large quadrupole moment, means that INCO is an ideal candidate for the method used to analyse the spectrum of BrNCO.

The preparation of INCO in solution was first reported in the 1930's by Birckenbach and Linhard (1). Since then it has commonly been used in solution as a reagent undergoing electrophilic stereospecific trans addition to alkenes:

$$\mathrm{INCO} + {>}\mathrm{C} = \mathrm{C}{<} \rightarrow \quad -\underset{\mathrm{I}}{\overset{|}{\mathrm{C}}}-\overset{\mathrm{NCO}}{\overset{|}{\mathrm{C}}}- \qquad (5.1)$$

INCO can be generated in situ as a reaction intermediate in an ether solution containing iodine, silver cyanate and an unsaturated compound. It is, however, sufficiently stable that it can be used from a preformed solution. The reaction between

INCO and alkenes produces iodoisocyanates which can then be treated to form a variety of molecules containing C-N bonds e.g. carbamates, ureas and amine hydrochlorides (2). Other uses of INCO in solution include the modification of unsaturated polymers (3) and the oxidative addition of INCO to organometallic complexes (4).

The only previous report of INCO in the gaseous phase was of its He(I) photoelectron spectrum (5), where it was prepared in a flow system by a method similar to the preparation of BrNCO. The photoelectron spectra of ClNCO, BrNCO and INCO are all similar, and it therefore seems likely that INCO will have a similar structure to the other halogen isocyanates.

5.2 Experimental Methods

Iodine isocyanate was prepared by passing I_2 vapour at a pressure of ≃30 mTorr over silver cyanate at 150-190°C.

$$I_{2(g)} + AgNCO_{(s)} \rightarrow INCO_{(g)} + AgI_{(s)} \qquad (5.2)$$

The silver cyanate, which was prepared as in section 4.2, had previously been dried by heating the sample to ≃150°C for ≃24 hours. This is crucial because INCO appears to be even more susceptible to hydrolysis than BrNCO. However, despite careful drying, the products of hydrolysis, NH_3 and HNCO, were observed initially. INCO was generated in a flow system, but it is sufficiently stable that it could be kept in the microwave cell

for several minutes without a noticeable decrease in the intensity of the spectrum. To resolve the nitrogen hyperfine splitting in the b-type Q branch transitions, the cell was cooled slightly using dry ice, although care had to be taken as INCO condenses at dry ice temperatures. All other measurements were made at room temperature.

5.3 Analysis of a-type Transitions

Initial estimates of the rotational constants were made using the bond lengths and angles transferred from ClNCO(6,7), as well as the I-N bond length in IN_3(8). The estimated constants predicted INCO to be a near-symmetric prolate rotor with the possibility of both a- and b-type transitions. The quadrupole coupling constants for ^{127}I were estimated by assuming that the ratio of χ_{zz} for I in INCO to χ_{zz} for Br in BrNCO is the same as the ratio of the quadrupole moments of the nuclei. The I-N bond was initially taken to be cylindrically symmetric.

As for BrNCO, the initial observation of the microwave spectrum of INCO was of a series of strong a-type R branch transitions. Figure 5.1 shows a typical a-type R branch group ($J = 9 \leftarrow 8$). The asymmetry split $K_a = 1$ transitions are easily distinguished on either side of the main group of lines, both for the ground state and for at least four excited vibrational states. The $K_a = 0$ lines were much more difficult to identify because many of them are partially overlapped by other lines.

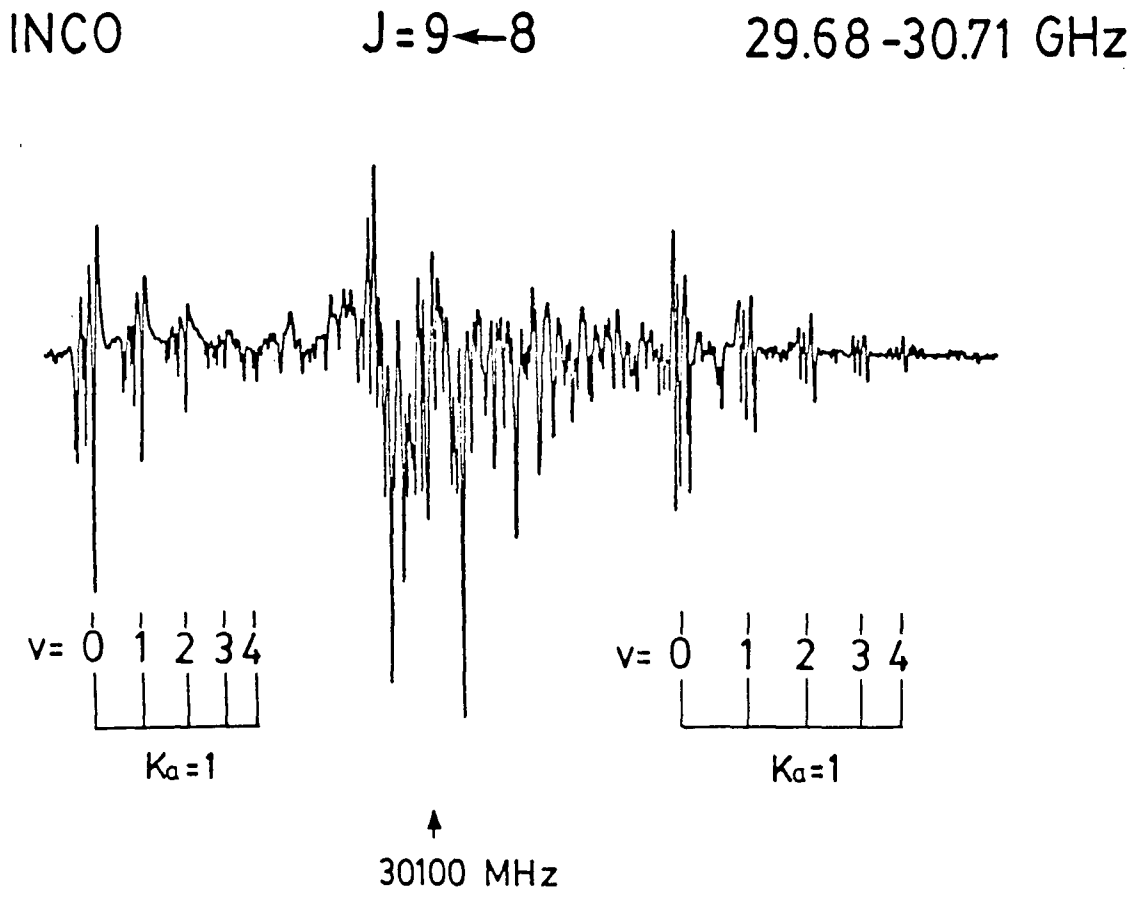

Figure 5.1 Broadband scan of the J = 9 ← 8 a-type R branch of INCO in the frequency range 29.68 - 30.71 GHz. The K_a = 1 transitions for the ground state and for four excited vibrational states are indicated.

Also, because ^{127}I has a spin of 5/2, each transition showed quadrupole hyperfine splitting with 6 strong components, many of which appeared to be significantly perturbed. No hyperfine splitting due to the nitrogen nucleus was observed in the a-type transitions.

Assignments were made on a trial and error basis for some of the less perturbed $K_a = 1$ and $K_a = 0$ lines, as well as the more highly perturbed transition $12_{0,12} - 11_{0,11}$. The hyperfine components of this transition were perturbed by as much as 49 MHz to lower frequency but were not overlapped by other lines. It is shown in Figure 5.2. Using the same method that was used to fit the a-type R-branches of BrNCO, the initial assignments were put into a least squares fit to simultaneously determine the rotational and I quadrupole coupling constants. The perturbations in the hyperfine structure allowed values of A_o and χ_{ab} to be determined along with B_o, C_o, χ_{aa} and $\chi_{bb}-\chi_{cc}$. These constants were then used to predict and assign further a-type lines with $K_a = 0$ and $K_a = 1$ for J between 5 and 15 in the range 18-54 GHz. No assignments for transitions with $K_a > 1$ could be made because of the overlapping hyperfine structure.

The two requirements for the success of the least squares fitting programme in finding accurate values of A_o from a-type R branches are met in INCO. The first, that is the requirement that χ_{ab} should be large, is met because the quadrupole moment of the nucleus is large and the angle between the principal quadrupolar z-axis and the inertial a-axis is $\approx 24°$ (see section

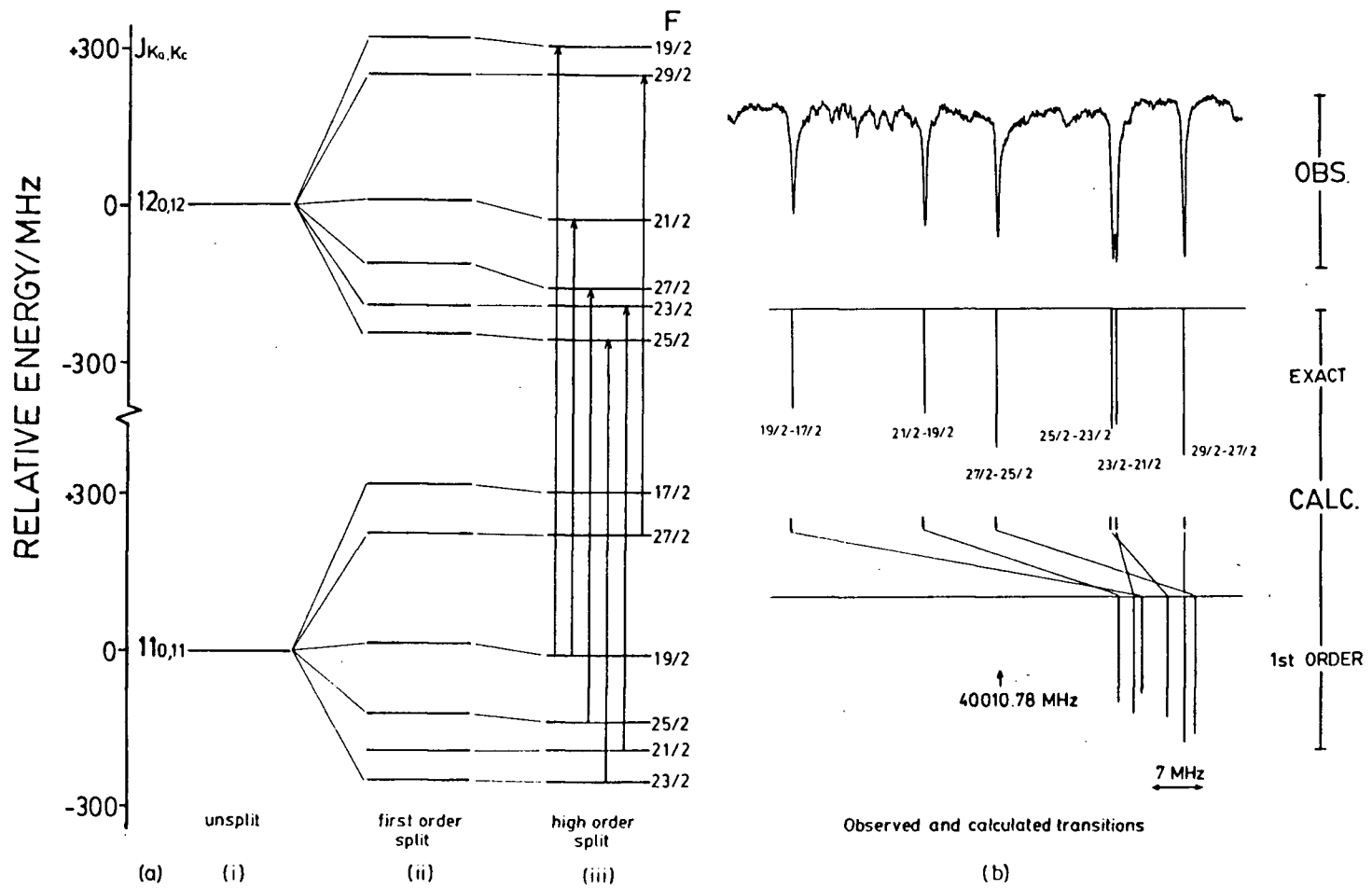

Figure 5.2 The $12_{0,12}$ - $11_{0,11}$ transitions of INCO. (a) The associated energy levels are shown: (i) the hypothetical unsplit rotational energies; (ii) the predicted first order I quadrupole energy levels; (iii) the I quadrupole energy levels derived from the exact Hamiltonian. (b) The observed transitions are compared with the calculated first order and exact Hamiltonian patterns.

5.5). The second condition, which arises because χ_{ab} has only a high-order effect, is that there is a number of near-degeneracies with the appropriate symmetry. Several of these involve rotational energy levels which take part in transitions in the frequency range studied.

An energy level diagram is shown in Figure 5.3. Some of the closest near-degeneracies, which produce the largest perturbations in the hyperfine structure, are indicated; those that involve measured a-type transitions are between $K_a = 0$ and $K_a = 1$ levels. Some hyperfine components were perturbed by relatively large amounts. For $12_{1,11} - 11_{1,10}$ and $13_{0,13} - 12_{0,12}$, these shifts were as large as 100 MHz. From these a-type transitions alone, values for A_o, B_o, C_o, Δ_J, Δ_{JK} and δ_J, as well as for χ_{aa}, $\chi_{bb}-\chi_{cc}$ and χ_{ab} for ^{127}I, were well-determined. These are shown in Table 5.1. The correlation coefficients in Table 5.2 show that all the constants, including A_o and χ_{ab}, are essentially uncorrelated. As in the analysis of the spectrum of BrNCO, an accurate value of A_o was evaluated for INCO solely from a-type R branch transitions. The accuracy of A_o to within one standard deviation is ≈0.5 MHz. This allowed us to predict, with a great deal of accuracy the frequencies of some $K_a = 1 \leftarrow 0$ b-type transitions.

5.4 Analysis of b-type Transitions

R and Q Branch $K_a = 1 \leftarrow 0$ b-type transitions were predicted using the constants in Table 5.1. The accuracy of the

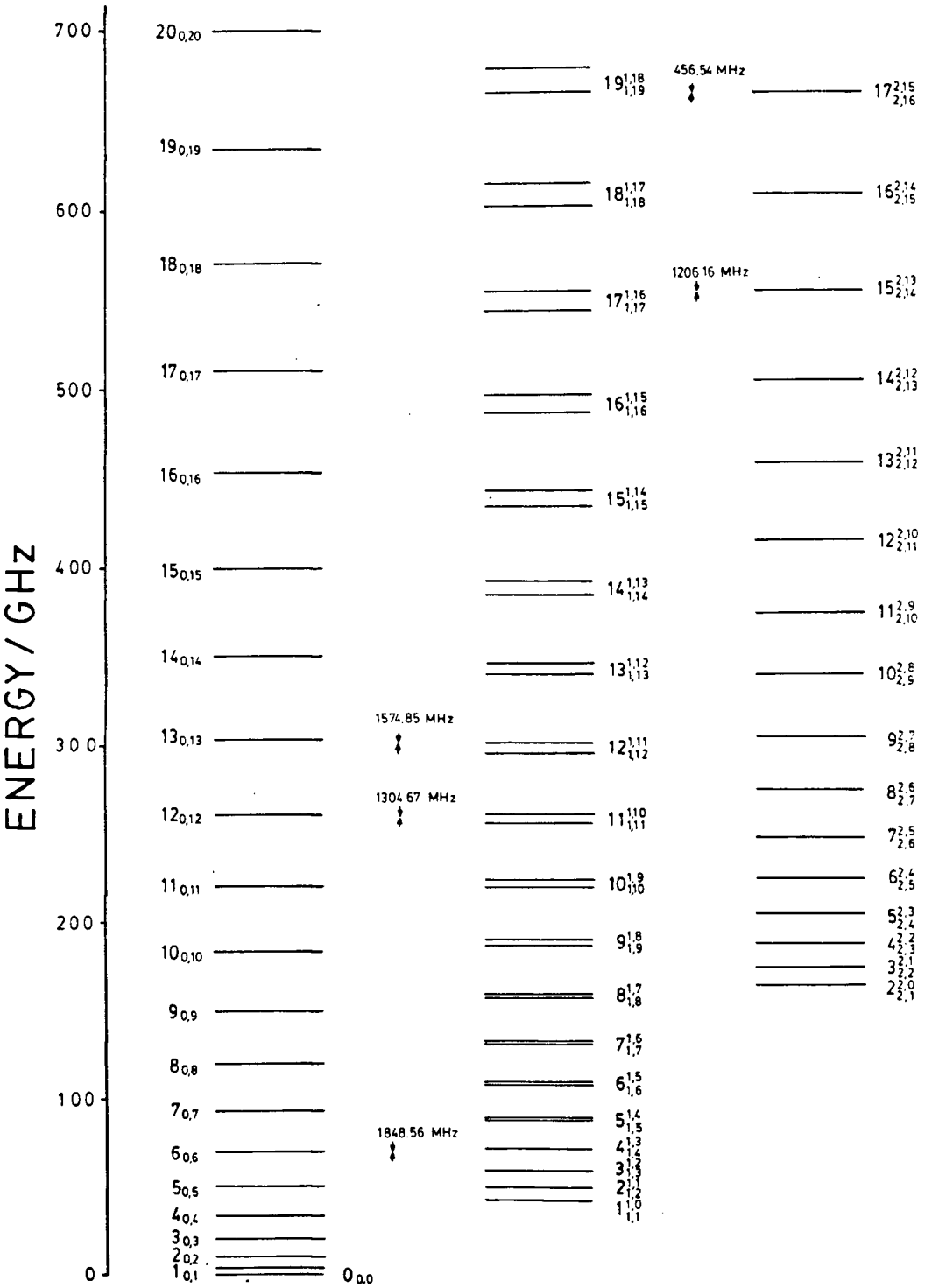

Figure 5.3 The rotational energy levels of INCO showing several important near-degeneracies between (i) K_a = 0 and 1 levels and (ii) K_a = 1 and 2 levels.

Table 5.1

Spectroscopic Constants of ^{127}INCO from a-type transitions only

Parameter	
Rotational Constants (MHz)	
A_o	40591.59(53)[1]
B_o	1704.9870(19)
C_o	1633.9090(17)
Centrifugal Distortion Constants (kHz)	
Δ_J	0.7571(20)
Δ_{JK}	-155.80(45)
δ_J	0.0941(25)
^{127}I Quadrupole Coupling Constants (MHz)	
χ_{aa}	-2235.2(16)
$\chi_{bb}-\chi_{cc}$	- 740.8(40)
χ_{ab}	-1671.95(25)

[1] Numbers in parentheses are one standard deviation in units of the last significant figure.

Table 5.2

Correlation coefficients of the spectroscopic constants of ^{127}INCO calculated from a-type transitions

A_o	1.00							
B_o	0.03	1.00						
C_o	0.12	-0.67	1.00					
Δ_J	0.04	0.43	0.27	1.00				
Δ_{JK}	0.17	0.22	0.13	0.03	1.00			
δ_J	-0.04	0.88	-0.84	-0.14	0.07	1.00		
χ_{aa}	-0.09	-0.04	-0.17	-0.20	-0.05	0.04	1.00	
$\chi_{bb}-\chi_{cc}$	-0.15	0.17	-0.20	-0.05	0.08	0.16	-0.01	1.00
χ_{ab}	-0.42	-0.03	0.06	0.06	-0.04	-0.41	-0.18	0.06 1.00

prediction was limited by the uncertainty in $(\chi_{bb}-\chi_{cc})$. Many of these transitions, which were much weaker than the a-type transitions and difficult to detect, were measured to within a few MHz of the predicted frequencies. Some transitions were not so easily identified from this early prediction because they were overlapped with a-type lines, although their assignments were confirmed after a further refinement of the constants.

There was, however, an obvious anomaly. When the hyperfine components of the transition $17_{1,16}-17_{0,17}$ were included in a least squares fit, which included only those constants that were

used to fit the a-type transitions, the differences between the observed and calculated frequencies were as large as 3 MHz. This was not due to a misassignment because there were no other lines overlapping this transition. However, from the energy level diagram, it was found that the level $17_{1,16}$ was ≃1200 MHz away from the $15_{2,14}$ level. Normally for Δ_K to be determined independently of A_o, transitions with $K_a = 2 \leftarrow 1$ are required. In BrNCO, no such transitions were measured and Δ_K was assimilated into A_o. In INCO, however, because the high-order shifts of the hyperfine components of the $17_{1,16}$ and $15_{2,14}$ levels are critically dependent on the magnitude of the near-degeneracy, they depend not only on the magnitudes of the rotational constants, but also on the magnitudes of the centrifugal distortion constants. Therefore the sizes of the perturbations are dependent on the value of Δ_K. Hence, it was possible that A_o and Δ_K could be separated. When Δ_K was included in the least squares fit, a reasonable value was obtained, and the calculated frequencies for the hyperfine components of the $17_{1,16}$-$17_{0,17}$ transition fell within the r.m.s. error of the observed frequencies.

Δ_K was still highly correlated with A_o. However, the value of Δ_K estimated from $17_{1,16}$-$17_{0,17}$ was used to predict the frequencies of the hyperfine components of the transition $20_{0,20}$-$19_{1,19}$. This is a particularly interesting case. The unsplit energy level difference between $19_{1,19}$ and $17_{2,15}$ is only ≃420 MHz. This is the smallest near-degeneracy involving

transitions in the frequency range studied. The two levels are in fact so close, that of the four F components that interact (i.e. they have the same F value), three of the $19_{1,19}$ levels lie below the corresponding levels of $17_{2,15}$ and are perturbed to lower energy, while the fourth, with F=15/2, lies above and is shifted to higher energy. This is shown in Figure 5.4. With the inclusion of this transition into the least-squares fit, Δ_K was now well-determined and independent of A_o.

Because the ^{14}N quadrupole structure was very small, nitrogen hyperfine splitting could be resolved only for the Q-branch b-type transitions. Using the same method as was used for BrNCO, $\chi_{bb}-\chi_{cc}$ for nitrogen was calculated in a fit using the quadrupole Hamiltonian of 2 nuclei using the coupling scheme: ($J + I_I = F_1$; $F_1 + I_N = F$). χ_{aa} and $\chi_{bb}-\chi_{cc}$ for iodine were held constant along with χ_{aa} for nitrogen which was not determinable from these transitions. It was calculated by assuming that χ_{cc} is the same as the average value of χ_{cc} in ^{79}BrNCO and ^{81}BrNCO. The effects of the ^{14}N quadrupole coupling were subtracted from the b-type Q-branch frequencies before the final values of the other constants were measured.

The final constants, derived from the global least-squares fit to all the measured transitions, both a and b type, are shown in Table 5.3 along with a comparison with the constants measured from a-type lines alone, where Δ_K was assimilated into A_o. Unfortunately, because the number of branches that could be observed was limited, δ_K could not be determined. Table 5.4

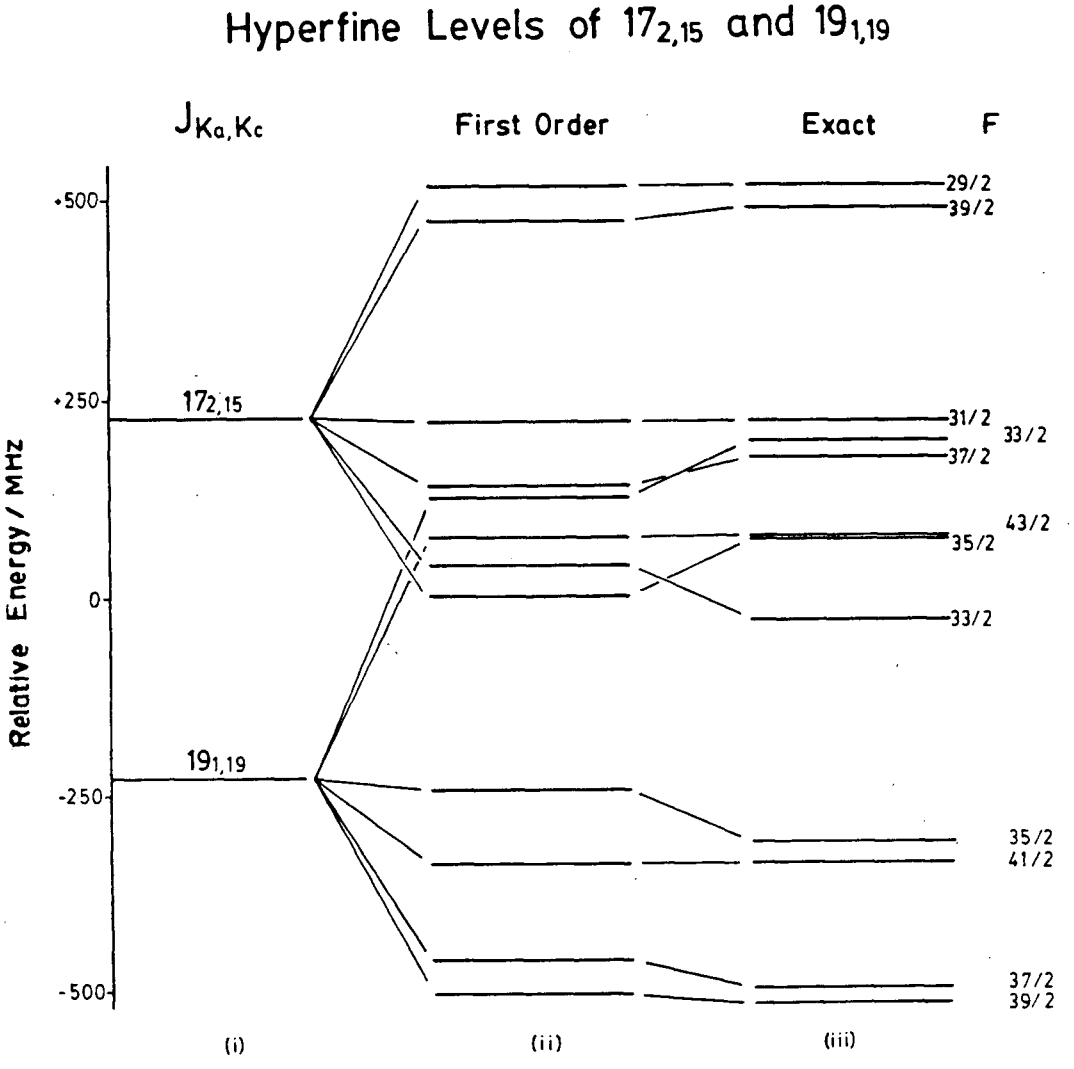

Figure 5.4 The energy levels of $17_{2,15}$ and $19_{1,19}$ of INCO showing

(i) the hypothetical unsplit rotational levels;
(ii) the calculated first order splittings and
(iii) the exact splittings.

For $19_{1,19}$ the levels with F = 35/2, 37/2 and 39/2 are pushed to lower energy by the corresponding levels of $17_{2,15}$, while the level with 33/2 of $19_{1,19}$ is pushed to higher energy.

Table 5.3

Spectroscopic Constants of ^{127}INCO

Parameter	a-Types Only	All Transitions
Rotational Constants (MHz)		
A_o	40591.59(53)[1]	40601.485(33)
B_o	1704.9870(19)	1704.98953(44)
C_o	1633.9090(17)	1633.90600(39)
Centrifugal Distortion Constants (kHz)		
Δ_J	0.7571(20)	0.7526(11)
Δ_{JK}	-155.80(45)	-155.605(79)
Δ_K	-	10948(15)
δ_J	0.0941(25)	0.09695(12)
^{127}I Quadrupole Coupling Constants (MHz)		
χ_{aa}	-2235.2(16)	-2238.33(75)
$\chi_{bb}-\chi_{cc}$	- 740.8(40)	- 734.830(80)
χ_{ab}	-1671.95(25)	-1671.81(14)
^{14}N Quadrupole Coupling Constants (MHz)		
χ_{aa}	-	5.2[2]
$\chi_{bb}-\chi_{cc}$	-	1.496(18)
Number of Rotational Transitions	27	47
Standard Deviation of fit (MHz)	0.058	0.038

[1] Numbers in parentheses are one standard deviation in units of the last significant figure.

[2] χ_{aa} was calculated by assuming that χ_{cc} is the same as the average value of χ_{cc} in ^{79}BrNCO and ^{81}BrNCO.

Table 5.4

Correlation coefficients of the spectroscopic constants of ^{127}INCO

A_o	1.00								
B_o	0.41	1.00							
C_o	0.82	-0.01	1.00						
Δ_J	0.84	0.16	0.94	1.00					
Δ_{JK}	0.81	0.70	0.56	0.73	1.00				
Δ_K	-0.09	0.67	-0.27	-0.17	0.09	1.00			
δ_J	-0.55	-0.77	-0.01	-0.22	-0.72	-0.24	1.00		
χ_{aa}	0.22	0.35	-0.26	-0.22	-0.11	0.77	-0.01	1.00	
$\chi_{bb}-\chi_{cc}$	0.00	-0.10	0.05	0.03	0.05	-0.09	0.06	-0.05	1.00
χ_{ab}	-0.10	-0.25	0.02	-0.03	-0.18	-0.07	0.15	0.03	-0.04	1.00

shows that none of the constants, in particular A_o and Δ_K, are correlated.

It is noteworthy that Δ_K was measured from these transitions. We have not only been able to determine an accurate A_o solely from a-type R branch transitions both in the analysis of the microwave spectrum of BrNCO and in the initial analysis of INCO, but also this method has been extended so that Δ_K was determined from transitions from which it would not normally be obtainable. Some of the energies of the $K_a = 1$ levels in $K_a = 1 \leftarrow 0$ b-type

transitions were perturbed by near degeneracies of the type $K_a = 2 \leftarrow 1$, which allowed Δ_K to be separated from A_o. No $K_a = 2 \leftarrow 1$ transitions could be measured. The relevant near-degeneracies are shown in the energy level diagram in Figure 5.3. Table 5.5 gives the measured frequencies as well as the calculated residuals, with χ_{ab} included and omitted to show the magnitude of the high-order shifts.

Table 5.5 Measured rotational transitions (in MHz) of INCO

Transition J'_{K_a,K_c} - J''_{K_a,K_c} F' - F"	Normalised[1] Weight	Observed[2] Frequency	Residuals[3] Without χ_{ab}	Residuals[3] With χ_{ab}
$6_{0,6}$ - $5_{0,5}$				
9/2 - 7/2	1.000	19978.071	-20.546	-0.004
11/2 - 9/2	1.000	19982.765	-23.761	-0.014
7/2 - 5/2	1.000	20003.661	-9.042	0.037
13/2 - 11/2	1.000	20012.940	-13.967	0.007
17/2 - 15/2	1.000	20038.666	0.123	0.009
15/2 - 13/2	1.000	20044.658	-0.460	-0.004
$7_{1,7}$ - $6_{1,6}$				
11/2 - 9/2	1.000	23101.368	-0.021	0.042
13/2 - 11/2	1.000	23104.899	0.382	0.058
9/2 - 7/2	1.000	23116.751	0.002	0.025
15/2 - 13/2	1.000	23119.941	1.095	0.050
17/2 - 15/2	1.000	23135.731	1.809	0.064
19/2 - 17/2	1.000	23136.812	1.486	0.049
$7_{0,7}$ - $6_{0,6}$				
9/2 - 7/2	1.000	23366.374	12.010	0.042
19/2 - 17/2	1.000	23372.965	0.047	-0.053
11/2 - 9/2	1.000	23376.151	31.713	0.027
17/2 - 15/2	1.000	23377.189	-0.653	-0.013
13/2 - 11/2	1.000	23391.934	41.411	0.026
15/2 - 13/2	1.000	23393.259	28.031	0.032
$7_{1,6}$ - $6_{1,5}$				
11/2 - 9/2	1.000	23606.211	0.979	0.006
13/2 - 11/2	1.000	23606.717	0.421	-0.026
15/2 - 13/2	1.000	23615.948	-0.069	-0.021
9/2 - 7/2	1.000	23617.646	-0.071	-0.055
17/2 - 15/2	1.000	23627.395	0.225	-0.030
19/2 - 17/2	1.000	23631.369	0.993	-0.009

[1] Measurements were weighted according to $1/\sigma^2$, where σ is the uncertainty in the measurements. Unit weight corresponded to an uncertainty of 0.03 MHz.

[2] Nitrogen hyperfine splitting has been subtracted from the b-type Q branch transitions.

[3] Observed frequency minus the frequency calculated using the constants in Table 5.3

Table 5.5 (Continued)

Transition F' - F"	Normalised Weight	Observed Frequency	Residuals Without χ_{ab}	Residuals With χ_{ab}
$8_{1\,8}$ - $7_{1\,7}$				
13/2 - 11/2	1.000	26409.229	-0.049	0.021
15/2 - 13/2	1.000	26412.527	0.163	0.053
11/2 - 9/2	1.000	26420.444	-0.025	0.006
17/2 - 15/2	1.000	26424.204	0.530	0.066
21/2 - 19/2	0.100	26435.761	0.738	0.083
19/2 - 17/2	0.100	26435.761	0.838	0.015
$8_{0\,8}$ - $7_{0\,7}$				
13/2 - 11/2	1.000	26681.085	-4.657	0.007
15/2 - 13/2	1.000	26684.285	-6.252	0.012
11/2 - 9/2	1.000	26690.587	-2.587	0.005
17/2 - 15/2	1.000	26695.709	-5.948	-0.001
21/2 - 19/2	1.000	26707.287	0.120	0.031
19/2 - 17/2	1.000	26710.014	-0.924	0.019
$8_{1\,7}$ - $7_{1\,6}$				
13/2 - 11/2	1.000	26983.957	1.614	0.017
15/2 - 13/2	1.000	26984.656	0.857	-0.005
17/2 - 15/2	0.100	26991.501	-0.112	-0.113
11/2 - 9/2	0.100	26991.501	0.095	0.138
19/2 - 17/2	1.000	27000.306	0.313	-0.049
21/2 - 19/2	1.000	27003.029	1.525	-0.025
$9_{1\,9}$ - $8_{1\,8}$				
15/2 - 13/2	1.000	29715.095	-0.072	0.004
17/2 - 15/2	1.000	29718.030	0.012	-0.019
13/2 - 11/2	1.000	29723.605	-0.054	-0.016
19/2 - 17/2	1.000	29727.382	0.245	-0.006
23/2 - 21/2	1.000	29735.782	0.451	0.076
21/2 - 19/2	1.000	29736.293	0.474	-0.007
$9_{0\,9}$ - $8_{0\,8}$				
15/2 - 13/2	1.000	30022.047	-2.102	0.012
17/2 - 15/2	1.000	30026.278	-1.718	-0.016
13/2 - 11/2	1.000	30027.800	-2.177	-0.021
19/2 - 17/2	1.000	30034.914	-1.789	-0.019
23/2 - 21/2	1.000	30040.998	0.082	0.003
21/2 - 19/2	1.000	30042.335	-1.510	-0.011
$9_{1\,8}$ - $8_{1\,7}$				
17/2 - 15/2	0.100	30361.131	1.591	-0.143
15/2 - 13/2	0.100	30361.131	3.120	0.091
13/2 - 11/2	1.000	30364.818	-0.048	0.012
19/2 - 17/2	1.000	30365.946	0.032	-0.041
21/2 - 19/2	1.000	30373.029	0.620	-0.007
23/2 - 21/2	1.000	30375.840	2.785	0.039

Table 5.5 (Continued)

Transition F' - F"	Normalised Weight	Observed Frequency	Residuals Without χ_{ab}	Residuals With χ_{ab}
$10_{1\,10}$ - $9_{1\,9}$				
17/2 - 15/2	1.000	33019.594	-0.051	0.030
19/2 - 17/2	1.000	33022.225	0.013	0.022
15/2 - 13/2	1.000	33026.293	-0.009	0.035
21/2 - 19/2	1.000	33029.908	0.203	0.056
25/2 - 23/2	1.000	33036.159	0.307	0.063
23/2 - 21/2	1.000	33036.938	0.343	0.028
$10_{0\,10}$ - $9_{0\,9}$				
17/2 - 15/2	1.000	33357.990	-2.382	-0.017
15/2 - 13/2	1.000	33361.740	-3.376	-0.011
19/2 - 17/2	1.000	33362.604	-0.898	-0.029
21/2 - 19/2	1.000	33369.228	-1.278	-0.008
23/2 - 21/2	1.000	33373.500	-2.697	0.004
25/2 - 23/2	1.000	33373.988	0.083	0.012
$10_{1\,9}$ - $9_{1\,8}$				
15/2 - 13/2	1.000	33737.846	-0.080	-0.004
19/2 - 17/2	1.000	33738.453	4.415	-0.002
21/2 - 19/2	1.000	33739.612	0.295	0.021
17/2 - 15/2	1.000	33740.192	7.626	-0.007
23/2 - 21/2	1.000	33745.940	1.455	0.003
25/2 - 23/2	1.000	33750.920	6.244	0.016
$11_{1\,11}$ - $10_{1\,10}$				
19/2 - 17/2	1.000	36322.903	-0.136	-0.048
21/2 - 19/2	1.000	36325.244	-0.085	-0.049
17/2 - 15/2	1.000	36328.272	-0.126	-0.076
23/2 - 21/2	1.000	36331.605	0.020	-0.066
27/2 - 25/2	1.000	36336.511	0.163	-0.009
25/2 - 23/2	1.000	36337.377	0.195	-0.026
$11_{0\,11}$ - $10_{0\,10}$				
19/2 - 17/2	1.000	36689.863	-4.872	-0.052
17/2 - 15/2	1.000	36690.757	-7.959	-0.070
21/2 - 19/2	0.100	36696.650	-0.659	0.088
23/2 - 21/2	0.100	36701.301	-1.763	0.064
25/2 - 23/2	0.100	36701.557	-6.171	0.015
27/2 - 25/2	1.000	36705.992	0.059	-0.006
$11_{1\,10}$ - $10_{1\,9}$				
17/2 - 15/2	1.000	37110.437	-0.065	0.026
23/2 - 21/2	1.000	37113.757	1.763	-0.053
25/2 - 23/2	1.000	37123.320	7.121	-0.076
21/2 - 19/2	0.100	37133.958	26.396	0.007
27/2 - 25/2	0.100	37143.750	27.600	0.090
19/2 - 17/2	0.100	37154.803	48.608	-0.021

Table 5.5 (Continued)

Transition F' - F"	Normalised Weight	Observed Frequency	Residuals Without χ_{ab}	Residuals With χ_{ab}
$12_{1\,12} - 11_{1\,11}$				
21/2 - 19/2	1.000	39625.450	-0.086	0.014
23/2 - 21/2	1.000	39627.502	-0.069	-0.008
19/2 - 17/2	1.000	39629.865	-0.082	-0.023
25/2 - 23/2	1.000	39632.897	0.028	-0.015
29/2 - 27/2	1.000	39636.822	0.160	0.032
27/2 - 25/2	1.000	39637.682	0.179	0.016
$12_{0\,12} - 11_{0\,11}$				
19/2 - 17/2	1.000	39982.019	-48.785	0.071
21/2 - 19/2	1.000	40000.702	-26.671	0.023
27/2 - 25/2	1.000	40010.776	-27.457	0.016
25/2 - 23/2	1.000	40026.890	-7.429	0.022
23/2 - 21/2	1.000	40027.370	-2.136	0.010
29/2 - 27/2	1.000	40036.962	0.126	0.068
$12_{1\,11} - 11_{1\,10}$				
21/2 - 19/2	0.100	40375.057	-103.942	0.065
29/2 - 27/2	1.000	40389.220	-98.109	-0.056
23/2 - 21/2	1.000	40417.708	-62.537	0.059
27/2 - 25/2	1.000	40465.533	-21.969	-0.015
25/2 - 23/2	1.000	40478.924	-5.089	0.006
19/2 - 17/2	1.000	40482.417	-0.123	-0.013
$13_{1\,13} - 12_{1\,12}$				
23/2 - 21/2	1.000	42927.130	-0.108	0.010
25/2 - 23/2	1.000	42928.972	-0.075	0.015
21/2 - 19/2	1.000	42930.875	-0.062	0.007
27/2 - 25/2	1.000	42933.616	0.029	0.022
31/2 - 29/2	1.000	42936.822	0.140	0.041
29/2 - 27/2	1.000	42937.644	0.155	0.031
$13_{0\,13} - 12_{0\,12}$				
25/2 - 23/2	1.000	43364.895	4.792	-0.038
31/2 - 29/2	1.000	43366.541	0.075	0.021
27/2 - 25/2	1.000	43385.969	21.783	0.018
23/2 - 21/2	0.100	43420.583	62.256	-0.070
21/2 - 19/2	1.000	43465.088	103.738	-0.039
29/2 - 27/2	0.100	43465.697	98.160	0.073
$13_{1\,12} - 12_{1\,11}$				
21/2 - 19/2	0.100	43853.888	-0.108	0.033
27/2 - 25/2	0.100	43856.716	1.325	0.017
29/2 - 27/2	1.000	43865.600	7.267	-0.046
25/2 - 23/2	1.000	43867.346	15.194	-0.026
23/2 - 21/2	1.000	43872.824	21.798	-0.022
31/2 - 29/2	1.000	43895.390	37.286	0.017

Table 5.5 (Continued)

Transition F' - F"	Normalised Weight	Observed Frequency	Residuals Without χ_{ab}	Residuals With χ_{ab}
$14_{1,14}$ - $13_{1,13}$				
25/2 - 23/2	1.000	46228.027	-0.175	-0.020
27/2 - 25/2	1.000	46229.708	-0.104	0.027
23/2 - 21/2	1.000	46231.267	-0.088	0.001
29/2 - 27/2	1.000	46233.761	0.017	0.047
33/2 - 31/2	1.000	46236.475	0.152	0.072
31/2 - 29/2	1.000	46237.204	0.128	0.032
$14_{0,14}$ - $13_{0,13}$				
31/2 - 29/2	1.000	46658.210	-37.280	-0.042
23/2 - 21/2	1.000	46668.225	-22.073	0.010
25/2 - 23/2	1.000	46672.091	-15.491	0.014
29/2 - 27/2	1.000	46685.082	-7.489	-0.023
27/2 - 25/2	1.000	46687.479	-1.585	-0.028
33/2 - 31/2	1.000	46694.714	0.023	-0.026
$14_{1,13}$ - $13_{1,12}$				
23/2 - 21/2	1.000	47224.639	-0.188	0.009
29/2 - 27/2	0.100	47226.213	0.097	-0.013
27/2 - 25/2	0.100	47226.602	3.298	-0.024
25/2 - 23/2	1.000	47227.535	5.243	-0.016
31/2 - 29/2	1.000	47230.022	1.388	-0.046
33/2 - 31/2	1.000	47235.438	7.051	-0.023
$15_{1,15}$ - $14_{1,14}$				
27/2 - 25/2	1.000	49528.210	-0.243	-0.030
29/2 - 27/2	1.000	49529.663	-0.226	-0.027
25/2 - 23/2	1.000	49531.029	-0.151	-0.030
31/2 - 29/2	1.000	49533.219	-0.107	-0.027
35/2 - 33/2	1.000	49535.589	0.071	0.006
33/2 - 31/2	1.000	49536.301	0.093	0.018
$15_{0,15}$ - $14_{0,14}$				
27/2 - 25/2	1.000	50011.379	-3.714	-0.022
25/2 - 23/2	1.000	50011.952	-5.624	-0.010
33/2 - 31/2	1.000	50014.908	-7.047	-0.002
29/2 - 27/2	1.000	50015.927	-0.402	-0.007
31/2 - 29/2	1.000	50017.802	-1.571	-0.007
35/2 - 33/2	1.000	50021.470	0.082	0.037
$15_{1,14}$ - $14_{1,13}$				
29/2 - 27/2	0.100	50594.701	1.000	-0.038
27/2 - 25/2	0.100	50594.701	1.908	-0.066
25/2 - 23/2	0.100	50594.701	-0.289	0.038
31/2 - 29/2	1.000	50595.926	-0.237	-0.012
33/2 - 31/2	0.100	50598.962	0.617	0.033
35/2 - 33/2	0.100	50601.151	3.048	0.070

Table 5.5 (Continued)

Transition F' - F"	Normalised Weight	Observed Frequency	Residuals Without χ_{ab}	Residuals With χ_{ab}
$13_{1\,12} - 13_{o\,13}$				
21/2 - 21/2	1.000	42183.411	-37.713	-0.044
31/2 - 31/2	1.000	42216.084	-16.610	-0.080
23/2 - 23/2	1.000	42239.340	-40.670	0.001
29/2 - 29/2	1.000	42243.386	-57.908	-0.004
25/2 - 25/2	1.000	42304.515	-12.888	0.039
27/2 - 27/2	1.000	42313.833	-13.036	0.025
$14_{1\,13} - 14_{o\,14}$				
23/2 - 23/2	1.000	42739.810	-15.843	-0.060
33/2 - 33/2	1.000	42756.815	-9.575	-0.069
25/2 - 25/2	1.000	42794.817	-19.903	0.003
31/2 - 31/2	1.000	42815.217	-19.222	0.012
27/2 - 27/2	1.000	42843.625	-8.018	0.029
29/2 - 29/2	1.000	42854.948	-5.466	0.019
$15_{1\,14} - 15_{o\,15}$				
25/2 - 25/2	1.000	43322.638	-10.429	0.067
35/2 - 35/2	1.000	43336.463	-6.643	-0.069
27/2 - 27/2	1.000	43378.182	-14.237	0.002
33/2 - 33/2	1.000	43399.216	-11.613	-0.008
$16_{1\,15} - 16_{o\,16}$				
35/2 - 35/2	1.000	44023.091	-8.341	0.017
31/2 - 31/2	1.000	44043.535	-6.977	0.056
$17_{1\,16} - 17_{o\,17}$				
29/2 - 29/2	1.000	44599.201	-21.555	-0.036
39/2 - 39/2	1.000	44625.663	-4.028	-0.052
31/2 - 31/2	1.000	44648.492	-32.432	-0.010
37/2 - 37/2	1.000	44690.701	-6.574	0.008
33/2 - 33/2	1.000	44692.445	-24.739	0.021
35/2 - 35/2	1.000	44712.003	-12.455	0.035
$18_{1\,17} - 18_{o\,18}$				
31/2 - 31/2	1.000	45330.177	-3.059	-0.009
41/2 - 41/2	1.000	45338.376	-3.352	-0.058
33/2 - 33/2	1.000	45391.355	-2.558	-0.011
39/2 - 39/2	1.000	45403.946	-5.494	-0.011
35/2 - 35/2	1.000	45432.338	2.211	0.060
37/2 - 37/2	1.000	45438.576	1.540	0.016
$19_{1\,18} - 19_{o\,19}$				
33/2 - 33/2	1.000	46089.540	-3.471	-0.005
43/2 - 43/2	1.000	46098.272	-2.843	-0.041
35/2 - 35/2	1.000	46150.472	-3.781	0.048
41/2 - 41/2	1.000	46164.294	-4.767	-0.009
37/2 - 37/2	1.000	46190.424	-0.063	0.013
39/2 - 39/2	1.000	46197.020	-0.055	0.0

Table 5.5 (Continued)

Transition F' - F"	Normalised Weight	Observed Frequency	Residuals Without χ_{ab}	Residuals With χ_{ab}
$20_{1\ 19}$ - $20_{o\ 20}$				
45/2 - 45/2	1.000	46906.578	-2.465	-0.033
37/2 - 37/2	1.000	46959.334	-3.803	0.047
43/2 - 43/2	1.000	46973.087	-4.225	0.038
39/2 - 39/2	1.000	46998.937	-0.510	0.052
41/2 - 41/2	1.000	47005.355	-0.399	0.021
$21_{1\ 20}$ - $21_{o\ 21}$				
47/2 - 47/2	1.000	47764.570	-2.167	-0.022
45/2 - 45/2	1.000	47831.497	-3.910	0.018
41/2 - 41/2	1.000	47857.554	-0.675	0.036
43/2 - 43/2	1.000	47863.753	-0.533	0.032
$22_{1\ 21}$ - $22_{o\ 22}$				
39/2 - 39/2	1.000	48665.105	-3.166	0.044
49/2 - 49/2	1.000	48673.524	-1.930	-0.014
41/2 - 41/2	1.000	48727.954	-3.532	0.001
47/2 - 47/2	1.000	48740.840	-3.753	-0.039
43/2 - 43/2	1.000	48767.260	-0.826	-0.074
45/2 - 45/2	1.000	48773.279	-0.639	0.006
$23_{1\ 22}$ - $23_{o\ 23}$				
43/2 - 43/2	1.000	49690.140	-3.363	0.038
45/2 - 45/2	1.000	49729.556	-0.748	0.004
47/2 - 47/2	1.000	49735.222	-0.706	0.003
$24_{1\ 23}$ - $24_{o\ 24}$				
53/2 - 53/2	1.000	50649.544	-1.546	0.031
45/2 - 45/2	1.000	50706.054	-3.339	-0.021
47/2 - 47/2	1.000	50745.651	-0.716	0.017
49/2 - 49/2	1.000	50750.848	-0.840	-0.052
$25_{1\ 24}$ - $25_{o\ 25}$				
45/2 - 45/2	1.000	51710.642	-3.393	0.043
55/2 - 55/2	1.000	51719.163	-1.449	-0.001
47/2 - 47/2	1.000	51776.247	-3.241	0.046
53/2 - 53/2	1.000	51787.779	-3.712	-0.024
49/2 - 49/2	1.000	51816.052	-0.723	-0.009
51/2 - 51/2	1.000	51821.258	-0.855	-0.008
$26_{1\ 25}$ - $26_{o\ 26}$				
57/2 - 57/2	1.000	52845.021	-1.327	0.012
49/2 - 49/2	1.000	52902.935	-3.327	0.014
55/2 - 55/2	1.000	52913.936	-3.960	-0.031
51/2 - 51/2	1.000	52943.130	-0.713	-0.024
53/2 - 53/2	1.000	52948.001	-1.018	-0.048

Table 5.5 (Continued)

Transition F' - F"	Normalised Weight	Observed Frequency	Residuals Without χ_{ab}	Residuals With χ_{ab}
$20_{0\,20} - 19_{1\,19}$				
35/2 - 33/2	1.000	33838.242	-67.392	-0.009
45/2 - 43/2	0.100	33913.537	-0.035	0.104
43/2 - 41/2	1.000	33964.972	4.166	-0.034
41/2 - 39/2	1.000	33995.752	16.966	0.012
39/2 - 37/2	1.000	34011.441	38.889	0.069
37/2 - 35/2	1.000	34018.275	71.534	-0.022
$21_{0\,21} - 20_{1\,20}$				
37/2 - 35/2	1.000	37828.243	1.715	0.015
47/2 - 45/2	1.000	37833.826	-0.094	0.046
39/2 - 37/2	1.000	37865.109	-2.224	0.035
45/2 - 43/2	1.000	37884.237	3.804	0.008
41/2 - 39/2	1.000	37888.182	-4.459	-0.034
43/2 - 41/2	1.000	37896.723	-1.725	-0.068
$22_{0\,22} - 21_{1\,21}$				
39/2 - 37/2	1.000	41767.255	2.346	0.005
49/2 - 47/2	1.000	41771.756	-0.054	0.085
41/2 - 39/2	1.000	41804.838	-0.483	-0.071
47/2 - 45/2	1.000	41821.010	3.458	-0.023
43/2 - 41/2	1.000	41828.062	-2.052	-0.061
45/2 - 43/2	1.000	41835.421	-0.115	-0.055
$23_{0\,23} - 22_{1\,22}$				
41/2 - 39/2	1.000	45721.705	2.486	0.054
51/2 - 49/2	1.000	45725.596	-0.087	0.050
43/2 - 41/2	0.100	45759.169	0.016	-0.098
49/2 - 47/2	1.000	45773.882	3.274	0.042
45/2 - 43/2	1.000	45782.108	-1.310	-0.060
47/2 - 45/2	1.000	45788.752	0.256	-0.103
$24_{0\,24} - 23_{1\,23}$				
43/2 - 41/2	1.000	49690.163	2.494	0.049
53/2 - 51/2	1.000	49693.957	0.017	0.151
45/2 - 43/2	1.000	49727.240	0.249	-0.091
51/2 - 49/2	1.000	49741.133	3.127	0.096
47/2 - 45/2	1.000	49749.800	-0.980	-0.081

Table 5.6

Observed hyperfine transition frequencies (in MHz) of $^{127}I^{14}NCO$ b-type Q branch transitions

Transition F_1' F' - F_1'' F''	Observed Frequency
$12_{1\ 11}$ - $12_{0\ 12}$	
29/2 29/2 - 29/2 29/2	41686.998
29/2 27/2 - 29/2 27/2	41687.308
29/2 31/2 - 29/2 31/2	41687.308
$13_{1\ 12}$ - $13_{0\ 13}$	
21/2 21/2 - 21/2 21/2	42183.259
21/2 19/2 - 21/2 19/2	42183.488
21/2 23/2 - 21/2 23/2	42183.488
31/2 31/2 - 31/2 31/2	42215.884
31/2 29/2 - 31/2 29/2	42216.185
31/2 33/2 - 31/2 33/2	42216.185
23/2 23/2 - 23/2 23/2	42239.187
23/2 21/2 - 23/2 21/2	42239.417
23/2 25/2 - 23/2 25/2	42239.417
29/2 29/2 - 29/2 29/2	42243.161
29/2 27/2 - 29/2 27/2	42243.499
29/2 31/2 - 29/2 31/2	42243.499
25/2 25/2 - 25/2 25/2	42304.329
25/2 23/2 - 25/2 23/2	42304.609
25/2 27/2 - 25/2 27/2	42304.609
27/2 27/2 - 27/2 27/2	42313.642
27/2 25/2 - 27/2 25/2	42313.929
27/2 29/2 - 27/2 29/2	42313.929
$14_{1\ 13}$ - $14_{0\ 14}$	
23/2 23/2 - 23/2 23/2	42739.633
23/2 21/2 - 23/2 21/2	42739.900
23/2 25/2 - 23/2 25/2	42739.900
33/2 33/2 - 33/2 33/2	42756.630
33/2 31/2 - 33/2 31/2	42756.909
33/2 35/2 - 33/2 35/2	42756.909
25/2 25/2 - 25/2 25/2	42794.621
25/2 23/2 - 25/2 23/2	42794.916
25/2 27/2 - 25/2 27/2	42794.916
31/2 31/2 - 31/2 31/2	42814.998
31/2 29/2 - 31/2 29/2	42815.327
31/2 33/2 - 31/2 33/2	42815.327
27/2 27/2 - 27/2 27/2	42843.416
27/2 25/2 - 27/2 25/2	42843.730
27/2 29/2 - 27/2 29/2	42843.730
29/2 29/2 - 29/2 29/2	42854.765
29/2 27/2 - 29/2 27/2	42855.040
29/2 31/2 - 29/2 31/2	42855.040

Table 5.6 (Continued)

Transition F_1'	F'	-	F_1''	F''	Observed Frequency
$15_{1\ 14}$		-	$15_{0\ 15}$		
25/2	25/2	-	25/2	25/2	43322.317
25/2	23/2	-	25/2	23/2	43322.638
25/2	27/2	-	25/2	27/2	43322.638
35/2	35/2	-	35/2	35/2	43336.245
35/2	33/2	-	35/2	33/2	43336.572
35/2	37/2	-	35/2	37/2	43336.572
27/2	27/2	-	27/2	27/2	43377.983
27/2	25/2	-	27/2	25/2	43378.282
27/2	29/2	-	27/2	29/2	43378.282
33/2	33/2	-	33/2	33/2	43399.060
33/2	31/2	-	33/2	31/2	43399.295
33/2	35/2	-	33/2	35/2	43399.295
$16_{1\ 15}$		-	$16_{0\ 16}$		
35/2	35/2	-	35/2	35/2	44022.898
35/2	33/2	-	35/2	33/2	44023.188
35/2	37/2	-	35/2	37/2	44023.188
31/2	31/2	-	31/2	31/2	44043.308
31/2	29/2	-	31/2	29/2	44043.649
31/2	33/2	-	31/2	33/2	44043.649
$17_{1\ 16}$		-	$17_{0\ 17}$		
29/2	29/2	-	29/2	29/2	44599.001
29/2	27/2	-	29/2	27/2	44599.302
29/2	31/2	-	29/2	31/2	44599.302
39/2	39/2	-	39/2	39/2	44625.469
39/2	37/2	-	39/2	37/2	44625.760
39/2	41/2	-	39/2	41/2	44625.760
31/2	31/2	-	31/2	31/2	44648.230
31/2	29/2	-	31/2	29/2	44648.589
31/2	33/2	-	31/2	33/2	44648.589
37/2	37/2	-	37/2	37/2	44690.483
37/2	35/2	-	37/2	35/2	44690.810
37/2	39/2	-	37/2	39/2	44690.810
33/2	33/2	-	33/2	33/2	44692.221
33/2	31/2	-	33/2	31/2	44692.557
33/2	35/2	-	33/2	35/2	44692.557
35/2	35/2	-	35/2	35/2	44711.831
35/2	33/2	-	35/2	33/2	44712.089
35/2	37/2	-	35/2	37/2	44712.089

Table 5.6 (Continued)

Transition F_1' F'			F_1'' F"	Observed Frequency
$18_{1\ 17}$		-	$18_{0\ 18}$	
31/2	31/2	-	31/2	31/2 45329.974
31/2	29/2	-	31/2	29/2 45330.279
31/2	33/2	-	31/2	33/2 45330.279
41/2	41/2	-	41/2	41/2 45338.181
41/2	39/2	-	41/2	39/2 45338.474
41/2	43/2	-	41/2	43/2 45338.474
33/2	33/2	-	33/2	33/2 45391.148
33/2	31/2	-	33/2	31/2 45391.451
33/2	35/2	-	33/2	35/2 45391.451
39/2	39/2	-	39/2	39/2 45403.765
39/2	37/2	-	39/2	37/2 45404.037
39/2	41/2	-	39/2	41/2 45404.037
35/2	35/2	-	35/2	35/2 45432.145
35/2	33/2	-	35/2	33/2 45432.435
35/2	37/2	-	35/2	37/2 45432.435
37/2	37/2	-	37/2	37/2 45438.399
37/2	35/2	-	37/2	35/2 45438.665
37/2	39/2	-	37/2	39/2 45438.665
$19_{1\ 18}$		-	$19_{0\ 19}$	
33/2	33/2	-	33/2	33/2 46089.349
33/2	31/2	-	33/2	31/2 46089.636
33/2	35/2	-	33/2	35/2 46089.636
43/2	43/2	-	43/2	43/2 46098.062
43/2	41/2	-	43/2	41/2 46098.378
43/2	45/2	-	43/2	45/2 46098.378
35/2	35/2	-	35/2	35/2 46150.272
35/2	33/2	-	35/2	33/2 46150.572
35/2	37/2	-	35/2	37/2 46150.572
41/2	41/2	-	41/2	41/2 46164.076
41/2	39/2	-	41/2	39/2 46164.404
41/2	43/2	-	41/2	43/2 46164.404
37/2	37/2	-	37/2	37/2 46190.242
37/2	35/2	-	37/2	35/2 46190.516
37/2	39/2	-	37/2	39/2 46190.516
39/2	39/2	-	39/2	39/2 46196.838
39/2	37/2	-	39/2	37/2 46197.111
39/2	41/2	-	39/2	41/2 46197.111
$20_{1\ 19}$		-	$20_{0\ 20}$	
45/2	45/2	-	45/2	45/2 46906.392
45/2	43/2	-	45/2	43/2 46906.676
45/2	47/2	-	45/2	47/2 46906.676
37/2	37/2	-	37/2	37/2 46959.082
37/2	35/2	-	37/2	35/2 46959.460
37/2	39/2	-	37/2	39/2 46959.460

Table 5.6 (Continued)

Transition F_1'	F'	-	F_1''	F''	Observed Frequency
$20_{1\ 19}$		-	$20_{0\ 20}$		
43/2	43/2	-	43/2	43/2	46972.851
43/2	41/2	-	43/2	41/2	46973.205
43/2	45/2	-	43/2	45/2	46973.205
39/2	39/2	-	39/2	39/2	46998.731
39/2	37/2	-	39/2	37/2	46999.040
39/2	41/2	-	39/2	41/2	46999.040
41/2	41/2	-	41/2	41/2	47005.155
41/2	39/2	-	41/2	39/2	47005.456
41/2	43/2	-	41/2	43/2	47005.456
$21_{1\ 20}$		-	$21_{0\ 21}$		
47/2	47/2	-	47/2	47/2	47764.358
47/2	45/2	-	47/2	45/2	47764.677
47/2	49/2	-	47/2	49/2	47764.677
45/2	45/2	-	45/2	45/2	47831.272
45/2	43/2	-	45/2	43/2	47831.610
45/2	47/2	-	45/2	47/2	47831.610
41/2	41/2	-	41/2	41/2	47857.340
41/2	39/2	-	41/2	39/2	47857.662
41/2	43/2	-	41/2	43/2	47857.662
43/2	43/2	-	43/2	43/2	47863.549
43/2	41/2	-	43/2	41/2	47863.856
43/2	45/2	-	43/2	45/2	47863.856
$22_{1\ 21}$		-	$22_{0\ 22}$		
39/2	39/2	-	39/2	39/2	48664.877
39/2	37/2	-	39/2	37/2	48665.220
39/2	41/2	-	39/2	41/2	48665.220
49/2	49/2	-	49/2	49/2	48673.310
49/2	47/2	-	49/2	47/2	48673.632
49/2	51/2	-	49/2	51/2	48673.632
41/2	41/2	-	41/2	41/2	48727.734
41/2	39/2	-	41/2	39/2	48728.065
41/2	43/2	-	41/2	43/2	48728.065
47/2	47/2	-	47/2	47/2	48740.616
47/2	45/2	-	47/2	45/2	48740.953
47/2	49/2	-	47/2	49/2	48740.953
43/2	43/2	-	43/2	43/2	48767.203
43/2	41/2	-	43/2	41/2	48767.513
43/2	45/2	-	43/2	45/2	48767.513
45/2	45/2	-	45/2	45/2	48773.066
45/2	43/2	-	45/2	43/2	48773.386
45/2	47/2	-	45/2	47/2	48773.386

Table 5.6 (Continued)

Transition F_1'	F'	-	F_1''	F''	Observed Frequency
$23_{1\ 22}$		-	$23_{0\ 23}$		
43/2	43/2	-	43/2	43/2	49689.953
43/2	41/2	-	43/2	41/2	49690.234
43/2	45/2	-	43/2	45/2	49690.234
45/2	45/2	-	45/2	45/2	49729.369
45/2	43/2	-	45/2	43/2	49729.650
45/2	47/2	-	45/2	47/2	49729.650
47/2	47/2	-	47/2	47/2	49735.010
47/2	45/2	-	47/2	45/2	49735.328
47/2	49/2	-	47/2	49/2	49735.328
$24_{1\ 23}$		-	$24_{0\ 24}$		
53/2	53/2	-	53/2	53/2	50649.327
53/2	51/2	-	53/2	51/2	50649.653
53/2	55/2	-	53/2	55/2	50649.653
45/2	45/2	-	45/2	45/2	50705.806
45/2	43/2	-	45/2	43/2	50706.179
45/2	47/2	-	45/2	47/2	50706.179
47/2	47/2	-	47/2	47/2	50745.420
47/2	45/2	-	47/2	45/2	50745.767
47/2	49/2	-	47/2	49/2	50745.767
49/2	49/2	-	49/2	49/2	50750.622
49/2	47/2	-	49/2	47/2	50750.961
49/2	51/2	-	49/2	51/2	50750.961
$25_{1\ 24}$		-	$25_{0\ 25}$		
45/2	45/2	-	45/2	45/2	51710.422
45/2	43/2	-	45/2	43/2	51710.753
45/2	47/2	-	45/2	47/2	51710.753
55/2	55/2	-	55/2	55/2	51718.925
55/2	53/2	-	55/2	53/2	51719.283
55/2	57/2	-	55/2	57/2	51719.283
47/2	47/2	-	47/2	47/2	51776.031
47/2	45/2	-	47/2	45/2	51776.355
47/2	49/2	-	47/2	49/2	51776.355
53/2	53/2	-	53/2	53/2	51787.543
53/2	51/2	-	53/2	51/2	51787.898
53/2	55/2	-	53/2	55/2	51787.898
49/2	49/2	-	49/2	49/2	51815.820
49/2	47/2	-	49/2	47/2	51816.169
49/2	51/2	-	49/2	51/2	51816.169
51/2	51/2	-	51/2	51/2	51821.028
51/2	49/2	-	51/2	49/2	51821.373
51/2	53/2	-	51/2	53/2	51821.373

Table 5.6 (Continued)

Transition					Observed
F_1'	F'	-	F_1''	F"	Frequency
$26_{1\ 25}$		-	$26_{0\ 26}$		
57/2	57/2	-	57/2	57/2	52844.797
57/2	55/2	-	57/2	55/2	52845.133
57/2	59/2	-	57/2	59/2	52845.133
49/2	49/2	-	49/2	49/2	52902.691
49/2	47/2	-	49/2	47/2	52903.057
49/2	51/2	-	49/2	51/2	52903.057
55/2	55/2	-	55/2	55/2	52913.689
55/2	53/2	-	55/2	53/2	52914.059
55/2	57/2	-	55/2	57/2	52914.059
51/2	51/2	-	51/2	51/2	52942.871
51/2	49/2	-	51/2	49/2	52943.259
51/2	53/2	-	51/2	53/2	52943.259
53/2	53/2	-	53/2	53/2	52947.791
53/2	51/2	-	53/2	51/2	52948.106
53/2	55/2	-	53/2	55/2	52948.106

5.5 The Structure of INCO

The moments of inertia of only one isotope of INCO have been measured in this study: $^{127}I^{14}N^{12}C^{16}O$. Hence, there is only limited structural information available.

The inertial defect for the ground state is 0.448 a.m.u. $Å^2$; INCO is therefore almost certainly planar.

Although only one of the nitrogen quadrupole coupling constants was determinable, the constants given in Table 5.7 are similar in magnitude to those of BrNCO and are therefore consistent with the configuration INCO rather than IOCN (see section 4.7).

Table 5.7

Quadrupole Coupling Constants of ^{14}N in Principal Inertial Axes

χ_{aa} (MHz)	5.2[1]
χ_{bb} (MHz)	-1.852(18)
χ_{cc} (MHz)	-3.348[1]

[1] χ_{aa} was calculated by assuming that χ_{cc} is the same as the average value of χ_{cc} in ^{79}BrNCO and ^{81}BrNCO. What was determined from the spectrum was $\chi_{bb} - \chi_{cc} = 1.496(18)$MHz.

A structure consistent with the measured rotational constants can be derived for INCO only by fixing some of the structural parameters. The N-C and C-O bond lengths were fixed at ClNCO values (6,7). The N-C-O angle was varied between 0°(linear) and 9.13°(<N-C-O in ClNCO), and values for the I-N

bond length and I-N-C angle were calculated (Table 5.8). The I-N bond length is comparable with other I-N bond lengths and the I-N-C angle is reasonable when compared with the X-N-C angles in the other halogen isocyanates (See Table 5.9). When compared with the sum of the single bond radii, the I-N bond length calculated for the various N-C-O angles (Table 5.8) is more consistent with a bent N-C-O chain. The position of the atoms relative to the inertial axes is shown in Figure 5.5.

Table 5.8

Structural parameters of INCO

	I	II	III
r(I-N)/Å	2.005	2.016	2.032
r(N-C)[1]/Å	1.225	1.225	1.225
r(C-O)[1]/Å	1.162	1.162	1.162
<(INC)	124.22°	122.07°	119.42°
<(NCO)[2]	0°	4°	9.13°
<(I-N-a)[3]	25.03°	25.20°	25.34°

[1] Constrained to ClNCO values.

[2] Constrained.

[3] Angle between the I-N bond axis and the a-inertial axis.

Table 5.9

Comparison of structural parameters of INCO with other molecules.

r(I-N)	
INCO	2.02 Å
I_2NCHO(9)	2.04 Å
Sum of single bond radii(10)	2.02 Å
<(X-N-C)	
INCO	122°
BrNCO	119°
ClNCO(6,7)	118°

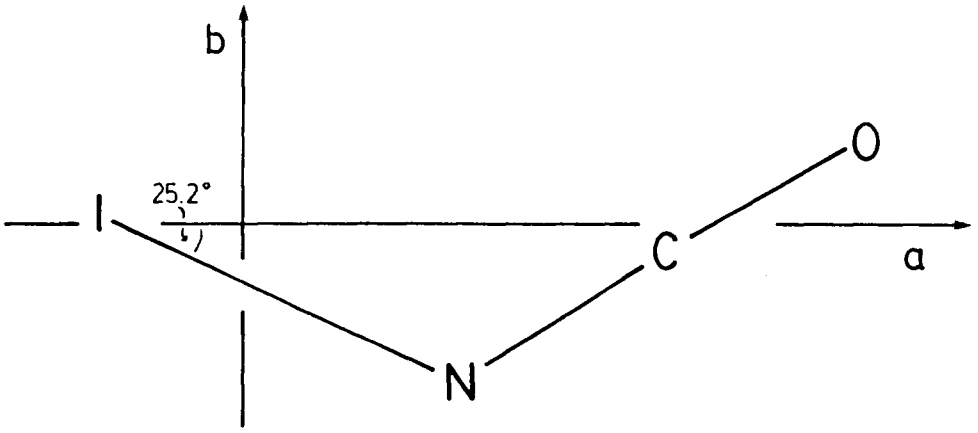

Figure 5.5 The relative positions of the atoms of INCO in its principal inertial axis system (from structure II in Table 5.8).

5.6 ^{127}I and ^{14}N Quadrupole Coupling

The procedure used to analyze the quadrupole coupling constants of bromine in BrNCO was also followed in INCO. The quadrupole tensor was diagonalized to find its principal values. These are given in Table 5.11. θ_{za}, which is the angle between the z-principal quadrupole axis and the a-inertial axis agrees to within ≃1° with the angle between the I-N bond and the a-inertial axis (see Table 5.8). The difference is probably not significant; hence the z-principal quadrupole axis and therefore the maximum electron density of the I-N bond lies along the I-N bond axis.

Table 5.10

Quadrupole Coupling Constants of ^{127}I in Principal Inertial axes

χ_{aa} (MHz)	-2238.33(75)
χ_{bb} (MHz)	751.75(41)
χ_{cc} (MHz)	1486.58(41)
χ_{ab} (MHz)	-1671.81(14)

Table 5.11

Quadrupole Coupling Constants of ^{127}I in Principal Quadrupole Axes

χ_{zz} (MHz)	-2986.1(15)
χ_{xx} (MHz)	1499.5(12)
χ_{yy} (MHz)	1486.58(41)
θ_{za} (deg)	24.097(7)

The difference between χ_{xx} and χ_{yy} is very small. Therefore the contribution of a π-bonded resonance structure to the overall structure of INCO is negligible (≈0.4%). The I-N bond is essentially cylindrically symmetric, as was assumed initially.

The two resonance forms which contribute most to the overall I-N bond are probably:

(I)

(II)

The positive charge is on the iodine in form (II) which represents an ionic I-N bond because $|\chi_{zz}| \geq |eQq_I|$. The contribution of this resonance form is estimated to be ≈23% (calculated as for BrNCO in section 4.8).

As in BrNCO, an attempt was made to reproduce the ^{14}N quadrupole coupling constants from p-orbital populations calculated in a semi-empirical CNDO calculation. The p orbital populations were calculated to be: $n_a = 0.9061$, $n_b = 1.3821$, $n_c = 1.6795$. The ^{14}N quadrupole coupling constants in the inertial axis system were calculated using equations 4.4 and 4.5. A comparison of the calculated constants with those obtained experimentally is given in Table 5.12. Once, again the theoretically calculated constants do not reproduce the experimental values very well. This further demonstrates the

need for improved theoretical calculations, particularly for molecules containing heavy atoms.

Table 5.12

Comparison of ^{14}N quadrupole coupling constants obtained experimentally with theoretically calculated values.

	Experimental	Calculated[1]
χ_{aa} (MHz)	5.2[2]	6.247
χ_{bb} (MHz)	-1.852(18)	-0.893
χ_{cc} (MHz)	-3.348[2]	-5.354

[1] Calculated using p-orbital populations from CNDO calculation.

[2] See text to see how obtained.

5.7 Discussion

In Chapter IV, perturbations in the quadrupole hyperfine structure in the microwave spectrum of BrNCO were demonstrated to be useful in evaluating all three rotational constants where otherwise they may not have all been determinable. The same method was also used for analyzing the microwave spectrum of INCO, and A_o was calculated solely from the analysis of a-type R branch transitions, using $K_a = 1 \leftarrow 0$ near-degeneracies. This study has further demonstrated the usefulness of using the 'exact' Hamiltonian to fit the rotational, centrifugal distortion and quadrupole coupling constants of a molecule. The energies are so sensitive to the magnitudes of the near-

degeneracies, that not only can the perturbations in the quadrupole structure be used to evaluate rotational constants, but also centrifugal distortion constants can be determined, in this case Δ_K. Δ_K would normally require $K_a = 2 \leftrightarrow 1$ transitions to be measured; this was impossible for INCO. Instead, perturbations in $K_a = 1 \leftarrow 0$ b-type transitions, caused by $K_a = 2 \leftrightarrow 1$ near-degeneracies contained enough information for Δ_K to be evaluated separately from A_o. This was a significant extension of the method developed to analyze the spectrum of BrNCO.

While not of general applicability, the method of using perturbations in the quadrupole hyperfine structure in the microwave spectrum of a molecule to evaluate otherwise undeterminable rotational and centrifugal distortion constants, will be useful when analyzing the spectra of molecules containing bromine and iodine, particularly when the spectrum has predominantly a-type R branch transitions. In fact, the microwave spectra of other molecules such as vinyl iodide are already being analyzed using this method (11). The major requirement for the usefulness of this method is that none of the angles between the bond axis, containing the quadrupolar nucleus and the atom to which it is attached, and the inertial axes is small, because χ_{ab} would be relatively small. The only other limitation is the relative magnitude of the rotational constants, which will determine the number of near-degeneracies with the correct symmetry relevant to the available frequency

range. If there are only a few near-degeneracies, then the accuracy of the constants obtained by this method will be limited.

In this microwave study, the rotational constants of INCO have been measured, along with 4 out of 5 quartic centrifugal distortion constants. The rotational constants have been used to determine a partial r_o structure for INCO which is consistent with the other halogen isocyanate structures.

In the microwave spectrum of INCO, several vibrational satellites were observed, the relative intensities of which provide an estimate of the lowest vibrational frequency of INCO at $\simeq 130 \pm 30 cm^{-1}$. This agrees quite well with the frequency of the lowest in plane bending vibration estimated from the inertial defect (equation 2.35) to be $\simeq 150 cm^{-1}$, probably corresponding to the I-N-C bending vibration.

In addition, an analysis of the quadrupole coupling constants of ^{127}I have established that there is approximately 23% ionic character in the I-N bond.

Table 5.13 summarises the ionic bond character of the halogen-nitrogen bond in the halogen isocyanates. The trend of decreasing electronegativity from Cl to I is reflected in the increasing ionic character of the halogen-nitrogen bond. This trend also apparently follows the stability of the halogen isocyanates with ClNCO being much less stable than INCO.

Table 5.13

Ionic bond character of the halogen isocyanates

	% Ionic Character	% π Bonding	% Single Bond Character
ClNCO	9.0	4.0	87.0
BrNCO	12.4	0.5	87.1
INCO	23.3	0.4	76.3

Bibliography

1. L. Birckenbach, M. Linhard, Ber. 63, 2544-2558, (1930); 64, 961-968, (1931).

2. S. Rosen, D. Swern, Anal. Chem. 38, 1392-1397, (1966).

3. C.G. Gebelein, J. Macromol. Sci.-Chem. A5, 433-442 (1971).

4. J. Macazaga, S. Delgado, J.R. Masaguer, J. Organometallic. Chem. 259, 233-236 (1983).

5. D.C. Frost, C.B. MacDonald, C.A. McDowell, N.P.C. Westwood, Chem. Phys. 47, 111-124 (1980).

6. W.H. Hocking, M.C.L. Gerry, J. Mol Spectrosc. 42, 547-566 (1972).

7. W.H. Hocking, M.L. Williams, M.C.L. Gerry, J. Mol Spectrosc. 58, 250-260 (1975).

8. J. Jander, Adv. Inorg. Chem. Radiochem. 19, 1-63 (1976).

9. H. Pritzkow, Monatsh. 105, 621-628 (1974).

10. L. Pauling. "The Nature of the Chemical Bond" 3rd ed., Cornell University Press, Ithaca, N.Y., 1960.

11. D. Cramb, Private Communication.

CHAPTER VI: THE MICROWAVE SPECTRUM OF BROMINE THIOCYANATE, BrSCN

6.1 Introduction

The chemistry of bromine thiocyanate, an unstable intermediate, has been studied in solution (1-4). In common with the other halogen thiocyanates, it can be prepared in a mixture of the halogen and the pseudohalogen $(SCN)_2$, which has previously been prepared by mixing $Pb(SCN)_2$ and a solution of bromine:

$$\text{(i)} \quad Pb(SCN)_2 + Br_2 \rightarrow (SCN)_2 + PbBr_2$$

$$\text{(ii)} \quad (SCN)_2 + X_2 \rightarrow 2XSCN \qquad X = Cl, Br, I \qquad (6.1)$$

In solution, BrSCN undergoes addition reactions with alkenes. However, the reaction products are not unique, with both bromothiocyanato and dibromo derivatives being formed (2). It has also being used as a reagent in thiocyanation reactions (8, 9).

Both infra-red solution studies and chemical studies of these halogen thiocyanates (1-7) confirm that the halogen is linked *via* the S atom.

The only previous gas-phase study of BrSCN was of its He(I) photoelectron spectrum by Frost *et al* (10). It was formed by the gas phase titration of $(SCN)_2$ with Br_2. Since the configuration of chlorine thiocyanate in the gas-phase has been shown in a microwave study to be ClSCN (11), it seems likely,

especially since the photoelectron spectrum of BrSCN directly parallels that of ClSCN, that BrSCN also has a thiocyanate structure.

Accordingly, the aim of this microwave study was to assign the ground state rotational spectrum of bromine thiocyanate and to determine whether the molecule has a thiocyanate or isothiocyanate structure.

6.2 Experimental Methods

BrSCN was prepared according to the method of Frost et al (10, 12). Silver thiocyanate was prepared by mixing aqueous solutions of potassium thiocyanate and silver nitrate. The resulting precipitate was filtered, washed, and then dried in the air and stored in the dark until use.

AgSCN was loosely packed using glass wool into a U-shaped tube, and dried thoroughly under vacuum for several hours while being heated to 100°C. The solid sample was then cooled to room temperature and gaseous bromine was passed over it. The reaction products depended on the pressure of the Br_2 and the way it came in contact with the solid.

If the Br_2 was simply passed through the solid sample, (Figure 6.1 (a)) the spectrum of $S(CN)_2$ resulted, along with some lines of SO_2 and HNCS. No lines belonging to $(SCN)_2$ could be identified, although this was the major reaction product expected (12). However, when the bromine was merely passed over the AgSCN at low pressure, in such a way that the gaseous

reaction products reacted with more bromine, the spectrum of BrSCN appeared almost immediately. (See Figure 6.1 (b)) Its formation is entirely analogous with its formation in solution:

$$\text{(i)} \quad 2AgNCS(s) + Br_2(g) \rightarrow (SCN)_2(g) + 2AgBr(s)$$

$$\text{(ii)} \quad (SCN)_2(g) + Br_2(g) \rightarrow 2BrSCN(g) \qquad (6.2)$$

Throughout the microwave study, BrSCN was produced solely in a flow system, and the cell was kept at room temperature.

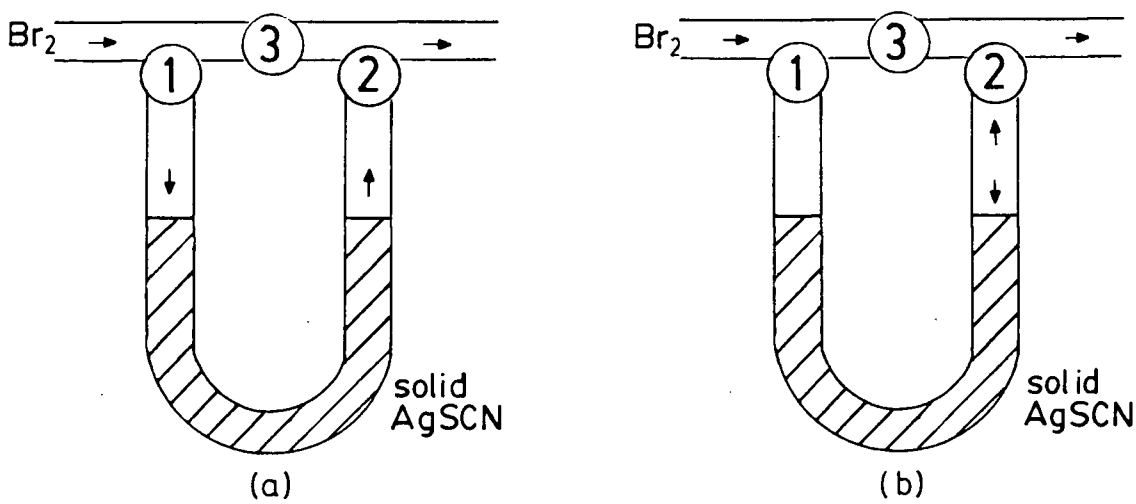

Figure 6.1 Preparation of BrSCN:

(a) Stopcocks 1 and 2 were open, stopcock 3 was closed. Gaseous Br_2 was passed through the solid AgSCN. the resulting microwave spectrum predominantly showed lines of $S(CN)_2$.

(b) Stopcock 1 was closed, stopcocks 2 and 3 were open. Gaseous Br_2 was passed over the AgSCN and the gaseous reaction products reacted with further bromine. The microwave spectrum predominately showed transitions of BrSCN.

6.3 Analysis of the Microwave Spectrum

The rotational constants of bromine thiocyanate were predicted for both isotopes of bromine and for both possible configurations: BrSCN and BrNCS. The former arrangement of atoms was more likely in analogy to ClSCN, although the latter configuration could not initially be ruled out. For BrSCN the structure was assumed by transferring the Br-S bond length from S_2Br_2 (13) and the S-C and C-N bond lengths and the S-C-N angle from $S(CN)_2$ (14). The Br-S-C angle was taken to be the same as the C-S-C angle in $S(CN)_2$. For BrNCS, the Br-N bond length was transferred from BrNCO. The Br-N-C angle was taken to be that of BrNCO, but increased by 7° in keeping with other isocyanates and isothiocyanates (15,16). The parameters of the N-C-S chain were transferred from HNCS (16). The predicted rotational constants for both possible configurations are shown in Table 6.1.

For both possible configurations, the molecule was predicted to be a planar near-symmetric prolate rotor having both a- and b-type transitions. However, the spectrum predicted for each configuration was quite different. The a-type transitions of BrNCS would be much more closely spaced than for the BrSCN isomer, while the magnitude of A_o for BrNCS is much larger than that predicted for BrSCN, and consequently it would be expected to have far fewer b-type transitions in the available frequency range.

The observed spectrum was similar to the spectra of BrNCO and INCO in that there was a series of strong a-type R branch

Table 6.1

The rotational constants of bromine thiocyanate and bromine isothiocyanate calculated from model structures.

	BrSCN	BrNCS
^{79}Br		
A_o (MHz)	9888.716	41482.906
B_o (MHz)	1882.847	1187.136
C_o (MHz)	1581.688	1154.109
^{81}Br		
A_o (MHz)	9872.200	41412.436
B_o (MHz)	1866.279	1176.730
C_o (MHz)	1569.562	1144.217

clusters throughout the spectrum; however, while the b-type transitions were extremely weak in the spectra of BrNCO and INCO so as to be very difficult to assign, they were reasonably intense in the spectrum of BrSCN. Consequently, their assignment was much more straightforward. The spacing of the a-type R branch clusters was found to be ≈3500 MHz, which was in reasonable agreement with the predicted (B+C) of BrSCN. Also, the pattern of the predicted b-type transitions for this configuration corresponded quite closely to those observed in the spectrum. It followed that this configuration was most likely to be the correct one.

All the transitions showed hyperfine splitting due to quadrupole coupling of the bromine nucleus (I = 3/2). Rough

values for the quadrupole coupling constants of the bromine nucleus in BrSCN were calculated by simply taking the ratio of χ_{aa} in BrSCN to χ_{aa} in ClSCN (11) to be the same as the ratio of the quadrupole moments of the bromine and chlorine nuclei. $(\chi_{bb} - \chi_{cc})$ was similarly estimated. These constants were then used to predict the first order hyperfine splitting patterns of both the a- and b-type transitions to facilitate the assignment of the spectrum. Unfortunately no hyperfine splitting due to the quadrupole coupling of the nitrogen nucleus was resolved for any transition.

Not all the transitions showed the predicted symmetrical splitting patterns. Some of the hyperfine structure was in fact significantly perturbed, indicating a higher order effect from the contribution of the off-diagonal term in the quadrupole coupling tensor, χ_{ab}. For BrSCN, χ_{ab}, calculated by assuming that the Br-S bond is a principal axis of the quadrupole tensor, was predicted to be large: the quadrupole moment of the Br atom is large, and θ_{za}, the angle between the z-axis in the principal quadrupole tensor and the a-inertial axis was calculated to be $\approx 33°$ (see Section 6.4). Also, several near-degeneracies of the type $\Delta F = 0$, $\Delta J = 0, \pm 1, \pm 2$, $\Delta K_a K_c$ = ee $\nleftrightarrow$ oe, oo $\nleftrightarrow$ eo, were likely, and transitions involving any of these energy levels were predicted to be significantly shifted from their first order prediction.

The complete analysis of the spectrum of BrSCN therefore required use of the global least-squares fitting procedure to obtain simultaneously the rotational, centrifugal distortion and

quadrupole coupling constants, including the off-diagonal term χ_{ab}. This was previously successfully employed in the analysis of BrNCO and INCO, which also have large perturbations in their hyperfine structure. However, unlike the analyses of these spectra, where the b-type transitions were relatively weak, the existence of strong, easily assignable, Q-branch b-type lines in the spectrum of BrSCN, precluded the necessity of using perturbations in the hyperfine structure of the a-type R branch transitions to find the rotational constant A_o.

First, B_o and C_o were calculated from a-type R branch K_a = 0 and the asymmetry split K_a = 1 transitions, which were either unperturbed or showed only small perturbations in their hyperfine structure. With the size of the asymmetry of the molecule (κ = -0.9263), these lines were well separated from the main cluster of lines. Transitions from one asymmetry branch of the $K_a = 2 \leftarrow 1$ b-type Q-branch ($J_{2,(J-2)} - J_{1,(J-1)}$) were assigned, to pinpoint a value of A_o. These were assigned from their hyperfine splitting patterns. Figure 6.2 shows the $13_{2,11} - 13_{1,12}$ transitions for both isotopes.

These transitions were used to fit values of A_o, B_o, C_o, χ_{aa}, $(\chi_{bb} - \chi_{cc})$, and χ_{ab}, so that further transitions could be assigned and these constants refined and the quartic distortion constants measured. K_a = 0 and 1 a-type R branch transitions were measured for J = 6 to 12. Several K_a = 2 and 3 asymmetry doublets from these branches were also measured. As well as several $K_a = 2 \leftarrow 1$ Q-branch transitions of the type mentioned, lines from the lower asymmetry sub-branches of the

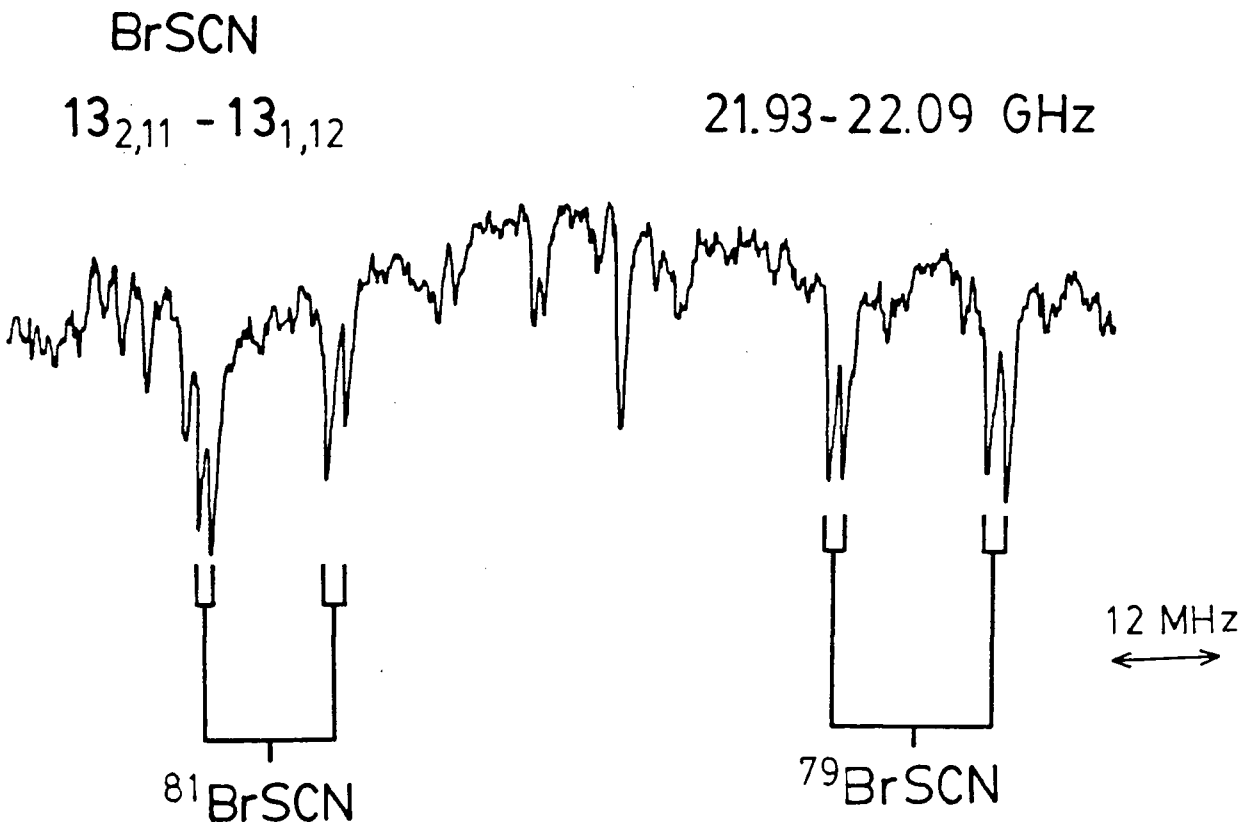

Figure 6.2 The transition $13_{2,11} - 13_{1,12}$ for ^{79}BrSCN and ^{81}BrSCN.

$K_a = 3 \leftarrow 2$ ($J_{3,(J-3)} - J_{2,(J-2)}$) and $K_a = 4 \leftarrow 3$ ($J_{4,(J-4)} - J_{3,(J-3)}$) Q branches were assigned. These were easily identified at the point where these sub-branches change direction to higher frequency. This is illustrated in Figure 6.3. A few lines of the other asymmetry sub-branch of the $K_a = 3 \leftarrow 2$ Q branch ($J_{3,(J-2)} - J_{2,(J-1)}$) and some $K_a = 1 \leftarrow 0$ and $K_a = 0 \leftarrow 1$ R branch transitions were measured to complete the analysis.

The final constants are shown in Table 6.2. As well as the

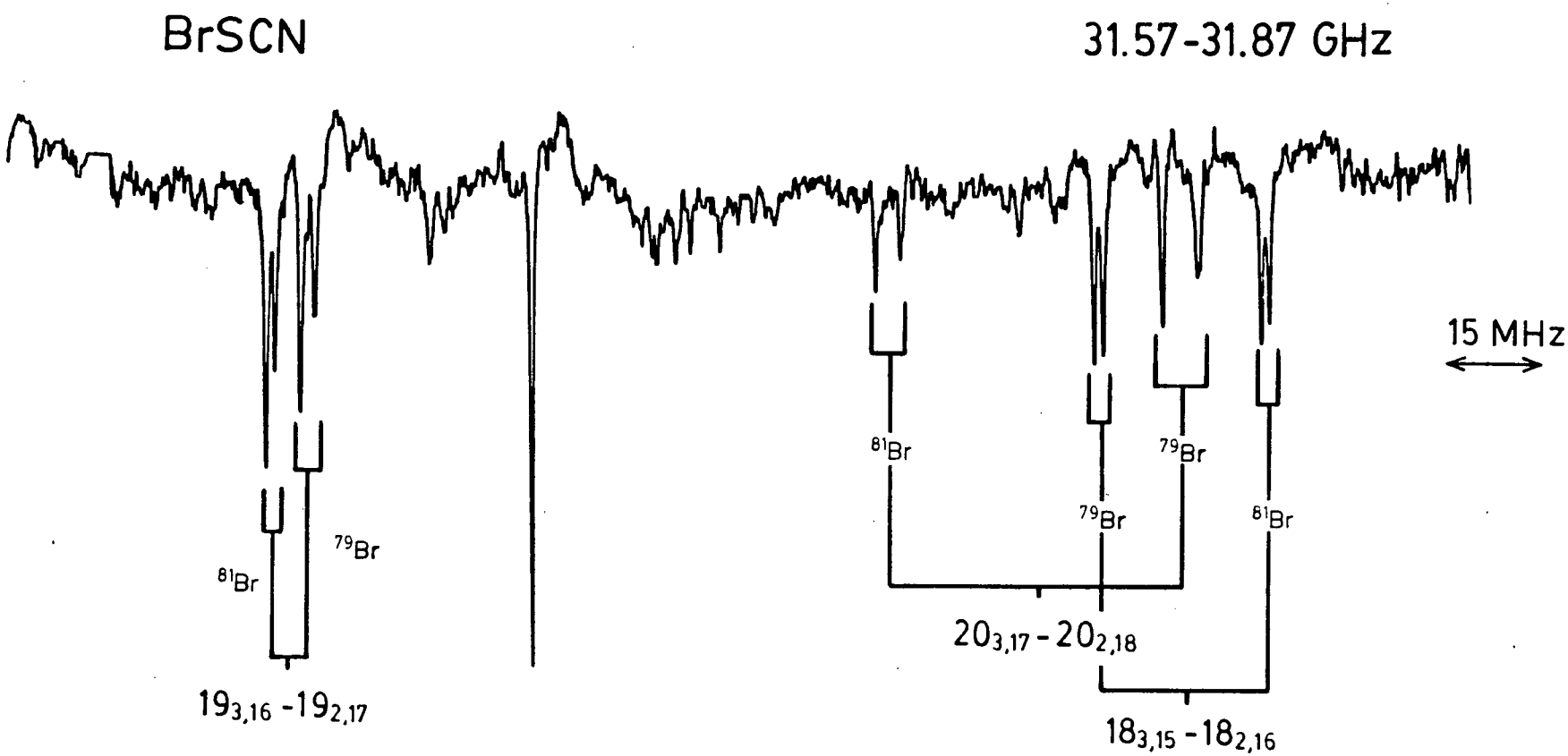

Figure 6.3 Broadband scan of the spectrum of BrSCN from 31.57 - 31.87 GHz. The transitions $18_{3,15}$ - $18_{2,16}$, $19_{3,16}$ - $19_{2,17}$ and $20_{3,17}$ - $20_{2,18}$ are shown for both isotopes.

Table 6.2

Spectroscopic constants of bromine thiocyanate

Parameter	^{79}BrSCN	^{81}BrSCN
Rotational Constants (MHz)		
A_o	10092.2012(68)[1]	10074.4731(78)
B_o	1944.40541(13)	1927.45095(13)
C_o	1627.94999(11)	1615.58914(10)
Centrifugal Distortion Constants (kHz)		
Δ_J	0.8477(18)	0.8271(22)
Δ_{JK}	-13.690(43)	-13.517(54)
Δ_K	104.2(12)	102.7(15)
δ_J	0.23956(43)	0.23530(55)
δ_K	2.010(39)	1.989(52)
Bromine Quadrupole Coupling Constants (MHz)		
χ_{aa}	402.62(77)	336.4(12)
$\chi_{bb}-\chi_{cc}$	366.20(16)	304.42(20)
χ_{ab}	478.41(23)	397.74(38)
Inertial defect (a.m.u. Å^2)		
Δ	0.448	0.449
Number of Rotational Transitions	56	55
Standard Deviation of fit (MHz)	0.044	0.055

[1] Numbers in parentheses are one standard deviation in units of the last significant figures.

rotational constants and the bromine quadrupole coupling constants, all five quartic centrifugal distortion constants were measured.

The frequencies of all the measured transitions are given in Tables 6.4 and 6.5. The transitions have been weighted according to their resolvability and whether they are partially overlapped by other transitions. The comparison of the residuals, with χ_{ab} included in the calculation of the exact frequencies, and with χ_{ab} omitted, which approximates a first order calculation, indicates that there are several important near-degeneracies, primarily affecting the measured a-type transitions. These are all of the type $K_a = 2 \leftrightarrow 1$ and $K_a = 3 \leftrightarrow 2$. The closest near-degeneracy separates the hypothetical unsplit rotational energy levels $9_{1,9}$ and $8_{2,7}$ by ≃265 MHz in the case of ^{79}BrSCN and ≃407 MHz in ^{81}BrSCN. This produces shifts in the hyperfine structure of measured transitions which involve the $9_{1,9}$ level, from a first-order pattern by as much as 30 MHz in ^{79}BrSCN and up to ≃13 MHz in ^{81}BrSCN. Table 6.3 indicates some of the closest near-degeneracies.

Table 6.3

Closest near degeneracies having the correct symmetry to cause perturbations in hyperfine structure in the spectrum of bromine thiocyanate.

Energy Levels	Difference in Energy (MHz) ^{79}BrSCN	^{81}BrSCN
$6_{1,5}$ - $5_{2,3}$	-590.84	-793.51
$9_{1,9}$ - $8_{2,7}$	-265.13	-406.54
$10_{1,9}$ - $9_{2,8}$	1584.16	1439.67
$11_{2,9}$ - $10_{3,7}$	1645.41	1247.23
$12_{2,11}$ - $11_{3,9}$	-694.41	-976.20
$13_{2,12}$ - $12_{3,10}$	2165.01	1872.17

Table 6.4 Measured rotational transitions (in MHz) of ^{79}BrSCN

Transition F' - F"	Normalised[1] Weight	Observed Frequency	Residuals[2] Without χ_{ab}	Residuals[2] With χ_{ab}
$7_{1,7}$ - $6_{1,6}$				
17/2 - 15/2	1.000	23786.693	0.053	0.016
15/2 - 13/2	1.000	23789.286	-0.376	-0.003
11/2 - 9/2	1.000	23790.086	-0.559	-0.068
13/2 - 11/2	1.000	23793.610	-0.092	0.018
$7_{0,7}$ - $6_{0,6}$				
17/2 - 15/2	1.000	24518.481	0.052	0.008
11/2 - 9/2	1.000	24520.856	-0.290	0.007
15/2 - 13/2	1.000	24523.468	-0.129	0.026
13/2 - 11/2	1.000	24526.252	-0.070	-0.028
$7_{1,6}$ - $6_{1,5}$				
17/2 - 15/2	1.000	25981.968	0.172	0.053
13/2 - 11/2	1.000	25987.525	1.319	0.080
11/2 - 9/2	0.100	25997.999	15.313	0.123
15/2 - 13/2	0.100	25997.999	12.732	-0.057
$8_{1,8}$ - $7_{1,7}$				
19/2 - 17/2	1.000	27148.453	0.035	0.005
17/2 - 15/2	0.500	27149.908	-1.042	0.049
13/2 - 11/2	0.500	27150.324	-1.199	-0.002
15/2 - 13/2	1.000	27153.938	-0.139	-0.043
$8_{0,8}$ - $7_{0,7}$				
19/2 - 17/2	1.000	27869.916	0.047	0.011
13/2 - 11/2	1.000	27871.645	-0.209	-0.018
17/2 - 15/2	1.000	27875.241	-0.044	0.059
15/2 - 13/2	1.000	27877.345	0.043	0.061
$8_{1,7}$ - $7_{1,6}$				
13/2 - 11/2	0.500	29638.808	-1.297	-0.018
19/2 - 17/2	0.500	29639.418	0.028	-0.057
17/2 - 15/2	1.000	29641.682	-0.930	-0.055
15/2 - 13/2	1.000	29643.412	0.054	0.036
$9_{1,9}$ - $8_{1,8}$				
19/2 - 17/2	1.000	30474.460	-25.762	-0.050
15/2 - 13/2	1.000	30488.289	-12.151	0.007
21/2 - 19/2	1.000	30498.014	0.045	0.019
17/2 - 15/2	1.000	30502.019	-0.688	-0.003

[1] Measurements were weighted according to $1/\sigma^2$, where σ is the uncertainty in the measurements. Unit weight corresponded to an uncertainty of 0.03 MHz.

[2] Observed frequency minus the frequency calculated using the constants in Table 6.2.

Table 6.4 (Continued)

Transition F' - F"	Normalised Weight	Observed Frequency	Residuals Without χ_{ab}	Residuals With χ_{ab}
$9_{0\,9}$ - $8_{0\,8}$				
21/2 - 19/2	1.000	31179.518	0.056	0.026
15/2 - 13/2	1.000	31180.779	-0.195	-0.062
19/2 - 17/2	1.000	31184.831	-0.036	0.038
17/2 - 15/2	1.000	31186.466	-0.004	0.005
$9_{1\,8}$ - $8_{1\,7}$				
21/2 - 19/2	0.100	33271.870	0.100	0.036
15/2 - 13/2	0.100	33271.870	-0.527	-0.128
19/2 - 17/2	1.000	33274.708	-0.302	-0.030
17/2 - 15/2	1.000	33275.656	-0.005	-0.055
$10_{1\,10}$ - $9_{1\,9}$				
23/2 - 21/2	1.000	33835.401	0.009	-0.012
19/2 - 17/2	1.000	33840.263	0.775	-0.042
17/2 - 15/2	0.500	33855.848	18.445	-0.107
21/2 - 19/2	1.000	33868.105	30.638	-0.038
$10_{0\,10}$ - $9_{0\,9}$				
23/2 - 21/2	1.000	34454.411	0.040	0.014
17/2 - 15/2	0.768	34455.325	-0.096	0.001
21/2 - 19/2	1.000	34459.303	-0.054	0.004
19/2 - 17/2	1.000	34460.878	-0.011	-0.004
$10_{2\,9}$ - $9_{2\,8}$				
17/2 - 15/2	0.100	35493.140	-0.192	0.154
23/2 - 21/2	0.100	35493.140	1.322	-0.054
21/2 - 19/2	1.000	35496.066	-0.189	0.033
19/2 - 17/2	1.000	35498.483	2.137	0.020
$10_{3\,8}$ - $9_{3\,7}$				
17/2 - 15/2	1.000	35863.912	-0.278	0.049
23/2 - 21/2	1.000	35864.916	0.997	0.013
21/2 - 19/2	1.000	35869.046	0.118	0.014
19/2 - 17/2	0.500	35869.799	0.514	0.044
$10_{3\,7}$ - $9_{3\,6}$				
23/2 - 21/2	1.000	35982.892	-5.508	0.036
19/2 - 17/2	1.000	35985.299	-7.246	-0.008
17/2 - 15/2	1.000	35988.357	-0.443	-0.131
21/2 - 19/2	1.000	35991.800	-0.264	-0.075
$10_{2\,8}$ - $9_{2\,7}$				
21/2 - 19/2	1.000	36751.031	-1.152	0.085
17/2 - 15/2	0.500	36753.317	-1.348	0.067
19/2 - 17/2	0.500	36753.317	0.004	-0.031
23/2 - 21/2	0.500	36753.653	0.077	-0.013

Table 6.4 (Continued)

Transition F' - F"	Normalised Weight	Observed Frequency	Residuals Without χ_{ab}	Residuals With χ_{ab}
$10_{1\,9}$ - $9_{1\,8}$				
23/2 - 21/2	0.500	36874.089	0.093	0.044
17/2 - 15/2	0.500	36874.089	-0.266	-0.064
21/2 - 19/2	1.000	36877.300	-0.112	0.026
19/2 - 17/2	1.000	36877.877	0.089	0.043
$11_{1\,11}$ - $10_{1\,10}$				
19/2 - 17/2	1.000	37160.568	-2.205	-0.043
25/2 - 23/2	1.000	37161.104	-0.002	-0.020
23/2 - 21/2	1.000	37161.668	-1.385	-0.019
21/2 - 19/2	1.000	37164.620	-0.106	-0.027
$11_{0\,11}$ - $10_{0\,10}$				
25/2 - 23/2	1.000	37703.711	-0.035	-0.057
19/2 - 17/2	1.000	37705.567	-0.098	-0.007
23/2 - 21/2	1.000	37709.293	0.014	0.042
21/2 - 19/2	1.000	37709.698	-0.033	-0.016
$11_{2\,10}$ - $10_{2\,9}$				
19/2 - 17/2	1.000	38985.034	-0.805	0.039
25/2 - 23/2	1.000	38985.679	0.405	-0.044
23/2 - 21/2	1.000	38987.672	-0.725	0.015
21/2 - 19/2	1.000	38990.044	0.557	-0.013
$11_{3\,9}$ - $10_{3\,8}$				
19/2 - 17/2	0.100	39464.936	-0.039	0.074
23/2 - 21/2	1.000	39468.320	-0.036	0.035
25/2 - 23/2	1.000	39472.350	7.727	0.037
21/2 - 19/2	1.000	39475.583	6.809	0.002
$11_{3\,8}$ - $10_{3\,7}$				
19/2 - 17/2	1.000	39664.034	-0.145	-0.029
23/2 - 21/2	1.000	39665.671	0.057	0.029
25/2 - 23/2	1.000	39666.155	2.528	-0.038
21/2 - 19/2	1.000	39669.494	3.270	-0.025
$11_{2\,9}$ - $10_{2\,8}$				
21/2 - 19/2	1.000	40563.801	0.233	0.027
25/2 - 23/2	1.000	40564.123	0.042	-0.020
23/2 - 21/2	1.000	40568.213	5.578	0.002
19/2 - 17/2	1.000	40571.828	6.844	-0.014
$11_{1\,10}$ - $10_{1\,9}$				
25/2 - 23/2	0.100	40440.946	0.179	0.140
19/2 - 17/2	0.100	40440.946	-0.129	-0.004
23/2 - 21/2	0.500	40444.394	-0.067	0.019
21/2 - 19/2	0.500	40444.779	-0.004	-0.043

Table 6.4 (Continued)

Transition F' - F"	Normalised Weight	Observed Frequency	Residuals Without χ_{ab}	Residuals With χ_{ab}
$12_{1\,12} - 11_{1\,11}$				
27/2 - 25/2	1.000	40475.840	0.029	0.013
21/2 - 19/2	1.000	40476.624	-0.623	0.0
25/2 - 23/2	1.000	40477.225	-0.428	-0.001
23/2 - 21/2	1.000	40479.106	0.010	0.045
$12_{0\,12} - 11_{0\,11}$				
27/2 - 25/2	1.000	40936.990	0.089	0.071
21/2 - 19/2	1.000	40937.318	-0.255	-0.083
25/2 - 23/2	1.000	40941.081	-0.001	0.031
23/2 - 21/2	1.000	40942.039	-0.209	0.001
$12_{2\,11} - 11_{2\,10}$				
21/2 - 19/2	1.000	42455.891	-6.872	0.017
25/2 - 23/2	0.500	42457.166	-7.934	-0.001
27/2 - 25/2	1.000	42462.373	0.238	0.015
23/2 - 21/2	1.000	42465.999	0.152	0.025
$12_{3\,10} - 11_{3\,9}$				
27/2 - 25/2	1.000	43051.182	-12.124	0.015
23/2 - 21/2	1.000	43054.541	-12.124	-0.072
21/2 - 19/2	1.000	43063.601	-0.110	0.006
25/2 - 23/2	1.000	43065.805	-0.395	-0.099
$12_{3\,9} - 11_{3\,8}$				
27/2 - 25/2	0.100	43366.981	0.528	0.122
21/2 - 19/2	0.100	43366.981	-0.092	0.036
25/2 - 23/2	0.100	43366.981	-0.186	-0.114
23/2 - 21/2	1.000	43368.254	0.425	-0.027
$12_{2\,10} - 11_{2\,9}$				
25/2 - 23/2	1.000	44368.265	-2.548	-0.004
21/2 - 19/2	1.000	44369.292	-3.444	-0.068
23/2 - 21/2	1.000	44371.522	-0.039	0.004
27/2 - 25/2	1.000	44372.018	0.009	-0.037
$12_{1\,11} - 11_{1\,10}$				
27/2 - 25/2	1.000	43966.862	0.112	0.081
21/2 - 19/2	1.000	43966.862	-0.102	-0.016
25/2 - 23/2	0.500	43970.747	-0.034	0.028
23/2 - 21/2	0.500	43970.993	-0.018	-0.050
$12_{1\,12} - 11_{0\,11}$				
27/2 - 25/2	0.100	42646.644	0.085	0.060
21/2 - 19/2	0.100	42646.644	0.592	-0.176
25/2 - 23/2	0.100	42659.909	0.498	-0.072
23/2 - 21/2	0.100	42659.909	0.285	0.209

Table 6.4 (Continued)

Transition F' - F"	Normalised Weight	Observed Frequency	Residuals Without χ_{ab}	Residuals With χ_{ab}
$13_{1\,13} - 12_{0\,12}$				
29/2 - 27/2	1.000	45490.044	-0.035	-0.055
23/2 - 21/2	1.000	45490.787	0.695	0.057
27/2 - 25/2	0.500	45500.964	0.466	0.070
25/2 - 23/2	0.500	45500.964	0.225	-0.041
$14_{1\,14} - 13_{0\,13}$				
31/2 - 29/2	1.000	48404.308	0.053	0.036
25/2 - 23/2	1.000	48404.795	0.316	-0.018
29/2 - 27/2	0.500	48412.841	0.316	0.019
27/2 - 25/2	0.500	48412.841	-0.042	-0.031
$15_{1\,15} - 14_{0\,14}$				
33/2 - 31/2	1.000	51383.554	0.022	0.009
27/2 - 25/2	1.000	51384.158	0.280	0.016
31/2 - 29/2	0.100	51390.373	0.324	0.091
29/2 - 27/2	0.100	51390.373	-0.116	-0.114
$12_{0\,12} - 11_{1\,11}$				
25/2 - 23/2	1.000	38758.334	-0.990	0.039
23/2 - 21/2	1.000	38761.409	-0.311	0.010
27/2 - 25/2	1.000	38766.203	0.050	0.041
21/2 - 19/2	0.500	38767.253	-1.514	0.048
$13_{0\,13} - 12_{1\,12}$				
27/2 - 25/2	1.000	42446.687	-0.603	0.019
25/2 - 23/2	1.000	42449.203	0.026	0.052
29/2 - 27/2	1.000	42452.130	-0.027	-0.036
23/2 - 21/2	1.000	42453.392	-0.779	0.032
$15_{0\,15} - 14_{1\,14}$				
31/2 - 29/2	1.000	49585.948	-0.351	-0.033
29/2 - 27/2	1.000	49587.495	-0.055	-0.035
33/2 - 31/2	1.000	49588.438	0.047	0.038
27/2 - 25/2	1.000	49589.282	-0.428	-0.020
$16_{0\,16} - 15_{1\,15}$				
33/2 - 31/2	1.000	53058.843	-0.240	0.004
31/2 - 29/2	0.100	53060.202	0.080	0.095
35/2 - 33/2	0.100	53060.202	-0.077	-0.085
29/2 - 27/2	1.000	53061.064	-0.308	0.003
$13_{2\,11} - 13_{1\,12}$				
27/2 - 27/2	1.000	22043.064	0.294	-0.025
25/2 - 25/2	1.000	22045.171	-0.036	-0.013
29/2 - 29/2	1.000	22064.703	0.016	0.012
23/2 - 23/2	0.500	22067.530	0.358	0.014

Table 6.4 (Continued)

Transition F' - F"	Normalised Weight	Observed Frequency	Residuals Without χ_{ab}	Residuals With χ_{ab}
$^{14}{}_{2\ 12}$ - $^{14}{}_{1\ 13}$				
29/2 - 29/2	1.000	23100.077	0.192	-0.010
27/2 - 27/2	1.000	23102.644	-0.031	-0.004
31/2 - 31/2	1.000	23126.847	0.045	0.032
25/2 - 25/2	1.000	23129.906	0.235	0.043
$^{15}{}_{2\ 13}$ - $^{15}{}_{1\ 14}$				
31/2 - 31/2	1.000	24522.033	0.139	-0.012
29/2 - 29/2	1.000	24524.821	-0.040	-0.016
33/2 - 33/2	1.000	24553.501	0.019	-0.002
27/2 - 27/2	1.000	24556.832	0.090	-0.035
$^{16}{}_{2\ 14}$ - $^{16}{}_{1\ 15}$				
33/2 - 33/2	1.000	26323.997	0.137	0.015
31/2 - 31/2	1.000	26327.378	0.022	0.009
35/2 - 35/2	1.000	26360.322	0.114	0.087
29/2 - 29/2	1.000	26363.405	0.074	-0.044
$^{17}{}_{2\ 15}$ - $^{17}{}_{1\ 16}$				
35/2 - 35/2	1.000	28513.068	0.103	-0.006
33/2 - 33/2	1.000	28516.505	-0.021	0.035
37/2 - 37/2	1.000	28553.209	-0.010	-0.044
31/2 - 31/2	1.000	28556.745	0.128	0.091
$^{18}{}_{2\ 16}$ - $^{18}{}_{1\ 17}$				
37/2 - 37/2	1.000	31083.442	0.117	0.016
35/2 - 35/2	0.500	31086.835	-0.128	-0.087
39/2 - 39/2	1.000	31127.053	0.060	0.020
33/2 - 33/2	1.000	31130.490	-0.013	-0.046
$^{17}{}_{3\ 15}$ - $^{17}{}_{2\ 16}$				
35/2 - 35/2	0.500	48953.793	1.748	0.0
33/2 - 33/2	0.500	48954.258	-0.202	-0.120
37/2 - 37/2	0.500	48979.983	-0.193	-0.135
31/2 - 31/2	1.000	48984.696	2.073	0.004
$^{18}{}_{3\ 15}$ - $^{18}{}_{2\ 16}$				
39/2 - 39/2	0.500	31796.927	0.033	0.030
33/2 - 33/2	0.500	31796.927	0.387	0.067
37/2 - 37/2	0.100	31798.831	0.458	0.185
35/2 - 35/2	0.100	31798.831	-0.107	-0.138
$^{18}{}_{3\ 16}$ - $^{18}{}_{2\ 17}$				
37/2 - 37/2	1.000	50483.824	0.644	0.004
35/2 - 35/2	1.000	50485.479	-0.062	0.007
39/2 - 39/2	1.000	50512.093	-0.075	-0.042
33/2 - 33/2	1.000	50515.192	0.649	-0.053

Table 6.4 (Continued)

Transition F' - F"	Normalised Weight	Observed Frequency	Residuals Without χ_{ab}	Residuals With χ_{ab}
$^{19}_{3\ 16} - {}^{19}_{2\ 17}$				
39/2 - 39/2	0.500	31633.001	0.223	0.057
37/2 - 37/2	0.500	31633.001	0.013	-0.002
41/2 - 41/2	1.000	31635.683	0.024	0.017
35/2 - 35/2	1.000	31636.091	0.191	0.0
$^{19}_{3\ 17} - {}^{19}_{2\ 18}$				
37/2 - 37/2	1.000	52186.309	-0.011	0.043
41/2 - 41/2	1.000	52213.579	0.039	0.056
35/2 - 35/2	0.500	52215.793	0.464	0.125
$^{20}_{3\ 17} - {}^{20}_{2\ 18}$				
41/2 - 41/2	1.000	31810.444	0.130	0.016
39/2 - 39/2	1.000	31810.820	-0.017	-0.029
43/2 - 43/2	1.000	31817.705	-0.004	-0.014
37/2 - 37/2	1.000	31818.401	0.119	-0.007
$^{22}_{3\ 19} - {}^{22}_{2\ 20}$				
45/2 - 45/2	1.000	33333.022	0.070	-0.002
43/2 - 43/2	1.000	33334.111	-0.060	-0.039
47/2 - 47/2	1.000	33349.587	0.055	0.040
41/2 - 41/2	1.000	33350.487	-0.026	-0.069
$^{23}_{3\ 20} - {}^{23}_{2\ 21}$				
47/2 - 47/2	1.000	34727.587	0.141	0.077
45/2 - 45/2	1.000	34728.833	-0.001	0.012
49/2 - 49/2	1.000	34748.251	-0.043	-0.062
43/2 - 43/2	1.000	34749.638	0.053	0.014
$^{24}_{3\ 21} - {}^{24}_{2\ 22}$				
49/2 - 49/2	1.000	36562.329	0.048	-0.012
47/2 - 47/2	1.000	36563.859	0.003	0.016
51/2 - 51/2	1.000	36587.216	0.014	-0.007
45/2 - 45/2	1.000	36588.710	0.008	-0.023
$^{26}_{4\ 22} - {}^{26}_{3\ 23}$				
49/2 - 49/2	0.500	42280.139	0.155	0.056
55/2 - 55/2	0.500	42280.139	-0.064	-0.073
51/2 - 51/2	0.100	42284.232	0.200	0.176
53/2 - 53/2	0.100	42284.232	-0.047	-0.127
$^{27}_{4\ 23} - {}^{27}_{3\ 24}$				
57/2 - 57/2	0.500	41864.304	0.056	0.046
51/2 - 51/2	0.500	41864.304	0.048	-0.046
53/2 - 53/2	0.500	41864.616	0.026	-0.018
55/2 - 55/2	0.500	41864.616	-0.023	-0.084

Table 6.4 (Continued)

Transition F' - F"	Normalised Weight	Observed Frequency	Residuals Without χ_{ab}	Residuals With χ_{ab}
$28_{4\ 24} - 28_{3\ 25}$				
59/2 - 59/2	1.000	41842.025	0.078	0.067
53/2 - 53/2	1.000	41842.715	-0.002	-0.043
55/2 - 55/2	0.500	41838.727	0.121	0.118
57/2 - 57/2	0.500	41839.301	0.014	-0.041

Table 6.5 Measured rotational transitions (in MHz) of ^{81}BrSCN

Transition F' - F"	Normalised[1] Weight	Observed Frequency	Residuals[2] Without χ_{ab}	Residuals[2] With χ_{ab}
$7_{1,7}$ - $6_{1,6}$				
17/2 - 15/2	1.000	23600.994	0.017	-0.011
15/2 - 13/2	1.000	23603.280	-0.207	0.035
11/2 - 9/2	1.000	23603.993	-0.332	-0.005
13/2 - 11/2	1.000	23606.793	-0.067	0.008
$7_{0,7}$ - $6_{0,6}$				
17/2 - 15/2	1.000	24327.058	0.026	-0.002
11/2 - 9/2	1.000	24329.117	-0.199	0.011
15/2 - 13/2	1.000	24331.202	-0.084	0.027
13/2 - 11/2	1.000	24333.615	0.041	0.073
$7_{1,6}$ - $6_{1,5}$				
17/2 - 15/2	1.000	25764.780	0.084	0.0
13/2 - 11/2	1.000	25769.026	0.654	-0.042
11/2 - 9/2	0.100	25774.304	8.842	0.245
15/2 - 13/2	0.100	25774.304	6.733	-0.100
$8_{1,8}$ - $7_{1,7}$				
19/2 - 17/2	1.000	26937.043	0.008	-0.016
17/2 - 15/2	0.500	26938.539	-0.596	0.081
13/2 - 11/2	0.500	26938.944	-0.686	0.080
15/2 - 13/2	1.000	26941.625	-0.121	-0.059
$8_{0,8}$ - $7_{0,7}$				
19/2 - 17/2	1.000	27654.686	0.021	-0.002
13/2 - 11/2	1.000	27656.179	-0.156	-0.020
17/2 - 15/2	1.000	27659.074	-0.059	0.015
15/2 - 13/2	1.000	27660.763	-0.061	-0.045
$8_{1,7}$ - $7_{1,6}$				
13/2 - 11/2	0.500	29392.619	-0.871	0.095
19/2 - 17/2	0.500	29392.907	0.032	-0.027
17/2 - 15/2	1.000	29394.885	-0.649	0.017
15/2 - 13/2	1.000	29396.091	-0.080	-0.088
$9_{1,9}$ - $8_{1,8}$				
19/2 - 17/2	1.000	30253.948	-9.082	-0.045
15/2 - 13/2	1.000	30256.989	-6.240	-0.009
21/2 - 19/2	1.000	30261.182	0.018	-0.002
17/2 - 15/2	1.000	30264.830	-0.275	0.015

[1] Measurements were weighted according to $1/\sigma^2$, where σ is the uncertainty in the measurements. Unit weight corresponded to an uncertainty of 0.03 MHz.

[2] Observed frequency minus the frequency calculated using the constants in Table 6.2.

Table 6.5 (Continued)

Transition F' - F"	Normalised Weight	Observed Frequency	Residuals Without χ_{ab}	Residuals With χ_{ab}
$9_{0\,9}$ - $8_{0\,8}$				
21/2 - 19/2	1.000	30941.085	0.050	0.032
15/2 - 13/2	1.000	30942.180	-0.132	-0.035
19/2 - 17/2	1.000	30945.499	-0.013	0.041
17/2 - 15/2	1.000	30946.853	0.006	0.016
$9_{1\,8}$ - $8_{1\,7}$				
21/2 - 19/2	1.000	32996.687	0.025	-0.020
15/2 - 13/2	1.000	32996.687	-0.360	-0.070
19/2 - 17/2	0.500	32999.105	-0.222	-0.024
17/2 - 15/2	0.500	32999.573	0.024	-0.014
$10_{1\,10}$ - $9_{1\,9}$				
23/2 - 21/2	1.000	33573.369	-0.058	-0.076
19/2 - 17/2	1.000	33577.213	0.381	-0.009
17/2 - 15/2	1.000	33585.911	10.803	-0.011
21/2 - 19/2	1.000	33587.745	12.601	0.016
$10_{0\,10}$ - $9_{0\,9}$				
23/2 - 21/2	1.000	34192.997	0.063	0.049
17/2 - 15/2	1.000	34193.776	-0.095	-0.018
21/2 - 19/2	1.000	34197.107	-0.033	0.005
19/2 - 17/2	1.000	34198.349	0.0	0.008
$10_{2\,9}$ - $9_{2\,8}$				
17/2 - 15/2	0.100	35206.758	-0.131	0.095
23/2 - 21/2	0.100	35206.758	1.048	-0.080
21/2 - 19/2	1.000	35209.164	-0.145	-0.011
19/2 - 17/2	1.000	35211.150	1.690	0.056
$10_{3\,8}$ - $9_{3\,7}$				
17/2 - 15/2	1.000	35567.891	-0.234	0.045
23/2 - 21/2	1.000	35568.498	0.612	0.060
21/2 - 19/2	0.500	35572.237	0.162	0.125
19/2 - 17/2	0.500	35572.610	0.233	0.032
$10_{3\,7}$ - $9_{3\,6}$				
23/2 - 21/2	1.000	35682.658	-4.473	-0.044
19/2 - 17/2	1.000	35684.728	-5.900	0.0
17/2 - 15/2	1.000	35687.130	-0.338	-0.075
21/2 - 19/2	1.000	35690.004	-0.229	-0.082
$10_{2\,8}$ - $9_{2\,7}$				
21/2 - 19/2	1.000	36434.114	-0.698	0.019
19/2 - 17/2	0.100	36435.943	0.183	0.153
17/2 - 15/2	0.100	36435.943	-0.937	-0.083
23/2 - 21/2	0.100	36435.943	-0.019	-0.083

Table 6.5 (Continued)

Transition F' - F"	Normalised Weight	Observed Frequency	Residuals Without χ_{ab}	Residuals With χ_{ab}
$10_{1\,9}$ - $9_{1\,8}$				
23/2 - 21/2	0.100	36571.444	0.169	0.134
17/2 - 15/2	0.100	36571.444	-0.297	-0.155
21/2 - 19/2	1.000	36574.014	-0.066	0.033
19/2 - 17/2	1.000	36574.717	-0.020	-0.049
$11_{1\,11}$ - $10_{1\,10}$				
19/2 - 17/2	0.100	36874.010	-1.589	0.098
25/2 - 23/2	0.100	36874.010	-0.195	-0.211
23/2 - 21/2	0.100	36874.703	-1.114	-0.017
21/2 - 19/2	1.000	36877.209	-0.006	0.051
$11_{0\,11}$ - $10_{0\,10}$				
25/2 - 23/2	1.000	37419.232	0.052	0.041
19/2 - 17/2	1.000	37420.629	-0.077	-0.034
23/2 - 21/2	0.500	37423.684	-0.006	0.038
21/2 - 19/2	0.500	37424.049	-0.108	-0.093
$11_{2\,10}$ - $10_{2\,9}$				
19/2 - 17/2	0.500	38671.818	-0.463	0.064
25/2 - 23/2	0.500	38672.088	0.273	-0.059
23/2 - 21/2	1.000	38673.928	-0.465	-0.012
21/2 - 19/2	1.000	38675.751	0.429	-0.004
$11_{3\,9}$ - $10_{3\,8}$				
19/2 - 17/2	1.000	39139.000	-0.097	-0.017
23/2 - 21/2	0.100	39142.099	0.173	0.222
25/2 - 23/2	0.100	39142.099	3.297	-0.036
21/2 - 19/2	1.000	39145.656	3.391	0.112
$11_{3\,8}$ - $10_{3\,7}$				
19/2 - 17/2	1.000	39329.998	-0.005	0.077
23/2 - 21/2	1.000	39331.230	-0.015	-0.057
25/2 - 23/2	1.000	39332.084	2.545	0.065
21/2 - 19/2	0.500	39334.902	3.152	-0.068
$11_{2\,9}$ - $10_{2\,8}$				
21/2 - 19/2	0.100	40213.278	0.314	0.154
25/2 - 23/2	0.100	40213.278	-0.112	-0.157
23/2 - 21/2	1.000	40216.691	4.513	0.061
19/2 - 17/2	1.000	40219.743	5.588	-0.009
$11_{1\,10}$ - $10_{1\,9}$				
25/2 - 23/2	0.100	40111.653	0.074	0.047
19/2 - 17/2	0.100	40111.653	-0.195	-0.106
23/2 - 21/2	0.500	40114.537	-0.070	-0.008
21/2 - 19/2	0.500	40114.863	-0.023	-0.049

Table 6.5 (Continued)

Transition F' - F"	Normalised Weight	Observed Frequency	Residuals Without χ_{ab}	Residuals With χ_{ab}
$12_{1\,12} - 11_{1\,11}$				
27/2 - 25/2	1.000	40164.185	0.028	0.013
21/2 - 19/2	1.000	40164.895	-0.469	-0.016
25/2 - 23/2	1.000	40165.308	-0.375	-0.057
23/2 - 21/2	1.000	40166.910	0.018	0.040
$12_{0\,12} - 11_{0\,11}$				
27/2 - 25/2	0.500	40628.925	0.051	0.043
21/2 - 19/2	0.500	40629.218	-0.198	-0.096
25/2 - 23/2	1.000	40632.326	-0.021	0.0
23/2 - 21/2	1.000	40633.231	-0.100	-0.021
$12_{2\,11} - 11_{2\,10}$				
21/2 - 19/2	1.000	42119.239	-3.274	0.066
25/2 - 23/2	1.000	42120.968	-3.470	-0.037
27/2 - 25/2	1.000	42122.147	0.167	0.004
23/2 - 21/2	1.000	42125.199	0.139	0.006
$12_{3\,10} - 11_{3\,9}$				
27/2 - 25/2	1.000	42701.442	-6.461	0.078
23/2 - 21/2	1.000	42703.598	-7.110	0.072
21/2 - 19/2	1.000	42708.194	-0.055	0.023
25/2 - 23/2	1.000	42710.197	-0.124	0.045
$12_{3\,9} - 11_{3\,8}$				
27/2 - 25/2	0.100	42999.136	0.464	0.151
21/2 - 19/2	0.100	42999.136	-0.054	0.032
25/2 - 23/2	0.100	42999.136	-0.183	-0.137
23/2 - 21/2	1.000	43000.226	0.359	0.010
$12_{2\,10} - 11_{2\,9}$				
25/2 - 23/2	1.000	43985.660	-2.489	-0.025
21/2 - 19/2	1.000	43986.501	-3.285	-0.005
23/2 - 21/2	1.000	43988.768	-0.013	0.037
27/2 - 25/2	1.000	43989.128	-0.041	-0.074
$12_{1\,11} - 11_{1\,10}$				
27/2 - 25/2	0.500	43612.402	0.030	0.008
21/2 - 19/2	0.500	43612.402	-0.161	-0.100
25/2 - 23/2	0.100	43615.752	0.077	0.121
23/2 - 21/2	0.100	43615.752	-0.124	-0.146
$12_{1\,12} - 11_{0\,11}$				
27/2 - 25/2	0.500	42376.320	0.110	0.028
21/2 - 19/2	0.500	42376.320	0.548	-0.090
23/2 - 21/2	0.100	42387.484	0.235	0.122
25/2 - 23/2	0.100	42387.484	0.404	-0.123

Table 6.5 (Continued)

Transition F' - F"	Normalised Weight	Observed Frequency	Residuals Without χ_{ab}	Residuals With χ_{ab}
$13_{1\,13}$ - $12_{0\,12}$				
29/2 - 27/2	0.500	45191.522	0.031	-0.057
23/2 - 21/2	0.500	45191.891	0.394	-0.134
27/2 - 25/2	1.000	45200.618	0.283	-0.119
25/2 - 23/2	1.000	45200.618	0.106	-0.077
$14_{1\,14}$ - $13_{0\,13}$				
31/2 - 29/2	0.500	48076.846	0.060	-0.036
25/2 - 23/2	0.500	48077.207	0.241	-0.120
29/2 - 27/2	0.500	48084.042	0.222	-0.119
27/2 - 25/2	0.500	48084.042	-0.056	-0.128
$15_{1\,15}$ - $14_{0\,14}$				
33/2 - 31/2	0.500	51027.030	0.046	-0.062
27/2 - 25/2	0.500	51027.401	0.133	-0.196
31/2 - 29/2	0.100	51032.750	0.213	-0.098
29/2 - 27/2	0.100	51032.750	-0.138	-0.231
$12_{0\,12}$ - $11_{1\,11}$				
25/2 - 23/2	0.500	38410.064	-0.886	-0.020
23/2 - 21/2	1.000	38412.821	-0.153	0.061
27/2 - 25/2	1.000	38416.798	-0.023	0.035
21/2 - 19/2	1.000	38417.818	-1.190	0.003
$13_{0\,13}$ - $12_{1\,12}$				
27/2 - 25/2	1.000	42077.895	-0.472	0.096
25/2 - 23/2	1.000	42079.944	-0.013	0.073
29/2 - 27/2	1.000	42082.530	-0.051	0.017
23/2 - 21/2	1.000	42083.585	-0.676	0.016
$15_{0\,15}$ - $14_{1\,14}$				
31/2 - 29/2	1.000	49176.783	-0.370	0.003
29/2 - 27/2	1.000	49178.124	-0.086	0.023
33/2 - 31/2	1.000	49178.942	-0.065	0.027
27/2 - 25/2	1.000	49179.644	-0.469	-0.036
$16_{0\,16}$ - $15_{1\,15}$				
33/2 - 31/2	1.000	52629.383	-0.197	0.142
31/2 - 29/2	0.100	52630.518	0.061	0.182
35/2 - 33/2	0.100	52630.518	-0.148	-0.039
29/2 - 27/2	1.000	52631.243	-0.338	0.045
$13_{2\,11}$ - $13_{1\,12}$				
27/2 - 27/2	1.000	21955.197	0.296	0.063
25/2 - 25/2	1.000	21956.873	-0.010	0.007
29/2 - 29/2	1.000	21972.735	0.038	0.036
23/2 - 23/2	1.000	21975.046	0.336	0.082

Table 6.5 (Continued)

Transition F' - F"	Normalised Weight	Observed Frequency	Residuals Without χ_{ab}	Residuals With χ_{ab}
$^{14}{}_{2\ 12}$ - $^{14}{}_{1\ 13}$				
29/2 - 29/2	1.000	22970.004	0.183	0.038
27/2 - 27/2	1.000	22972.062	-0.037	-0.018
31/2 - 31/2	1.000	22991.750	-0.019	-0.027
25/2 - 25/2	1.000	22994.208	0.111	-0.029
$^{15}{}_{2\ 13}$ - $^{15}{}_{1\ 14}$				
31/2 - 31/2	1.000	24342.389	0.122	0.015
29/2 - 29/2	1.000	24344.708	-0.021	-0.004
33/2 - 33/2	1.000	24368.156	0.022	0.008
27/2 - 27/2	1.000	24370.858	0.102	0.012
$^{16}{}_{2\ 14}$ - $^{16}{}_{1\ 15}$				
33/2 - 33/2	1.000	26088.090	0.139	0.052
31/2 - 31/2	1.000	26090.776	-0.049	-0.048
35/2 - 35/2	1.000	26117.835	0.080	0.061
29/2 - 29/2	1.000	26120.347	0.053	-0.025
$^{17}{}_{2\ 15}$ - $^{17}{}_{1\ 16}$				
35/2 - 35/2	1.000	28214.886	0.048	-0.029
33/2 - 33/2	1.000	28217.702	-0.051	-0.009
37/2 - 37/2	1.000	28247.880	-0.021	-0.045
31/2 - 31/2	1.000	28250.666	-0.030	-0.054
$^{18}{}_{2\ 16}$ - $^{18}{}_{1\ 17}$				
37/2 - 37/2	1.000	30718.746	0.023	-0.047
35/2 - 35/2	1.000	30721.620	-0.087	-0.058
39/2 - 39/2	1.000	30754.684	0.013	-0.014
33/2 - 33/2	1.000	30757.595	0.031	0.007
$^{17}{}_{3\ 15}$ - $^{17}{}_{2\ 16}$				
35/2 - 35/2	0.500	48760.444	1.370	-0.131
33/2 - 33/2	1.000	48761.000	-0.071	-0.013
37/2 - 37/2	1.000	48782.276	-0.062	-0.018
$^{18}{}_{3\ 15}$ - $^{18}{}_{2\ 16}$				
35/2 - 35/2	1.000	31832.303	0.045	0.030
37/2 - 37/2	1.000	31832.654	0.229	0.024
39/2 - 39/2	0.500	31830.840	0.126	0.125
33/2 - 33/2	0.500	31830.840	0.271	0.029
$^{18}{}_{3\ 16}$ - $^{18}{}_{2\ 17}$				
37/2 - 37/2	1.000	50257.717	0.468	-0.026
35/2 - 35/2	1.000	50259.092	-0.108	-0.059
39/2 - 39/2	1.000	50281.177	-0.051	-0.025
33/2 - 33/2	0.500	50283.626	0.435	-0.109

Table 6.5 (Continued)

Transition F' - F"	Normalised Weight	Observed Frequency	Residuals Without χ_{ab}	Residuals With χ_{ab}
$19_{3\ 16} - 19_{2\ 17}$				
39/2 - 39/2	1.000	31626.135	0.159	0.036
37/2 - 37/2	1.000	31626.135	0.023	0.012
41/2 - 41/2	0.500	31627.936	0.093	0.089
35/2 - 35/2	0.500	31628.167	0.168	0.027
$19_{3\ 17} - 19_{2\ 18}$				
37/2 - 37/2	0.500	51924.463	0.099	0.138
41/2 - 41/2	0.500	51947.175	0.059	0.072
35/2 - 35/2	0.500	51949.413	0.401	0.133
$20_{3\ 17} - 20_{2\ 18}$				
41/2 - 41/2	0.500	31752.252	0.169	0.086
39/2 - 39/2	0.500	31752.527	0.046	0.038
43/2 - 43/2	1.000	31757.655	-0.015	-0.022
37/2 - 37/2	1.000	31758.181	0.082	-0.010
$22_{3\ 19} - 22_{2\ 20}$				
45/2 - 45/2	1.000	33141.743	0.129	0.078
43/2 - 43/2	1.000	33142.585	-0.024	-0.003
47/2 - 47/2	1.000	33154.851	0.027	0.017
41/2 - 41/2	1.000	33155.562	-0.006	-0.032
$24_{3\ 21} - 24_{2\ 22}$				
49/2 - 49/2	1.000	36202.721	0.122	0.080
47/2 - 47/2	1.000	36203.810	-0.058	-0.048
51/2 - 51/2	1.000	36222.795	0.056	0.043
45/2 - 45/2	1.000	36223.924	-0.029	-0.051
$26_{4\ 22} - 26_{3\ 23}$				
49/2 - 49/2	0.500	42384.580	0.149	0.077
55/2 - 55/2	0.500	42384.580	-0.068	-0.074
51/2 - 51/2	0.100	42388.465	0.098	0.081
53/2 - 53/2	0.100	42388.465	-0.138	-0.196
$27_{4\ 23} - 27_{3\ 24}$				
57/2 - 57/2	1.000	41902.265	0.010	0.003
51/2 - 51/2	1.000	41902.265	0.046	-0.014
53/2 - 53/2	0.500	41903.148	0.014	-0.007
55/2 - 55/2	0.500	41903.148	-0.054	-0.098
$28_{4\ 24} - 28_{3\ 25}$				
55/2 - 55/2	1.000	41796.875	-0.007	-0.007
57/2 - 57/2	1.000	41796.875	0.025	-0.011
59/2 - 59/2	0.100	41799.153	0.129	0.121
53/2 - 53/2	0.100	41799.153	-0.077	-0.107

6.4 The Structure of BrSCN

Despite only having rotational constants for ^{79}BrSCN and ^{81}BrSCN, some deductions can be made about the structure of the molecule. It is most probably planar, as indicated by the inertial defect which is small and positive, and is essentially the same for both isotopes (see Section 2.5). This is confirmed by the ratio of the out-of-plane quadrupole coupling constants χ_{cc} (^{81}Br) / χ_{cc} (^{79}Br) = 0.8335, which is close to the ratio of the quadrupole moments of the bromine nuclei (0.8353).

As was mentioned previously, the measured rotational constants confirm that the correct configuration of bromine thiocyanate is BrSCN rather than BrNCS. A comparison of the predicted rotational constants for each of these configurations with the measured constants are shown in Table 6.6.

A fit of the rotational constants to the structural parameters of BrSCN was made. The S-C and C-N bond lengths were held fixed at their values in $S(CN)_2$(14). The SCN angle was fixed at 5° with the N atom in a trans configuration to the Br atom. This is the deviation from linearity in the S-C-N group in $S(CN)_2$. This S-C-N angle was also used in calculating a partial r_o structure for ClSCN (11), giving reasonable values for the structural parameters. Values for the Br-S bond length and the Br-S-C angle were found in the least squares fit (Table 6.7). Comparisons of these values with those in similar molecules, and with the sum of the single bond radii, show that they are reasonable (Table 6.8). The Br-S bond length is similar to that found in other molecules, while the BrSC angle

Table 6.6

Comparison of the measured rotational constants of bromine thiocyanate with those calculated from model structures

	Calculated		Experimental
	BrSCN	BrNCS	
^{79}Br			
A_o (MHz)	9888.716	41482.906	10092.2012(68)
B_o (MHz)	1882.847	1187.136	1944.40541(13)
C_o (MHz)	1581.688	1154.109	1627.94999(11)
^{81}Br			
A_o (MHz)	9872.200	41412.436	10074.4731(78)
B_o (MHz)	1866.279	1176.730	1927.45095(13)
C_o (MHz)	1569.562	1144.217	1615.58914(10)

Table 6.7

Structural parameters of bromine thiocyanate

r(Br-S)	2.18 Å
r(S-C)[1]	1.701 Å
r(C-N)[1]	1.156 Å
<(Br-S-C)	99.75°
<(S-C-N)[1]	5.0°
<(Br-S-a)[2]	34.4°

[1] Constrained to values transferred from $S(CN)_2$ (11)

[2] The angle between the Br-S bond and the a-inertial axis.

Table 6.8

Comparison of structural parameters of BrSCN with structures of other molecules

r(Br-S)/Å	
BrSCN	2.18
S_2Br_2 (13)	2.237
$SOBr_2$ (17)	2.27
SO_2BrF (18)	2.155
$BrSF_5$ (19)	2.190
Sum of single bond radii (20)	2.162
<(X-S-C)/deg	
BrSCN	99.75
ClSCN (8)	99.8
$S(CN)_2$ (14)	98.4
CH_3SCN (15)	99.9

is ≈99° in common with other molecules containing the -SCN group with the thiocyanate configuration. The position of the atoms relative to the principal axes are shown in Figure 6.4.

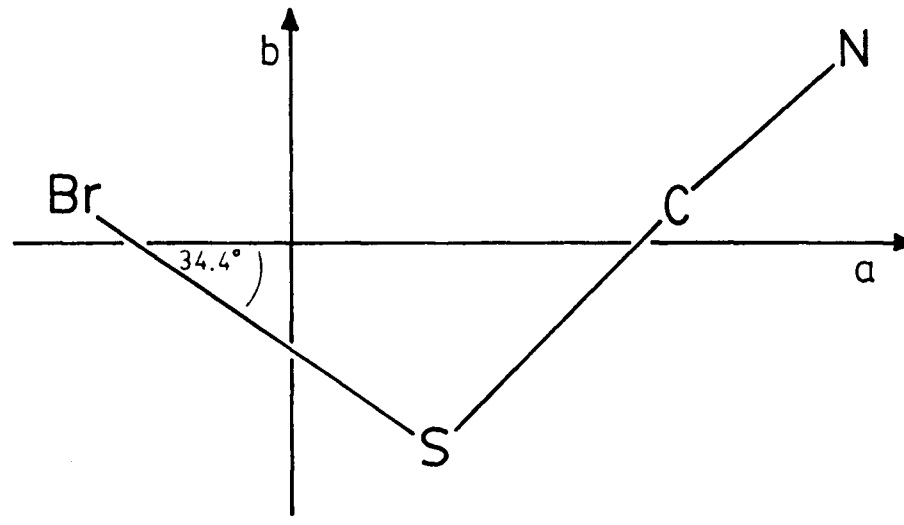

Figure 6.4 The positions of the atoms of BrSCN relative to its principal inertial axis system.

6.5 Bromine Quadrupole Coupling

The quadrupole coupling constants for the bromine nucleus in BrSCN in the inertial axis system are given in Table 6.9. Unfortunately no nitrogen quadrupole coupling could be resolved at all. Once again, the Br quadrupole tensors were diagonalized, to give the principal values of the bromine quadrupole coupling tensors, as well as θ_{za}, the angle between the z-principal axis and the a-inertial axis (Table 6.10).

Table 6.9

Quadrupole coupling constants of bromine thiocyanate in the principal inertial axes system

	^{79}BrSCN	^{81}BrSCN
χ_{aa} (MHz)	402.62(77)	336.4(12)
χ_{bb} (MHz)	- 18.21(39)	-16.00(20)
χ_{cc} (MHz)	-384.41(39)	-320.42(62)
χ_{ab} (MHz)	478.41(23)	397.74(38)

Table 6.10

Principal values of the bromine quadrupole coupling tensor of bromine thiocyanate

	^{79}BrSCN	^{81}BrSCN
χ_{zz} (MHz)	714.85(63)	595.2(10)
χ_{xx} (MHz)	-330.44(26)	-274.82(71)
χ_{yy} (MHz)	-384.41(39)	-320.42(62)
θ_{za} (deg)	33.12(2)	33.05(4)

A comparison of θ_{za} with the angle between the Br-S bond axis and the a-inertial axis (see Table 6.7) indicates that principal z axis essentially lies along the Br-S bond, i.e., it is not a bent bond (the maximum electron density lies along the Br-S bond). It is interesting that θ_{za} is $\approx$1° less than <(Br-S-a), in common with the corresponding comparisons in BrNCO and INCO.

This trend has also been observed in other molecules (21). No theory has been proposed which would account for this; however the effect probably arises because the electrons in the bond between the quadrupolar nucleus and the atom to which it is attached are not independent of the other electrons in the molecule.

The amount of π character in the Br-S bond is calculated from the difference between χ_{xx} and χ_{yy}, reflecting a difference in the p-orbital populations along these directions (see equation 4.6). The contribution of a π bonded resonance structure to the overall structure is calculated to be $\approx$4.6%. Hence, there is more electronic charge in the p_y (out of plane) orbital than in the p_x orbital. It cannot be ascertained whether this π bonding character is out-of-plane, with electron density donated from the sulfur atom towards the bromine atom, or whether there is π character in the plane of the molecule, with the p_x orbital of the Br atom sharing its electrons with an orbital of the sulfur atom. The corresponding resonance forms are:

I(a) I(b)

Using the theory of Townes and Dailey, as described in Section 4.8, the contribution of the various possible resonance forms to the Br-S bond can be calculated. The two other possible resonance forms affecting the nature of the Br-S bond

are:

II III

Form II shows a totally covalent Br-S bond, while form III indicates a totally ionic Br-S bond, with the negative pole on the bromine atom because $|\chi_{zz}| < |eQq_{Br}|$.

The contribution of form III, representing the ionic character of the Br-S bond, is designated i, and is calculated by comparing χ_{zz} and eQq_{Br}:

$$\chi_{zz} = -eQq_{Br} \left[(U_p)_z^{II} \ (1-i-\pi) + i(U_p)_z^{III} + \pi(U_p)_z^{I} \right]$$

In form III, the ionic character produces a closed shell on the bromine, so that it has zero coupling ($(U_p)_z^{III} = 0$). Because it is uncertain whether form I(a) or form I(b) is the correct resonance structure representing π bonding, values for i were calculated for both possibilities. For the former i $\approx$ 5%, and for the latter i $\approx$ 9%. Hence, whichever π-bonded resonance structure is the correct one, the Br-S bond is predominately covalent, which agrees with the comparison of the Br-S bond length with the sum of the covalent radii of the Br and S atoms (see Table 6.8).

6.6 Discussion

BrSCN has only previously been studied in the gaseous phase in a photoelectron study (12). Analysis of the microwave spectrum of BrSCN has yielded values for all three rotational constants, as well as all five quartic centrifugal distortion constants for both isotopic species. Both a-type R branch transitions and b-type transitions from several different branches were measured.

Many lines due to transitions within excited vibrational states of the molecule were also observed. Relative intensity measurements indicate that the lowest excited vibrational state lies $\approx 154 \pm 30$ cm^{-1} above the ground state. This is in excellent agreement with the frequency of the lowest-in-plane bending vibration which was calculated, using the inertial defect in equation 2.35, to be ≈ 150 cm^{-1}.

It was unfortunate that I could not detect any transitions of the pseudohalogen $(SCN)_2$. This was probably partly due to the instability of the molecule, with any $(SCN)_2$ that was formed decomposing before it could be detected. Also, because the dipole moment of $S(CN)_2$, the transitions of which were observed spectroscopically when searching for transitions of $(SCN)_2$, is relatively large, the multitude of intense lines due to this molecule may have obscured transitions of any $(SCN)_2$ that might otherwise have been detected. The mechanism for the formation of $S(CN)_2$ is not known.

This study has allowed us to determine that BrSCN does indeed have a thiocyanate configuration rather than an

isothiocyanate one. A partial r_o structure was calculated to give reasonable values for the Br-S bond length and Br-S-C angle. No equilibrium or average structure was calculated for BrSCN. However the distortion constants measured in this study, coupled with the solution vibrational frequencies (4), although incomplete, may enable a force field calculation to be done which would allow a ground state average structure to be calculated. This avenue was not pursued at this time because a full structure requires a complete set of isotopic data.

In addition, the quadrupole coupling constants for the bromine nucleus have been measured, including the off-diagonal term, χ_{ab}, which was available because of the large number of perturbations in the hyperfine structure. The Br-S bond has been demonstrated to be essentially covalent with small amounts of ionic and π bonded character.

Bibliography

1. C. Raby, J. Claude, J. Buxeraud, Bull. Soc. Pharm. Bordeaux 114, 147-152, (1975).

2. C. Raby, J. Claude, J. Buxeraud, Bull. Soc. Pharm. Bordeaux 115, 153-161, (1976).

3. C. Raby, J. Buxeraud, C. Moesch, J. Claude, Bull. Soc. Pharm. Bordeaux 120, 33-38, (1981).

4. M.J. Nelson, A.D.E. Pullin. J. Chem. Soc. 604-612, (1960).

5. A.B. Angus, R.G.R. Bacon, J. Chem. Soc. 774-778, (1958).

6. R.G.R. Bacon, R.S. Irwin, J. Chem. Soc. 778-784, (1958).

7. C. Raby, J. Buxeraud, J. Claude, J. Ann Chim., 1, 65-7, (1976).

8. K. Yamane, K. Fujimori, S. Ichikawa, S. Miyoshi, K. Hashizume; Heterocycles. 20, 1263-1266 (1983).

9. K. Fujimori, N. Hirako, K. Yamane, Bull. Chem. Soc. Jpn. 56, 1247-1248, (1983).

10. D.C. Frost, C.B. MacDonald, C.A. McDowell, N.P.C. Westwood, J. Am. Chem. Soc. 103, 4423-4427, (1981).

11. R.J. Richards, R.W. Davis, M.C.L. Gerry, J. Chem. Soc. Chem., Comm., 915-916 (1980).

12. D.C. Frost, C. Kirby, W.M. Lau, C.B. MacDonald, C.A. McDowell, N.P.C. Westwood, Chem. Phys. Lett., 69, 1-6, (1980).

13. R. Kniep, L. Korte, D. Mootz, Z. Naturforsch, b38, 1-6, (1983).

14. L. Pierce, R. Nelson, C.H. Thomas, J. Chem. Phys. 43, 3423-3431, (1965).

15. R.G. Lett, W.H. Flygare, J. Chem. Phys. 47, 4730-4750, (1976).

16. K. Yamada, M. Winnewisser, G. Winnewisser, L.B. Szalanski, M.C.L. Gerry, J. Mol Spectrosc. 79, 295 - 313, (1980).

17. J. Brunvoll, I. Hargittai, B. Rozsondai, J. Mol. Struct. 84, 153-155, (1982).

18. J. Raley, J.E. Wollrab, R.W. Lovejoy, J. Mol. Spectrosc. 48, 100-106, (1973).

19. R. Jurek, P. Goulet, C. Verry, A. Poinsot, Can. J. Phys. 61, 1405-1415 (1983).

20. L. Pauling. "The Chemical Bond" 3rd ed., Cornell University Press, Ithaca, New York, 1960.

21. M.C.L. Gerry, W. Lewis - Bevan, N.P.C. Westwood, J. Chem. Phys. 79, 4655-4663, (1983).

CHAPTER VII: THE INFRA-RED SPECTRUM OF AMINODIFLUOROBORANE, BF_2NH_2

7.1 Introduction

The aminoboranes can often be prepared by the pyrolysis of borane-amine complexes, e.g.:

$$R_3N{:}BR'_3 \xrightarrow{\Delta} R_2N\text{-}BR'_2 + R\text{-}R' \qquad (7.1)$$

For example, the parent compound, BH_2NH_2, the inorganic analogue of ethylene, is reported to be prepared by the thermal decomposition of BH_3NH_3 (1).

Similarly, gaseous aminodifluoroborane, BF_2NH_2, which is the inorganic analogue of 1,1-difluoroethylene, may be prepared by heating ammonia-boron trifluoride, BF_3NH_3. Early studies of the products of heating BF_3NH_3 suggested that the decomposition of the adduct above 125° took place according to (2):

$$4BF_3NH_3 \rightarrow 3NH_4^+BF_4^- + BN \qquad (7.2)$$

However, it was later shown that no boron nitride is present in the decomposition products, which do however contain several H-N-B-F species (3). The mass spectrum of the volatile decomposition products of the pyrolysis of BF_3NH_3 at 185° has been monitored carefully by Rothgery *et al* (4), showing that primarily BF_2NH_2 is formed, along with some trifluoroborazine, $(BFNH)_3$. The vapour can also be condensed to form polymeric

aminodifluoroborane (4,5).

Lovas and Johnson (6) have studied the microwave spectrum of BF_2NH_2, which was produced in a simple gas phase reaction of a mixture of NH_3 and BF_3, and later by the revaporization of the condensation products of this reaction by heating to 140°C. The measurement of the rotational constants of 6 isotopic species confirmed the ethylene-like planar structure of the molecule. The work also produced ground state centrifugal distortion constants and a value for the dipole moment.

No infra-red data is available in the literature for BF_2NH_2. The aim of this study was therefore to measure the infra-red spectrum of this molecule in the gas phase, and to evaluate the wavenumbers of the fundamental vibrations. The rotational structure of the 2_0^1 band was also investigated at high resolution to improve the accuracy of the ground state constants, and to measure for the first time rotational parameters of the 2^1 level.

7.2 Experimental Methods

BF_2NH_2 was prepared by heating solid BF_3NH_3:

$$BF_3NH_{3(s)} \xrightarrow{\Delta} BF_2NH_{2(g)} + HF_{(g)} \qquad (7.3)$$

The adduct was prepared by passing a stream of ammonia gas over a stirred solution of boron trifluoride etherate (BDH Chemicals), which was diluted with twice its volume of diethyl

ether (7). A white precipitate, which was BF_3NH_3, was formed. It was then washed with diethyl ether and dried under vacuum. Care was taken to keep the reaction flask flushed with nitrogen because BF_3NH_3 hydrolyses easily.

BF_3NH_3 was then loosely packed in a 20 cm pyrex tube and was heated to between 125° and 140°C. The reaction products were flowed through the long path cell with path length 8.25 m. Initially only residual solvent, diethyl ether was produced, but gradually the spectrum of BF_2NH_2 was detected, although some diethyl ether was still present contaminating the spectrum. When the BF_3NH_3 was heated to higher temperatures, the spectrum of the more stable trifluoroborazine, $(BFNH)_3$, started to appear, and above ≃180°, the sample decomposed rather rapidly and the spectrum disappeared.

Very little vapour pressure could be maintained, probably because the aminodifluoroborane was polymerizing in the cell. Therefore the spectra obtained were not very intense. High and low resolution spectra were recorded at low pressures (≈20-50 microns), some of which was due to diethyl ether. Portions of the spectrum between 400 and 3700 cm^{-1} were recorded at 0.05 and 0.01 cm^{-1} resolution to identify the fundamentals, and one band, the 2_0^1 band near 1608 cm^{-1}, was recorded at 0.004 cm^{-1} resolution. For this band, a total of 90 interferograms was co-added for the final interferogram. 10 interferograms were collected at a time, with each scan taking ≃$3\frac{1}{2}$ minutes, between which a low resolution scan was taken to ensure the continued

presence of BF_2NH_2. The empty cell was also scanned to give a background spectrum. No apodization function was used (boxcar truncation), and the interferograms were converted by the Fourier transformation operation to total intensity spectra, and then ratioed to give a transmittance spectrum. Finally the spectrum was converted to absorbance. A Bomem software peak-finding programme, which differentiates the peaks, was used to find the line positions.

A deuterated sample, BF_2ND_2, was also prepared by heating BF_3ND_3 which was prepared as above using gaseous ND_3 (MSD isotopes, 99.2 atom %D). Low resolution (0.05 cm^{-1}) spectra were recorded, as above.

7.3 Analysis of the Infra-red Spectrum

BF_2NH_2 is a planar, oblate near-symmetric rotor (κ = 0.8326) (6). The alignment of the principal inertial axes is shown in Figure 7.1. The molecule has C_{2v} symmetry and 3N - 6 = 12 vibrational degrees of freedom, which transform under the symmetry operations of this point group according to:

$$\Gamma_{(vib)} = 5A_1 + A_2 + 2B_1 + 4B_2 \qquad (7.4)$$

The fundamentals with A_1 symmetry give A-type bands, those with B_1 symmetry have C-type spectra, B-type bands correspond to B_2 symmetry, while the vibration with A_2 symmetry corresponds to the torsion and is infra-red inactive.

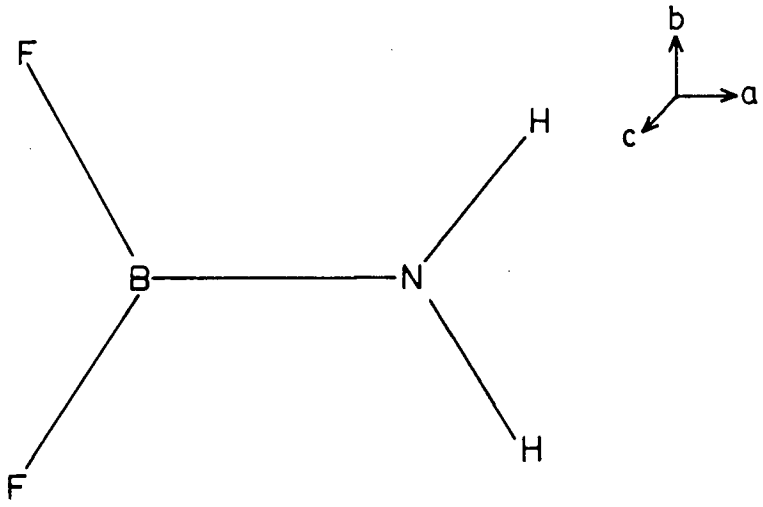

Figure 7.1 The configuration of the atoms of BF_2NH_2. The direction of the principal inertial axes is indicated.

Unfortunately the infra-red spectrum of BF_2NH_2 could not be completely assigned in this study. Some bands were too weak to be observed while others were overlapped. The bands which were observed have been assigned from the band contours (8), by analogy with the frequencies of the fundamentals of NH_2BH_2 (1,9) and HBF_2 (10,11), and from the frequencies calculated using ab-initio SCF calculations (12). The deuterated spectrum was even weaker, and it provided very limited information, although it did help to assign one band (see below).

A low resolution spectrum of BF_2NH_2, from 800 to 3700 cm^{-1} is shown in Figure 7.2. The pair of fundamentals at $\approx$3500 cm^{-1} is assigned to the N-H symmetric and asymmetric stretching vibrations ν_1, and ν_9, by analogy with BH_2NH_2. The band contours indicate that the band at 3576 cm^{-1} is a B-type band

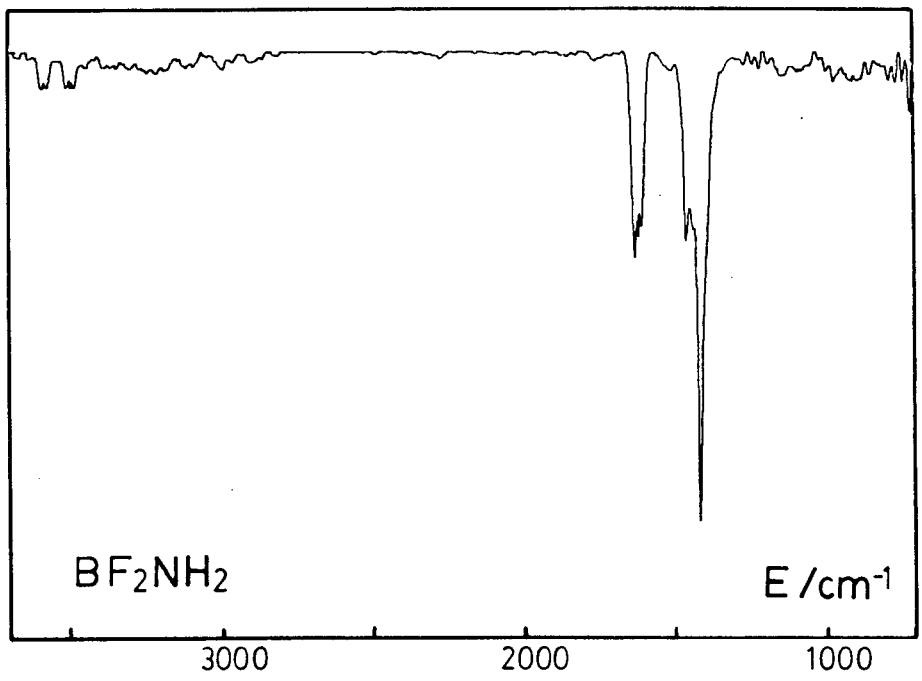

Figure 7.2 Low-resolution transmittance spectrum of gaseous BF_2NH_2 in the region 750-3700 cm^{-1}.

and therefore corresponds to ν_9, while the band at 3487 cm^{-1} is an A-type band and is the ν_1 fundamental. The A-type band at $\simeq$1608 cm^{-1} is the NH_2 symmetric bending vibration, again following BH_2NH_2. There are at least two overlapping fundamentals between 1360 and 1460 cm^{-1}. This region was investigated at 0.01 cm^{-1} resolution in order to make an assignment. A B-type band contour could be distinguished with a band centre at $\simeq$ 1339 cm^{-1}. This is probably the BF_2 asymmetric stretching mode. A tentative assignment for the B-N stretching vibration was made at 1406 cm^{-1}, which corresponds to the most intense portion of this region. Two bands were observed below 700 cm^{-1}. One, a C-type band centred at 661 cm^{-1} was assigned

to the BF_2 out-of-plane bending motion following the theoretical calculations. Also, this was the only band identified in the deuterated spectrum. Its frequency did not change much upon deuteration; it must therefore correspond to the BF_2 out-of-plane bending motion and not the NH_2 out-of-plane bending motion. The other lies at 439 cm^{-1} and corresponds to the BF_2 symmetric bend. This agrees extremely well with the rough approximation of the frequency of the lowest in-plane bending vibration calculated by Lovas and Johnson using the inertial defect to be $\simeq$440 cm^{-1}. A summary of these assignments is given in Table 7.1 along with any $^{10}BF_2NH_2$ band centres that could be identified and a comparison with the ab-initio calculations which are consistently higher than the measured frequencies, for both BF_2NH_2, and for BH_2NH_2 for which frequencies were also calculated (10). Table 7.2 gives a comparison of the fundamentals of BH_2NH_2 with the corresponding frequencies of the fundamentals of BF_2NH_2 and HBF_2.

7.4 Analysis of the Rotational Structure of the 2_0^1 Band.

The ν_2 fundamental at 1608 cm^{-1} is assigned to be due predominantly to the NH_2 symmetric bending motion. It was recorded at $\simeq$0.004 cm^{-1} resolution. It is an A-type band of a near-oblate asymmetric rotor with selection rules: $\Delta J = 0, \pm 1$, $\Delta K_a = 0, \pm 2 \ldots\ldots$ and $\Delta K_c = \pm 1, \pm 3 \ldots\ldots$. The spectrum at 0.05 cm^{-1} resolution is shown in Figure 7.3. It shows two intense central Q branch features belonging to the overlapping Q

Table 7.1

Vibrational frequencies of BF_2NH_2 (in cm^{-1})

Symmetry		$^{11}BF_2NH_2$	$^{10}BF_2NH_2$	$^{11}BF_2ND_2$	Calculated[1]
A_1	ν_1	3487[2]	-	-	3629
	ν_2	1608	1619	-	1793
	ν_3	(1406)[3]	-	-	1590
	ν_4	-	-	-	940
	ν_5	439	464	-	488
A_2	ν_6	I.R. inactive			553
B_1	ν_7	661	687	684	713
	ν_8	-	-	-	562
B_2	ν_9	3576	-	-	3736
	ν_{10}	1339	-	-	1663
	ν_{11}	-	-	-	1061
	ν_{12}	-	-	-	417

[1] From reference 12.

[2] Uncertanties are ±1 cm^{-1}.

[3] Estimated from most intense portion of spectrum.

Table 7.2

Vibrational Frequencies of BF_2NH_2 (in cm^{-1})

$^{11}BF_2NH_2$	$^{11}BH_2NH_2$[1]	$H^{11}BF_2$[2]	Type of Motion
3487	3451	-	NH symm. stretch
1608	1617	-	NH_2 symm. bend
(1406)[3]	1337	-	BN stretch
-	-	1167	BF symm. stretch
439	-	544	BF_2 symm. bend
I.R. inactive	830		Torsion
661	-	-	BF_2 out-of-plane
-	1005	-	NH_2 out-of-plane
3576	3534	-	NH asymm. stretch
1339	-	1404	BF asymm. stretch
-	1122	-	NH_2 asymm. bend
-	-	-	BF_2 asymm. bend

[1] From reference (1, 9).

[2] From reference (10, 11)

[3] Estimated from most intense portion of spectrum.

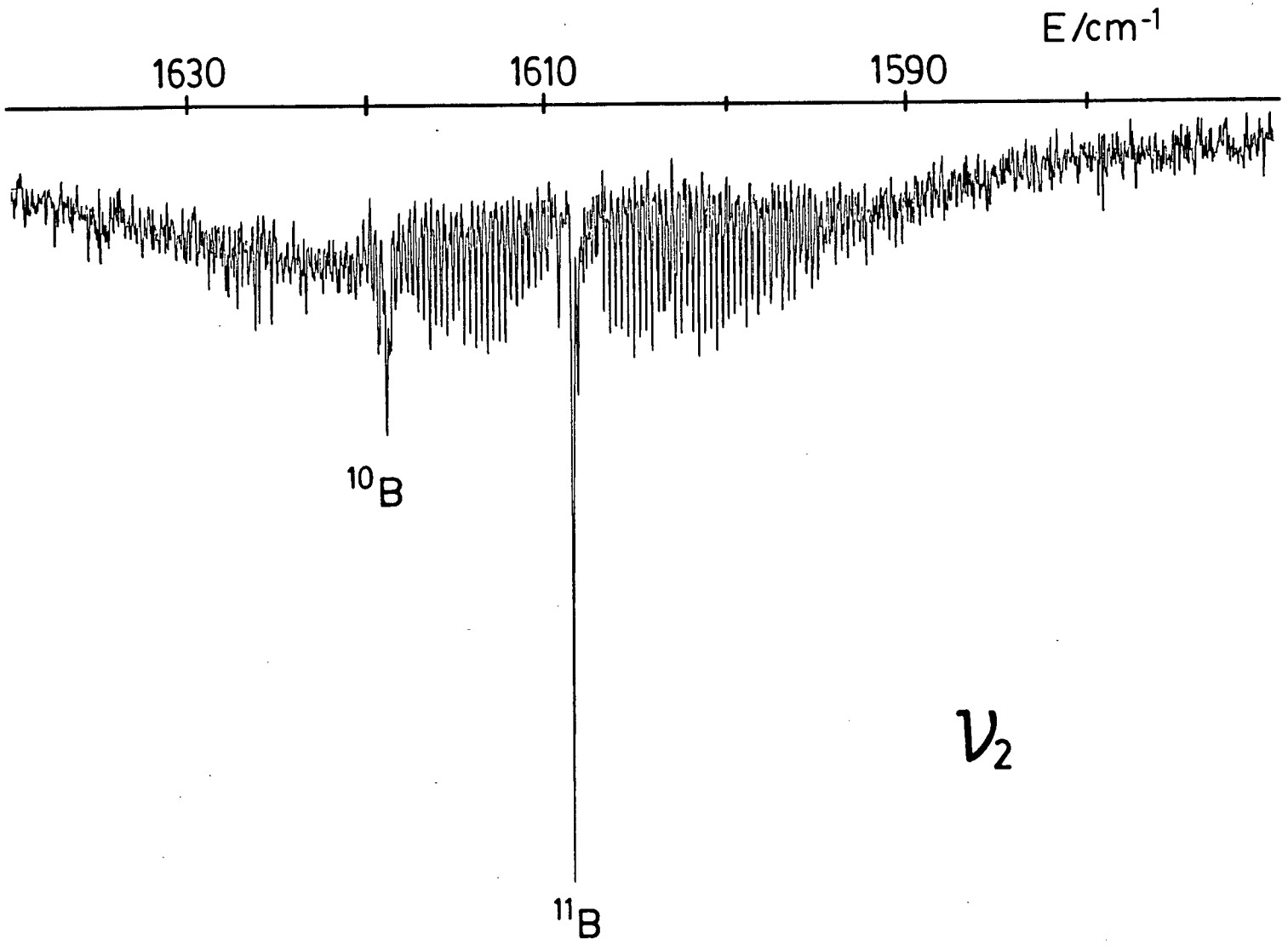

Figure 7.3 Medium resolution transmittance spectrum of the ν_2 fundamental of gaseous BF_2NH_2. The ^{10}B - ^{11}B shift is indicated.

branch lines of $^{11}BF_2NH_2$ and $^{10}BF_2NH_2$. The relative intensities of these features do not exactly reflect the relative abundances of each isotope ($^{11}B \simeq 80\%$ and $^{10}B \simeq 20\%$) probably because of underlying R branch transitions in the case of ^{10}B Q-branch spike. On either side of the band centre lie clusters of approximately equally spaced R- and P- branch transitions. The grouping together of transitions is common in oblate near-symmetric rotors when the rotational constants do not change much upon vibrational excitation and $C \simeq \frac{1}{4}(A + B)$ (13). Each cluster has a different value of $(2J-K_c)$ and they alternate between even and odd K_c. Within each cluster, the lower state quantum numbers of the transitions are $(J, K_c = J)$, $(J-1, K_c = J-2)$,... down to $((J+1)/2, K_c = 1)$ or $(J/2, K_c = 0)$. The spectrum therefore becomes more dense away from the band centre, both to high and low frequency. A section of the P branch side is shown in Figure 7.4. For a molecule with two equivalent H's and two equivalent F's the relative intensities of asymmetry split transitions given by the spin statistics are: $5(K_aK_c$ = ee or eo): $3(K_aK_c$ = oo or oe). However, because only a few asymmetry split transitions could be assigned because of the multitude of overlapped lines, it was difficult to see the exact intensity alternation.

Assignment of the quantum numbers of the ^{p}P and ^{r}R branch transitions, which were the strongest lines in the spectrum, were made using combination differences. The difference in frequency between pairs of ^{r}R and ^{p}P branch transitions, having

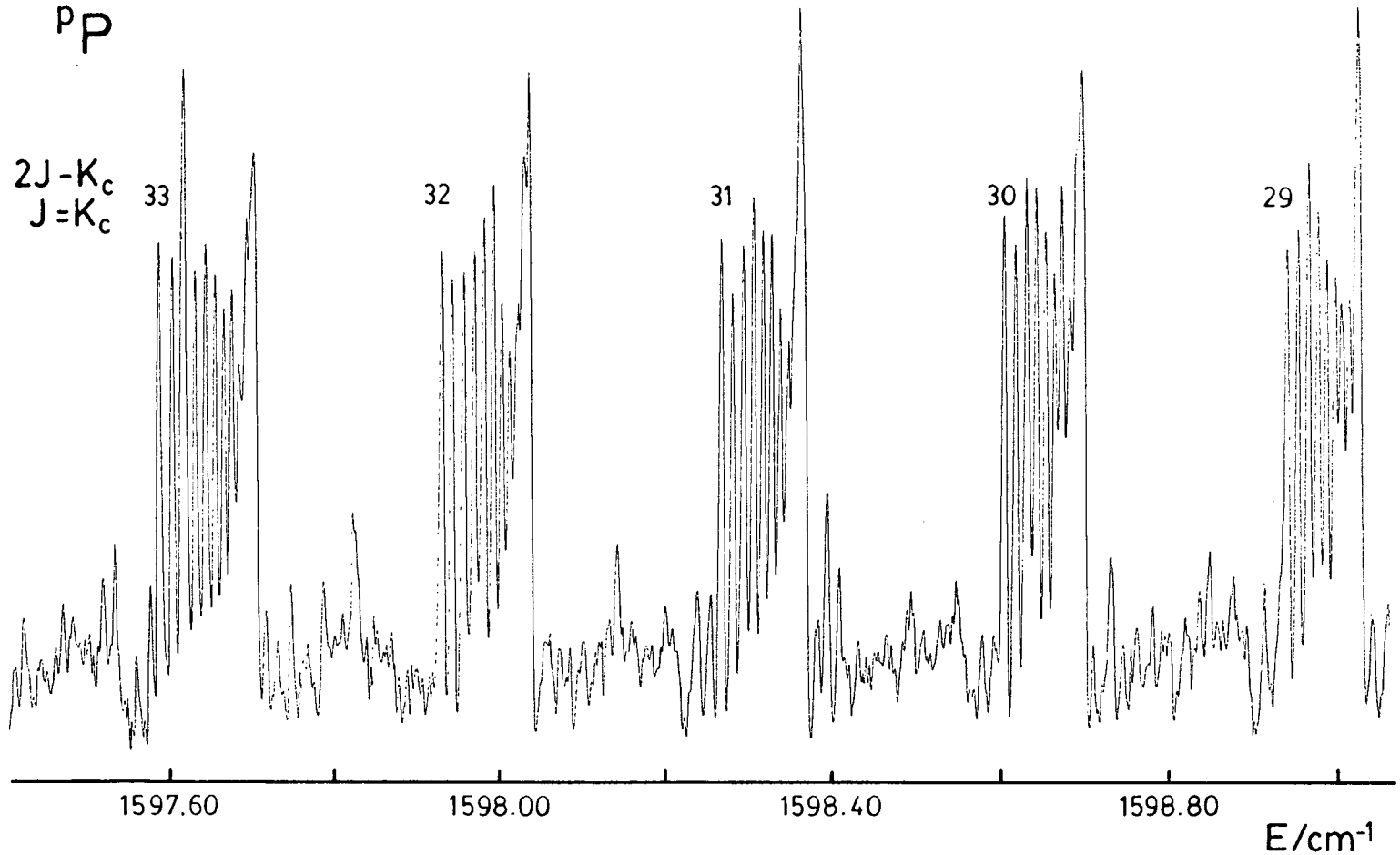

Figure 7.4 High resolution absorbance spectrum of a portion of the ^{P}P branch side of the 2_0^1 band of gaseous BF_2NH_2. The value of $2J-K_c$ for the ground state for each cluster of lines is indicated. This is also the value of J and K_c for the peak to the lowest frequency side of each cluster. J decreases by 1 and K_c decreases by 2 towards to higher frequency.

common upper state but different ground state rotational energy levels, were calculated and compared with the frequency of the corresponding transition predicted using the microwave constants of Lovas and Johnson (6).

Once correct assignments were made for several lines, as determined by a good agreement of the combination differences and the predicted frequencies, the remainder of the assignments were clear from the spectral patterns. An infra-red least squares fitting procedure was used to determine the rotational and quartic centrifugal distortion constants of both the ground and 2^1 levels.

Both the microwave transitions, measured by Lovas and Johnson (6), and the combination differences, were used to improve the determination of the ground state quartic centrifugal distortion constants. These were limited in accuracy in the microwave study because primarily only μ_a Q branch transitions could be measured in the frequency range studied. The microwave data were given uncertainties $\simeq$100 times smaller than the combination differences; the weights are proportional to $(\text{uncertainty})^{-2}$. The results are given in Table 7.3, along with a comparison with the microwave constants which were converted from MHz into cm^{-1}. The microwave distortion constants were converted from the τ's using the equations given in Section 2.4.

Finally, a least squares fit was made to the excited state constants using the measured transition frequencies. The ground

Table 7.3

Ground state rotational constants $^{11}BF_2NH_2$

Parameter	This work[1]	Microwave data[2]
Rotational Constants (cm^{-1})		
A	0.33421379(34)	0.3342132(17)
B	0.31990223(32)	0.3199009(17)
C	0.16320694(31)	0.1632092(17)
Centrifugal Distortion Constants (cm^{-1})		
$10^6\Delta_J$	0.17560(23)	0.188(24)
$10^7\Delta_{JK}$	0.335(10)	-
$10^6\Delta_K$	0.2067(14)	0.233(58)
$10^7\delta_J$	0.7669(16)	0.688(12)
$10^6\delta_K$	0.21307(41)	-

[1] Calculated from combination differences of the 2_0^1 band and the microwave data from reference (6).

[2] Converted from MHz to cm^{-1} (using c = 2.99792458 x 10^8 ms^{-1}) from values given in reference (6).

state constants were held fixed at the values calculated as above. The rotational and quartic centrifugal distortion constants of the 2^1 level are given in Table 7.4.

No calibration of the spectrum was done; however the band origin was corrected using the average shift of the peak positions of some lines of H_2O (0.00109(50) cm^{-1}). The wavenumbers of the observed transitions are given in Table 7.5. The standard deviation of the least squares fit was 0.0005 cm^{-1}

Table 7.4

Rotational constants of the 2^1 level of $^{11}BF_2NH_2$

Parameter	
Rotational Constants (cm^{-1})	
A	0.3342448(13)
B	0.3196908(11)
C	0.16303486(12)
Centrifugal Distortion Constants (cm^{-1})	
$10^6\Delta_J$	0.17725(23)
$10^7\Delta_{JK}$	0.418(52)
$10^6\Delta_K$	0.1828(65)
$10^7\delta_J$	0.7744(44)
$10^6\delta_K$	0.2203(18)
Band Centre (cm^{-1})	
T_o	1608.70691(50)

which also corresponds to unit weight. Some transitions were given less than unit weight because they were slightly overlapped with other transitions.

Not all the transitions could be fitted to this model. The rotational structure of the ν_2 fundamental is significantly perturbed by a Coriolis interaction. This is clearly illustrated in Figure 7.5; a gap appears in both the P and R branch clusters at the same value of K_c. Certain rotational levels of the 2^1 state are shifted, with the largest shifts for $K_c = 31$. The shifts, which are calculated from the

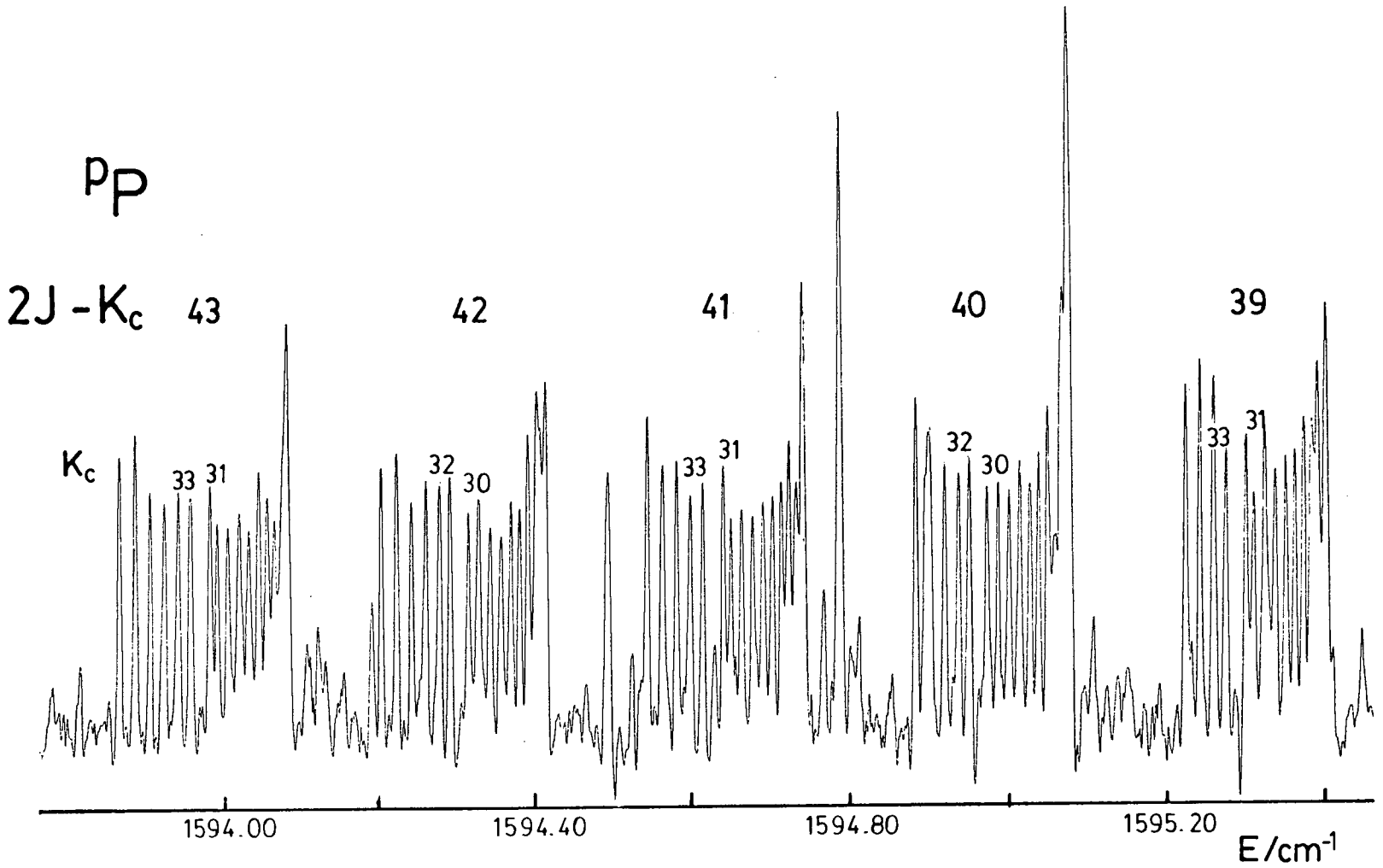

Figure 7.5 High resolution absorbance spectrum of a portion of the ^{P}P branch side of the 2_0^1 band of BF_2NH_2 indicating a small Coriolis perturbation. The value of $2J-K_c$ for the 2^1 level is indicated for each cluster as well as the value of K_c for the peaks on either side of the gap in the rotational structure.

Table 7.5

Observed infrared transitions of $^{11}BF_2NH_2$

J'	K_a'	K_c'	-	J"	K_a"	K_c"	Observed Wavenumber (cm^{-1})	Deviation[1] (cm^{-1})	Normalised Weight[2]
7	6	1	-	7	6	2	1609.00673	0.00100	1.0
10	8	2	-	10	8	3	1609.29112	0.00032	1.0
12	10	2	-	12	10	3	1609.15716	0.00011	1.0
13	12	2	-	13	10	3	1609.97330	-0.00100	0.5
17	15	2	-	17	15	3	1608.83798	-0.00028	1.0
10	7	3	-	10	7	4	1609.77828	0.00035	0.5
13	10	3	-	13	10	4	1609.63400	-0.00000	0.5
16	14	3	-	16	12	4	1610.05792	0.00088	1.0
17	14	3	-	17	14	4	1609.30626	-0.00040	1.0
19	16	3	-	19	16	4	1609.12325	0.00039	1.0
23	20	3	-	23	20	4	1608.82741	0.00073	1.0
19	16	4	-	19	14	5	1610.20539	0.00069	1.0
15	10	5	-	15	10	6	1610.44284	-0.00059	0.5
19	14	5	-	19	14	6	1610.34129	0.00006	1.0
29	24	5	-	29	24	6	1609.34159	-0.00034	0.5
33	27	6	-	33	27	7	1609.60739	0.00048	0.0
17	10	7	-	17	10	8	1611.10592	-0.00004	0.5
28	22	7	-	28	20	8	1610.94038	-0.00057	0.5
24	16	8	-	24	16	9	1611.36479	-0.00068	1.0
29	22	8	-	29	20	9	1611.27539	0.00037	1.0
24	16	9	-	24	14	10	1611.70709	-0.00053	0.5
25	16	9	-	25	16	10	1611.69498	-0.00014	1.0
26	18	9	-	26	16	10	1611.68094	-0.00063	1.0
27	18	9	-	27	18	10	1611.66652	-0.00000	1.0
28	20	9	-	28	18	10	1611.65000	-0.00054	1.0
29	20	9	-	29	20	10	1611.63268	0.00043	1.0
24	14	10	-	24	14	11	1612.04264	-0.00089	0.5
25	16	10	-	25	14	11	1612.03246	-0.00043	1.0
26	16	10	-	26	16	11	1612.02122	-0.00012	1.0
27	18	10	-	27	16	11	1612.00893	0.00009	1.0
28	18	10	-	28	18	11	1611.99491	-0.00037	1.0
29	20	10	-	29	18	11	1611.98168	0.00102	0.5
25	14	11	-	25	14	12	1612.36605	-0.00048	1.0
26	16	11	-	26	14	12	1612.35576	-0.00058	1.0
27	16	11	-	27	16	12	1612.34431	-0.00106	0.5
29	18	11	-	29	18	12	1612.32105	0.00016	1.0
30	20	11	-	30	18	12	1612.30719	-0.00009	1.0
25	14	12	-	25	12	13	1612.69739	-0.00027	1.0
26	14	12	-	26	14	13	1612.68763	-0.00075	0.5
27	16	12	-	27	14	13	1612.67850	0.00006	1.0
28	16	12	-	28	16	13	1612.66795	0.00013	1.0
29	18	12	-	29	16	13	1612.65698	0.00052	1.0

[1] The deviation represents the difference between the observed wavenumber and that calculated using the constants in Tables 7.3 and 7.4.

[2] Measurements were weighted according to $1/\sigma^2$ where σ is the uncertainty in the measurements. Unit weight corresponded to an uncertainty of 0.0005 cm^{-1}.

J'	K_a'	K_c'	-	J"	$K_a"$	$K_c"$	Observed Wavenumber (cm^{-1})	Deviation (cm^{-1})	Normalised Weight
33	22	12	-	33	20	13	1612.60241	-0.00048	1.0
34	22	12	-	34	22	13	1612.58733	0.00012	0.0
28	16	13	-	28	14	14	1612.99928	-0.00019	1.0
30	18	13	-	30	16	14	1612.97775	-0.00020	1.0
33	20	13	-	33	20	14	1612.94005	-0.00034	1.0
34	22	13	-	34	20	14	1612.92550	-0.00082	1.0
27	14	14	-	27	12	15	1613.33808	-0.00052	1.0
28	14	14	-	28	14	15	1613.33001	0.00063	1.0
29	16	14	-	29	14	15	1613.32023	0.00063	0.5
29	14	15	-	29	14	16	1613.64897	0.00020	1.0
30	16	15	-	30	14	16	1613.63891	-0.00005	1.0
31	16	15	-	31	16	16	1613.62883	0.00022	1.0
32	18	15	-	32	16	16	1613.61759	-0.00011	1.0
33	18	15	-	33	18	16	1613.60631	0.00011	1.0
34	20	15	-	34	18	16	1613.59429	0.00019	1.0
29	14	16	-	29	12	17	1613.97644	-0.00050	1.0
31	16	16	-	31	14	17	1613.95650	-0.00112	1.0
32	16	16	-	32	16	17	1613.94623	-0.00098	1.0
33	18	16	-	33	16	17	1613.93517	-0.00110	1.0
34	18	16	-	34	18	17	1613.92402	-0.00076	1.0
35	20	16	-	35	18	17	1613.91250	-0.00023	1.0
36	20	16	-	36	20	17	1613.90096	0.00087	0.0
37	22	18	-	37	20	17	1613.88773	0.00089	0.0
28	12	17	-	28	10	18	1614.31198	-0.00107	0.5
29	12	17	-	29	12	18	1614.30397	-0.00040	0.5
30	14	17	-	30	12	18	1614.29392	-0.00133	0.5
31	14	17	-	31	14	18	1614.28508	-0.00060	1.0
32	16	17	-	32	14	18	1614.27446	-0.00118	0.5
33	16	17	-	33	16	18	1614.26402	-0.00110	1.0
38	22	17	-	38	20	18	1614.20503	0.00037	0.0
27	10	18	-	27	8	19	1614.64754	-0.00030	1.0
30	12	18	-	30	12	19	1614.62172	-0.00064	1.0
31	14	18	-	31	12	19	1614.61227	-0.00077	1.0
32	14	18	-	32	14	19	1614.60220	-0.00108	0.5
33	16	18	-	33	14	19	1614.59304	-0.00003	1.0
30	12	19	-	30	10	20	1614.94948	0.00048	0.5
31	12	19	-	31	12	20	1614.93934	-0.00052	1.0
32	14	19	-	32	12	20	1614.92995	-0.00036	1.0
33	14	19	-	33	14	20	1614.92006	-0.00028	1.0
34	16	19	-	34	14	20	1614.90990	-0.00003	1.0
35	16	19	-	35	16	20	1614.89905	-0.00002	1.0
36	18	19	-	36	16	20	1614.88826	0.00050	1.0
37	18	19	-	37	18	20	1614.87694	0.00097	0.0
37	18	20	-	37	16	21	1615.20302	-0.00065	1.0
38	18	20	-	38	18	21	1615.19173	0.00002	0.0
27	6	21	-	27	6	22	1615.62629	0.00043	0.5
32	12	21	-	32	10	22	1615.58385	0.00074	0.5
36	16	21	-	36	14	22	1615.54278	0.00074	0.5
37	16	21	-	37	16	22	1615.53167	0.00092	0.5
38	18	21	-	38	16	22	1615.51863	-0.00039	1.0
39	18	21	-	39	18	22	1615.50744	0.00060	0.0
8	8	0	-	9	8	1	1603.37571	-0.00027	0.5
9	9	0	-	10	9	1	1602.81751	0.00039	1.0
10	10	0	-	11	10	1	1602.26330	0.00066	1.0
18	18	0	-	19	18	1	1597.79182	-0.00083	0.5
6	6	1	-	7	6	2	1604.76624	-0.00040	0.5
15	14	1	-	16	14	2	1599.23587	0.00032	1.0
17	16	1	-	18	16	2	1598.14454	-0.00028	1.0
7	6	2	-	8	6	3	1604.32317	-0.00062	0.5
10	9	2	-	11	9	3	1602.43521	-0.00000	1.0
11	10	2	-	12	10	3	1601.81900	0.00037	1.0
13	11	2	-	14	11	3	1600.23899	0.00083	0.5
13	12	2	-	14	12	3	1600.60565	-0.00023	0.5

J'	K_a'	K_c'	-	J"	K_a''	K_c''	Observed Wavenumber (cm^{-1})	Deviation (cm^{-1})	Normalised Weight
15	14	2	-	16	14	3	1599.41808	-0.00064	0.5
16	14	2	-	17	14	3	1598.41023	0.00041	1.0
22	20	2	-	23	20	3	1595.10937	0.00002	1.0
9	7	3	-	10	7	4	1603.30966	-0.00001	0.5
10	7	3	-	11	7	4	1602.60527	-0.00096	0.5
11	8	3	-	12	8	4	1601.92746	0.00083	0.5
12	10	3	-	13	10	4	1601.36698	-0.00072	1.0
13	10	3	-	14	10	4	1600.55169	0.00056	1.0
14	12	3	-	15	12	4	1600.09526	0.00008	1.0
15	12	3	-	16	12	4	1599.17484	0.00106	1.0
16	14	3	-	17	14	4	1598.84750	0.00012	0.5
17	14	3	-	18	14	4	1597.82735	-0.00076	0.5
19	16	3	-	20	16	4	1596.54118	-0.00077	0.5
20	18	3	-	21	18	4	1596.43331	-0.00089	0.5
23	20	3	-	24	20	4	1594.19396	0.00076	0.5
24	21	3	-	25	21	4	1593.64794	0.00038	0.5
15	12	4	-	16	12	5	1599.69470	0.00070	1.0
17	14	4	-	18	14	5	1598.39590	-0.00008	1.0
18	14	4	-	19	14	5	1597.53961	-0.00074	1.0
18	15	4	-	19	15	5	1597.75292	-0.00040	1.0
19	15	4	-	20	15	5	1596.83960	0.00057	0.5
19	16	4	-	20	16	5	1597.11611	0.00002	1.0
20	16	4	-	21	16	5	1596.14045	-0.00008	1.0
21	18	4	-	22	18	5	1595.86125	0.00051	1.0
21	17	4	-	22	17	5	1595.44954	-0.00017	0.5
24	20	4	-	25	20	5	1593.46417	-0.00066	1.0
23	18	5	-	24	18	6	1594.52632	0.00059	0.5
28	22	6	-	29	22	7	1591.51025	0.00101	0.5
29	22	7	-	30	22	8	1591.33304	0.00026	1.0
20	4	16	-	21	4	17	1600.32007	-0.00021	0.5
21	6	16	-	22	6	17	1599.66282	-0.00033	0.5
20	4	17	-	21	4	18	1600.64480	0.00005	0.5
21	4	17	-	22	4	18	1599.98748	-0.00008	0.5
22	6	17	-	23	6	18	1599.32997	-0.00033	0.5
24	8	17	-	25	8	18	1598.01515	-0.00043	1.0
25	8	17	-	26	8	18	1597.35787	-0.00026	1.0
21	4	18	-	22	4	19	1600.31146	-0.00038	0.5
22	4	18	-	23	4	19	1599.65418	-0.00033	0.5
23	6	18	-	24	6	19	1598.99750	0.00038	0.5
24	6	18	-	25	6	19	1598.33981	0.00013	1.0
25	8	18	-	26	8	19	1597.68200	-0.00018	1.0
27	10	18	-	28	10	19	1596.36656	-0.00046	1.0
28	10	18	-	29	10	19	1595.70925	-0.00011	0.5
29	12	18	-	30	12	19	1595.05179	0.00014	0.5
34	16	18	-	35	16	19	1591.76233	-0.00003	0.5
21	2	19	-	22	2	20	1600.63588	-0.00014	1.0
22	4	19	-	23	4	20	1599.97904	0.00043	1.0
23	4	19	-	24	4	20	1599.32120	0.00006	1.0
24	6	19	-	25	6	20	1598.66342	-0.00020	1.0
25	6	19	-	26	6	20	1598.00569	-0.00036	0.5
26	8	19	-	27	8	20	1597.34822	-0.00022	1.0
27	8	19	-	28	8	20	1596.69041	-0.00037	1.0
28	10	19	-	29	10	20	1596.03249	-0.00060	1.0
29	10	19	-	30	10	20	1595.37557	0.00021	1.0
30	12	19	-	31	12	20	1594.71765	0.00006	0.5
31	12	19	-	32	12	20	1594.06014	0.00035	0.5
33	14	19	-	34	14	20	1592.74380	-0.00028	0.5
22	2	20	-	23	2	21	1600.30249	-0.00011	0.5
23	4	20	-	24	4	21	1599.64479	-0.00025	1.0
24	4	20	-	25	4	21	1598.98732	-0.00011	1.0
25	6	20	-	26	6	21	1598.32988	0.00010	1.0
26	6	20	-	27	6	21	1597.67210	0.00001	1.0
27	8	20	-	28	8	21	1597.01414	-0.00023	1.0

J'	K_a'	K_c'	-	J"	K_a''	K_c''	Observed Wavenumber (cm^{-1})	Deviation (cm^{-1})	Normalised Weight
28	8	20	-	29	8	21	1596.35632	-0.00029	1.0
29	10	20	-	30	10	21	1595.69873	-0.00010	1.0
30	10	20	-	31	10	21	1595.04090	-0.00012	1.0
31	12	20	-	32	12	21	1594.38297	-0.00022	1.0
32	12	20	-	33	12	21	1593.72503	-0.00031	0.5
33	14	20	-	34	14	21	1593.06742	-0.00004	1.0
22	2	21	-	23	2	22	1600.62659	0.00008	1.0
23	2	21	-	24	2	22	1599.96884	-0.00000	1.0
24	4	21	-	25	4	22	1599.31113	-0.00001	1.0
25	4	21	-	26	4	22	1598.65309	-0.00030	1.0
26	6	21	-	27	6	22	1597.99551	-0.00010	1.0
27	6	21	-	28	6	22	1597.33805	0.00025	1.0
28	8	21	-	29	8	22	1596.67970	-0.00027	1.0
29	8	21	-	30	8	22	1596.02234	0.00023	1.0
30	10	21	-	31	10	22	1595.36411	-0.00013	1.0
31	10	21	-	32	10	22	1594.70679	0.00044	1.0
32	12	21	-	33	12	22	1594.04902	0.00057	1.0
33	12	21	-	34	12	22	1593.39085	0.00031	1.0
36	16	21	-	37	16	22	1591.41708	0.00030	1.0
23	2	22	-	24	2	23	1600.29261	0.00003	1.0
24	2	22	-	25	2	23	1599.63480	0.00004	1.0
25	4	22	-	26	4	23	1598.97706	0.00015	1.0
26	4	22	-	27	4	23	1598.31915	0.00013	1.0
27	6	22	-	28	6	23	1597.66127	0.00016	1.0
28	6	22	-	29	6	23	1597.00333	0.00015	1.0
29	8	22	-	30	8	23	1596.34542	0.00018	1.0
30	8	22	-	31	8	23	1595.68780	0.00052	0.5
31	10	22	-	32	10	23	1595.02971	0.00040	1.0
32	10	22	-	33	10	23	1594.37183	0.00048	1.0
33	12	22	-	34	12	23	1593.71356	0.00018	0.5
34	12	22	-	35	12	23	1593.05589	0.00048	1.0
23	0	23	-	24	0	24	1600.61638	0.00013	1.0
24	2	23	-	25	2	24	1599.95832	0.00001	1.0
25	2	23	-	26	2	24	1599.30040	0.00006	1.0
26	4	23	-	27	4	24	1598.64228	-0.00007	1.0
27	4	23	-	28	4	24	1597.98438	0.00005	1.0
28	6	23	-	29	6	24	1597.32653	0.00024	1.0
29	6	23	-	30	6	24	1596.66880	0.00056	0.5
30	8	23	-	31	8	24	1596.01090	0.00072	1.0
31	8	23	-	32	8	24	1595.35257	0.00045	1.0
32	10	23	-	33	10	24	1594.69448	0.00042	1.0
33	10	23	-	34	10	24	1594.03632	0.00031	1.0
34	12	23	-	35	12	24	1593.37852	0.00055	1.0
35	12	23	-	36	12	24	1592.72083	0.00089	1.0
36	14	23	-	37	14	24	1592.06204	0.00011	1.0
37	14	23	-	38	14	24	1591.40459	0.00065	1.0
24	0	24	-	25	0	25	1600.28170	-0.00011	1.0
25	2	24	-	26	2	25	1599.62362	-0.00010	1.0
26	2	24	-	27	2	25	1598.96580	0.00020	1.0
27	4	24	-	28	4	25	1598.30795	0.00049	1.0
28	4	24	-	29	4	25	1597.64993	0.00063	1.0
29	6	24	-	30	6	25	1596.99169	0.00055	1.0
30	6	24	-	31	6	25	1596.33353	0.00056	0.5
31	8	24	-	32	8	25	1595.67539	0.00059	1.0
32	8	24	-	33	8	25	1595.01691	0.00027	1.0
33	10	24	-	34	10	25	1594.35902	0.00053	1.0
34	10	24	-	35	10	25	1593.70060	0.00025	1.0
35	12	24	-	36	12	25	1593.04268	0.00044	1.0
37	14	24	-	38	14	25	1591.72642	0.00033	1.0
25	0	25	-	26	0	26	1599.94737	0.00033	1.0
26	2	25	-	27	2	26	1599.28926	0.00047	1.0

J'	K_a'	K_c'	-	J"	K_a''	K_c''	Observed Wavenumber (cm^{-1})	Deviation (cm^{-1})	Normalised Weight
27	2	25	-	28	2	26	1598.63105	0.00052	1.0
28	4	25	-	29	4	26	1597.97287	0.00063	1.0
29	4	25	-	30	4	26	1597.31494	0.00099	0.5
30	6	25	-	31	6	26	1596.65598	0.00032	1.0
31	6	25	-	32	6	26	1595.99780	0.00043	1.0
32	8	25	-	33	8	26	1595.33904	-0.00005	1.0
33	8	25	-	34	8	26	1594.68127	0.00044	1.0
35	10	25	-	36	10	26	1593.36463	0.00026	1.0
38	14	25	-	39	14	26	1591.39027	0.00036	1.0
26	0	26	-	27	0	27	1599.61171	-0.00023	1.0
27	2	26	-	28	2	27	1598.95363	0.00009	1.0
28	2	26	-	29	2	27	1598.29543	0.00031	1.0
29	4	26	-	30	4	27	1597.63711	0.00041	1.0
30	4	26	-	31	4	27	1596.97915	0.00087	0.5
31	6	26	-	32	6	27	1596.32038	0.00052	1.0
32	6	26	-	33	6	27	1595.66171	0.00026	1.0
33	8	26	-	34	8	27	1595.00317	0.00011	1.0
34	8	26	-	35	8	27	1594.34528	0.00058	1.0
35	10	26	-	36	10	27	1593.68712	0.00076	0.5
36	10	26	-	37	10	27	1593.02873	0.00067	1.0
37	12	26	-	38	12	27	1592.37087	0.00108	1.0
27	0	27	-	28	0	28	1599.27666	0.00015	1.0
28	2	27	-	29	2	28	1598.61837	0.00042	1.0
29	2	27	-	30	2	28	1597.96001	0.00062	1.0
30	4	27	-	31	4	28	1597.30157	0.00074	1.0
31	4	27	-	32	4	28	1596.64330	0.00103	0.5
32	6	27	-	33	6	28	1595.98464	0.00091	1.0
33	6	27	-	34	6	28	1595.32576	0.00056	0.5
34	8	27	-	35	8	28	1594.66722	0.00051	1.0
35	8	27	-	36	8	28	1594.00901	0.00077	1.0
38	12	27	-	39	12	28	1592.03361	0.00052	1.0
41	14	27	-	42	14	28	1590.05927	0.00086	1.0
28	0	28	-	29	0	29	1598.94073	-0.00002	1.0
29	2	28	-	30	2	29	1598.28211	0.00007	1.0
31	4	28	-	32	4	29	1596.96541	0.00078	1.0
32	4	28	-	33	4	29	1596.30662	0.00068	1.0
33	6	28	-	34	6	29	1595.64809	0.00082	0.5
34	6	28	-	35	6	29	1594.98944	0.00081	0.5
35	8	28	-	36	8	29	1594.33066	0.00063	0.5
36	8	28	-	37	8	29	1593.67298	0.00152	0.0
37	10	28	-	38	10	29	1593.01438	0.00144	0.0
39	12	28	-	40	12	29	1591.69694	0.00088	1.0
29	0	29	-	30	0	30	1598.60501	0.00035	1.0
30	2	29	-	31	2	30	1597.94605	0.00025	1.0
31	2	29	-	32	2	30	1597.28753	0.00059	1.0
32	4	29	-	33	4	30	1596.62923	0.00113	0.0
33	4	29	-	34	4	30	1595.97035	0.00106	0.0
34	6	29	-	35	6	30	1595.31202	0.00152	0.0
35	6	29	-	36	6	30	1594.65327	0.00153	0.0
36	8	29	-	37	8	30	1593.99478	0.00175	0.0
37	8	29	-	38	8	30	1593.33576	0.00140	0.0
39	10	29	-	40	10	30	1592.01992	0.00273	0.0
38	10	29	-	39	10	30	1592.67809	0.00234	0.0
40	12	29	-	41	12	30	1591.36183	0.00312	0.0
41	12	29	-	42	12	30	1590.70307	0.00278	0.0
42	14	29	-	43	14	30	1590.04645	0.00450	0.0
43	14	29	-	44	14	30	1589.38588	0.00219	0.0
30	0	30	-	31	0	31	1598.26858	0.00034	0.0
31	2	30	-	32	2	31	1597.61004	0.00081	0.0
32	2	30	-	33	2	31	1596.95104	0.00081	0.0
33	4	30	-	34	4	31	1596.29272	0.00147	0.0
34	4	30	-	35	4	31	1595.63421	0.00190	0.0
35	6	30	-	36	6	31	1594.97539	0.00200	0.0

J'	K_a'	K_c'	-	J"	$K_a"$	$K_c"$	Observed Wavenumber (cm^{-1})	Deviation (cm^{-1})	Normalised Weight
36	6	30	-	37	6	31	1594.31708	0.00256	0.0
37	8	30	-	38	8	31	1593.65830	0.00260	0.0
38	8	30	-	39	8	31	1592.99978	0.00284	0.0
39	10	30	-	40	10	31	1592.34130	0.00307	0.0
42	12	30	-	43	12	31	1590.36521	0.00266	0.0
31	0	31	-	32	0	32	1597.93368	0.00219	0.0
32	2	31	-	33	2	32	1597.27639	0.00406	0.0
33	2	31	-	34	2	32	1596.61914	0.00595	0.0
34	4	31	-	35	4	32	1595.96111	0.00703	0.0
35	4	31	-	36	4	32	1595.30250	0.00750	0.0
36	6	31	-	37	6	32	1594.64376	0.00779	0.0
37	6	31	-	38	6	32	1593.98398	0.00700	0.0
38	8	31	-	39	8	32	1593.32618	0.00812	0.0
39	8	31	-	40	8	32	1592.66816	0.00897	0.0
40	10	31	-	41	10	32	1592.00983	0.00943	0.0
41	10	31	-	42	10	32	1591.35121	0.00953	0.0
43	12	31	-	44	12	32	1590.03451	0.01001	0.0
44	14	31	-	45	14	32	1589.37578	0.00974	0.0
32	0	32	-	33	0	33	1597.59412	-0.00029	0.0
33	2	32	-	34	2	33	1596.93368	-0.00142	0.0
34	2	32	-	35	2	33	1596.27408	-0.00174	0.0
35	4	32	-	36	4	33	1595.61377	-0.00281	0.0
36	4	32	-	37	4	33	1594.95325	-0.00412	0.0
37	6	32	-	38	6	33	1594.29338	-0.00484	0.0
38	6	32	-	39	6	33	1593.63370	-0.00542	0.0
39	8	32	-	40	8	33	1592.97323	-0.00686	0.0
40	8	32	-	41	8	33	1592.31312	-0.00801	0.0
33	0	33	-	34	0	34	1597.25694	-0.00007	0.0
34	2	33	-	35	2	34	1596.59714	-0.00041	0.0
35	2	33	-	36	2	34	1595.93662	-0.00151	0.0
36	4	33	-	37	4	34	1595.27734	-0.00141	0.0
37	4	33	-	38	4	34	1594.61751	-0.00191	0.0
39	6	33	-	40	6	34	1593.29795	-0.00299	0.0
40	8	33	-	41	8	34	1592.63886	-0.00294	0.0
41	8	33	-	42	8	34	1591.97994	-0.00281	0.0
42	10	33	-	43	10	34	1591.32063	-0.00314	0.0
43	10	33	-	44	10	34	1590.66094	-0.00395	0.0
45	12	33	-	46	12	34	1589.34232	-0.00511	0.0
34	0	34	-	35	0	35	1596.91926	-0.00002	1.0
35	2	34	-	36	2	35	1596.25936	-0.00031	1.0
36	2	34	-	37	2	35	1595.59968	-0.00043	1.0
37	4	34	-	38	4	35	1594.93956	-0.00104	0.5
38	4	34	-	39	4	35	1594.28040	-0.00075	0.5
39	6	34	-	40	6	35	1593.62045	-0.00131	0.0
40	6	34	-	41	6	35	1592.96099	-0.00145	0.0
41	8	34	-	42	8	35	1592.30127	-0.00193	0.0
42	8	34	-	43	8	35	1591.64236	-0.00168	0.0
35	0	35	-	36	0	36	1596.58115	-0.00007	1.0
36	2	35	-	37	2	36	1595.92155	0.00008	1.0
37	2	35	-	38	2	36	1595.26145	-0.00032	1.0
38	4	35	-	39	4	36	1594.60108	-0.00105	0.5
39	4	35	-	40	4	36	1593.94212	-0.00043	0.5
40	6	35	-	41	6	36	1593.28206	-0.00098	0.5
41	6	35	-	42	6	36	1592.62216	-0.00145	0.0
42	8	35	-	43	8	36	1591.96262	-0.00165	0.0
43	8	35	-	44	8	36	1591.30334	-0.00168	0.0
44	10	35	-	45	10	36	1590.64393	-0.00194	0.0
45	10	35	-	46	10	36	1589.98441	-0.00242	0.0
36	0	36	-	37	0	37	1596.24264	-0.00019	1.0
37	2	36	-	38	2	37	1595.58259	-0.00035	1.0
38	2	36	-	39	2	37	1594.92248	-0.00062	1.0
39	4	36	-	40	4	37	1594.26274	-0.00059	1.0
40	4	36	-	41	4	37	1593.60263	-0.00100	1.0

J'	K_a'	K_c'	-	J"	K_a"	K_c"	Observed Wavenumber (cm^{-1})	Deviation (cm^{-1})	Normalised Weight
41	6	36	-	42	6	37	1592.94294	-0.00106	0.0
42	6	36	-	43	6	37	1592.28334	-0.00113	0.0
37	0	37	-	38	0	38	1595.90409	-0.00003	0.5
38	2	37	-	39	2	38	1595.24418	0.00010	1.0
39	2	37	-	40	2	38	1594.58351	-0.00060	1.0
40	4	37	-	41	4	38	1593.92362	-0.00059	1.0
41	4	37	-	42	4	38	1593.26357	-0.00082	1.0
42	6	37	-	43	6	38	1592.60332	-0.00133	0.0
43	6	37	-	44	6	38	1591.94385	-0.00115	0.0
44	8	37	-	45	8	38	1591.28440	-0.00106	0.0
46	10	37	-	47	10	38	1589.96646	-0.00024	0.0
47	10	37	-	48	10	38	1589.30685	-0.00066	0.0
38	0	38	-	39	0	39	1595.56485	-0.00023	1.0
40	2	38	-	41	2	39	1594.24415	-0.00064	1.0
41	4	38	-	42	4	39	1593.58425	-0.00052	1.0
42	4	38	-	43	4	39	1592.92373	-0.00109	1.0
43	6	38	-	44	6	39	1592.26385	-0.00112	0.5
44	6	38	-	45	6	39	1591.60425	-0.00097	1.0
46	8	38	-	47	8	39	1590.28629	0.00024	1.0
39	0	39	-	40	0	40	1595.22524	-0.00047	1.0
40	2	39	-	41	2	40	1594.56548	0.00009	1.0
41	2	39	-	42	2	40	1593.90493	-0.00023	1.0
42	4	39	-	43	4	40	1593.24452	-0.00048	1.0
43	4	39	-	44	4	40	1592.58417	-0.00077	1.0
44	6	39	-	45	6	40	1591.92414	-0.00083	0.5
48	10	39	-	49	10	40	1589.28591	-0.00036	1.0
40	0	40	-	41	0	41	1594.88587	-0.00015	1.0
41	2	40	-	42	2	41	1594.22503	-0.00053	1.0
42	2	40	-	43	2	41	1593.56496	-0.00023	1.0
43	4	40	-	44	4	41	1592.90423	-0.00068	1.0
48	8	40	-	49	8	41	1589.60503	-0.00012	1.0
41	0	41	-	42	0	42	1594.54602	0.00002	1.0
42	2	41	-	43	2	42	1593.88563	0.00022	1.0
43	2	41	-	44	2	42	1593.22485	-0.00006	1.0
44	4	41	-	45	4	42	1592.56491	0.00040	0.5
45	4	41	-	46	4	42	1591.90381	-0.00040	1.0
46	6	41	-	47	6	42	1591.24436	0.00034	1.0
47	6	41	-	48	6	42	1590.58346	-0.00050	1.0
49	8	41	-	50	8	42	1589.26424	0.00001	1.0
42	0	42	-	43	0	43	1594.20587	0.00021	1.0
43	2	42	-	44	2	43	1593.54482	-0.00012	1.0
44	2	42	-	45	2	43	1592.88446	0.00016	1.0
45	4	42	-	46	4	43	1592.22396	0.00018	1.0
46	4	42	-	47	4	43	1591.56354	0.00018	1.0
48	6	42	-	49	6	43	1590.24314	0.00024	1.0
49	8	42	-	50	8	43	1589.58309	0.00021	1.0
43	0	43	-	44	0	44	1593.86509	0.00009	1.0
44	2	43	-	45	2	44	1593.20427	0.00013	1.0
45	2	43	-	46	2	44	1592.54358	0.00020	1.0
46	4	43	-	47	4	44	1591.88305	0.00032	1.0
47	4	43	-	48	4	44	1591.22264	0.00044	1.0
48	6	43	-	49	6	44	1590.56199	0.00019	1.0
44	0	44	-	45	0	45	1593.52379	-0.00022	1.0
45	2	44	-	46	2	45	1592.86300	-0.00001	0.5
46	2	44	-	47	2	45	1592.20244	0.00031	1.0
49	6	44	-	50	6	45	1590.22041	0.00020	1.0
50	6	44	-	51	6	45	1589.56021	0.00037	1.0
45	0	45	-	46	0	46	1593.18309	0.00039	1.0
46	2	45	-	47	2	46	1592.52195	0.00038	1.0
47	2	45	-	48	2	46	1591.86149	0.00093	1.0
46	0	46	-	47	0	47	1592.84179	0.00072	1.0
47	2	46	-	48	2	47	1592.17943	-0.00037	1.0
48	2	46	-	49	2	47	1591.51888	0.00022	1.0

J'	K_a'	K_c'	-	J"	K_a"	K_c"	Observed Wavenumber (cm^{-1})	Deviation (cm^{-1})	Normalised Weight
50	4	46	-	51	4	47	1590.19618	-0.00061	1.0
51	6	46	-	52	6	47	1589.53530	-0.00078	1.0
47	0	47	-	48	0	48	1592.49958	0.00047	1.0
48	2	47	-	49	2	48	1591.83852	0.00080	1.0
49	2	47	-	50	2	48	1591.17661	0.00016	1.0
50	4	47	-	51	4	48	1590.51491	-0.00042	1.0
48	0	48	-	49	0	49	1592.15737	0.00054	1.0
49	2	48	-	50	2	49	1591.49548	0.00017	1.0
50	2	48	-	51	2	49	1590.83461	0.00069	1.0
51	4	48	-	52	4	49	1590.17190	-0.00078	1.0
52	4	48	-	53	4	49	1589.51201	0.00041	1.0
49	0	49	-	50	0	50	1591.81513	0.00090	1.0
50	2	49	-	51	2	50	1591.15258	0.00000	1.0
51	2	49	-	52	2	50	1590.49083	-0.00024	1.0
51	2	50	-	52	2	51	1590.81059	0.00106	1.0
53	4	50	-	54	4	51	1589.48647	0.00003	1.0
4	2	2	-	4	4	1	1608.12462	-0.00019	1.0
6	4	2	-	6	6	1	1607.99243	0.00003	1.0
8	6	3	-	8	6	2	1607.99243	0.00001	1.0
9	7	3	-	9	7	2	1608.03995	0.00101	0.5
11	9	3	-	11	9	2	1608.15255	-0.00010	0.5
9	6	4	-	9	6	3	1607.58534	-0.00063	1.0
19	16	4	-	19	16	3	1608.19593	0.00079	1.0
17	12	5	-	17	14	4	1607.19255	-0.00106	0.5
20	16	5	-	20	16	4	1607.62740	0.00109	0.5
21	16	5	-	21	18	4	1606.96913	-0.00085	0.5
24	20	5	-	24	20	4	1608.02499	-0.00032	1.0
26	22	5	-	26	22	4	1608.21528	-0.00002	1.0
17	12	6	-	17	12	5	1606.93483	0.00001	1.0
18	13	6	-	18	13	5	1606.95311	0.00005	0.5
20	15	6	-	20	15	5	1607.01411	0.00079	1.0
22	16	6	-	22	18	5	1606.87952	0.00067	1.0
23	17	6	-	23	19	5	1606.84906	-0.00019	1.0
24	18	6	-	24	20	5	1606.80500	0.00022	1.0
25	20	6	-	25	20	5	1607.37524	-0.00056	1.0
30	24	6	-	30	26	5	1606.03838	0.00047	1.0
31	26	6	-	31	26	5	1608.06097	0.00009	1.0
22	16	7	-	22	16	6	1606.62164	-0.00050	1.0
24	18	7	-	24	18	6	1606.67338	-0.00046	1.0
29	23	7	-	29	23	6	1607.00411	0.00019	1.0
29	22	8	-	29	22	7	1606.36646	0.00031	1.0
13	12	1	-	12	12	0	1616.24304	0.00109	0.5
15	14	1	-	14	14	0	1617.35769	0.00098	1.0
4	2	2	-	3	2	1	1610.85716	-0.00023	1.0
6	4	2	-	5	4	1	1612.17960	-0.00014	0.5
8	6	2	-	7	6	1	1613.47157	0.00099	0.5
9	7	2	-	8	7	1	1614.09878	-0.00018	1.0
10	9	2	-	9	9	1	1614.43123	-0.00093	0.5
12	10	2	-	11	10	1	1615.90077	-0.00072	1.0
12	11	2	-	11	11	1	1615.60060	0.00037	1.0
5	2	3	-	4	2	2	1611.16120	0.00098	1.0
8	5	3	-	7	5	2	1613.16121	0.00064	0.5
9	6	3	-	8	6	2	1613.83466	0.00031	0.5
11	8	3	-	10	8	2	1615.17602	0.00080	1.0
12	9	3	-	11	9	2	1615.83481	0.00009	1.0
13	10	3	-	12	10	2	1616.48335	0.00066	0.5
13	11	3	-	12	11	2	1616.17436	-0.00037	1.0
14	11	3	-	13	11	2	1617.11643	-0.00049	1.0
15	12	3	-	14	12	2	1617.73611	0.00023	1.0
16	13	3	-	15	13	2	1618.33884	0.00026	1.0
4	0	4	-	3	0	3	1610.17152	-0.00053	1.0
12	8	4	-	11	8	3	1615.44846	-0.00018	0.5

J'	K_a'	K_c'	-	J"	$K_a"$	$K_c"$	Observed Wavenumber (cm^{-1})	Deviation (cm^{-1})	Normalised Weight
20	16	4	-	19	16	3	1620.75200	-0.00018	1.0
26	22	4	-	25	22	3	1624.13973	-0.00063	0.5
5	0	5	-	4	0	4	1610.49661	-0.00018	0.5
14	9	5	-	13	9	4	1616.38916	0.00009	0.5
15	10	5	-	14	10	4	1617.05440	-0.00034	1.0
16	11	5	-	15	11	4	1617.72660	0.00064	0.5
17	12	5	-	16	12	4	1618.40338	0.00011	1.0
6	0	6	-	5	0	5	1610.82188	0.00067	0.5
18	13	6	-	17	13	5	1618.64555	0.00001	1.0
19	14	6	-	18	14	5	1619.29583	-0.00023	1.0
20	14	6	-	19	14	5	1619.99592	0.00003	1.0
23	18	6	-	22	18	5	1621.87527	-0.00096	1.0
21	14	7	-	20	14	6	1620.27792	0.00057	1.0
23	17	7	-	22	17	6	1621.57296	0.00058	1.0
15	8	8	-	14	8	7	1616.02859	0.00000	1.0
18	10	8	-	17	10	7	1617.98033	-0.00044	1.0
20	12	8	-	19	12	7	1619.28183	-0.00065	1.0
26	19	8	-	25	19	7	1623.19022	0.00005	1.0
19	10	9	-	18	10	8	1618.30107	0.00082	1.0
21	12	9	-	20	12	8	1619.60058	0.00057	1.0
16	6	10	-	15	6	9	1616.02094	-0.00003	0.5
17	8	10	-	16	8	9	1616.67074	-0.00030	0.5
18	8	10	-	17	8	9	1617.32080	-0.00008	1.0
19	10	10	-	18	10	9	1617.97023	-0.00028	1.0
21	12	10	-	20	12	9	1619.26895	-0.00027	1.0
22	12	10	-	21	12	9	1619.91821	-0.00013	1.0
24	14	10	-	23	14	9	1621.21626	0.00002	1.0
16	6	11	-	15	6	10	1615.69181	-0.00036	0.5
17	6	11	-	16	6	10	1616.34129	-0.00088	0.5
18	8	11	-	17	8	10	1616.99164	-0.00027	1.0
19	8	11	-	18	8	10	1617.64092	-0.00047	1.0
20	10	11	-	19	10	10	1618.29044	-0.00018	1.0
23	12	11	-	22	12	10	1620.23659	-0.00033	0.5
24	14	11	-	23	14	10	1620.88559	0.00033	0.5
25	14	11	-	24	14	10	1621.53303	-0.00038	1.0
26	16	11	-	25	16	10	1622.18116	-0.00024	1.0
27	16	11	-	26	16	10	1622.82947	0.00023	1.0
18	6	12	-	17	6	11	1616.66246	-0.00059	0.5
19	8	12	-	18	8	11	1617.31244	-0.00004	1.0
23	12	12	-	22	12	11	1619.90708	-0.00035	1.0
24	12	12	-	23	12	11	1620.55591	0.00043	1.0
25	14	12	-	24	14	11	1621.20332	0.00003	1.0
26	14	12	-	25	14	11	1621.85033	-0.00051	1.0
27	16	12	-	26	16	11	1622.49815	-0.00001	1.0
18	6	13	-	17	6	12	1616.33368	-0.00045	1.0
19	6	13	-	18	6	12	1616.98305	-0.00054	0.5
20	8	13	-	19	8	12	1617.63267	-0.00007	1.0
21	8	13	-	20	8	12	1618.28146	-0.00012	1.0
23	10	13	-	22	10	12	1619.57856	0.00021	0.5
24	12	13	-	23	12	12	1620.22594	-0.00034	1.0
25	12	13	-	24	12	12	1620.87375	-0.00016	1.0
26	14	13	-	25	14	12	1621.52123	-0.00002	1.0
27	14	13	-	26	14	12	1622.16851	0.00021	1.0
28	16	13	-	27	16	12	1622.81603	0.00097	0.5
29	16	13	-	28	16	12	1623.46160	0.00006	1.0
18	4	14	-	17	4	13	1616.00555	0.00046	0.5
19	6	14	-	18	6	13	1616.65379	-0.00081	0.5
20	6	14	-	19	6	13	1617.30363	-0.00016	1.0
21	8	14	-	20	8	13	1617.95277	0.00011	1.0
22	8	14	-	21	8	13	1618.60139	0.00018	1.0
23	10	14	-	22	10	13	1619.24947	0.00004	1.0
24	10	14	-	23	10	13	1619.89708	-0.00024	1.0

J'	K_a'	K_c'	-	J"	K_a"	K_c"	Observed Wavenumber (cm^{-1})	Deviation (cm^{-1})	Normalised Weight
25	12	14	-	24	12	13	1620.54485	-0.00004	1.0
26	12	14	-	25	12	13	1621.19132	-0.00081	1.0
27	14	14	-	26	14	13	1621.83827	-0.00078	1.0
29	16	14	-	28	16	13	1623.13118	-0.00073	1.0
18	4	15	-	17	4	14	1615.67630	0.00043	0.5
19	4	15	-	18	4	14	1616.32548	0.00002	0.5
20	6	15	-	19	6	14	1616.97403	-0.00069	0.5
21	6	15	-	20	6	14	1617.62322	-0.00042	1.0
22	8	15	-	21	8	14	1618.27235	0.00011	1.0
25	10	15	-	24	10	14	1620.21574	-0.00025	0.5
26	12	15	-	25	12	14	1620.86289	-0.00032	1.0
27	12	15	-	26	12	14	1621.50968	-0.00041	1.0
29	14	15	-	28	14	14	1622.80278	-0.00001	0.5
30	16	15	-	29	16	14	1623.44927	0.00065	1.0
31	16	15	-	30	16	14	1624.09416	0.00007	1.0
19	4	16	-	18	4	15	1615.99642	0.00030	0.5
21	6	16	-	20	6	15	1617.29416	-0.00032	1.0
22	6	16	-	21	6	15	1617.94294	-0.00021	1.0
23	8	16	-	22	8	15	1618.59129	-0.00018	1.0
24	8	16	-	23	8	15	1619.23957	0.00012	1.0
25	10	16	-	24	10	15	1619.88687	-0.00020	1.0
26	10	16	-	25	10	15	1620.53397	-0.00036	1.0
27	12	16	-	26	12	15	1621.18065	-0.00058	1.0
28	12	16	-	27	12	15	1621.82766	-0.00010	1.0
29	14	16	-	28	14	15	1622.47415	0.00023	1.0
30	14	16	-	29	14	15	1623.11983	0.00013	1.0
19	2	17	-	18	2	16	1615.66624	-0.00033	1.0
20	4	17	-	19	4	16	1616.31551	-0.00050	1.0
21	4	17	-	20	4	16	1616.96447	-0.00065	1.0
22	6	17	-	21	6	16	1617.61320	-0.00068	1.0
23	6	17	-	22	6	16	1618.26224	-0.00006	0.5
25	8	17	-	24	8	16	1619.55758	-0.00047	1.0
26	10	17	-	25	10	16	1620.20628	0.00090	0.5
27	10	17	-	26	10	16	1620.85228	-0.00006	1.0
28	12	17	-	27	12	16	1621.49875	-0.00016	1.0
29	12	17	-	28	12	16	1622.14472	-0.00039	1.0
30	14	17	-	29	14	16	1622.79105	0.00013	1.0
31	14	17	-	30	14	16	1623.43668	0.00035	1.0
32	16	17	-	31	16	16	1624.08152	0.00017	1.0
20	2	18	-	19	2	17	1615.98631	-0.00003	1.0
21	4	18	-	20	4	17	1616.63513	-0.00042	1.0
22	4	18	-	21	4	17	1617.28391	-0.00051	1.0
23	6	18	-	22	6	17	1617.93255	-0.00039	1.0
24	6	18	-	23	6	17	1618.58123	0.00014	1.0
25	8	18	-	24	8	17	1619.22886	-0.00002	1.0
26	8	18	-	25	8	17	1619.87640	0.00010	1.0
27	10	18	-	26	10	17	1620.52338	0.00004	1.0
28	10	18	-	27	10	17	1621.17001	0.00001	1.0
29	12	18	-	28	12	17	1621.81722	0.00095	0.5
30	12	18	-	29	12	17	1622.46160	-0.00054	1.0
31	14	18	-	30	14	17	1623.10752	-0.00008	1.0
20	2	19	-	19	2	18	1615.65669	0.00027	1.0
21	2	19	-	20	2	18	1616.30554	-0.00021	1.0
22	4	19	-	21	4	18	1616.95474	0.00001	1.0
23	4	19	-	22	4	18	1617.60310	-0.00026	1.0
24	6	19	-	23	6	18	1618.25168	0.00005	1.0
25	6	19	-	24	6	18	1618.89978	0.00025	1.0
27	8	19	-	26	8	18	1620.19452	0.00032	1.0
28	10	19	-	27	10	18	1620.84083	-0.00013	1.0
29	10	19	-	28	10	18	1621.48713	-0.00019	1.0
30	12	19	-	29	12	18	1622.13378	0.00050	1.0
31	12	19	-	30	12	18	1622.77835	-0.00047	0.5

J'	K_a'	K_c'	-	J"	$K_a"$	$K_c"$	Observed Wavenumber (cm^{-1})	Deviation (cm^{-1})	Normalised Weight
33	14	19	-	32	14	18	1624.06889	0.00022	0.5
21	2	20	-	20	2	19	1615.97572	0.00002	1.0
22	2	20	-	21	2	19	1616.62481	0.00001	0.5
23	4	20	-	22	4	19	1617.27271	-0.00084	1.0
24	4	20	-	23	4	19	1617.92169	-0.00025	1.0
25	6	20	-	24	6	19	1618.57002	0.00006	1.0
27	8	20	-	26	8	19	1619.86492	0.00005	1.0
28	8	20	-	27	8	19	1620.51237	0.00063	1.0
29	10	20	-	28	10	19	1621.15864	0.00043	1.0
30	10	20	-	29	10	19	1621.80491	0.00063	1.0
31	12	20	-	30	12	19	1622.45015	0.00021	1.0
32	12	20	-	31	12	19	1623.09517	0.00000	1.0
21	0	21	-	20	0	20	1615.64556	0.00016	1.0
22	2	21	-	21	2	20	1616.29439	-0.00023	1.0
23	2	21	-	22	2	20	1616.94317	-0.00033	1.0
24	4	21	-	23	4	20	1617.59193	-0.00008	1.0
25	4	21	-	24	4	20	1618.24005	-0.00011	1.0
26	6	21	-	25	6	20	1618.88796	0.00002	1.0
27	6	21	-	26	6	20	1619.53531	-0.00002	1.0
28	8	21	-	27	8	20	1620.18251	0.00019	1.0
29	8	21	-	28	8	20	1620.82955	0.00063	1.0
30	10	21	-	29	10	20	1621.47573	0.00062	1.0
31	10	21	-	30	10	20	1622.12117	0.00028	0.5
32	12	21	-	31	12	20	1622.76640	0.00016	1.0
34	14	21	-	33	14	20	1624.05524	-0.00041	0.5
22	0	22	-	21	0	21	1615.96437	0.00019	1.0
23	2	22	-	22	2	21	1616.61305	-0.00014	1.0
24	2	22	-	23	2	21	1617.26166	-0.00017	1.0
25	4	22	-	24	4	21	1617.90972	-0.00040	1.0
26	4	22	-	25	4	21	1618.55778	-0.00024	1.0
27	6	22	-	26	6	21	1619.20540	-0.00015	1.0
28	6	22	-	27	6	21	1619.85267	-0.00001	1.0
29	8	22	-	28	8	21	1620.49969	0.00027	1.0
30	8	22	-	29	8	21	1621.14545	-0.00029	1.0
31	10	22	-	30	10	21	1621.79191	0.00026	1.0
32	10	22	-	31	10	21	1622.43753	0.00039	1.0
33	12	22	-	32	12	21	1623.08147	-0.00072	0.5
34	12	22	-	33	12	21	1623.72659	-0.00022	1.0
23	0	23	-	22	0	22	1616.28288	0.00027	1.0
24	2	23	-	23	2	22	1616.93116	-0.00023	1.0
25	2	23	-	24	2	22	1617.57930	-0.00051	1.0
26	4	23	-	25	4	22	1618.22776	-0.00010	1.0
27	4	23	-	26	4	22	1618.87558	0.00005	1.0
28	6	23	-	27	6	22	1619.52277	-0.00003	1.0
29	6	23	-	28	6	22	1620.17005	0.00037	1.0
30	8	23	-	29	8	22	1620.81700	0.00085	1.0
31	8	23	-	30	8	22	1621.46230	0.00010	1.0
32	10	23	-	31	10	22	1622.10788	0.00005	1.0
33	10	23	-	32	10	22	1622.75357	0.00054	1.0
35	12	23	-	34	12	22	1624.04243	0.00034	1.0
24	0	24	-	23	0	23	1616.60077	0.00009	1.0
25	2	24	-	24	2	23	1617.24888	-0.00036	1.0
26	2	24	-	25	2	23	1617.89719	-0.00024	1.0
27	4	24	-	26	4	23	1618.54519	-0.00005	1.0
28	4	24	-	27	4	23	1619.19215	-0.00052	1.0
29	6	24	-	28	6	23	1619.83970	0.00001	1.0
30	6	24	-	29	6	23	1620.48644	0.00013	1.0
31	8	24	-	30	8	23	1621.13344	0.00093	0.5
32	8	24	-	31	8	23	1621.77831	0.00002	1.0
34	10	24	-	33	10	23	1623.06868	0.00013	1.0
36	12	24	-	35	12	23	1624.35703	0.00002	1.0
25	0	25	-	24	0	24	1616.91852	0.00013	1.0

J'	K_a'	K_c'	-	J"	K_a''	K_c''	Observed Wavenumber (cm^{-1})	Deviation (cm^{-1})	Normalised Weight
26	2	25	-	25	2	24	1617.56662	-0.00011	1.0
27	2	25	-	26	2	24	1618.21440	-0.00029	1.0
28	4	25	-	27	4	24	1618.86226	-0.00000	1.0
29	4	25	-	28	4	24	1619.50859	-0.00085	0.5
30	6	25	-	29	6	24	1620.15601	-0.00021	1.0
31	6	25	-	30	6	24	1620.80298	0.00040	1.0
32	8	25	-	31	8	24	1621.44823	-0.00029	0.5
34	10	25	-	33	10	24	1622.74010	0.00101	0.5
35	10	25	-	34	10	24	1623.38419	0.00048	1.0
36	12	25	-	35	12	24	1624.02866	0.00079	1.0
26	0	26	-	25	0	25	1617.23529	-0.00045	1.0
27	2	26	-	26	2	25	1617.88372	-0.00014	1.0
28	2	26	-	27	2	25	1618.53176	0.00017	1.0
29	4	26	-	28	4	25	1619.17870	-0.00022	1.0
30	4	26	-	29	4	25	1619.82622	0.00036	1.0
31	6	26	-	30	6	25	1620.47262	0.00024	1.0
32	6	26	-	31	6	25	1621.11863	0.00015	1.0
33	8	26	-	32	8	25	1621.76458	0.00043	1.0
34	8	26	-	33	8	25	1622.41029	0.00090	1.0
35	10	26	-	34	10	25	1623.05466	0.00048	1.0
36	10	26	-	35	10	25	1623.69922	0.00071	1.0
37	12	26	-	36	12	25	1624.34175	-0.00062	0.5
27	0	27	-	26	0	26	1617.55258	-0.00015	1.0
28	2	27	-	27	2	26	1618.20039	-0.00023	1.0
30	4	27	-	29	4	26	1619.49534	0.00012	0.5
31	4	27	-	30	4	26	1620.14208	0.00017	1.0
32	6	27	-	31	6	26	1620.78888	0.00070	0.5
33	6	27	-	32	6	26	1621.43430	0.00028	1.0
28	0	28	-	27	0	27	1617.86911	-0.00026	1.0
29	2	28	-	28	2	27	1618.51714	0.00011	1.0
30	2	28	-	29	2	27	1619.16475	0.00045	1.0
32	4	28	-	31	4	27	1620.45825	0.00065	1.0
34	6	28	-	33	6	27	1621.74971	0.00052	0.5
35	8	28	-	34	8	27	1622.39520	0.00087	0.5
36	8	28	-	35	8	27	1623.04057	0.00155	0.0
37	10	28	-	36	10	27	1623.68544	0.00220	0.0
38	10	28	-	37	10	27	1624.32793	0.00094	0.0
29	0	29	-	28	0	28	1618.18632	0.00068	0.5
31	2	29	-	30	2	28	1619.48039	0.00028	0.5
32	4	29	-	31	4	28	1620.12746	0.00074	0.5
33	4	29	-	32	4	28	1620.77377	0.00085	0.5
34	6	29	-	33	6	28	1621.41985	0.00117	0.0
35	6	29	-	34	6	28	1622.06526	0.00126	0.0
39	10	29	-	38	10	28	1624.64357	0.00289	0.0
40	12	29	-	39	12	28	1625.28601	0.00235	0.0
30	0	30	-	29	0	29	1618.50211	0.00056	0.0
32	2	30	-	31	2	29	1619.79674	0.00119	0.0
33	4	30	-	32	4	29	1620.44310	0.00117	0.0
34	4	30	-	33	4	29	1621.08963	0.00175	0.0
35	6	30	-	34	6	29	1621.73543	0.00205	0.0
36	6	30	-	35	6	29	1622.38031	0.00187	0.0
37	8	30	-	36	8	29	1623.02569	0.00265	0.0
39	10	30	-	38	10	29	1624.31401	0.00318	0.0
31	0	31	-	30	0	30	1618.82037	0.00327	0.0
32	2	31	-	31	2	30	1619.46854	0.00446	0.0
33	2	31	-	32	2	30	1620.11620	0.00556	0.0
34	4	31	-	33	4	30	1620.76298	0.00621	0.0
35	4	31	-	34	4	30	1621.40957	0.00710	0.0
36	6	31	-	35	6	30	1622.05543	0.00771	0.0
39	8	31	-	38	8	30	1623.98971	0.00901	0.0
40	10	31	-	39	10	30	1624.63369	0.00962	0.0
41	10	31	-	40	10	30	1625.27660	0.00965	0.0

J'	K_a'	K_c'	-	J"	K_a''	K_c''	Observed Wavenumber (cm^{-1})	Deviation (cm^{-1})	Normalised Weight
33	2	32	-	32	2	31	1619.77745	-0.00158	0.0
34	2	32	-	33	2	31	1620.42337	-0.00198	0.0
35	4	32	-	34	4	31	1621.06865	-0.00259	0.0
36	4	32	-	35	4	31	1621.71346	-0.00323	0.0
37	6	32	-	36	6	31	1622.35763	-0.00405	0.0
38	6	32	-	37	6	31	1623.00096	-0.00526	0.0
39	8	32	-	38	8	31	1623.64302	-0.00726	0.0
40	8	32	-	39	8	31	1624.28581	-0.00804	0.0
34	2	33	-	33	2	32	1620.09305	-0.00057	0.0
35	2	33	-	34	2	32	1620.73902	-0.00069	0.0
36	4	33	-	35	4	32	1621.38413	-0.00122	0.0
37	4	33	-	36	4	32	1622.02880	-0.00175	0.0
39	6	33	-	38	6	32	1623.31682	-0.00273	0.0
40	8	33	-	39	8	32	1623.96018	-0.00316	0.0
41	8	33	-	40	8	32	1624.60333	-0.00331	0.0
34	0	34	-	33	0	33	1619.76108	-0.00048	1.0
35	2	34	-	34	2	33	1620.40740	-0.00045	1.0
36	2	34	-	35	2	33	1621.05327	-0.00042	1.0
37	4	34	-	36	4	33	1621.69855	-0.00054	0.5
38	4	34	-	37	4	33	1622.34329	-0.00074	0.5
39	6	34	-	38	6	33	1622.98678	-0.00173	0.0
40	6	34	-	39	6	33	1623.63147	-0.00104	0.0
41	8	34	-	40	8	33	1624.27381	-0.00222	0.0
35	0	35	-	34	0	34	1620.07519	-0.00047	1.0
36	2	35	-	35	2	34	1620.72176	0.00005	1.0
37	2	35	-	36	2	34	1621.36683	-0.00048	0.5
38	4	35	-	37	4	34	1622.01215	-0.00032	1.0
39	4	35	-	38	4	34	1622.65676	-0.00039	0.0
40	6	35	-	39	6	34	1623.29972	-0.00165	0.0
41	6	35	-	40	6	34	1623.94379	-0.00131	0.0
42	8	35	-	41	8	34	1624.58705	-0.00130	0.0
43	8	35	-	42	8	34	1625.22958	-0.00151	0.0
36	0	36	-	35	0	35	1620.38889	-0.00050	1.0
37	2	36	-	36	2	35	1621.03509	-0.00011	1.0
38	2	36	-	37	2	35	1621.68107	0.00050	1.0
39	4	36	-	38	4	35	1622.32486	-0.00061	0.0
40	4	36	-	39	4	35	1622.96886	-0.00104	0.0
42	6	36	-	41	6	35	1624.25641	-0.00092	0.0
41	6	36	-	40	6	35	1623.61266	-0.00120	1.0
37	0	37	-	36	0	36	1620.70260	-0.00015	1.0
38	2	37	-	37	2	36	1621.34833	0.00000	1.0
39	2	37	-	38	2	36	1621.99305	-0.00040	1.0
40	4	37	-	39	4	36	1622.63748	-0.00063	1.0
41	4	37	-	40	4	36	1623.28162	-0.00066	1.0
38	0	38	-	37	0	37	1621.01538	-0.00036	1.0
39	2	38	-	38	2	37	1621.66084	-0.00025	1.0
41	4	38	-	40	4	37	1622.95074	0.00037	1.0
43	6	38	-	42	6	37	1624.23707	-0.00065	1.0
44	6	38	-	43	6	37	1624.88004	-0.00061	1.0
39	0	39	-	38	0	38	1621.32850	0.00013	1.0
40	2	39	-	39	2	38	1621.97374	0.00026	1.0
41	2	39	-	40	2	38	1622.61799	-0.00012	1.0
43	4	39	-	42	4	38	1623.90537	-0.00056	1.0
44	6	39	-	43	6	38	1624.54860	-0.00050	1.0
45	6	39	-	44	6	38	1625.19169	-0.00006	1.0
46	8	39	-	45	8	38	1625.83349	-0.00040	1.0
40	0	40	-	39	0	39	1621.64058	-0.00005	1.0
41	2	40	-	40	2	39	1622.28565	0.00015	1.0
42	2	40	-	41	2	39	1622.92955	-0.00034	1.0
44	4	40	-	43	4	39	1624.21725	0.00005	1.0
41	0	41	-	40	0	40	1621.95258	0.00006	1.0
43	2	41	-	42	2	40	1623.24142	0.00013	1.0

J'	K_a'	K_c'	-	J"	K_a"	K_c"	Observed Wavenumber (cm^{-1})	Deviation (cm^{-1})	Normalised Weight
44	4	41	-	43	4	40	1623.88416	-0.00078	1.0
45	4	41	-	44	4	40	1624.52847	0.00038	1.0
46	6	41	-	45	6	40	1625.17085	0.00013	1.0
47	6	41	-	46	6	40	1625.81239	-0.00045	1.0
42	0	42	-	41	0	41	1622.26400	-0.00005	1.0
43	2	42	-	42	2	41	1622.90866	0.00023	1.0
45	4	42	-	44	4	41	1624.19558	-0.00014	1.0
46	4	42	-	45	4	41	1624.83828	-0.00033	1.0
43	0	43	-	42	0	42	1622.57502	-0.00018	1.0

difference between the observed and calculated frequencies and are relatively small ($<\simeq 0.01\ cm^{-1}$), were found to be roughly proportional to $[J(J+1) - K_c(K_c \pm 1)]^1$ for values of K_c = 29 to 33. For a molecule with C_{2v} symmetry this means that:

$$\Gamma\nu_2\ (A_1) \times \Gamma_{(perturbing)} = A_2 \text{ or } B_1 \qquad (7.5)$$

Therefore the perturbing mode must have the symmetry species A_2 or B_1. Furthermore, the direction of the shifts indicate that it is a ΔK_c = -1 interaction with a mode lying just below the ν_2 fundamental. A rough estimate of the frequency of the perturbing mode was made. The level with the largest shift (K_c = 31) was assumed to lie equal in energy to the level with K_c = 30 in the perturbing mode for the same value of J (see Figure 7.6). When symmetric top rigid rotor energies are assumed and the rotational constants are taken to be the same for both

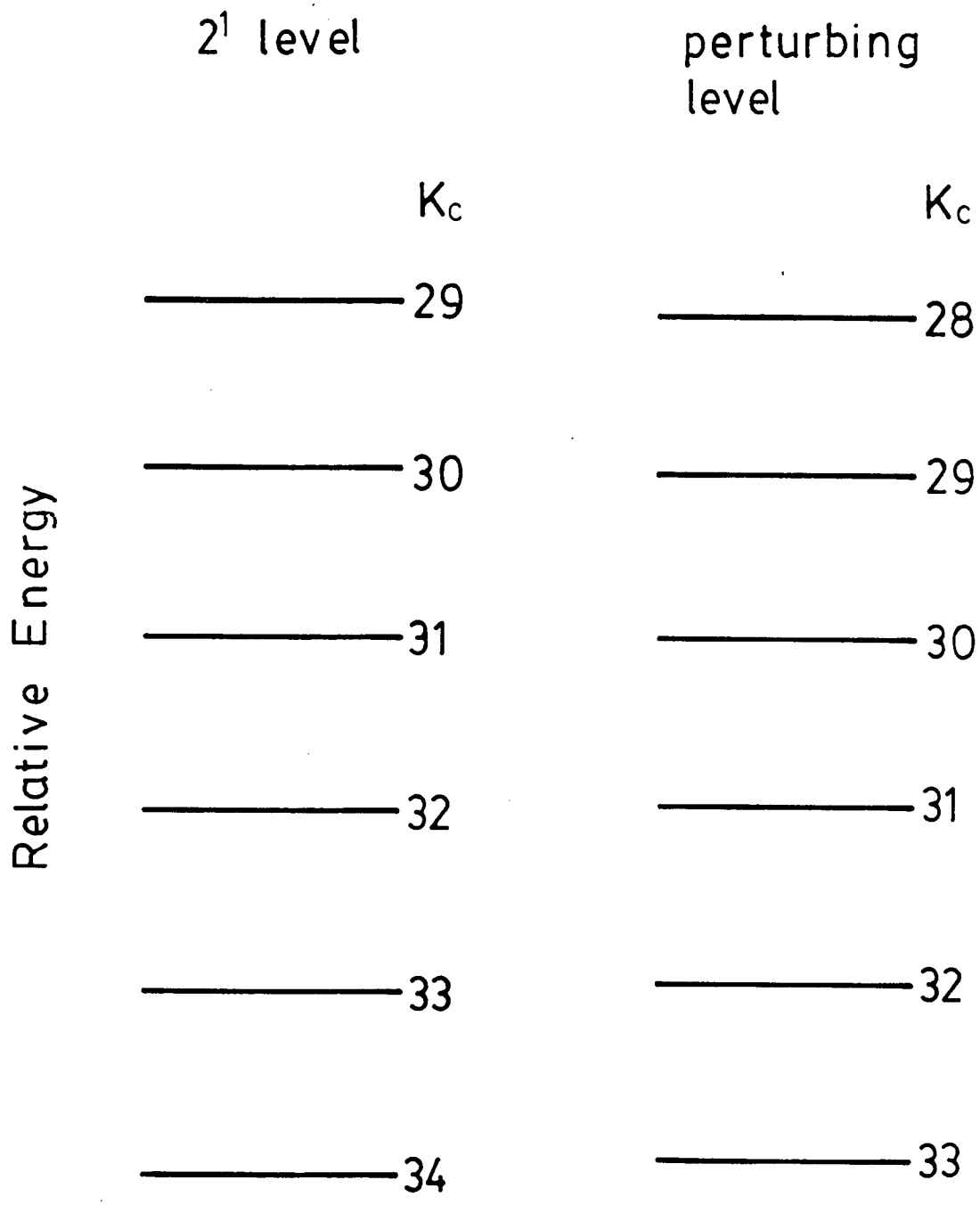

Figure 7.6 Relative positions of the K stacks of the 2^1 and perturbing level for a particular value of J.

levels, the perturbing level is found to lie below the 2^1 level by:

$$T(\nu_2) - T(\nu_p) \approx [\tfrac{1}{2}(A+B)-C][(31)^2-(30)^2] \qquad (7.6)$$

$$\approx 10 \text{ cm}^{-1}$$

The perturbing level cannot be a fundamental: the shifts are too small, there are no bands overlapping ν_2 and it is highly unlikely that the torsion will lie at such a high frequency. Also, since it cannot be an overtone, which would have symmetry A_1, it must therefore be a combination level. Unfortunately, because not all the frequencies of the fundamentals have been identified, it is uncertain which combination of fundamentals produces the perturbation. One possibility, although unlikely because it would lie at too low a frequency is $2\nu_5 + \nu_7$ ($\approx$1540 cm^{-1}) which has B_1 symmetry. Using the calculated frequencies (12) for bands which have not yet been identified (see Table 7.1), other possibilities for the perturbing combination band are $\nu_4 + \nu_7$ and $\nu_7 + \nu_{11}$ which have B_1 and A_2 symmetries respectively. The latter is more likely as the calculated frequencies are high when compared to the corresponding experimental frequencies.

7.5 Discussion

For the first time, the infra-red spectrum of BF_2NH_2 has been investigated. The wavenumbers of 7 of the 11 infra-red active fundamentals have been evaluated. The other fundamentals

may have been too weak to detect, especially since only a low vapour pressure of BF_2NH_2 could be maintained, or they may have been obscured by other bands, particularly bands of the impurity diethyl ether.

In addition, one of the fundamentals, the 2_0^1 band, has been examined in greater detail and the rotational and quartic centrifugal distortion constants for the ground and the first excited state have been calculated. The centrifugal distortion constants for the ground state were improved in accuracy over those calculated solely from microwave transitions (6). There is also a small Coriolis perturbation in this band; it is uncertain which combination band is causing the perturbation, though it is likely to be $\nu_7 + \nu_{11}$. This level is estimated to lie $\approx$10 cm^{-1} below the 2^1 level which would mean that the frequency of ν_{11} is $\approx$937 cm^{-1}.

Bibliography

1. M.C.L. Gerry, W. Lewis-Bevan, A.J. Merer, N.P.C. Westwood, J. Mol. Spectrosc. 110, 153-163, (1985).

2. A.W. Laubengayer, G.F. Condike, J. Am. Chem. Soc. 70, 2274-2276, (1948).

3. I.G. Ryss, N.G. Parkhomenko, Russ. J. Inorg. Chem. (Eng. Transl.) 11, 55-59 (1966)

4. E.F. Rothgery, H.A. McGee, Jr., S. Pusatcioglu, Inorg. Chem. 14, 2236-2239, (1975).

5. S.Y. Pusatcioglu, H.A. McGee Jr., A.L. Fricke, J.C. Hassler, J Appl. Polym. Sci. 21, 1561-1567, (1967).

6. F.J. Lovas, D.R. Johnson, J. Chem. Phys. 59, 2347-2353, (1973).

7. H.J. Becher, "Handbook of Preparative Inorganic Chemistry", Ed. G. Brauer., Vol. 1., Academic, New York, 1963.

8. G. Herzberg. "Infrared and Raman Spectra of Polyatomic Molecules", pp. 469-484, Van Nostrand, New York, 1945.

9. Work in progress at the University of British Columbia, Vancouver.

10. M. Perec, L.N. Becka, J. Chem. Phys., 43, 721-727 (1965).

11. A.G. Robiette, M.C.L. Gerry, J. Mol. Spectrosc. 80, 403-410 (1980).

12. T.-K. Ha, J. Mol. Struct. (Theochem) 136, 165-176, (1986).

13. W. Lewis-Bevan, A.J. Merer, M.C.L. Gerry, P.B. Davies, A.J. Morton-Jones, P.A. Hamilton, J. Mol. Spectrosc. 113, 458-471, (1985).